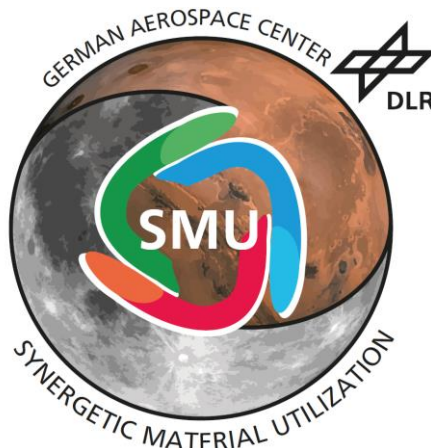Master's Thesis

Development of a Testbed for the Beneficiation of Lunar Regolith

Concentrating an Ilmenite-Rich Feedstock for In-Situ Oxygen Production on the Moon

Submitted to the
Faculty of Production Engineering
at the
University of Bremen

Author:	Michel Fabien Franke (3218889)
Examiners:	Dr.-Ing. Paul Zabel
	Prof. Dr.-Ing. Andreas Rittweger
Submission date:	5th of February 2022

Declaration of Authorship

Nachname: Franke   Vorname: Michel Fabien

Matrikelnr.: 3218889

A)   Eigenständigkeitserklärung

Ich versichere, dass ich die vorliegende Arbeit selbstständig verfasst und keine anderen als die angegebenen Quellen und Hilfsmittel verwendet habe.

Alle Teile meiner Arbeit, die wortwörtlich oder dem Sinn nach anderen Werken entnommen sind, wurden unter Angabe der Quelle kenntlich gemacht. Gleiches gilt auch für Zeichnungen, Skizzen, bildliche Darstellungen sowie für Quellen aus dem Internet.

Die Arbeit wurde in gleicher oder ähnlicher Form noch nicht als Prüfungsleistung eingereicht.

Die elektronische Fassung der Arbeit stimmt mit der gedruckten Version überein.

Mir ist bewusst, dass wahrheitswidrige Angaben als Täuschung behandelt werden.

B)   Erklärung zur Veröffentlichung von Bachelor- oder Masterarbeiten

Die Abschlussarbeit wird zwei Jahre nach Studienabschluss dem Archiv der Universität Bremen zur dauerhaften Archivierung angeboten. Archiviert werden:

1) Masterarbeiten mit lokalem oder regionalem Bezug sowie pro Studienfach und Studienjahr 10 % aller Abschlussarbeiten

2) Bachelorarbeiten des jeweils ersten und letzten Bachelorabschlusses pro Studienfach u. Jahr.

☒ Ich bin damit einverstanden, dass meine Abschlussarbeit im Universitätsarchiv für wissenschaftliche Zwecke von Dritten eingesehen werden darf.

☐ Ich bin damit einverstanden, dass meine Abschlussarbeit nach 30 Jahren (gem. §7 Abs. 2 BremArchivG) im Universitätsarchiv für wissenschaftliche Zwecke von Dritten eingesehen werden darf.

☐ Ich bin nicht damit einverstanden, dass meine Abschlussarbeit im Universitätsarchiv für wissenschaftliche Zwecke von Dritten eingesehen werden darf.

C)   Einverständniserklärung über die Bereitstellung und Nutzung der Bachelorarbeit / Masterarbeit / Hausarbeit in elektronischer Form zur Überprüfung durch Plagiatssoftware

Eingereichte Arbeiten können mit der Software *Plagscan* auf einen hauseigenen Server auf Übereinstimmung mit externen Quellen und der institutionseigenen Datenbank untersucht werden.

Zum Zweck des Abgleichs mit zukünftig zu überprüfenden Studien- und Prüfungsarbeiten kann die Arbeit dauerhaft in der institutionseigenen Datenbank der Universität Bremen gespeichert werden.

☒ Ich bin damit einverstanden, dass die von mir vorgelegte und verfasste Arbeit zum Zweck der Überprüfung auf Plagiate auf den *Plagscan*-Server der Universität Bremen hochgeladen wird.

☐ Ich bin ebenfalls damit einverstanden, dass die von mir vorgelegte und verfasste Arbeit zum o.g. Zweck auf dem *Plagscan*-Server der Universität Bremen hochgeladen u. dauerhaft auf dem *Plagscan*-Server gespeichert wird.

☐ Ich bin nicht damit einverstanden, dass die von mir vorgelegte u. verfasste Arbeit zum o.g. Zweck auf dem *Plagscan*-Server der Universität Bremen hochgeladen u. dauerhaft gespeichert wird.

Mit meiner Unterschrift versichere ich, dass ich die oben stehenden Erklärungen gelesen und verstanden habe. Mit meiner Unterschrift bestätige ich die Richtigkeit der oben gemachten Angaben.

_____   _____

Datum, Ort   Unterschrift

Abstract

The utilization of extraterrestrial resources may one day enable mankind's further exploration and sustainable colonization of the Solar System. An easily accessible and very versatile resource found on Earth's celestial neighbor, the Moon, is lunar regolith. This unconsolidated mixture of soil and rocks contains large quantities of oxygen, which in return can be used to produce consumables for propulsion and life support systems. However, the oxygen is chemically bound to minerals and must, thus, be extracted. The preparation of a feedstock that is chemically and physically suited for the extraction is termed beneficiation and depicts a vital stage in the context of in-situ oxygen production.

Developing a test stand that demonstrates the technical feasibility of lunar mineral beneficiation in a laboratory setting is the purpose of this master's thesis. The testbed's main function is to concentrate the target mineral ilmenite (a titanium-iron oxide), to reject unwanted gangue minerals (like silicates), and to remove unfavored size fractions (e.g., dedusting and oversize grain removal). To ensure that the end product fulfills this function in a satisfactory manner, a systematic engineering design process consisting of seven work packages is applied. This involves a review of existing studies and an investigation of available processes, the definition of requirements and specification, as well as various conceptualization activities (process and setup selection plus sketching). Moreover, results of design calculations and data of methodically selected components are integrated into a 3D model, to be created using computer-aided design software. Production planning activities like the preparation of procurement-related documentation completes the development.

The outcome of this thesis is a well-engineered and methodically mature beneficiation system that encompasses three dry separation stages: Particle size separation, magnetic separation, and electrostatic separation. This multi-stage approach guarantees the reliable and efficient enrichment of ilmenite from lunar regolith simulant. Hence, it is ready to be brought into being through assembly, integration, and test and can eventually be used for beneficiation-related experiments.

Keywords related to this work:

- In-situ resource utilization (ISRU)
- Space resource utilization (SRU)
- Extraterrestrial oxygen production
- Lunar mineral beneficiation
- Mineral enrichment of ilmenite

Kurzfassung

Die Nutzung extraterrestrischer Ressourcen könnte sich als der Schlüssel zur Expansion unserer Spezies in das Sonnensystem erweisen. Auf dem Mond, dem einzigen natürlichen Satelliten unseres Heimatplaneten, stellt der sogenannte Regolith eine leicht zugängliche und vielfältig nutzbare Ressource dar. Diese lose Masse aus Schutt und Gestein enthält große Mengen an Sauerstoff, der wiederum zum Betrieb von Antriebs- und Lebenserhaltungssystemen genutzt werden könnte. Allerdings ist der Sauerstoff chemisch an Minerale gebunden und muss daher extrahiert werden. Die Herstellung eines Ausgangsmaterials, das chemisch und physikalisch für diesen Extraktionsprozess geeignet ist, wird in der Fachsprache als Aufbereitung bezeichnet, welche einen wichtigen Schritt im Rahmen der in-situ Sauerstoffproduktion auf dem Mond darstellt.

Ziel dieser Masterarbeit ist die Entwicklung eines Prüfstandes, der die technische Umsetzbarkeit der Aufbereitung von Mondmineralen unter Laborbedingungen demonstriert. Die Hauptfunktion dieses Prüfstandes soll darin bestehen, das Zielmineral Ilmenit (ein Titan-Eisenoxid) anzureichern, unerwünschte Gangminerale (wie Silikate) auszusortieren und zu große oder zu kleine Partikel zu entfernen (d.h. Entstaubung und Überkornabsiebung). Um sicherzustellen, dass das Endprodukt diese Funktionen in hinreichendem Maße erfüllt, wird ein systematischer Produktentstehungsprozess zur Anwendung gebracht, der aus insgesamt sieben Arbeitspaketen besteht. Dazu gehören die Sichtung vorhandener Publikationen und die Identifikation potenzieller Verfahren, die Definition von Anforderungen und Spezifikationen sowie verschiedene Konzeptionsaktivitäten (Auswahl von Methoden, Beschreibung des Aufbaus und Anfertigung von Entwurfsskizzen). Darüber hinaus werden die Ergebnisse von Auslegungsberechnungen sowie Daten methodisch ausgewählter Komponenten in ein 3D-Modell eingearbeitet, welches mit Hilfe einer computergestützten Konstruktionssoftware erstellt wird. Produktionsplanerische Tätigkeiten wie die Erstellung von beschaffungsrelevanten Unterlagen schließen die Entwicklung ab.

Das Ergebnis dieser Arbeit ist ein technisch hochwertiges und methodisch ausgereiftes Aufbereitungssystem, das drei Abschnitte beinhaltet: Partikelgrößensortierung, magnetische Trennung und elektrostatische Aufbereitung. Der mehrstufige Ansatz ermöglicht es, die Ilmenitkonzentration von synthetischem Mondregolith effizient und zuverlässig zu erhöhen. Das fertiggestellte System ist somit optimal für die Montage, Integration und Erprobung vorbereitet und kann zukünftig zu experimentellen Zwecken eingesetzt werden.

Stichwörter zu dieser Arbeit:

- Vorort-Verwendung von Ressourcen (ISRU)
- Nutzung von Weltraumressourcen (SRU)
- Extraterrestrische Sauerstoffgewinnung
- Aufbereitung von Mondmineralen
- Anreicherung von Ilmenit

Acknowledgements

I have received a great deal of both professional and personal support throughout the writing of this document. I would therefore like to express my deepest gratitude to all the special individuals who stuck with me along the way and therethrough helped in making this thesis become a reality.

First and foremost, I would like to thank my supervisor *Dr.-Ing. Paul Zabel* for giving me the opportunity to join his newly founded research group Synergetic Material Utilization. I feel very privileged to work among so many bright minds and am honored to contribute to research that will have a profound impact on interplanetary spaceflight in the not-too-distant future. The time I got to spend at the German Aerospace Center has been truly enriching to me.

Even before becoming my supervisor, Mr. Zabel sparked my passion for human space exploration through his very insightful lecture at the University of Bremen, which inspired me to specialize in the field of in-situ resource utilization from early on. His enthusiasm and encouragement ever since helped me in making the most of my workdays. I am utterly grateful for his indispensable guidance and the valuable feedback he provided.

I would like to extend my sincere thanks to the director of DLR's Institute of Space Systems in Bremen *Prof. Dr.-Ing. Andreas Rittweger* for being my thesis examiner and for equipping me with the necessary knowledge and skills in classes like Design of Space Vehicles or Structural Design and Analysis.

Furthermore, I would like to recognize the expert advice I received from *Dr. rer. nat. Peter Spietz* (in regards to high voltage technology) and acknowledge the efforts of the whole System Analysis Space Segment department.

I would also like to express my deepest appreciation to my peers. To my colleagues at DLR: I greatly appreciate the warm-hearted and welcoming atmosphere you created in the Mission Control Room. The many enlightening discussions during work and get-togethers in our free time were a real blessing. And to my fellow students at the University of Bremen, many of whom have become close friends: I am really glad to have met so many kind and open-minded people. I dearly hope that we will never lose sight of one another.

And finally, I am extremely grateful to my parents, grandparents, and girlfriend. Their relentless support during this challenging time has once more proven that they are always there for me, no matter the circumstances. I am deeply indebted to you, for you have lightened my workload whenever possible. Your moral and emotional support will never be forgotten. I would not have gotten so far without you!

Table of Contents

List of Figures

List of Tables

List of Abbreviations

Abbreviation	*Explanation*
AIT	Assembly, Integration and Test
BOM	Bill of Materials
CAD	Computer-Aided Design
COTS	Commercial Off-The-Shelf
DC	Direct Current
DD	Detailed Design
DLR	German Aerospace Center
ECLSS	Environmental Control and Life Support System
ECSS	European Cooperation for Space Standardization
ESA	European Space Agency
ETW	Electrostatic Travelling Wave
FEMM	Finite Element Method Magnetics
GSD	Generative Shape Design
HV	High Voltage
ISRU	In-Situ Resource Utilization
LCROSS	Lunar Crater Observation and Sensing Satellite
LEO	Low Earth Orbit
LSPS	Lunar Soil Particle Separator
NASA	National Aeronautics and Space Administration
PD	Preliminary Design
PSR	Permanently Shadowed Region
RPM	Revolutions Per Minute
RQ	Requirement
SMU	Synergetic Material Utilization
SRU	Space Resource Utilization
TRL	Technology Readiness Level
WP	Work Package

List of Symbols

Symbol	Denotation	Unit
$\vec{F}_g$	Gravitational force	[N]
$\vec{F}_c$	Centrifugal force	[N]
$\vec{F}_p$	Net force on a particle	[N]
$\vec{F}_{ad}$	Adhesive force	[N]
$\vec{F}_{vdW}$	Van der Waals force	[N]
$\vec{F}_{char}$	Characteristic force	[N]
σ	Electrical conductivity	[S*m^{-1}]
ε_r	Relative permittivity / dielectric constant	[-]
$\vec{F}_C$	Coulomb Force	[N]
q_p	Electric charge of a particle	[C]
$\vec{E}$	Electrostatic field strength	[V*m^{-1}]
$\vec{F}_{de}$	Dielectrophoresis force	[N]
r_p	Diameter of particle	[m]
ε_p	Permittivity of particle	[F*m^{-1}]
ε_0	Vacuum permittivity	[F*m^{-1}]
C	Capacitance of particles	[F]
ϕ_p	Work function of particle	[eV]
ϱ_p	Equivalent total resistance of particle	[Ω]
d_p	Diameter of particle	[m]
$q_{p,max}/m$	Charge to mass ratio	[C/kg]
ϕ_s	Work function of surface	[eV]
ρ_p	Density of particle	[kg*m^{-3}]
p	Pauthenier limit constant	[-]
$\vec{F}_m$	Magnetic force	[N]
V_p	Volume of particle	[m^3]
χ_p	Magnetic susceptibility of particle	[m^3*kg^{-1}]
χ_f	Magnetic susceptibility of fluid	[m^3*kg^{-1}]
$\vec{H}$	Magnetic field intensity	[A*m^{-1}]
$\vec{B}$	Magnetic flux density	[T]

C	Curie constant	[K]
T	Temperature	[K]
θ_C	Curie temperature	[K]
Q	Capacity of the permanent magnet drum separator	[kg/h]
L	Length of the drum	[m]
v	Linear drum velocity	[m*s^{-1}]]
f	Looseness of the feed	[-]
ρ	Bulk density (mean density of the feed)	[kg*m^{-3}]
ω	Angular velocity	[rad/s]
L_{eff}	Effective length of the drum	[m]
r	Radius of the drum	[m]
n	Rotational frequency	[1/min]
m	Mass of particle	[kg]
R	Diameter of the drum	[m]
g	Gravitational acceleration	[m/s^{-2}]
V	Volume	[m^3]
μ	Friction coefficient	[-]
θ	Separation angle	[°]
U	Voltage	[V]
d	Distance between plates	[m]
A	Plate area	[m^2]
C_{vac}	Capacity of a parallel-plate capacitor in vacuum	[F]
$E_{el,vac}$	Energy stored in a parallel-plate capacitor in vacuum	[W]
x	x-position of a particle in a uniform electrostatic field	[m]
y	y-position of a particle in a uniform electrostatic field	[m]
v_x	x-velocity of a particle in a uniform electrostatic field	[m/s^2]
v_y	y-velocity of a particle in a uniform electrostatic field	[m/s^2]
t	Time	[s]
I	Electric current	[A]
P	Power	[W]
t	Wall thickness	[mm]
α	Draft angle	[°]

Chapter 1   Introduction

1.1 Motivation & Subject Matter

"Magnificent desolation" [1] – this is how Buzz Aldrin vocalized his first impression of the moonscape, when he became the second man to walk on the lunar surface in July 1969. It seemed like the Moon, lacking in a notable atmosphere, hydrosphere, or magnetosphere [2], could not bear anything that is of interest for the human species. However, our perspective on the Moon as a source of resources has shifted dramatically since then; international space missions like India's Chandrayaan-1 (2008-2009) and the National Aeronautics and Space Administration (*short:* NASA) mission LCROSS (2009), concerned with examining, prospecting, and assessing the lunar resource potential, have revealed that our Earth's only natural satellite is not as *desolate* as once believed.

In fact, the Moon is thought to host many useful goods like oxygen, water ice, and precious metals, which in turn are often bound to a variety of valuable minerals. Not only do these resources merely *exist*, but they are also available in abundance, widely spread and well distributed. Data, collected through remote sensing (from orbiters) and sample collection (from landers), have shown that roughly two-fifths (by mass) of the lunar crust are constituted by oxygen atoms [3]. The measurements additionally suggest that permanently shadowed regions (*short:* PSR) at the lunar poles would stock billions of metric tons of H_2O at cryogenic temperatures [4], keeping the water frozen and preventing it from evaporating into space. Moreover, the findings imply that lunar regolith – the unconsolidated, heterogenous layer of debris that covers the lunar surface – is of special interest, as it comprises large quantities of oxygen (>40 wt.%) and is rich in elements like Silicon (>20 wt.%), Iron (>10 wt.%), Calcium, Aluminum, and Magnesium (see figure 1) – all of which are sought-after materials.
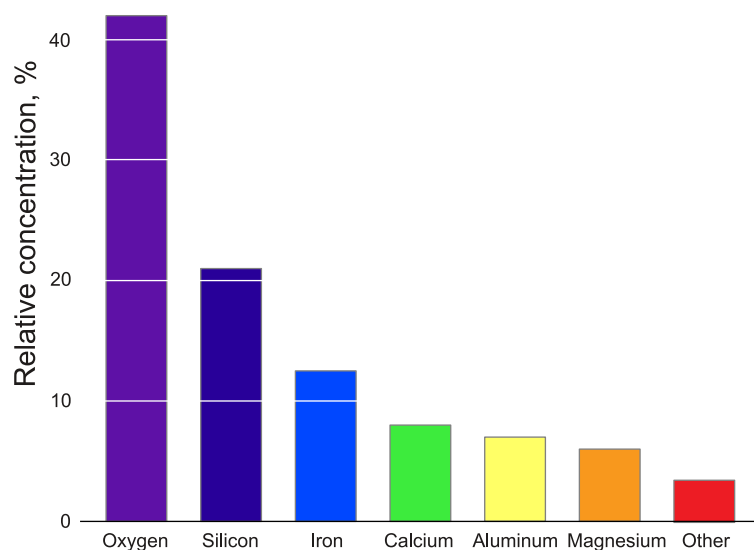
Figure 1: Average composition of lunar regolith [5]

However, these resources do not provide any value on their own – it is the *utilization* of a resource that constitutes its value [6]. In the space sector, this field is known as *In-Situ Resource Utilization* (*short:* ISRU) or *Space Resource Utilization* (*short:* SRU). Both terms equally describe the act of collecting, processing, storing, and using materials encountered on other astronomical objects to circumvent the necessity of bringing materials from Earth, drastically reducing launch mass, energy demand, costs, and risks associated with space missions [7]. When applied to the Moon, our nearest celestial neighbor, ISRU "has the potential to be the breakthrough technology that enables the further exploration of space by humankind" [8]. Its O_2-rich soil and rocks are an ideal basis for the extraterrestrial production of oxygen, which may be used in rocket propellants or to operate life support systems (e.g., in crewed spacecrafts or habitats). At this, space agencies like the European Space Agency (*short:* ESA) already consider the Moon as a future "spaceport to the universe" [9]: In its *Space Resources Strategy* from 2019, ESA emphasizes that the usage of the easily accessible lunar regolith for in-situ oxygen production is inevitable to *sustainably* explore or even colonize our solar system within the conceivable future [10].

Even though oxygen holds a high relative share within the lunar regolith, it does not appear in its pure form, but rather as part of a more sophisticated chemical compound (e.g., $FeTiO_3$ for the mineral ilmenite), meaning that it needs to be extracted first. This can be achieved using thermo-chemical reduction processes, all of which "require a consistent feedstock from the regolith to reliably and consistently produce oxygen" [11]. Hence, a preprocessing of the regolith is essential to guarantee a high oxygen yield and efficiency. This stage is called beneficiation and constitutes a major intermediate step in the domain of ISRU. It involves activities such as size sorting or mineral enrichment to create a higher-grade feedstock by separating the target mineral from the residuals.

Although being an essential part of ISRU, beneficiation as a research area has often been overlooked, while the attention of the scientific community mainly focused on the preceding and subsequent steps, i.e., excavation and extraction. This issue is also addressed in the most recent *ISRU Gap Assessment Report*, published in 2021 by the International Space Exploration Coordination Group: "There is currently limited work on crushing, size sorting, and mineral beneficiation, most likely due to lack of firm requirements" [12]. While a number of concepts exist in theory, only few of them have actually been built and put to the test in real life. Therefore, the report's authors call to action to remedy this situation [12]. Answering this call is the main purpose of this thesis: In consequence of the mentioned importance and topicality of this domain, it aims to demonstrate the feasibility and practicability of beneficiation as a preparation step for in-situ oxygen generation on the Moon.

1.2 Scope & Structure of Work

More specifically, it is the dedicated objective of the present scientific work to develop a laboratory test stand that is able to beneficiate lunar regolith simulant (as an input), converting it into an ilmenite-rich feedstock (output), which, in the end, could be used for in-situ oxygen generation on the Moon. The following main work packages have been defined to reach this goal:

- Perform a literature **research** and investigate possible processes for regolith beneficiation (chapter 3.1)
- State technical **requirements and specifications** that sufficiently characterize the test stand's wanted performance (chapter 3.2)
- Conceive a beneficiation **concept** by selecting processes, depicting a rough setup, and illustrating this setup as part of a technical sketch (chapter 3.3)
- **Calculate** the parameters and derive the **dimensions** that are needed to ensure that all requirements are met (chapter 3.4)
- **Select** readily available **components** that fulfill the demanded tasks (chapter 3.5)
- **Design** a preliminary and a detailed 3D model of the test stand using computer-aided design (*short:* CAD) software (chapter 3.6)
- **Plan** the **production** by sourcing the selected components, deriving technical drawings, and issuing a bill of materials from the previously created, final model (chapter 3.7)

Before getting to the practical part, however, some fundamental knowledge must be acquired. Thus, the foregoing section will outline the theoretic background and scientific context concerning the basic steps of ISRU (chapter 2.1), the properties of the processed materials (chapter 2.2), and the environmental conditions present on the Moon and Earth (chapter 2.3), in order to optimally prepare the application-oriented activities in section 3.

Both sections are enclosed by an introductive prelude in the beginning (chapter 1), as well as a summary (chapter 4), a conclusion, and a brief outlook into the future (chapter 5) at the very end. Now, before proceeding with chapter 2, the reader will concisely be provided with context as to where and in which environment the thesis is conducted.

1.3 Professional Environment

The work portrayed in this paper is executed at the *Institute of Space Systems* of the German Aerospace Center (*short:* DLR), which is located in Bremen, Germany. More specifically, it is part of the research group *Synergetic Material Utilization* (*short:* SMU), which was founded in 2021 by Dr.-Ing. Paul Zabel. SMU seeks to combine SRU with Environmental Control and Life Support Systems (*short:* ECLSS) "in order to exploit the many synergies among both fields to enable sustainable exploration of the solar system" [13] (e.g., common materials, processes, and products). Currently, SMU has seven dedicated research topics, dealt with by three PhD candidates, two M.Sc. candidates, and two interns, as well as Dr. Zabel himself. In the beginning, three areas are focused on:

- Regolith Beneficiation and Utilization
- In-Situ Propellant and Consumables Production
- Shared Water, Hydrogen and Oxygen Infrastructure

This scientific work is part of the first-mentioned pillar, but its end product, namely the beneficiation test stand, will be used to supply the other topics (e.g., the second group with the raw material needed to create an oxidizer for chemical propulsion systems). Accordingly, it must be noted that this thesis is part of a bigger (space) value chain and, thus, shares interfaces to and interdependencies with all the other SMU researchers, which will be highlighted throughout in the course of this document.

Chapter 2   Fundamentals

To facilitate the activities relating to the development of the beneficiation test stand (see chapter 3), it is of utter importance to learn about the theory behind what may affect the prospective device. As such, the present chapter will provide essential background knowledge, familiarize the reader with the bigger picture of relevant topics and raise awareness for potential interconnections.

It is important to note that the interdisciplinary nature of this document's subject matter demands a precognition in more than just one scientific field, with space engineering (specialized in ISRU), lunar geology & mineralogy, and planetary science being the most prominent ones. Accordingly, there are three main topics to be dealt with in chapter 2, that all constitute an independent subchapter:

- The **processes** of all main ISRU stages (excavation, beneficiation, and extraction / utilization)
- The **materials** to be processed (the ingoing regolith as well as the outgoing mineral streams)
- The **environment** to be experienced (the real, lunar and the artificial laboratory conditions)

2.1 The Processes: ISRU for Lunar Oxygen Production

As described in chapter 1, ISRU describes the usage of local resources from astronomical bodies other than Earth for the application on site or elsewhere in space. More specifically, it encompasses "any hardware or operation that harnesses and utilizes local or in-situ resources to create products and services for robotic, and human exploration and sustained presence" [12], to allow for reduced launch mass and numbers, thus, making space more affordable and accessible. Commodities of interest include solar wind implanted volatiles (such as helium-3), metals (like titanium, iron, silicon and aluminum) in mineral rocks, atmospheric constituents (e.g., oxygen and nitrogen) or even human waste, which may contain potentially useful organic matter like impure water [11].

On the Moon, which "represents a critical location for the expansion of humanity beyond Low Earth Orbit" (*short:* LEO) [12], oxygen is one of the prime in-situ resources due to its versatility and abundance. It can leverage human space flight within decades, as it is crucial for propulsion systems, constitutes one of the main life support consumables, and is needed for metal powder processing. Therefore, developing technology critical for oxygen extraction from lunar regolith is one of the top priorities within ESA's ISRU strategy. At this, ESA demands an "end to end demonstration of the production of […] oxygen at the lunar surface from locally sourced materials" as early as 2030 [10]. In this respect, 'end to end' already implies that oxygen production in view of ISRU is a multistage *product chain*. With the aim of universalizing this chain, Dr. Kathryn Hadler and her colleagues from the Imperial College in London developed a high-level framework, flowsheet, and terminology [14]. According to the researchers, in-situ oxygen production on the Moon comprises three steps: The procedure starts with the *excavation* of a given raw material, including its collection and conveyance. Excavation is followed by the second step *beneficiation*, where regolith is prepared into a suitable feedstock through particle sizing and mineral enrichment. Lastly follows *extraction* where the prepared feedstock is reduced, and emerging oxygen is captured (see figure 2) [8].
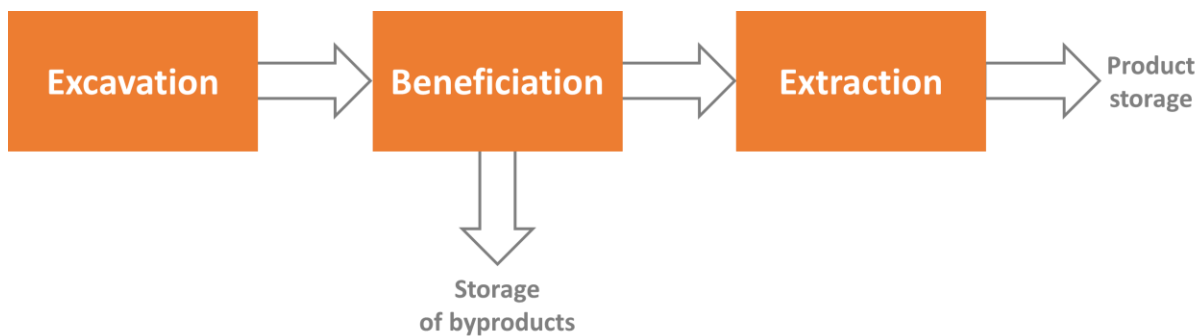
Figure 2: A universal flowsheet for ISRU in the framework of lunar oxygen production based on [14, p. 2]

Illuminating these processes in a scientific way is the purpose of subchapter 2.1. To put the desired laboratory test stand into a context, the following paragraphs will explain the basic principles behind not only beneficiation (2.1.2), but also behind the adjacent stages excavation (2.1.1) and extraction. Focusing on beneficiation, it will elaborate on the physics of dry separation techniques, which might be employed during the development as shown in chapter 3.

2.1.1 First Step: Excavation

According to the flowsheet in figure 2, the first step of in-situ oxygen production on the Moon is *excavation*. It denotes the act of mining, hauling, and handling a *raw material* (alias *ore* in terrestrial mining) such as lunar regolith that contains a desired *resource* (like oxygen) in some form or another (e.g., *pure* or bound to an *ore mineral* like ilmenite). Chronologically, excavation takes place after a resource-rich area has been spotted and assessed as suitable for quarrying (during antecedent prospecting missions) and before the raw material is forwarded to the ensuing processing (i.e., beneficiation) [12]. Being the first stage of the ISRU product chain makes excavation utterly important, as it represents "the foundation of any attempt to utilize lunar regolith resources effectively" [15, p. 2].

Despite being so important – and a well-understood technique in terrestrial mining – relatively few scientific studies have been conducted with respect to excavation on the Moon. The underreported research engenders a low design maturity in lunar excavators, as indicated by a Technology Readiness Level (*short*: TRL) of under four [15, p. 2]. However, lunar excavation needs completely new approaches, as necessitated by the different nature of materials (see chapter 2.2) and environment (see chapter 2.3) found on Earth and the Moon. Some differentiators are listed hereafter:

- Whereas underground mining (sub-surface) is often needed to reach deeply buried rock stratum in terrestrial mining, lunar regolith is easily accessible and can, thus, be harvested using **surface mining only**
- While mining drills and crushing equipment are needed to dislodge rocks (to get to the ore mineral) on Earth, the fine lunar regolith can be loaded onto the excavator **without any pre-comminution**
- Whilst terrestrial excavation appliances (like bulldozers) are operated by personnel, it is not viable nor economically tenable to adopt this scheme to space. Extraterrestrial excavators must be **highly automatic robots**

Furthermore, lunar excavators – like all space systems on the Moon – have to withstand the abrasive power of miniscule lunar dust particles, the thermal cycling, highly energetic radiation, and a low gravity environment. Especially, the last named imposes a challenge on lunar excavation: To dig on Earth, excavators rely on their weight; the 1/6th of Earth's gravity present on the Moon, however, reduces the weight and, as a result, reduces the vehicle's maximum excavation force, which is one of the most valuable performance parameters of an excavation vehicle [15, p. 3]. Another reason why terrestrial "excavators are designed as mass-intensive machinery" [15, p. 3] is to avoid lifting or slippage during operation (as mass has a significant influence on traction), which is in conflict with the requirements given by launch vehicles for their payloads to be lightweight and restricted in volume. Both effects add up and make it increasingly hard for lunar excavators to cope with the low gravitation.

In order to address these difficulties, NASA introduced an annual engineering competition, as part of its Centennial Challenges program. The first one to be brought into being was named *Regolith Excavation Challenge* and lasted from 2007 to 2010 [15, p. 2]. Since then, the competition was followed by several successors (like the Lunabotics Mining Competition), which all have different names but share a mutual objective: To offer an opportunity to the general public (students, entrepreneurs, and professionals) to invent, improve or test their own excavation-related robots. So far, these competitions yielded a multitude of feasible concepts and prototypes; a selection of examples can be seen in the following picture:
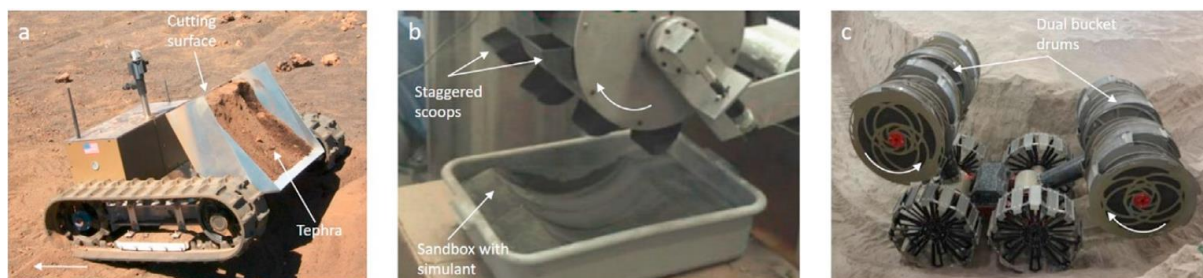
Figure 3: Examples of excavators invented during NASA's competitions [15, p. 5]

All of them have their own advantages and drawbacks, so that "there is currently no consensus as to which options are best suited for different lunar surface conditions or manufacturing needs" [15, p. 2]. Hence, a categorization scheme was established to keep track of the many designs: Just et al., who reviewed existing regolith excavation techniques for lunar ISRU in 2020, grouped "thirteen processes […] into *discrete* and *continuous* excavators" and further differentiated between "systems with and without connection to a mobility platform – referred to as *complete* and *partial* systems" [15, p. 1], as can be seen in figure 4. In this context, discrete systems have only one, relatively big cutting surface (as indicated in figure 3a) and, as such, must break contact with the bottom when dumping the excavated material (figuratively speaking, it takes a 'single large bite' at a time). Examples of discrete excavators are dozers, front-loaders or backhoes [15, p. 4]. Continuous systems, on the other hand, have multiple, relatively smaller cutting surfaces (as shown in 3b) and consequently remain in contact with the soil. To elaborate: "Once one cutting surface or bucket has gathered a sufficient amount of soil, it then clears the contact area while the next cutting surface has already started accumulating soil" (i.e., it takes 'many small bites') [15, p. 4]. Examples here are bucket wheels or bucket chains.
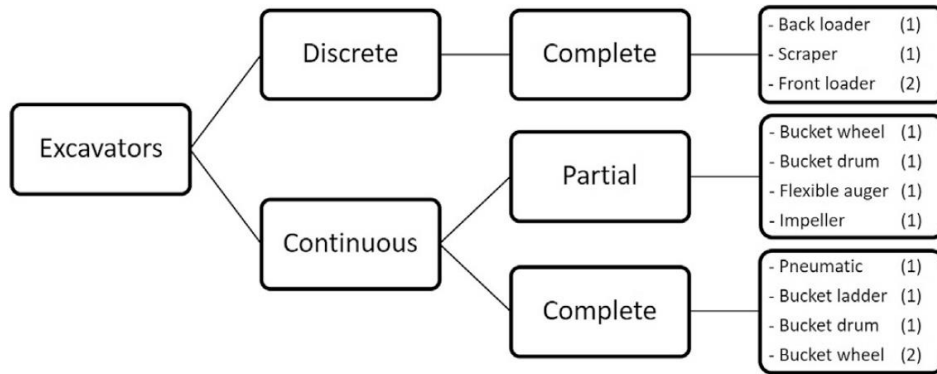
Figure 4: Types of excavators [15, p. 4]

Since in ISRU "the performance of each downstream stage is dependent on the preceding operation" [14, p. 2], the most prominent excavation performance metrics in the domain of O_2-related ISRU shall be mentioned, as they can have an effect on beneficiation. Those are [15, p. 8]:

- Excavation Rate
- Traverse Speed
- Power Consumption
- Regolith Consistency

The first-named characterizes the amount of e.g. regolith (either given as volume or mass) collected within a certain time; its unit would accordingly be given as kg/h or m^3/h [15, p. 9]. The *excavation rate* is highly application-driven: "Machinery in support of oxygen extraction will have to excavate less material than systems for habitat construction for example" [15, p. 9]. Since it accounts for all the necessary steps (acquisition, driving, dumping, repositioning), it is also highly intertwined with the second parameter – the *traverse speed* [15, p. 9]. Traverse speed quantifies "the driving speed of the vehicle used to provide mobility" on a given terrain or in a special scenario [15, p. 9], i.e. in the unit meters per second. Thirdly, excavation is quantifiable by its *power consumption* in Watts. It may either be given as a total value, or more ideally as a breakdown of consumption per subsystem or operation, respectively [15, p. 9]. This productivity measure, again, depends on yet another metric, namely the regolith consistency or – when thinking of analogue testing – the simulant properties [15, p. 9], as quarrying "dense cohesive materials requires more power" [15, p. 9]. Using denser (analogue) material can also diminish the excavation rate (as more excavation force is needed) or affect traverse speed (as driving on solid ground is faster than traversing a loose layer of debris).

2.1.2 Second Step: Beneficiation

Once gathered up, the excavated material will eventually be brought to a stockpile for temporary storage or directly to a processing facility [14, p. 3], where *beneficiation* takes place. This second step in Hadler's flowsheet will be regarded in the subsequent paragraphs.

Beneficiation is a term that originated in the terrestrial mining industry [15, p. 2]. It describes the act of transforming freshly excavated, raw material (e.g., lunar regolith) into a high-grade *feedstock* that is chemically and physically suitable for further processing.

At this, preparing the feedstock is either accomplished by *particle sizing* (filtering a specific size range) or by means of *mineral enrichment*, where the component of interest (i.e., an ore mineral like ilmenite) is separated from the undesired constituents contained in the mined material. The product streams that result in this process are typically called *(ore) concentrate* – the desired product rich in the ore mineral – and *tailings* (a 'waste' stream of non-valuable or less useful g*angue minerals*) [14, p. 3].

The main objective of beneficiation is to improve efficiency of later processes in the value chain. For in-situ oxygen production, this translates into a higher oxygen *yield* during extraction thanks to the reactant's elevated concentration. The enhanced mass fraction of the extraction's source material simultaneously helps in diminishing undesirable interference with other ingredients [12]. Another aim of beneficiation is to increase consistency, i.e., to decrease variability of the feedstock. The improved predictability of the utilized ore concentrate ensures process-stability and an overall higher reliability in downstream steps, as it prevents major disturbances [8]. As such, beneficiation depicts a vital intermediate step of the ISRU framework. Some authors even claim that size separation and mineral separation are indispensable when it comes to establishing a sustainable oxygen production infrastructure on the Moon [15, p. 2].

However, these goals can only be reached to some extent, as no beneficiation system is perfect: "Unwanted waste (gangue) minerals pass into the product stream and desired mineral particles are lost to the waste stream. To account for this misreporting of particles in terrestrial mineral processing, the terms *recovery* and *grade*", as well as *enrichment ratio* are used [14, p. 3]. These key performance metrics for beneficiation are defined as follows [8]:

- **Recovery** $= \dfrac{\text{Mass of produced product (e.g.,ilmenite)}}{\text{Mass of product in raw material (e.g.,ilmenite in regolith fed to the beneficiation system)}}$

- **Grade** $= \dfrac{Mass\ of\ product\ (ilmenite\ in\ feedstock)}{Mass\ of\ stream\ (total\ mass\ of\ feedstock)}$

- **Enrichment ratio** $= \dfrac{Grade\ of\ given\ species\ in\ outlet\ (ilmenite\ content\ in\ the\ ore\ concentrate\ )}{Grade\ of\ the\ same\ species\ in\ input\ (ilmenite\ content\ in\ the\ raw\ material)}$

In order to optimize these key performance metrics, any beneficiation system must be adapted to the selected extraction process (see chapter 2.1.3) and its source material (see chapter 2.2.2.2). As of today, "the beneficiation of lunar regolith to increase ilmenite content to improve the oxygen yield from hydrogen reduction is the most widely studied beneficiation strategy for lunar regolith" [14, p. 2], which is also the purpose of SMU's beneficiation test stand. The individual (sub-)processes employable in this context and their respective functional principles will be regarded as separate subchapters for both particle sizing (2.1.2.1) and mineral enrichment (2.1.2.2) to be found hereinafter.

2.1.2.1 Particle Sizing

Comminution, the reduction of particle sizes in a mined material, and *sizing*, the separation of particles according to their size, are both preliminary steps in the terrestrial beneficiation process [16, p. 276]. However, lunar regolith is generally so fine-grained (see 2.2.1.2) that comminution-related activities such as crushing and grinding are not needed for ISRU on the Moon [16, p. 276]. This leaves particle

sizing as the only available technique to be applied prior to mineral enrichment in the context of lunar feedstock preparation [14, p. 3]. Within this setting, sizing can serve two purposes: Firstly and more obviously, it controls the feedstock's physical properties as it puts its "particle size into a narrow range by removing coarse and fine particles from the mined regolith", which may be explicitly demanded by an oxygen extraction reactor's requirements [17, p. 7]. Secondly, sizing may control the feedstock's chemical composition, too, as in an inhomogeneous raw material, size distribution and mineral occurrence can be connected [11, p. 3]. This holds true for lunar regolith, as the relative abundance of its different particle types depends on size [18, p. 288] and other factors like excavation site (2.2.1).

When it comes to sizing, there are two subprocesses to choose from. The simplest of them is *screening*, where the ore is passed through one or more sieve(s), so that particles bigger than a certain size threshold are withheld. Terrestrial screening equipment can have many faces, from a simple metal lattice to sophisticated machines; further, they can be static (for very coarse material) or dynamically shake or vibrate the material with the aid of mechanisms [19]. Moreover, the aperture size, shape, orientation, and screen material can be adapted to the processed material. Large-scale sifter machines that incorporate a working fluid like water are often used on Earth [19].

Another option would be *classification*, which is described as sizing by exploiting "the differences in settling velocities exhibited by particles of different size" [19] under the influence of gravity. It either involves gravitational particle settling or centrifugally enhanced settling. As such, it "depends on relative movement in response to" gravitational ($\vec{F}_g$) and centrifugal ($\vec{F}_c$) "plus other forces such as resistance to motion by water or air" to discriminate different sizes [20]. On Earth, classification is done using gas cyclones, hydro-cyclones (see figure 5), ore sorters, rotating trommels of fluidized classifiers.
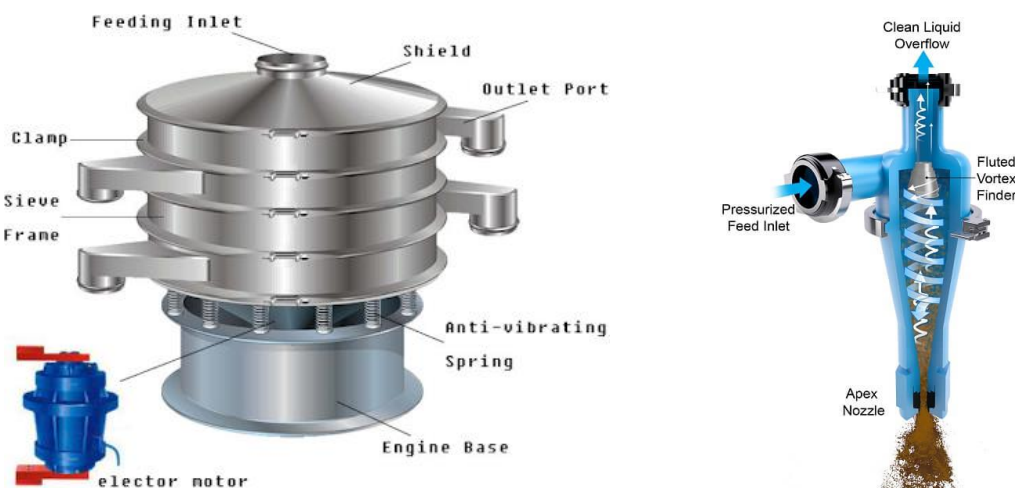
Figure 5: A schematic depiction of a vibratory sifter [21] and a hydro-cyclone [22] for sizing

New and disruptive techniques have recently been proposed for the size-driven sorting of regolith. They build up on the fact that other physical features of lunar soil such as electrostatic and magnetic properties are size-dependent (as will be explained in 2.2). However, these factors are also exploited to filter certain mineral types, which is termed *mineral enrichment.* To avoid ambiguity, the principles of magnetic and electrostatic separation will only be regarded as part of the following subchapter.

2.1.2.2 Mineral Enrichment

Mineral enrichment is a technique in beneficiation used "to separate minerals of different type based on their [distinct] physical properties" [14, p. 2]. The technique is used extensively and at huge scale in the terrestrial mining industry [14, p. 2]; however, the vast experience and knowledge here on Earth cannot be transferred to the Moon easily, as there is one major difference: Whereas water-intensive enrichment methods like froth flotation dominate in terrestrial mining, processes that rely on a process fluid are not suitable for lunar ISRU uses, because transport to the Moon and replenishment would be too costly (not to mention the challenging environment [3.2]). Correspondingly, *dry separation* is the only viable option for mineral enrichment on the Moon in the foreseeable future.

In dry separation, the movement of a particle is governed by the sum of various forces that act on it. On the Moon, those can be summarized as three *general terms* ($\vec{F}_g, \vec{F}_{ad}, \vec{F}_{vdW}$) that affect all mineral enrichment processes, as well as one or more *characteristic terms*, specific to each process:

$$\vec{F}_{net} = \sum \vec{F}_p = \vec{F}_g + \vec{F}_{ad} + \vec{F}_{vdW} + \vec{F}_{char} \tag{1}$$

As mentioned earlier, $\vec{F}_g$ is the *gravitational force* as experienced by any given object. Although the lunar gravitation is substantially lower (see 2.3), many beneficiation devices rely on the pull of gravity for conveyance – so-called free-fall systems. $\vec{F}_{ad}$ describes the *adhesive force*, the electrostatic attraction among a material's charged and non-charged particles (due to the resulting potential). It must be considered – as lunar regolith is very fine and highly charged – that the adhesive force can become dominant. The van der Waals force $\vec{F}_{vdW}$ is characterized as the distance-dependent interaction among nearby particles caused by their fluctuating polarization. It becomes dominant for lunar particles with a diameter less than 50 μm. Other general terms known from Earth, like drag or buoyant forces, can be neglected in the lunar context due to the hard vacuum present on the Moon.

The *characteristic force* $\vec{F}_{char}$ is applied deliberately by the beneficiation apparatus, i.e., in the form of a controlled, external field. It separates different minerals within the ore by exploiting their difference in physical properties, as its magnitude is not only governed by the field strength, but also by substance-specific coefficients. Describing the characteristic forces for the most frequently applied dry separation methods – *electrostatic* (2.1.2.2.1) and *magnetic separation* (2.1.2.2.2) – while also explaining their functioning will be the goal of two low-tier subchapters, which follow hereupon.

2.1.2.2.1 Electrostatic Separation

"Electrostatic separation is the selective sorting of solids by utilizing the [characteristic] forces acting on charged or polarized bodies in an electric field" [23, p. 23]. More specifically, it is based on the fact that some materials – such as minerals – can be electrically charged. The polarity and magnitude of the obtained charge depends on properties such as *conductivity σ* (a measure of how easily an electric current can flow through a mineral and how readily it releases an obtained, electrical charge; basis for categorization into *conductor* $\left[> 10^{-5} \frac{1}{\Omega m} \right]$, *semi-conductor* or *insulators* $\left[< 10^{-8} \frac{1}{\Omega m} \right]$) or *relative*

permittivity ε_r (formerly known as the *dielectric constant*, which indicates the electric polarizability of the mineral; bigger than 81 for conductors, normally between three and ten for insulators [unitless]) [23, p. 26], which are specific to any given substance. This specificness can be exploited to discriminate a wanted material from the undesired bulk by applying an electric field of appropriate strength [23].

In the context of electrostatic separation, there are two characteristic forces, called *coulomb force* and *dielectrophoresis force*. Starting with the former, it can be sensed as attraction or repulsion of charged particles, i.e., positively charged particles being repelled by a positive electrode and vice versa. Other than its counterpart, it acts on charged particles in *any* electrostatic field [11, p. 5]. Its magnitude is described by the product of a particle's electric charge and the electric field strength [11, p. 5]:

$$\vec{F}_C = q_p * \vec{E} \tag{2}$$

The latter – the dielectrophoresis force – "acts through the polarization of neutral particles in non-uniform electrostatic fields" [11, p. 5], only. Compared to the Coulomb force, it is considerably small, which gets even lower with increasing distance (negligible over large distances [11, p. 5]). Although mineral enrichment based on dielectrophoresis has some terrestrial heritage, it has not yet "been demonstrated for lunar applications on its own" [11, p. 5]. To compute this force's magnitude, the following formula can be used, which depends on the particle's diameter r_p, the permittivity of the particle's material ε_p, the vacuum permittivity ε_0 (natural constant), and the field strength $\vec{E}$:

$$\vec{F}_{de} = 2\pi r_p^3 \varepsilon_0 \left(\frac{\varepsilon_p - \varepsilon_0}{\varepsilon_p + 2\varepsilon_0} \right) \nabla \vec{E}^2 \tag{3}$$

Apart from these parameters, particle shape and size also seem to play an important role in both, electrostatic separation based on Coulomb or dielectrophoresis forces. At this, it is reported that "irregular particles tumbling down an incline attain a higher change than those that slide on one plane" [11, p. 5]. Further, another author states that "because the electrostatic force is proportional to the surface charge of the available surface area of the particles [...], fine, thin and light particles can be greatly influenced by the electrostatic force" (high charge-to-mass ratio) [23, p. 23].

Generally, electrostatic separation for mineral enrichment purposes is especially interesting on the Moon, as lunar regolith found at the surface already possesses a natural electrostatic charge (read 2.2.1.2 for more detail), that may be taken advantage of. This, however, is not the case for regolith simulants (2.2.1.3), which are used for lab testing on Earth (as for the test stand). To address this, several means of imparting charge have been proposed in the literature, as there are [11, p. 5]:

- Induction Charging
- Tribocharging
- Ion, electron, and UV bombardment

The first named occurs when an uncharged particle passes a non-ionizing electrostatic field. In doing so, the particle acquires the polarity of the field. "If a *conducting* or *semi-conducting* polarised particle then contacts an earthed surface, it loses one polarity to the conductive surface resulting in a net charge of opposite polarity" [11, p. 5]. The magnitude of this charge is determined by the physical and

chemical character of the mineral – the resulting differences in charge can later be exploited, as higher charges will lead to bigger deviations in a particle's path through a subsequent electrostatic field [23, p. 23]. *Non-conductive* particles, on the other hand, do not acquire any charge whatsoever, thus, will not show any response (neither being repelled nor attracted). Note that as conductivity increases with temperature, non-conductors might still be heated to such an extent that their conductivity becomes high enough for them to be charged. If the charge gained from induction was to be calculated, the following formulas, containing the capacitance of a particles C [F], its work function ϕ_p [eV] and its equivalent total resistance ϱ_p [Ω], should be used (d_p in the capacitance's formula is the particle diameter in meter) [11, p. 5]:

$$q_p = C\Delta\phi_p[1 - e^{-t/\varrho_p C}] \quad \text{with} \quad C = 2\pi\varepsilon_0 d_p \tag{4}$$

Since most minerals share a high resistivity, i.e., low conductivity, it may be hard to efficiently separate them using induction charging, as acquiring enough charge may happen too slowly for a distinguishable separation to occur. To circumvent this drawback, an alternative like *tribocharging* could be considered. Tribocharging is described as "a process by which particles (conductors, semiconductors and insulators) acquire [electric] charge through frictional rubbing and subsequent separation", also known as the triboelectric effect [11, p. 5]. The charge's magnitude is a product of two phases: It builds up during particle-particle contact, when the charge is transferred from one to another, and after the contact is broken, through the backflow of charge. Contact electrification is based on the energetically beneficial transfer of electrons, as defined by a particle's *Fermi level*: "When a particle with a higher Fermi level (lower work function) contacts a material with a lower Fermi level (higher work function), the former will lose an electron and the latter will gain it" [11, p. 5]. There is a strong relation in Fermi level delta and charging for metals; however, the charging of insulators is not so straightforward and other factors (like particle size, shape, angularity water adsorption) also play a role. This makes the calculation of the charge's magnitude complex: "A universal tribocharging model may not exist" [11, p. 5]. The absence of an analytical solution can still be bypassed through an empirical model, the so-called Harper equation that approximates the charge to mass ratio in $C * kg^{-1}$ with the aid of the work function of the particle ϕ_p and surface ϕ_s, as well as particle density ρ_p and diameter r_p:

$$\frac{q_{p,max}}{m} = 2.66 * 10^{-13} \left(\frac{\phi_s - \phi_p}{\rho_p * r_p^2}\right)(8.85 + 1.151\log_{10} r_p) \tag{5}$$

Tribocharging is considered as the simplest process "for imparting charge on particles, making it an attractive option for lunar SRU" [11, p. 6]. However, it is also possible to charge particles through the bombardment with ions, electrons, or UV radiation, which also constitute promising options. Starting with ion bombardment, this process involves a "corona-generating electrode mounted above an earthed metallic surface and a gas to ionise" [11, p. 6]. The charge is transferred by the ionized gas as it impinges the particles while they pass under the corona. After exiting the corona, conductive particles lose all their obtained charge to the earthed surface underneath them, which renders them neutral. Semi- and non-conductors, on the other hand, will get polarized and accordingly adhere to the underlying earthed surface [11, p. 6]. This adherence can now be exploited to distinguish the polarized semi- and non-conductors from the uncharged conductors, by putting the surface in motion. This is exemplarily done in roller separators (see figure 6): Semi- and non-conductors will adhere to

the rotating drum and end up in the closest collection hoppers, whereas conductors will already lose contact at the rotation's beginning, so they end up in the farthest collection container.
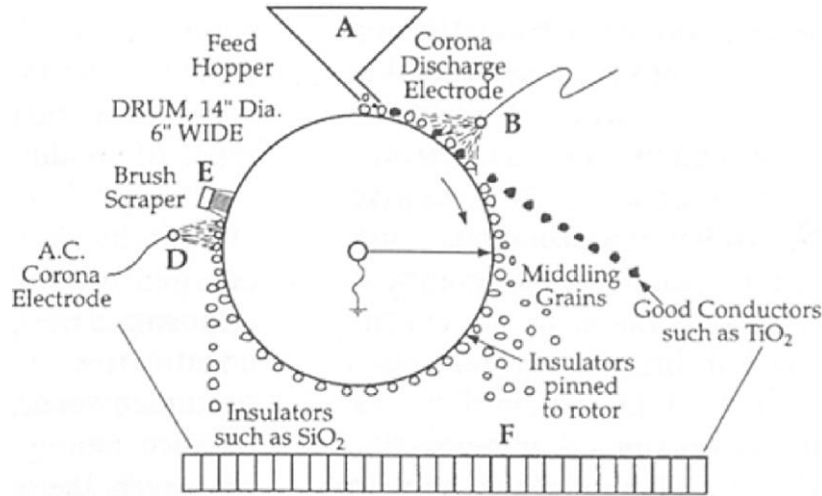
Figure 6: Earthed drum separator according to Manouchehri [23, p. 31]

It is likely that this technology could be employed for lunar SRU. Furthermore, the ions could also be replaced by electrons – the working principle remains the same – as electron beam charging is more energy efficient. This option would also eliminate the need for an ion source, making it more practical for outer space [11, p. 6]. It even seems superior when compared to UV bombardment, as some studies suggest that the imparted charge would be "an order of magnitude greater than the combined ion/electron bombardment, and three orders of magnitude greater than the UV method" [11, p. 6]. Independent of the ultimately selected beam type, there is one, universal formula that can be used to quantify the theoretically highest charge obtainable through bombardment: The Pauthenier Limit. It includes the constant p ($p = 3$ for conductors; $p = 3\varepsilon_p/(\varepsilon_p + 2)$ for dielectrics):

$$q_{p,max} = 4\pi r_p^2 \varepsilon_0 p |\vec{E}| \qquad (6)$$

2.1.2.2.2 Magnetic Separation

Magnetic separation is a dry enrichment process in which the differences in magnetic susceptibility within a mineral mixture are exploited through a magnetic field [19], either to "separate magnetic gangue from the desired ore, or conversely to remove a magnetic target ore from nonmagnetic gangue" [24]. There is only one characteristic force to be considered in this regard, termed *magnetic force*. It can be modelled using the following formula, which comprises an observed particle's volume V_p, its density ρ_p and magnetic susceptibility χ_p, as well as the surrounding fluid's susceptibility χ_f, the magnetic field intensity $\vec{H}$, and the magnetic field gradient (flux density's derivative) $\frac{d\vec{B}}{dx}$:

$$\vec{F}_m = V_p \rho_p (\chi_p - \chi_f) \vec{H} \frac{d\vec{B}}{dx} \quad \text{with} \quad \chi_p = \frac{C}{T - \theta_C} \qquad (7)$$

At this, χ_p can be calculated using the Curie-Law, which divides the Curie constant of a material C [K] by the difference between temperature T and the Curie temperature θ_C (0 for paramagnetism).

Speaking of paramagnetism, the validity of formula 7 is generally restricted to ferro- or paramagnetic materials. These terms originate from a categorization scheme based on a material's magnetic susceptibility, which indicates how much any given material will become magnetized by a magnetic field (a measure for how much it will interact with this field – if it is going to be attracted or repelled; χ is given in $m^3 * kg^{-1}$), which shall be explained hereinafter. There are three major classes:

- **Diamagnetism** ($\chi < 0$)
- **Paramagnetism** ($\chi > 0$)
- **Ferromagnetism** ($\chi \gg 0$)

Diamagnetic materials appear nonmagnetic in magnetic fields of low or moderate field strength, but have the tendency to oppose very strong magnetic fields (elevated field strengths) [25]. Theoretically, all types of materials have a diamagnetic component to them. However, the typical diamagnetic behavior is only exhibited by materials where this component is dominant, such as many terrestrial and extraterrestrial minerals.

Paramagnetic refers to weakly magnetic materials like ilmenite (2.2.2). In contrast to diamagnetic behavior, paramagnetic materials are attracted and not repelled when an external magnetic field is applied [25]. This can be attributed to the unaligned magnetic moments, that they occupy. "These moments react independently to applied magnetic fields and thermal energy […]. Without an applied magnetic field, the moments are randomly oriented" [11, p. 6], resulting in a net zero magnetization. To force a magnetic response anyway, strong magnetic fields are generally needed.

The term *ferromagnetic* is used when referring to materials that are strongly attracted to magnets, with iron being the most famous example (even though nickel, cobalt and their alloys are also members of this category) [25]. They get highly magnetized when exposed to a magnetic field and accordingly possess high susceptibility levels. Even low-intensity magnets will suffice to separate ferromagnetic minerals from other constituents in a mixture.

2.1.3 Third Step: Extraction

The completion of chapter 2.1.2 leads us to the third and last stage of the ISRU flowsheet: *Extraction*. It delineates the liberation of a product of interest, such as O_2 when speaking of oxygen production, from a pre-processed feedstock rich in the designated ore mineral (i.e., ilmenite) by means of chemical processing [12]. After extraction, the product may be consumed, sold, or further processed (e.g., pressurizing and cooling the O_2 to obtain a propellant's oxidizer). A broad variety of techniques are available when it comes to oxygen production on the Moon; the most frequently considered chemical processes to extract oxygen from lunar regolith are chemical reduction, acid treatment, electrolysis, and pyrolysis [26, p. 51].

At this, *chemical reduction* is characterized as a type of chemical reaction that entails "the gain of electrons […] of an atom, an ion, or of certain atoms in a molecule" [27], the so-called oxidizing agent. As such, it is the opposite of an oxidation, i.e., the loss of electrons in the reduction agent. Both are consolidated as the redox reaction, as reduction and oxidation always occur together.

Acid treatment refers to the more technical term of chemical dissociation, where the presence of an acid – a molecule or ion that is able to donate a proton or form a covalent bond with an electron pair [28] – triggers a process that breaks and dismantles chemical compounds (e.g., molecules or salts) into lower-level elements like atoms, ions or radicals [29].

Electrolysis, on the other hand, harnesses direct electric current to trigger an interchange of atoms and force a redox reaction. More specifically, two electrodes inject the direct current (*short*: DC) into an electrolyte and thereby ionize it. Positive ions discharge at the cathode by gaining electrons, which, as explained above, depicts a chemical reduction. The negatively charged anions lose electrons at the anode and accordingly, oxidize. Such being the case, electrolysis means converting electric energy into chemical energy. In other words, it is an inversion of a battery's working principle [30].

Lastly, the term *pyrolysis* refers to "the thermal decomposition of materials at elevated temperatures in an inert atmosphere" [31]. The absence of oxygen or other reagents helps in avoiding a full combustion. Like all the other mentioned processes, it aims to change the chemical makeup of the educt; in this case, the products can be solid (like char), condensable liquids or permanent gasses [31].

Further, each of the mentioned chemical processes has several methods and can be executed with different reactants, which is multiplying the number of possibilities: So far, the research community has proposed more than twenty methods [11] that could potentially be utilized to extract oxygen from lunar feedstock, some of them having been enhanced for several decades now and others being fairly novel (e.g., the *FFC-Cambridge process*, also known as molten salt electrolysis [15, p. 2]). To name but a few examples, reduction can either be conducted using *hydrogen* (yielding water as a primary product) or *methane*, whereas electrolysis is available for *molten* or *solid lunar regolith*. For pyrolysis there is a special approach called *vapor phase pyrolysis*, which requires temperatures beyond 2000°C, while acid treatment of ilmenite-rich feedstocks may be done with *sulfuric* acid (H_2SO_4) [26, p. 51].

"At present, the reduction of lunar regolith using hydrogen has been the most widely studied of the oxygen production techniques" [14, p. 2]. This can be attributed to hydrogen reduction being a very energy efficient process, as it is operated at moderate temperatures (700°C as opposed to 1600°C for methane reduction). Besides, it is a conceptually plain approach of two, well-established reaction steps, only: Water is the outcome of the initial hydrogen reduction; a subsequent electrolysis must be performed to get from water to oxygen (with hydrogen as a by-product). The process relies on a pre-processed feedstock with a high grade in iron-oxides, which is to be generated through beneficiation. In the case of ilmenite as a source material, the reduction equation look as follows [26, p. 51]:

$$FeTiO_{3(s)} + H_{2(g)} \rightarrow Fe_{(s)} + TiO_{2(s)} + H_2O_{(g)} \tag{8}$$
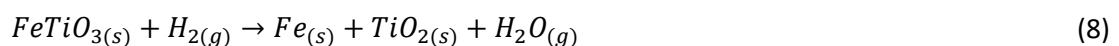
As mentioned before, a subsequent electrolysis then liberates the wanted oxygen from the water:

$$2H_2O_{(l)} \rightarrow 2H_{2(g)} + O_{2(g)} \tag{9}$$

For the sake of sustainability, the outputted hydrogen may be reused as an input to a later repetition of equation 8, making it a closed-loop process [26, p. 51].

"This reaction could ideally produce 10.5 wt.% O_2 from a given mass of ilmenite" as shown by several preliminary studies that have proven the feasibility of this concept [18, p. 142]. Ilmenite is also the most popular ore mineral to be used in this context, despite the fact that other minerals in the lunar regolith occur considerably more often (e.g., silicates), the reason being that "silicates present more difficult process engineering problems because they must be reduced at temperatures of 1100°C or more" [32, p. 543].

However, there are also limitations and dependencies associated with this method. The biggest disadvantage of ilmenite as a source material is that its abundance is restricted to mare regions (one of two main geological units on the Moon, as will be explained in chapter 2.2), making it unsuitable for processing plants in other areas [26, p. 51], where they would operate in an economically inviable manner. This statement is based on the fact that cutting the concentration of ilmenite in half would double the hydrogen reduction reactor size and increase energy requirements by a factor of two for the same rate of oxygen production [20, p. 1]. On top of that, the hydrogen needed for the reduction is viewed as a given input, although its provision is both expensive and time-consuming, as it would either be supplied from Earth or generated in-situ, from solar wind implanted hydrogen nuclei in the lunar soil [18, p. 142] or ice deposits in PSRs. Furthermore, fluctuations in the feedstock might deteriorate the process efficiency, as it relies on the presence of a consistently high ilmenite grade (as visualized in figure 7) and an absence of disturbing elements like sulfides, which would react to toxic hydrogen sulfide and would accordingly demand a post-purification step [26, p. 51].
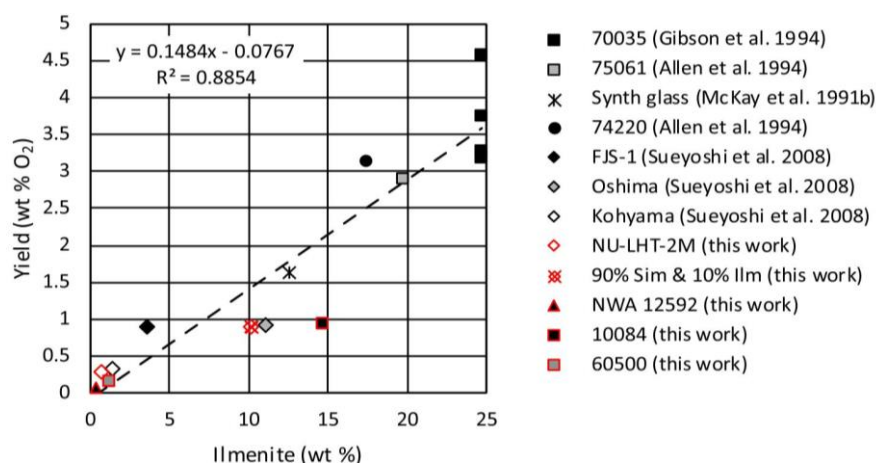
Figure 7: Oxygen yield as a function of the ilmenite grade for hydrogen reduction of regolith [33, p. 9]

When it comes to the extraction stage, there are three important performance parameters to remember, all originating from the discipline of chemical reaction engineering [14, p. 3]:

- **Refresh Ratio** is the "mass of fresh reactant required (e.g. H_2) per mass of product produced (e.g. O_2)"
- **Conversion** describing the "mass of reactant consumed (e.g. H_2) per fresh reactant input"
- **Yield** is defined as "mass of product produced (e.g. O_2) per mass of feedstock"

The word *yield* is widely used and not restricted to extraction. Instead, it can also be used at any other stage of the flow sheet (e.g., as mass of concentrate output compared to the initial raw material mass).

2.2 The Materials: Raw Material, Ore Concentrate & Gangue

Although the processes explained in chapter 2.1 constitute a vital part of ISRU, it represents only one of the many facets. Such being the case, ISRU is also always "underpinned by knowledge of the lunar or planetary *geology*, including *mineralogy*, *physical characteristics*, and the variability" [8] of the respective substance. In recognition of this fact, chapter 2.2 will characterize the materials to be inserted into and dispensed by the beneficiation apparatus. The following pages will consequently deal with the physical and chemical properties and most prominent features of those materials, while also providing a succinct overview of their origin, occurrence, purpose, and structure.
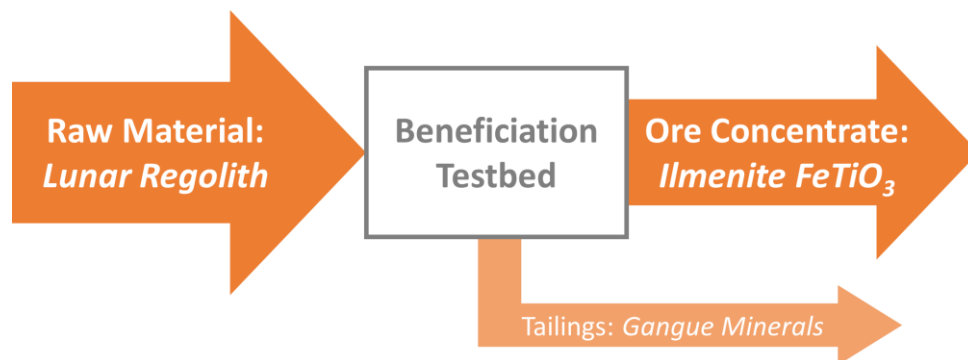
Figure 8: Material flow during the beneficiation of lunar regolith

Within chapter 2.2, the beneficiation testbed is being viewed as a black box, so that the ingoing and outgoing material flow can be focused on. As illustrated in figure 8, these can be identified as the raw material, i.e., the freshly excavated lunar regolith (2.2.1), the wanted ore mineral that is being enriched to a concentrate – in this case an iron oxide called ilmenite – and the tailings that are being removed, i.e., the waste stream of so-called gangue minerals (2.2.2). Describing these materials will help in designing a system that can optimally exploit the properties of different constituents of lunar regolith to separate the wanted from the unwanted part.

2.2.1 Input: Lunar Regolith

Geophysical data suggest that the Moon, just like Earth, is a differentiated body that possesses a tripartite shell structure composed of crust, mantle, and core. However, unlike on Earth, geological processes like volcanism or plate tectonics had halted almost 3 billion years ago [34, p. 537]. Instead, the transformation of the Moon's outermost shell is nowadays driven by non-endogenous dynamics, only. More specifically, it is the impact of cosmic objects like meteorites, asteroids, or comets, that represents the only abrupt geologic force. The impact-events fling away parts of the solid lunar bedrock, leaving massive craters behind, which in the end trench and sculpt the moonscape [34, p. 541]. The erosion is accompanied by a shockwave, which initiates the "shattering, pulverization, melting, mixing, and dispersal of the original coherent bedrock to new locations in and around the crater. […] As the impacts continue, the original bedrock is covered by a fragmental layer of broken, melted, and otherwise altered debris from innumerable superimposed craters" [18, p. 286]. This layer is called *lunar regolith*.

Knowing how regolith formed in the first place helps in defining what it is: From a geological point of view, lunar regolith can be perceived as a greyish, unconsolidated layer of debris containing fine-grained soil as well as rock material (whether transported or endemic), which almost completely overlies the Moon's bedrock. Consequently, it can be recognized as the predominant top-layer of the lunar surface or, to put it differently, as a boundary "between the solid Moon and the matter and energy that fill the solar system" [18, p. 286]. Only very few exceptions like crater walls and lava tunnels exist, where steep slopes make it impossible for the regolith to adhere to the underlaying ground, so that bedrock would be exposed [18, p. 285]. Yet the abundance of regolith is not limited to the surficial dimensions: The average depth of the regolith layer is estimated to be between 4 and 5 meters in the lighter areas and 10 to 15 meters in the darker regions. While there is consensus on the median thickness, the scientific community has not yet agreed on a maximum, as some sources suggest that it hardly ever exceeds 20 meters [18, p. 286], while others claim that that the deepest points might be in the kilometer order of magnitude [34, p. 542].

Being so abundant and readily accessible, lunar regolith holds a great economic value and "[…] will probably be the first extraterrestrial material to be exploited for resource recovery" [35, p. 804]. Beyond that, it is a highly versatile resource, so that its usage is not limited to oxygen production only. It is conceivable that regolith will also be used for almost any construction work, be it for landing pads or lunar bases. It therefore bears the potential to enable the establishment of a permanent presence already in the foreseeable future [18, p. 286].

As mentioned earlier, regolith is a collective term for both, fine-grained soil, and larger rock material. By definition, the size threshold between the two was set arbitrarily at 1 cm (for cataloging purposes), meaning that the sub-centimeter fraction is considered as soil and vice versa [18, p. 285]. The bulk of lunar regolith is constituted by the soil, "a somewhat cohesive, dark grey to light grey, […] loose, clastic material", which itself is a complex mixture, classifiable into five basic particle types [18, p. 288]:

- **Mineral** fragments
- Pristine, crystalline **rock** fragments
- **Breccia** fragments
- **Glasses** of various kinds
- Constructional particles unique to the Moon called **agglutinates**

In this connection, *minerals* are solid compounds of several chemical elements with a characteristic, crystalline structure. The term *rock*, on the other hand, describes an aggregate of one or more mineral types, which forms a "bulk solid geologic material that is relatively homogeneous at a large enough scale" [36]. *Breccia* can be described as a mixture of both, as they are "composed of broken fragments of minerals or rocks cemented together by a fine-grained matrix that can be similar to or different from the composition of the fragments" [37]. They form due to the solidification of pulverized lunar 'dust' during impact events, when a shockwave produces enough heat and overpressure necessary to weld fragments together [34, p. 541]. At this, the matrix embedding the fragments forms from locally available materials and can be glassy (mostly at the rim of craters) or glassless. Generally, breccias represent a significant portion of the regolith and contribute to its complexity [18, p. 285].

Glasses are different from the aforementioned constituents: Other than minerals or rocks, they are not crystalline but amorphous, which makes them appear transparent. They form when a suitable compound (e.g., silica) is molten and then rapidly cooled; on the Moon, this happens as part of impact melting or formerly through volcanic eruptions. "Completely glassy fragments (glasses without either crystal or rock inclusions) of both impact and volcanic origin are present in all sampled lunar soils" [18, p. 294]. Lastly, *agglutinates* are a special type of glass-bonded aggregates that can be found solely on the Moon. They appear as heterogeneous clasts or 'fringed' swirls (see figure 9) and entail a number of smaller soil particles (like mineral or glass grains), which are held together through vesicular, flow-banded glass [18, p. 296]. They are small in size (mostly smaller than 1 mm) and contain irregular lines "of Fe metal (much of which is very fine-grained, single domain Fe°), and troilite (FeS)" [18, p.296] embedded in the glass. They, too, can be traced back to micro-meteoritic bombardment, in which silicate melt adhered to nearby soil grains [18, p. 296].
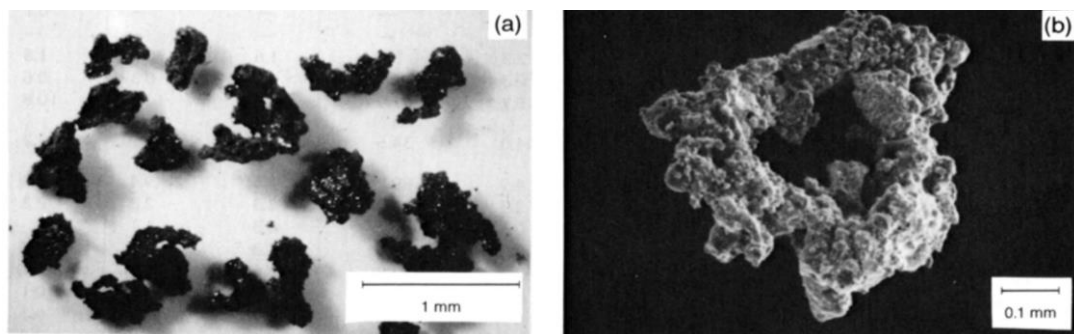
Figure 9: Typical lunar soil agglutinates found in Apollo samples [18, p. 296]

The ratio of these constituents within the regolith are inhomogeneous and depend on multiple factors (e.g., the location). But in general, it can be stated that agglutinates and breccias predominate: As an example, Apollo 11 samples contained 60% agglutinates and 20% breccias, so that only a small part of the sample was occupied by rock fragments and mineral grains [18, p. 307]. Beyond the sampling *location*, there is one other important influence factor that affects the mixing proportion called *maturity*, as "mature (old) and immature (young) soils from the same area may also have" very different attributes [18, p. 294]. In this connection, maturation describes how newly formed regolith is progressively altered when exposed to the high-energy solar wind environment, micrometeorites, and cosmic charged particles, which pulverize the soil to even finer grains and change its composition [38, p. 46]. As such, the geologic processes that modify the regolith over time are inherently different from terrestrial weathering (chemical weathering, running water, wind, and glaciation) [18, p. 476].

With the Moon being the only other body in space that has been systematically sampled, lunar regolith samples have been subject to a multitude of experiments in the past [18, p. 5]: Almost 2200 specimens with a total mass of approximately 382 kg were collected and returned to Earth during the course of NASA's Apollo program, which helped scientists to qualitatively and quantitatively characterize the soil and rocks [34, p. 537]. A broad spectrum of measuring devices in the laboratory (like spectrometers) but also on the lunar surface (e.g., magnetometers, heat flux probes) [34, p. 537] revealed both, the geochemical features (2.2.1.1) and the physical properties (2.2.1.2) of the lunar soil and rocks. These findings shall be presented within the next two subchapters.

2.2.1.1 Geochemical Composition

Centering upon its geochemical composition, it can be stated that lunar regolith is considerably nonuniform. Its varying chemical makeup is mainly caused by the complex structure it possesses, as it reflects how regolith is a mechanical mixture of different broken and molten fragments, whose ratio depends on several factors [18, p. 329], as explained above. Apollo samples, for instance, have shown remarkable differences even when picked up from the same landing site [18, p. 288]. Despite the chemical heterogeneity, the modal mineralogy of lunar rock seems relatively monotonous when compared to a thriving world like Earth: "Fewer than a hundred minerals have been found on the Moon, compared to several thousand on Earth" [18, p. 475]. This, on the other side, can be attributed to the absence of running water, wind, life or other geologic forces that are present on Earth but missing on the Moon [39, p. 406]. As a soil's composition heavily depends on the mineralogy of the source rocks it originates from, lunar soils can be classified into three distinct affinities [18, p. 288]:

- **Basaltic**, meaning that they predominately contain basalt, a fine-grained, dark grey, and very hard rock formed through rapid cooling of lava that is rich in iron and magnesium
- **Anorthositic**, i.e., mostly containing anorthosite, a coarse-grained, brightly textured rock formed when magma solidifies after intruding rock, majorly made of plagioclase feldspar
- **Meteoritic** constituents, which only make up a small fraction (<2%) of the regolith

Whereas meteoritic parts can be found all over the place, anorthosites and basalts are unevenly distributed, forming distinct geographic units called *highlands* (or terrae in Latin) and *maria* (as in the plural for mare, the Latin word for sea); the ancient highlands are considered anorthositic (*Ca*, *Al*-rich), whereas the younger maria are predominantly basaltic (*Fe*, *Ti*-rich) [18, p. 306]. This is also why the feldspar-rich highlands appear light-colored and have a rougher topography, while the iron-rich maria, which originated as cavities on the nearside formed by massive meteorite-impacts that were later filled with lava, seem darker (i.e., low-albedo surfaces) and finer [34, p. 538].

Generally, the most prominent mineral group within these soils are *silicates* (i.e., minerals dominated by silicon and oxygen), which constitute up to 90% by volume. The most abundant among them are *plagioclase feldspar* [(Ca,Na)(Al,Si)$_4$O$_8$], *pyroxene* [(Ca,Fe,Mg)$_2$Si$_2$O$_6$], and *olivine* [(Mg,Fe)$_2$SiO$_4$] as can be seen in table 1, with a tendency of mare soils being richer in pyroxene, whereas highland soils are more plagioclase-dominated [18, p. 122].

Table 1: Content of minerals and glasses (vol.%) in Apollo (A) and Luna (L) samples [18, p. 123]

	A-11	A-12	A-14	A-15 (H)	A-15 (M)	A-16	A-17 (H)	A-17 (M)	L-16	L-20	L-24
Plagioclase	21.4	23.2	31.8	34.1	12.9	69.1	39.3	34.1	14.2	52.1	20.9
Pyroxene	44.9	38.2	31.9	38.0	61.1	8.5	27.7	30.1	57.3	27.0	51.6
Olivine	2.1	5.4	6.7	5.9	5.3	3.9	11.6	0.2	10.0	6.6	17.5
Silica	0.7	1.1	0.7	0.9	-	0.0	0.1	-	0.0	0.5	1.7
Ilmenite	6.5	2.7	1.3	0.4	0.8	0.4	3.7	12.8	1.8	0.0	1.0
Mare Glass	16.0	15.1	2.6	15.9	6.7	0.9	9.0	17.2	5.5	0.9	3.4
Highland Glass	8.3	14.2	25.0	4.8	10.9	17.1	8.5	4.7	11.2	12.8	3.8
Others	-	-	-	-	2.3	-	-	0.7	-	-	
Total	99.9	99.9	100.0	100.0	100.0	99.9	99.9	99.8	100.0	99.9	99.9

Data from *Papike et al.* (1982), *Simon et al.* (1982), *Laul et al.* (1978a), and Papike and Simon (unpublished). (H) Denotes highland. (M) Denotes mare.

"*Oxide minerals*, composed chiefly of metals and oxygen, are next in abundance after silicate minerals" [18, p. 122]. They primarily accumulate in mare basalts, where they may represent up to one fifth by volume [18, p. 121]. The most common oxide, which simultaneously depicts the target mineral for our test stand, is *ilmenite* [(Fe,Mg)TiO$_3$], an opaque, black (due to its high TiO$_2$ content) substance [18, p. 122]. Ilmenite is followed by *spinel* (a complex series containing members like chromite, ulvöspinel, hercynite and sensu stricto) and *armalcolite* [(Fe,Mg)Ti$_2$O$_5$]) [18, p. 122].

Apart from silicates and oxides, there are also other mineral groups that exist – although occurring notably less frequent – like sulfides, phosphides, and carbides [18, p. 122]. An example of scarce minerals are *apatite* [Ca$_5$(PO$_4$)$_3$(OH,F,Cl)], *whitlockite* [Ca$_3$(PO$_4$)$_2$], *potassium feldspar* [KAlSi$_3$O$_8$], and *zircon* [ZrSiO$_4$]. Despite their scarcity, they are of major interest for ISRU as they "carry the bulk of such vital trace elements such as K, the rare earth elements (REE), P, and Zr" [18, p. 306]. Equally seldom are *schreibersite* [(Fe,Ni)3P], *cohenite* [(Fe,Ni)3C], and *niningerite* [(Mg,Fe,Mn)S], which are often of meteoritic origin [18, p. 122].

There is one oddity that all these mineral groups – from silicates over oxides to phosphides – have in common, which is strictly confined to the Moon: The lunar mineralogic repertoire completely lacks in hydrates, i.e., the lunar regolith does not accommodate any water-bearing minerals like clays, which oppositely are plentiful here on Earth [18, p. 122].

As mentioned earlier, agglutinates are a unique entity and accordingly differ from other lunar constituents in geochemical respects. Although their composition will be generally similar to that of the bulk regolith, they invariably contain metal droplets of single domain iron (np-Fe^0) and troilite (FeS) [18, p. 296], leading to a generally higher concentration of Fe in the agglutinates, triggered by the auto-reduction of FeO as a result of the low-oxygen, highly-reducing environment on the Moon. Although recent findings indicate that nano-phase iron and troilite are not unique to agglutinates but can also form a vapor-deposited patina on the surface of other lunar soil and rock particles, its concentration in bulk regolith is substantially lower than in agglutinic glass [40].

At this point, it is noteworthy that the geochemical composition cannot be considered individually, as it is heavily intertwined with the regolith's physical properties. This includes, but is not limited to, the variation of mineral shares with grain size. "Minerals that were originally present as small crystals in parent rocks may dominate the composition of the finest-grained sizes of a lunar soil, even though they made up only a small percentage of the parent rock" [18, p. 306].

2.2.1.2 Physical Properties

Accordingly, it is necessary to deal with the mechanical, magnetic, and electrostatic features of regolith in the following. Even though "the chemical compositions of lunar soils show considerable variation, physical properties such as grain size, density, packing, and compressibility are rather uniform" [18, p. 288] as a direct consequence of the confined lunar environment (see chapter 2.1.3) which prohibits more complex geologic processes that would result in a more diverse lunar surface material [18, p. 475].

Beginning with the first-named, figure 10 depicts the statistical *grain size distribution* of lunar regolith, with the middle curve indicating the average distribution and the upper and lower curves showing the ±1 standard deviation. The graph indicates that the bulk of regolith (~92%) is made up by the <1 mm fraction (so-called *fine fines*). It is important to remark that "most of the scientific studies have been performed on [this] fraction", while the *coarse fines* (>1 mm) "have not been studied in such a way that their data can be easily integrated with results from the fine fines" [18, p. 287]. Furthermore, the *average diameter* of regolith is $D_{50} = 72$ μm, the lunar soil's average *grain size* can be quantified as approx. 60 μm [18, p. 294] and the *average size* of *rock* fragments within it is at <250 μm [18, p. 288]. Agglutinates, on the other hand, can reach up to >1 mm in size [18, p. 298], whilst its single-domain metal droplets are sub-microscopic (30–100 Å) [18, p. 297]. With respect to the soils, the *mean grain size* can still be relatively heterogeneous, as it "ranges from 40 to 800 μm, with most means falling between 45 and 100 μm" depending on the individual sample (and e.g. the thickness of the regolith layer at the landing site) [18, p. 305]. As an example, Apollo 16 samples showed a mean grain size of 101 to 268 μm, whereas the parameter ranged from 41.5 to 166 μm for Apollo 17 [18, p. 305]. Moreover, mature soils are tendentially finer grained due to longer exposure [18, p. 294].
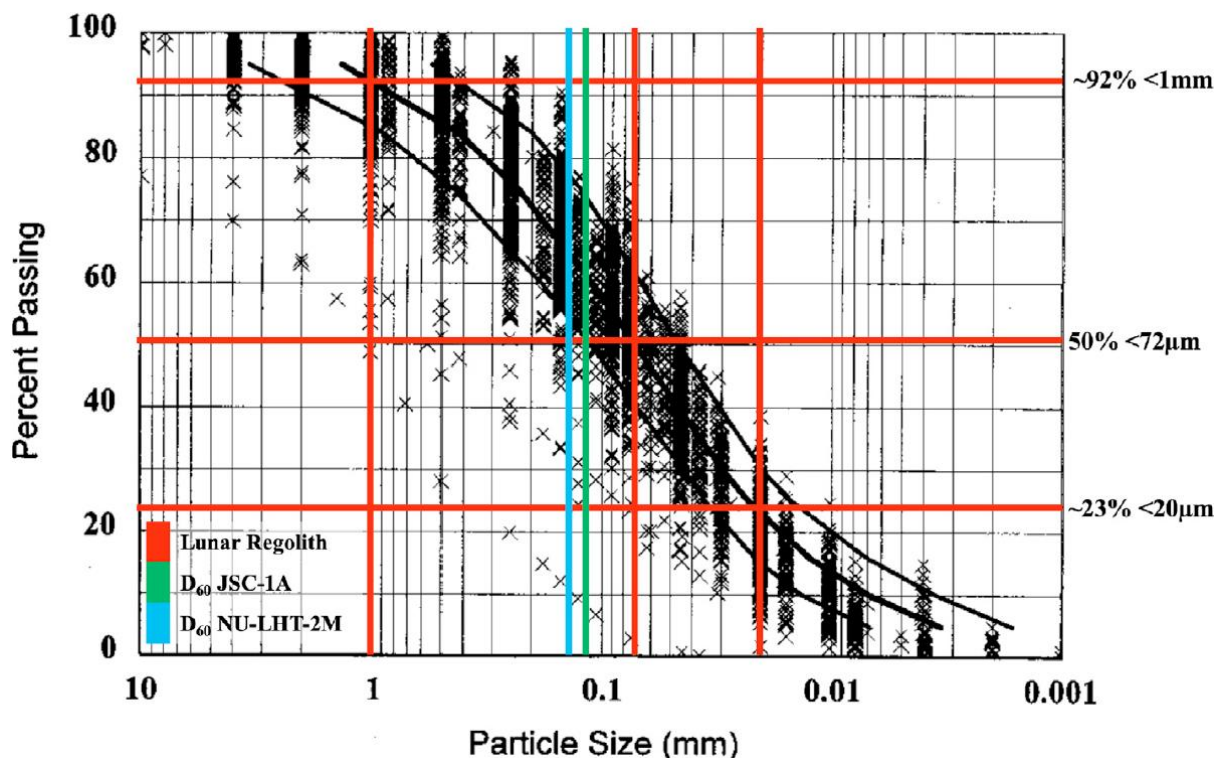
Figure 10: Particle size distribution of the lunar regolith based on 350 samples [11, p. 2]

As implied in chapter 2.2.1.1, the mineralogic composition of regolith is not evenly distributed across all size fractions. Exemplarily, the presence of polymineralic fragments (i.e., containing more than one mineral type) is a function of the mineral grain size in the parent rock. More specifically: "Rocks composed of minerals >60 μm in size will, when crushed, produce mostly single mineral fragments" [18, p. 294], while 30% of the 90…150 μm rock fragments of one sample were multi-mineralic [41, p. 1415]. Also, certain mineral fragments occupy more space than others, which will be elaborated in 2.2.2. Thus, sizing of lunar regolith may significantly contribute to an efficient beneficiation process.

Other mechanical properties like the particle shape, specific gravity, and bulk density are just as relevant as size, but are less crucial to the beneficiation-related activities. Thus, they will only be regarded briefly. The *shape* of a soil particle also influences the other physical properties. In lunar soil, the particle shape is "highly variable, ranging from spherical to extremely angular" [18, p. 478]. It is mainly expressed by two geotechnical parameters called *elongation*, which describes the ratio of the major to the intermediate axis of a particle, and the *aspect ratio*, which is inversely related to elongation (minor to major axis of an ellipse fitted to the particle). The elongation of regolith is averaged to 1.35, meaning that it exceeds a threshold and can accordingly be considered as *somewhat elongated* (equant ≤ 1.3 ≤ elongated) [18, p. 479]. "Because of the elongation, the particles tend to pack together with a preferred orientation of the long axes. [...] Because of this preferred particle orientation, the physical properties of the lunar soil [...] are expected to be anisotropic" [18, p. 478]. As can be seen in table 2, another attribute of lunar soil is its *porosity*. It describes the ratio of the volume of empty space between particles to the total volume and changes with depth [18, p. 483].

Table 2: Lunar soil in-situ porosity in dependence of regolith depth [18, p. 492]

Depth Range (cm)	Average Porosity, n (%)	Average Void Ratio, e
0 – 15	52 ± 2	1.07 ± 0.07
0 – 30	49 ± 2	0.96 ± 0.07
30 – 60	44 ± 2	0.78 ± 0.07
0 – 60	46 ± 2	0.87 ± 0.07

"The *specific gravity, G,* of a soil particle is defined as the ratio of its mass to the mass of an equal volume of water at 4°C" [18, p. 481], making it a dimensionless factor that describes how much bigger the density of a specific substance is compared to that of water (1 g/cm^3). As a reference, many terrestrial soils have a specific gravity of 2.7 [18, p. 481], whereas the lunar soils range from 2.3 to 3.2. Literature recommends a "value of 3.1 for general scientific and engineering" purposes [18, p. 481].

So by definition, G is greatly interrelated with the next parameter, the *bulk density ρ*, which is a property of unconsolidated solids (like soil) describing its mass contained within a given volume [18, p. 483]. It significantly varies with depth: The average for the top layer (0-15 cm depth) is given at 1.50 g/cm^3, whereas at an intermediate depth (30-60 cm) it can reach up to 1.74 g/cm^3 [18, p. 492].

The magnetic features of lunar regolith, on the other hand, can be summarized in four main observations. Firstly, the magnetic properties of every mineral type within the lunar soil differs greatly due to the distinct atomic structures and molecule arrangement (specific values will be listed individually in 2.2.2); some authors even state that "chemistry is the main factor that controls the magnetic susceptibility of minerals" [25]. Secondly, the magnetic behavior of bulk lunar material is dominated by the miniscule, ferromagnetic nano-phase iron particles (np-Fe^0) on the soil and in the agglutinates (see chapter 2.2.1), instead of iron-bearing minerals (other than on Earth where iron oxides prevail) [42, p. 2386]. Besides the abundant ferromagnetic constituents, "measurements indicate a significant amount of weakly magnetic [i.e., paramagnetic] material including the possibility of [...] diamagnetism" in the samples (see figure 11) [35, p. 804]. Thirdly, the magnetic response is size-dependent. In particular, it can be observed that the "<50 μm size fractions behaved as if virtually

most of the particles had relatively higher magnetic susceptibilities than the coarser particles" [40]. This phenomenon also relates to the np-Fe^0: The ferromagnetic "patina has been found on >90% of particles in the <10 μm fraction" and the "np-Fe0-bearing agglutinates comprise up to 80% of the <20 μm (dust) fraction" [11, p. 12]. On the other hand, heavier and coarser grains appear to be relatively less magnetic [43], as "the magnetic force is volume dependent" [44, p. 1]. This also affects big agglutinates: Though they are highly susceptible, their fairly large size and mass make them less responsive to magnetic fields [35, p. 804]. Lastly, the soil maturity also plays a role in the magnetic behavior: "Generally the soil magnetism increases with maturity" [45, p. 5367].
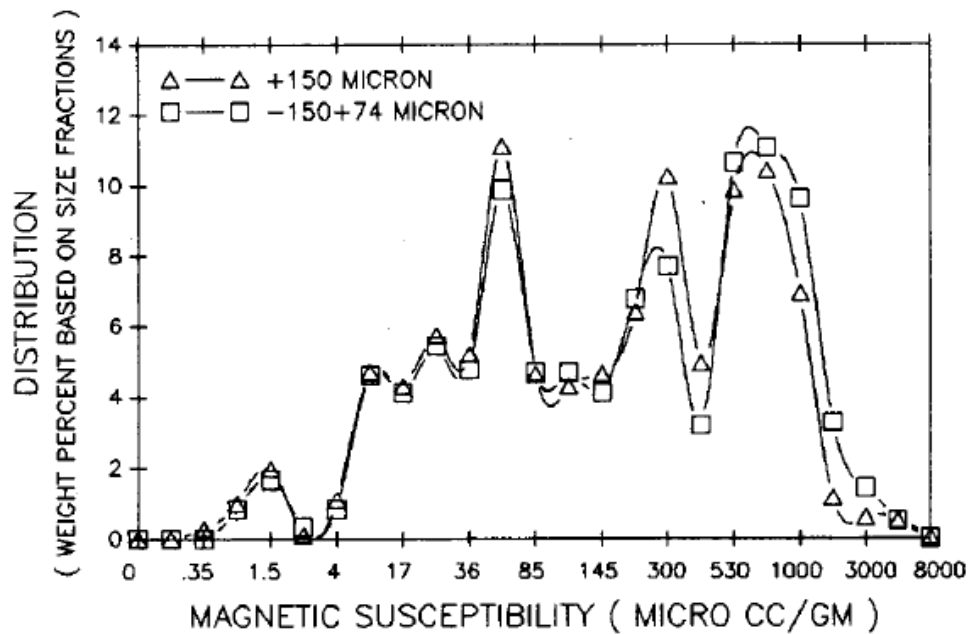
Figure 11: Magnetic distribution for a typical mature highland soil (67501) [45, p. 5367]

Generally, the electrostatic character of lunar regolith is dominated by a low *electrical conductivity* ("conductivity ranges from 10^{-14} S/m for lunar soils to 10^{-9} S/m for lunar rocks at 300 K in darkness" [18, p. 531]) and extremely low *dielectric losses*, typical for silicate mixes. The *relative dielectric permittivity* of regolith is heavily controlled by the bulk density and can consequently be approximated by the formula $k=1.9^{\rho}$ (ρ = bulk density in g/cm^3) [18, p. 531]). The combination of these traits paves the way for a unique phenomenon: When regolith is exposed to (solar) UV irradiation, an internal *polarization mechanism* is triggered [18] so that a radiation-induced *electrostatic charge* builds up. This charge leads to an extensive cohesion among dust particles and adhesion to surroundings [46]. When experimentally measured, the bulk net charge of Apollo 15 samples was found to range between 10^{-11} and 10^{-13} coul/kg and was almost entirely *negative* [46]. Furthermore, the electrostatic features of lunar material underly complex dependencies, with daytime (highest chargeability during night because of lower conductivity), particle size (charge density decreases with particle size), and mineral type (certain minerals gather charge more efficiently than others) being the most influential factors [46]. Graphic representations of these relations can be found in annex 1.

2.2.1.3 Simulants

The availability of lunar regolith samples here on Earth is strictly limited. However, academia and industry are both in need of large quantities in order to conduct all their scientific experiments and laboratory testing [11, p. 3]. This circumstance motivated researchers to engage in the development of *regolith simulants*, which are terrestrially synthesized copycats of lunar material that aim to mimic the original in all relevant matters. The quality features to be approximated can be, among others, a suitable mineralogy and bulk chemistry, the correct particle size distribution, the right particle shape with a corresponding grain density, and an adequate magnetic susceptibility or electrostatic chargeability [47].

However, earthly simulants can emulate these properties only to a certain extent and imperfections are almost inevitable. That is to say, there are fundamental limitations to simulants: Firstly, it is extremely hard to produce a simulant in bulk while also maintaining uniform and consistent properties [48, p. 1], so that variations within one simulant type are likely. Secondly, it is impossible to recreate all lunar peculiarities in one simulant type, because the environmental conditions present during the formation of lunar regolith and its earthly imitator are inherently different. Exemplarily, mineral formation in simulants occurs in presence of water [11, p. 3] and artificial agglutinates are created without the high temperatures and energy present at micrometeorite impacts. Therefore, different simulant manufactures focus on different aspects and perform trade-offs (chemistry vs. physics), so that "there is no universal simulant that replicates ideally the regolith and meets all research needs" [11, p. 3]. Instead, customers must choose the simulant type that best suits their research purpose.

Generally, the variety of lunar regolith simulants is immense: Taylor, who analyzed the market and compared different specimens in 2016, names 29 different types [11, p. 3], but many new have been developed thenceforth. The SMU research group performed a comparison of the major lunar regolith simulants and eventually opted for products by the at-cost organization Exolith Lab, which belongs to the University of Central Florida. DLR accordingly purchased 20 kg respectively of:

- **LHS-1** Lunar Highlands Simulant
- **LMS-1** Lunar Mare Simulant (see figure 12)
- **LHS-1D** Lunar Highlands Dust Simulant

Figure 12: LMS-1 Lunar Mare Simulant appearance and microscopic image [49]

Exolith Lab "simulants aim to accurately represent the mineralogy and particle size distribution of Lunar regolith to provide a useful simulation tool for the scientific community" [47]. Being state-of-the-art products with a high accuracy regarding composition, size, and shape, they are especially well-suited for ISRU-related research needs. Furthermore, "Exolith Lab is […] capable of adding agglutinates to small amounts of simulant, further increasing the fidelity and usefulness of [those] lunar regolith simulants" [47]. It even allows the manufacturer "to characterize [its] simulants in terms of maturity as well as glass content" [47], making LHS-1 and LHS-1D, but especially LMS-1 the perfect fit for SMU and the use for beneficiation testing. Data sheets, containing the simulants' most important physical properties, mineralogy, and bulk chemistry, are given in annex 2.

2.2.2 Output: Ilmenite & Tailings

Having regarded the input material extensively, a succinct description of the outputs is yet to follow. The beneficiation testbed will dispense two separate mass flows: For one thing, it will collect a feedstock rich in the valuable target mineral – which in our case is ilmenite – and for another it will release the tailings, i.e., unwanted gangue minerals (e.g., pyroxene and olivine) as well as too massive particles (e.g., coarse fines, or big agglutinates). Knowledge of the ore concentrate and how it differs from the residual constituents, as to be portrayed in 2.2.2, will later serve as a foundation for drafting an ideal beneficiation device, as it helps in understanding how to best exploit the mineral's properties.

In general terms, *ilmenite* is a titanium-iron oxide mineral that can be expressed by the idealized chemical formula $FeTiO_3$ [18, p. 140]. However, even though "the vast bulk of ilmenites are restricted to close to [this] ideal composition" [50], it sometimes also contains minute (minor mole percentages) amounts of magnesium and manganese, so that its full, non-idealized formula would read $(Fe,Mg,Mn,Ti)O_3$ [50]. Broadly speaking, its main properties are an iron-black to gray color with a brownish tint in reflected light (as shown in figure 13), a brittle tenacity, as well as a granular to massive and lamellar crystal habit [50]; ilmenite commonly occurs as "bladed crystals" in lunar regolith [18, p. 141]. Figure 13 additionally depicts how the mineral crystallizes in a trigonal structure (in TiO_2 bearing magmas) that "consists of alternating layers of Ti- and Fe-containing octrahedra" [18, p. 140].
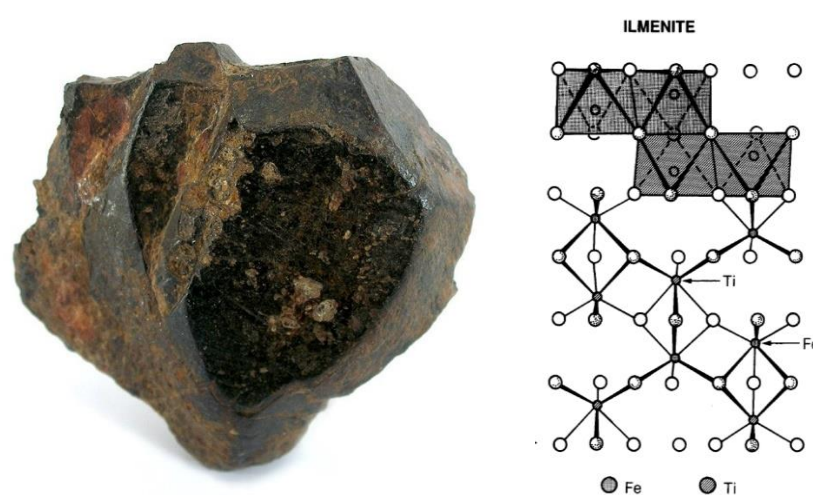
Figure 13: The mineral ilmenite in its macroscopic (L) [50] and atomic (R) [18] appearance

Ilmenite is often chosen as a target source material when it comes to lunar oxygen extraction (e.g., through hydrogen reduction, where it is reduced to rutile and iron while water is gained [18, p. 142]), due to its high processing efficiency [14, p. 1]. Consequently, it constitutes the mineral of interest for most extra-terrestrial beneficiation studies [11, p. 13]. But it may serve more than just one purpose in the time to come, as it is also under investigation as a base material for the construction of lunar bases, with its other constituents, iron and titanium, being predestined for the building of structures [50].

The occurrence and amount of ilmenite are subject to vast fluctuations and vary with, e.g., the former composition of the magma that the ilmenite crystallized in as well as the region and maturity of any given sample [18, p. 140]. The stake can reach high double-digit numbers in immature mare basalts, or less than one-hundredth in older highland soils. By way of example, it forms 15% to 20% of several Apollo 11 and 17 samples, while representing less than one volume percent in Apollo 16 highland specimens. At this, it should be noted that literature values of the ilmenite content are often derived stoichiometrically, as a function of a sample's TiO_2 content (interpreting ilmenite as a certain part of the easily detectable titanium dioxides), which correlates with the fluctuations mentioned above [18, p. 140]. In mature soils, ilmenite within the lunar regolith may already be converted to impact glasses, "lowering the ilmenite content, while preserving the bulk TiO_2 content", leading to bigger inaccuracies with respect to the ilmenite contents [33, p. 10].

The occurrence of ilmenite is also size-dependent. Usually, single domain ilmenite grains do not get smaller than 45 µm or bigger than 0.5 mm, other than tailings like agglutinates or glasses. Besides, the highest ilmenite concentration can be found in the 45 µm to 75 µm domain. This and more in-depth information on the size distribution of target and gangue minerals can be found in table number 3.

Table 3: Petrography of grain size fractions from a typical Apollo 17 mare soil [18, p. 289]

Components	Petrographic Description, vol.%							%, Visual Estimate in Lunar Receiving Laboratory			
	<20 µm	20–45 µm	45–75 µm	75–90 µm	90–150 µm	150–250 µm	250–500 µm	0.5–1 mm	1–2 mm	2–4 mm	4–10 mm
*Soil 71061,1**											
Agglutinates	17.0	17.3	13.0	17.3	9.3	11.8	10.0	10.0	—	—	—
Basalt, equigranular			9.0	15.0	30.9	—	—	—	—	—	—
Basalt, variolitic			0.6	1.6	19.6	3.4	51.5	65.0	100.0	100.0	100.0
Breccia											
Low grade, brown			1.0	4.0	3.6	5.1	6.9	—	—	—	—
Low grade, colorless			0.3	1.3	0.6	—	—	5.0	—	—	—
Medium, high grade			1.0	1.3	1.6	2.8	1.5	—	—	—	—
Anorthosite			—	—	0.3	—	—	—	—	—	—
Cataclastic anorthosite			1.0	—	—	—	—	—	—	—	—
Norite			—	—	—	—	—	—	—	—	—
Gabbro			—	—	—	—	0.5	5.0	—	—	—
Plagioclase			16.3	7.0	17.3	9.0	8.5	—	—	—	—
Clinopyroxene			21.3	26.3	21.0	17.4	10.8	—	—	—	—
Orthopyroxene			—	—	—	—	—	—	—	—	—
Olivine			—	—	—	0.6	—	—	—	—	—
Ilmenite			6.0	3.3	4.6	3.3	2.3	—	—	—	—
Glass											
Orange			7.6	5.0	6.3	4.5	0.8	—	—	—	—
"Black"			18.7	10.6	9.6	5.1	6.1	5.0	—	—	—
Colorless			1.0	1.0	1.3	—	1.5	—	—	—	—
Brown			0.3	5.2	4.6	3.3	—	—	—	—	—
Gray, ropy			0.7	0.6	—	1.7	—	10.0	—	—	—
Other			2.0	—	—	1.0	—	—	—	—	—
Total number of grains counted	300	161	300	300	300	178	130	20	100	?	?
Wt.% of total sample for each size fraction	17.98	12.21	8.39	3.0	8.66	7.04	7.08	3.44	6.15	6.74	10.16

Having said that, like other minerals, ilmenite does not always appear in its pure form, but is often embedded in a multi-mineralic composite grain. To avoid those "impure" fractions, it is better to focus on smaller portions, because "as grain size decreases, the degree of liberation of phases becomes more complete" [41, p. 1415], meaning that the smaller a grain, the cleaner (i.e., single-phase) it is. This has been experimentally proven by Taylor [41], who examined two lunar rock samples and found that the ilmenite-rich split of the 45 to 90 µm size fraction consisted of 85% single-phase grains, other than the 90 to 150 µm fraction, where multi-phase grains prevailed.

Two other important mechanical properties of ilmenite are its specific gravity of 4.70…4.79 and a density of 4.5…5 g/cm³, which are significantly higher than the bulk of regolith (G=3.1 and ρ=1.50 g/cm³) and very different from most gangue minerals (see annex 3), making them suitable differentiators that could be exploited through beneficiation [50].

Another widely used physical differentiator for beneficiation is a mineral's magnetic nature. If ilmenite's magnetic properties were to be summarized in one sentence, it may be described as *paramagnetic* with a *low magnetic susceptibility* (which is temperature dependent) [50]. For instance, the magnetic susceptibility of one lunar ilmenite sample has been quantified as $\chi \cong 60\ \mu cc/gm$ [51] (imperial notation for CGS massic susceptiblity) and given at $\chi \cong 76\ \mu cc\ cgs\ mass\ units$ for another one [52, p. 453]. Correspondingly, ilmenite generally exhibits a weak attraction to hand magnets, only [50]. Yet, the presence of a strong magnetic field (≥2 T) can change this low magnetic response into a noteworthy attraction, which might help to separate ilmenite from non-magnetic tailings [11, p. 7]. A gangue mineral in the lunar regolith that exhibits a similar paramagnetic behavior is pyroxene. "The specific susceptibilities of [those paramagnetic] minerals generally range up to $100\ \mu cc/gm$" [51].

Many other gangue minerals are diamagnetic (therefore carry a minus-sign) and have a very weak susceptibility like anorthite (with $\chi = -0.39\ \mu cc/gm$ [51]), feldspars, ice or some basalts [43, p. 14]. There are also ferromagnetic tailings, like the native iron particles, which have a high susceptibility of at least $\chi > 130\ \mu cc/gm$ and, thus, dominate the magnetic response. Other tailings like agglutinates also possess a high magnetic susceptibility [35, p. 805] due to their high native iron content. Lastly, as explained earlier, the very fine dust is strongly attracted by magnetic fields. It is worth pointing out that the above values underly stochastic fluctuations and vary with maturity ("the more mature soils are more magnetic" [51]) and – thanks to the Curie-Law – with temperature (the lower the temperature, the higher the susceptibility). The results of two experiments that aimed to characterize the magnetic susceptibility of lunar samples can be found in the now following table 4 and figure 14.

Table 4: Distribution of susceptibility for >150 µm fraction of mature highland soil No. 64421 [35, p. 804]

Magnetic Susceptibility Range (10^{-6} cc/gm)			Wt. Rec. >150 um Fraction (Wt.%)	Concentration Anorth. %	Aggl. %
	<	0.75	12.7	95.0	0.0
>	0.75 <	5.58	24.6	70.0	5.0
>	5.58 <	64.9	48.6	20.0*	10.0
>	64.9 <	699	12.5	1.7	55.0
>	699	<7470	1.7	1.0	95.0
>	7470			* Estimated	
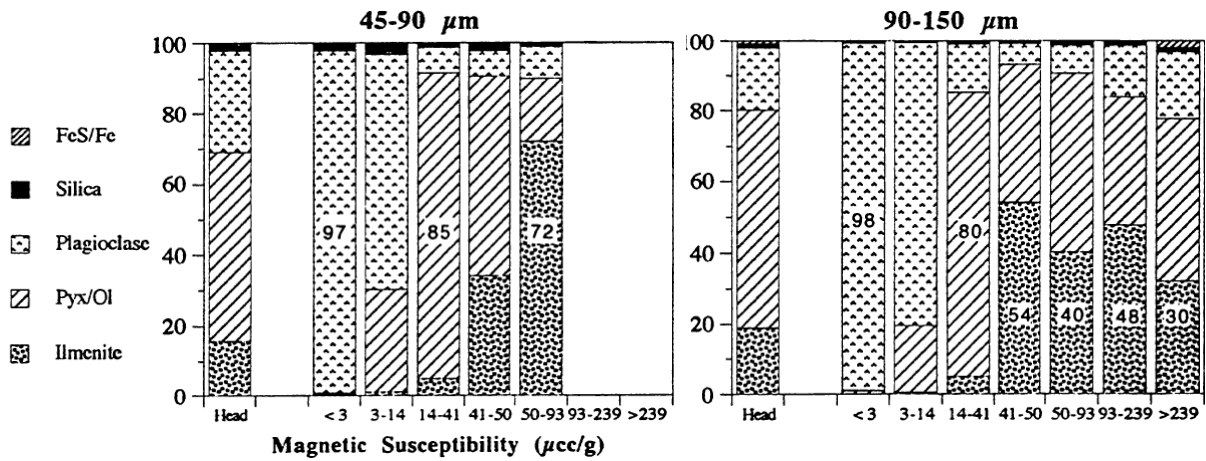
Figure 14: Distribution of susceptibility for different sizes within the mare basalt sample No. 71055 [41]

The last physical attribute of ilmenite to be regarded in this chapter is its electro-physical nature. As mentioned in 2.1.2.2.1, minerals can be classified as conductors, semiconductors, and non-conductors. While the majority of gangue minerals (silicates like feldspars) and other tailing (e.g., glasses, agglutinates [20, p. 4]) belong to the semi- or non-conductor category [23, p. 26], ilmenite can be considered as a conductor [53]. Being a conductor, ilmenite does not readily retain charge, but transports it to the surrounding (*poor chargeability*). This is mainly caused by its high Fe-content, where electricity is transmitted via the drift of electrons [54]. Its exact electrical conductivity Ω is highly temperature-dependent (and sensitive to water-content), so that no single value can be given. However, experiments on terrestrial ilmenite samples have delivered diagrams, that depict the conductivity as a function of temperature; a plot of the relative (dielectric) permittivity can be found in annex 3. Before closing subchapter 2.2, the triboelectric properties of ilmenite and gangue shall briefly be regarded. Most importantly, values of the *work functions* are provided in annex 3. Ilmenite's position in the triboelectric series has been the subject of several studies: Li et al. (1999) found a selection of terrestrial minerals to progress as follows: quartz > augite > albite > ilmenite > copper > fosterite [11, p. 9]. Another team of researchers tribocharged several lunar minerals and came to the results illustrated in table 5.

Table 5: Tribocharging series of minerals within the lunar regolith [43, p. 18]

Component	Relative Charging
Olivine	Very negative
Ilmenite	About neutral
Pyroxene	Very positive
Anorthosite	Very positive
Basalt	Very positive
Ice	Extremely positive

2.3 The Environment: Conditions on Moon and Earth

One of the most influential design drivers that must be considered in almost any engineering project is the environment a product must cope with. For space systems, parameters like the targeted celestial body's gravitational acceleration, its atmospheric pressure, and the temperature range found at its surface (as governed by the day/night cycle) are of utter importance for specifying an appropriate device. Since our beneficiation test stand is conceived as a technology demonstrator for later in-situ use on the *Moon*, while actually being built and operated in a laboratory on *Earth*, both environments will have to be illuminated and characterized to allow for an optimal design during later development.

Table 6: Comparison of the ambient conditions found on the Moon and Earth in line with [11, p. 4]

Feature	Comparison		Implications for lunar beneficiation
	Moon	Earth	
Gravitational Acceleration	$1.625 \frac{m}{s}$	$9.81 \frac{m}{s}$	Impacts density separation; Reduces gravity-driven fluid/particle flow; Reduces particle inertia, thus reducing the magnitude of any external force required to overcome it;
Surface Temperature (d/n)	$127°C/-173°C$	$14°C$	Temperature variation will affect particle properties; Hot particles more easily charged, but less magnetically susceptible and vis versa; Equipment must survive the lunar night;
Atmosphere	*Hard vacuum*	*Abundant*	Process fluids not readily available, and must be generated *in-situ*, or imported from Earth; Fluids, if any, must be used in a closed system; Cooling of equipment (e.g., electromagnets) only possible via heat pipe or radiative exchange
Human Access	*None*	*Abundant*	High reliability (uncommon in terrestrial mining) is necessary; Modular designs will facilitate repairs / replacements;
Day / Night cycle	$324h$	$12h$	Regolith becomes less charged at night (no UV charging); Equipment cooling/heating is power-intensive; Power generation at night becomes challenging;

As can be seen in the overview provided above, the ambient conditions on both astronomical objects differ greatly and dissimilarities can be found in almost any regard. This poses drastic implications for beneficiation, too (see table 6, right column). To address this in more depth, the following subchapter will give a succinct outline of the *lunar* (2.3.1) and *terrestrial environment* (2.3.2), with the aim of increasing the transparency of design decisions taken throughout the development process.

2.3.1 Theory: Lunar Environment

With a mass of $7.342*10^{22}$ kg and an equatorial radius of around 1738.1 km, the Moon is much lighter and smaller than planet Earth (1.2% of the mass and at a quarter of the diameter), resulting in a relatively low *gravitational acceleration* of 1.625 m/s [2]. Thus, the weight of objects that are situated on its surface is reduced by a factor of 0.166 (compared to Earth). This does not only affect the beneficiation machine itself, but also the weight and inertia of every single regolith grain transiting it. Free-fall separators are impacted the most, as a falling particle's final velocity is significantly reduced, so that characteristic forces in, e.g., magnetic or electrostatic separation can act upon it for an extended period of time. This may be beneficial as it permits a more compact design.

In contrast to Earth, the Moon does not possess a biosphere (absence of organic matter), magnetosphere (negligible magnetic field; too weak to protect the lunar surface), real hydrosphere (the Moon does not have liquid water deposits) or remaining tectonic activity [2]. But most importantly in the context of beneficiation, it also does not have a notable *atmosphere*, i.e., it is almost completely airless due to the low gravity present, which makes it impossible for the Moon to retain a thicker gaseous envelope. The atmospheric pressure is as tenuous as 1 pico-bar during daytime and 1 femto-bar during night, which is classified as an ultra-high vacuum [2]. In fact, it is so low that many substances, which would be liquid under terrestrial conditions, turn gaseous and volatize, due to the surrounding pressure being smaller than the substance's vapor pressure. For beneficiation, this means that potentially needed process fluids are not readily available and – even when brought from Earth – could not be used in non-closed or unpressurized systems. The same holds true for liquid coolants, so that radiative cooling is to be preferred. On the other side, no air flow also means an undisturbed particle movement, as air drag, turbulent vortexes or lateral gusts are non-existent. The absence of unwanted deflections would translate into an improved yield due to better predictability.

Even though the low gravitation and the almost perfect vacuum may facilitate the efficiency of certain processes to a certain extent, there are also *hazards* that can be harmful to space technology if not properly taken care of. One of those hazards is whirled up lunar dust, which either unwantedly *adheres* to surfaces, where it could accumulate and impair a (beneficiation) system's performance or acts like an *abrasive* when its minute particles hit the system at high velocities. Another challenge to be coped with is the constant exposure to *ionizing radiation*, either by cosmic rays or solar wind particles [18, p. 27]. The possibility of *micrometeoroid bombardments* can also be considered as an additional risk. However, the likelihood of an impact event is rather low and it strongly varies with location (e.g., extremely unlikely to occur on the nearside). Countermeasures like radiation-hardened electronics and protective shields would have to be taken for fail-safe ISRU systems used on the Moon.

Proceeding with the next environmental factor, a celestial body's *day / night cycle* is governed by its orbit. At this, Earth's only natural satellite revolves around our home planet within approximately 27.32 days [2]. Being tidally locked, this is also the exact same time needed for the Moon to rotate around its own axis (which is why there is a near and a far side) [18, p. 27]. With our Earth also orbiting the sun, this interval is slightly shorter than the Moon's synodic period of 29.53 days [2] – more commonly referred to as a lunar day. The lunar day is further divided into its illuminated daytime and the dark lunar night, which in consequence last approximately 324 h each. The sequence of night and day affects beneficiation systems, too, as UV irradiation, for instance, governs the charge of regolith, which is exploited in electrostatic separation (see chapter 2.1.2.2.1). With solar power being the major source of energy in outer space, it also influences the power generation for any beneficiating machine.

Furthermore, the sunlight cycle also dominates the thermal conditions on the lunar surface, as the Moon's atmosphere is too sparse to store a notable amount of heat. Hence, the *surface temperature* can vary greatly over the day: "Lunar surface temperatures increase about 280 K from just before lunar dawn to lunar noon" [18, p. 34]. The daily "thermal cycle certainly implicates more design criteria that have to be addressed" [15, p. 3]. It should be mentioned that seasonal effects do not play a big

role in this matter, as the axial tilt with respect to the ecliptic is only 1.5424° [2], resulting in a more or less constant solar illumination over the course of the year. However, the sunlight-induced heat is not only a function of time, but also depends on the location (see table 7). Firstly, this is due to the differing incidence angle of the incoming sunlight: At the equator, for instance, the sun rays impinge perpendicularly on the absorbing surface, resulting in a high incoming irradiance. The poles, in contrast, receive a significantly smaller power per unit area. Secondly, it is influenced by the Moon's topology, as the Moon has many different surface features such as elevated mountains, crater rims and rocky boulders. At the poles, these kinds of obstacles can cast permanent shadows, preventing sunlight from ever heating the soil behind them (this is how the previously mentioned PSRs are formed). Accordingly, heating or active cooling may be needed depending on the location of an ISRU processing plant, which can become very power consuming. The extreme temperatures also have a special impact on mineral enrichment, in the way that they directly manipulate the electrical chargeability and magnetic susceptibility of processed minerals (hotter particles can be charged more easily but lose in magnetic susceptibility).

Table 7: Estimated average lunar surface temperatures depending on location [18]

	Shadowed Polar Craters	Other Polar Areas	Front Equatorial	Back Equatorial	Limb Equatorial	Typical Mid-Latitudes
Average temp.	40 K(?)	220 K	254 K	256 K*	255 K	220 < T < 255 K
Monthly range	none	±10 K†	±140 K	±140 K	±140 K	±110 K

* The farside of the Moon is closer to the sun at noon than the nearside is, so it gets ≈1% more solar energy.
† Average temperature has a yearly variation that makes it very cold (T < 200 K) for several weeks.

Lastly, another important factor to be taken into account when speaking of ISRU under lunar conditions is the very limited *human access*. With no personnel available, any beneficiation system to be used on the Moon should require as little maintenance as possible. This can already be assured during development: Reliability and maintainability should be viewed as key priorities during development (for example through modular design approaches); expensive hardware that is able to survive the entire mission duration without replenishment should be preferred over components that come at low acquisition costs but demand frequent servicing or even replacement.

2.3.2 Practice: Laboratory Environment

For obvious reasons, the environmental conditions found in a laboratory here on Earth differ fiercely from the ones explained in chapter 2.3.1. Generally, a laboratory's ambience can be rated as less demanding to materials, mechanical parts, and processes, as well as electrical hardware and software, relaxing many vital technical requirements. The design of a space technology demonstrator operated in a controlled environment can accordingly be simpler than that of the real machine, which in turn has to be equipped with more sophisticated components suited for outer space usage. Sometimes, however, factors like the higher gravitational potential or the denser atmosphere on planet Earth may interfere with experiments, as in this case for beneficiation. To address both, the advantageous and adverse external influence factors, the following lines will concisely portray the main properties of the environment in a terrestrial laboratory, while comparing it to the conditions present on the Moon.

First off, the gravitational acceleration on Earth – quantifiable as 9.81 m/s – is substantially bigger than that of the Moon, attributable to its higher mass of $5.976*10^{24}$ kg, which is distributed over an – in simplified terms – spherical volume with a radius of 6371 km (the more exact shape is called a geoid) [18, p. 28]. Without any means to compensate for the higher gravitational pull, the simulant particles will fall faster to the ground. Furthermore, stronger characteristic forces will be needed to cope with the resulting higher inertia in order to appreciably manipulate the particle's trajectory. More powerful components and a sturdy structure will henceforth be needed for the beneficiation testbed.

Aside from gravity, a particle's trajectory can also be affected by the presence of a surrounding medium like air. As Earth possesses a dense atmosphere ($2.5*10^{19}$ molecules/cm^3 [18, p. 28]; sea level atmospheric pressure of approx. 1 bar or exactly 1 atm), air drag, draughts and other confounding effects like inadvertent gas ionization (during electrostatic separation) may occur and could potentially perturb mineral enrichment [11, p. 6]. In a laboratory, the use of facilities like vacuum chambers or inert atmosphere chambers (flooded with nitrogen to oust the reactive oxygen) may help in mitigating these interferences and emulate the airlessness (or at least the absence of gaseous oxygen) on the Moon, for more representative results. The DLR Institute for Space Systems itself possesses a vacuum chamber, which may be used during testing and operation of the beneficiation testbed. Atmospheric humidity represents yet another factor that should also be considered and appropriately controlled, in order to prevent interactions with the dry regolith simulant.

As mentioned earlier, the analog setting is typically more forgiving than the harsh space environment; this is also demonstrated by the absence of the most disruptive lunar hazards like ionizing radiation or micrometeorite impacts. This consequently eases the requirement profile drastically, thereby making way for an overall simplified design. Components like passive or active radiation shields, as well as Whipple shields (which protect a space system from harmful high-velocity impacts of micrometeorites by dispersing them) henceforth become obsolete. In addition, risks associated with the super-fine part of the regolith (simulant) like abrasion or congestion vanish. Lastly, even if a malfunction due to external factors occurred, laboratory personnel could still intervene and suppress it with ease, so that reliability loses its high-priority status during development.

With Earth only requiring 24 hours to revolve around its own axis, the heat coming from the sun is distributed more evenly, so that Earth maintains a well-spread and life-friendly average surface temperature of 22°C [18, p. 28]. The daily temperature fluctuations are – compared to other planets outside the habitable zone – very limited. The only noteworthy temperature variation comes with seasons, as the Earth is tilted by 23°28' [18, p. 28]. The narrow temperature range, too, helps to abolish the necessity for extra components, like a sophisticated thermal control subsystem. In a laboratory setting, a temperature of choice (mostly between 20°C and 25°C) is set in, monitored, and maintained.

This concludes chapter two and with it the theoretical part of the present thesis. Such being the case, the succeeding practical activities have been prepared thoroughly and extensively.

Chapter 3   Development

Now that a profound knowledge of beneficiation's scientific context has been imparted, the hands-on work, i.e., the *development* of the laboratory test stand, can commence. A common approach when tackling such an engineering task is to apply a systematic process and, thus, subdivide the total workload into consecutive groups of tasks – so called work packages (*short:* WP). The relevant WPs for this project are portrayed in figure 15. The shown sequence of activities also acts as a guideline for the structure of chapter 3, as an individual subsection is dedicated to each WP. Pursuing this procedure will help to transform a vague idea into a rough concept and eventually deliver a feasible and functional CAD model, while successively increasing the design's maturity in a methodic manner.
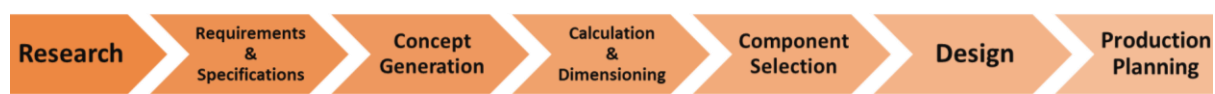
Figure 15: Engineering design process similar to the one found in [55]

3.1 Research

This thesis is not the first attempt to demonstrate the feasibility of lunar mineral beneficiation in a laboratory setting. In fact, scientists, and research groups from all over the world have been working eagerly to accomplish this goal by deliberating sophisticated machines and conducting thorough experiments with them over the course of the last decades [11]. However, not all researchers approached the challenge in the same way; in fact, each author chose the separation method and settings best serving his or her research needs, and, accordingly, each paper reports different results. Considering this, the purpose of the first WP in the development process is to *review* the most relevant beneficiation *studies* conducted hitherto, to *investigate* the *(sub-)processes* they employed, and to *summarize* their experiment *setups* and *outcomes*. In doing so, the literature review to be presented in chapter 3.1 is one of the project's most important tasks, as it paves the way for all subsequent activities, e.g., the specification of technical requirements or the creation of a suitable concept.

In **2020**, Dr. Hadler [8], who was already cited throughout chapter 2.1, as well as her colleagues from Imperial College – first and foremost J.N. **Rasera** [11] – published a paper called "The beneficiation of lunar regolith for space resource utilisation: A review". In it, the authors list many previous publications (see table 8) and summarize the methods that were used. The summary itself (hereinafter called the *main source* or *Rasera et al.*) as well as the referenced documents (*secondary sources*) will be consulted to fulfill the above declared purposes. Thus, these publications act as a starting point for getting a better picture regarding gravitational (3.1.1), electrostatic (3.1.2), and magnetic (3.1.3) separation. Each of these subchapters follows the main source's structure and introduces the respective studies one by one, while relevant details and insights from secondary sources will be given when needed.

Table 8: Summary of previous studies on lunar dry beneficiation by Rasera et al. [11, p. 12]

Category	Process	Target Mineral	Fraction (µm)	Feed	Testing Conditions	Ref.
Gravitational	Size Sorting	n/a	75–150	JSC-1A NU-LHT-2M OB-1	Vacuum Lunar-g	Wilkinson (2011)
	Enrichment	n/a	n/a	n/a	n/a	None.
Magnetic	Size Sorting	n/a	n/a	n/a	n/a	None.
	Enrichment	Ilmenite	20–200	n/a	n/a	Williams et al. (1979)
		Anorthite	>150 45–150	Apollo 64421	No data	Oder et al. (1989)
		Ilmenite	90–150 45–90	Apollo 10058 Apollo 71055	No data	Taylor et al. (1992)
		Ilmenite Iron Oxide	150–425	Custom JSC-1A NU-LHT-2M	Vacuum	Berggren et al. (2011)
Electrostatic	Size Sorting	n/a	<106	FJS-1	Air, Vacuum	Adachi et al. (2017a)
	Size Sorting & Enrichment	Ilmenite	90–150	KSC-1 Apollo 10084	Air	Agosto (1984)
		Ilmenite	20–200	n/a	n/a	Williams et al. (1979)
	Enrichment	Ilmenite	<45 45–90 90–150 150–250 250–500	Custom	Air, N$_2$, Vacuum Heated: 100–200 °C Washed Samples	Agosto (1983)
		Ilmenite	90–150 150–200	KSC-1 Apollo 10084	Air, N$_2$, Vacuum Heated: 100–200 °C Washed Samples	Agosto (1985)
		n/a	50–75	JSC-1	Vacuum	Captain et al. (2007)
		Ilmenite	75–106	Custom	Air	Li et al. (1999)
		Ilmenite	<1000	NU-LHT-2M (+ilmenite)	Air Lunar-g	Quinn et al. (2012)
		n/a	<25 >100	JSC-1 MLS-1	Air	Trigwell et al. (2006)
		Ilmenite	50–75	JSC-1 JSC-1A KSC-1	Air, Vacuum	Trigwell et al. (2009)
		Ilmenite	50–75 75–100	JSC-1A NU-LHT-2M Apollo 14163 Apollo 70051	Vacuum	Trigwell et al. (2012)
		n/a	210–420 104–420	Custom	Vacuum Heated: 100–104 °C	Fraas (1970)

3.1.1 Gravitational Beneficiation

The authors of the main source do not explicitly cover *gravitational* beneficiation themselves. However, they at least designate one secondary source, which addresses the topic of gravitational size sorting extensively; this paper carries the title 'Size Beneficiation of Regolith for Simplicity and Efficiency' and was published by Allen **Wilkinson** in **2011** [56] as part of the 'Planetary & Terrestrial Mining and Sciences Symposium'. It is concerned with evaluating the performance of several options for gravity-based sizing of lunar regolith, aiming to conceive a simple yet efficient particle size control system for NASA's ROxygen (a demonstration plant that extracts oxygen from lunar soil).

In doing so, several criteria determined Wilkinson's work. Firstly, the project he worked on obliged him to target a production mass of approx. 13kg size sorted material per hour – a requirement that radically predefined the system sizing choices [56]. Secondly, his hardware choices were governed by four driving forces: Gravity independence, simplicity and reliability, energy efficiency as well as volume and mass [56]. Lastly, another guideline was to stick to the simplest, i.e., most robust solutions, as exemplified by the terrestrial granular handling industry; this line of thoughts led Wilkinson to sieve-

based *screening* techniques, as they are "the oldest and most trusted size beneficiation method" according to an internal industry survey [56]. However, he noted that stationary sieves may be prone to failure in low-g environments, as particles may get caught and halt the granular flow – a phenomenon called *blinding*. *De-blinding* is, thus, a necessary countermeasure to guarantee a reliable process: External forces are exerted on the sieve and, in consequence, transferred onto the lodged particles, which hence get released [56]. This may be achieved through vibration, shearing motion, ultrasound, flexing the screen, or brushing. To select the best option, Wilkinson and others conducted experiments under low-g (simulated during parabolic flights); Wilkinson concluded that a *rotary flat shearing sifter* (similar to a domestic flour sifter) was superior when compared to a *horizontal vibratory sifter* (see figure 16) [56]. Others pointed out that vibratory sifters would be beneficial regarding their wear-life perspective, simplicity, and compactness – whereas Wilkinson deplored their vulnerability to low gravity environments. Later, Wilkinson additionally examined sonic and shearing barrel sifters – with the former being unfavorable (as it is slow for smaller particles and would demand a pressurized gas) and the latter performing only moderately [56].
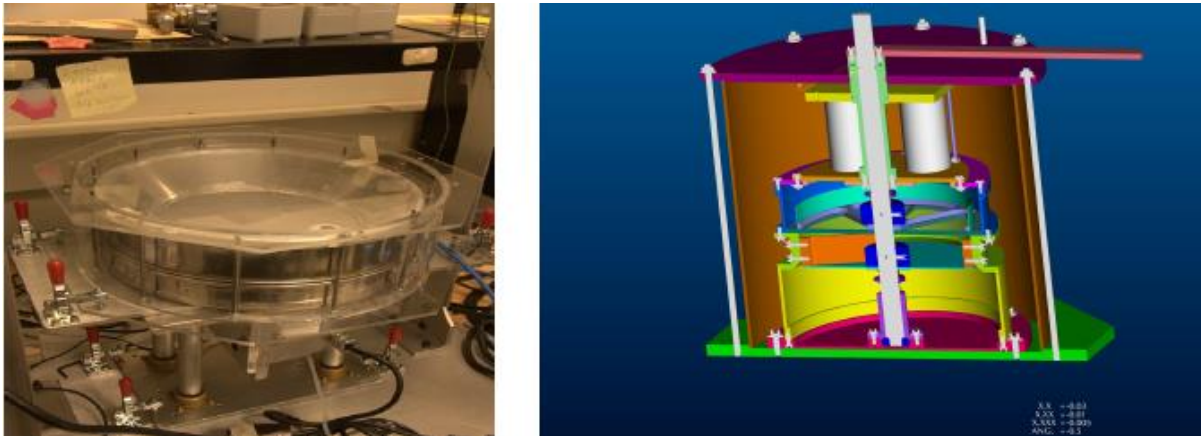
Figure 16: Horizontal vibratory (L) and rotary shearing (R) sifters used by Wilkinson [56]

At the end of his paper, Wilkinson concludes that shearing sieve-based sizing systems are best at coping with the many challenges of lunar size beneficiation (e.g., low-g and vacuum environment, high reliability, and efficiency requirements). However, the author notes that shearing alone is not sufficient to de-blind – he instead recommends to additionally implement a modest screen flexure. He also remarks that "Wear does remain an issue and must be solved by development of wear-resistant materials" [56], which from his point of view is still a gap in the ISRU domain. The paper ends with the statement that shearing sifters can be adapted to the needs of any given mission: Not only can it be sized according to the demanded volume flow rate, it also can be adjusted in respect of shear bar shape or shearing clearance [56].

Another publication listed by Rasera et al. is 'Mining and Beneficiation of Lunar Ores' by Richard J. **Williams** and others – a paper published in **1979** [16] as part of the compilation 'Space Resources and Space Settlements'. Although the essay primarily focusses on other beneficiation methods (which is why it does not appear under the table's "gravitational" section), it also involves a *screening* pre-step, in which bigger fragments are filtered out, and a *classification* step incorporating a cyclone: "The ore

is first passed through a coarse *sieve* to remove fragments larger than 1 cm. [...] It is then treated with an *air cyclone* that disaggregates the soil and removes the <20 µm particles" [16, p. 276]. However, Williams admits that size-sorting cyclones require large volumes of high-velocity gas, which are evidently unavailable on the Moon. He further elaborates how this may also pose the risk of "significant losses of air" that may occur at the inlet or outlet of the cyclone (where the processed material escapes into vacuum through an airlock), which in his words depicts "a formidable technical problem" [16, p. 276].

Yet, the utilization of cyclones in the context of lunar gravitational beneficiation is still suggested today. During a talk at **2021**'s Space Resources Week given by Dr. Philip **Metzger** [43], a planetary scientist at the University of Central Florida, the speaker suggested pneumatic dedusting and size separation for the handling of icy lunar regolith. He justified his choice of using cyclones with the drastic difference in ballistic coefficients between lithic and icy particles (so that classification becomes very efficient) as opposed to the more homogeneous size distribution (making sieving less fruitful). In the case of pneumatic sizing, he even proposed to cascade several cyclones to achieve a higher resolution, so that a size overlap of lithic material and ice could be avoided [43]. However, the sequence Metzger developed (which also employs magnetic and electrostatic beneficiation in later steps) so far only exists in theory; an experimental proof has not been delivered until now. It is also doubtful whether the idea of pneumatic processing is transferable to non-icy regolith, as the disparity regarding the ballistic coefficient is substantially less significant; not to mention the logistic implications that come along with using a process fluid.

Fortunately, alternative classification methods exist, which can be operated without such a fluid. These were investigated and tested by Mark **Berggren** and colleagues in **2011** [20], when the team developed a beneficiation system – named the Lunar Soil Particle Separator (*short*: LSPS) – that is able to concentrate ilmenite from dry lunar regolith to facilitate in-situ oxygen production in three main stages; aside from magnetic and electrostatic separation, the researchers also examined two rather unconventional options for dry classification to dodge the technical problems alleged above.

According to Berggren, "the lunar vacuum environment precludes the use of a working fluid to provide a resistive force during size separations" [20, p. 5]. Instead, he argues that "in vacuum particles can be subjected to flow resistance across engineered, roughened surfaces to take advantage of the relative friction differences between finer and coarser particles" [20, p. 5]. This is the idea of the *rotating cone*. The basic principle is abstracted in figure 17: The lunar soil is fed uniformly onto the textured surface of a rotating cone (Berggren mentions a feed rate of 15 grams per minute), which is of predefined dimensions (angle of 30° and diameter of 15 cm) and spinning at a given speed (40...250 1/min). All particles get accelerated by the rotary motion, but coarser particles (lower surface area to mass ratio) cascading down the cone's inclined plane reach the outer edge quicker than the finer ones [20, p. 9]. The different trajectories result in the particles exiting the circumference in different collection zones, effectively dividing them into different size classes. Wear and blinding (the main problems of sieving) are of no concern using this technique, says Berggren [20, p. 6]. On the other hand, the authors denote that coarsest material, larger than one millimeter, would have to be removed beforehand.
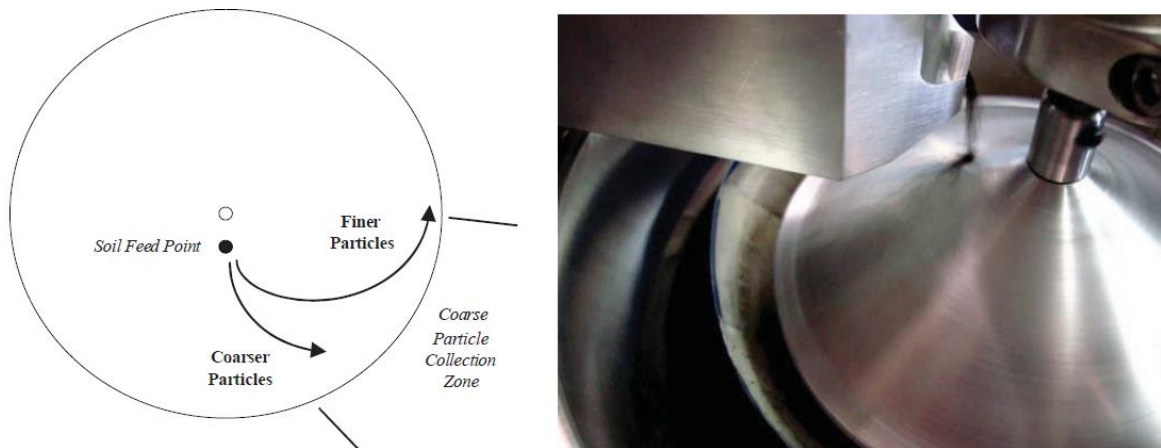
Figure 17: Rotating cone particle separation schematic (L) and test hardware (R) [20, p. 6]

This might be done through screening (grizzly screens were suggested) or with the aid of yet another technique portrayed in Berggren's study labelled the *slotted ramp separator* [20, p. 6]. The team's experimental setup found in figure 18 already indicates the operating principal; it exploits "differences in friction between coarse and fine particles during flow across a surface" [20, p. 9], but – other than the rotating cone – with a fixed (not moving) separation surface. Along this surface there are slots of different gap sizes to successively remove particles of increasing (average) size. "The finest particles tend to drop through a slot in the ramp while coarser particles proceed to the next ramp section" [20, p. 9] as the reduction of a particle's velocity by friction is size-dependent (the finer, the more it gets retarded). The ramps design parameters were defined following the results of initial experiments. Here is an overview of the most important criteria:

- **Ramp angle:** 45°
- **Ramp length:** 20 cm for fines; 8 cm for coarse product (from dispersion to slot)
- **Slot number:** initial setup 2; final setup 7
- **Slot gap:** initial setup 0.17 cm (fines) and 1.3 cm (coarse product); final setup 0.17…1.9 cm
- **Soil feed rate:** 195…294 g/min for fine product; ~200…209 g/min for coarse product
- **Material:** Sheet metal

Figure 18: Slotted ramp particle size separator after assembly (L) and in vacuum chamber (R) [20, p. 11]

When testing the slotted ramp separator's experimental setup, it already showed that the concept is feasible and that cross-contamination is minimal [20, p. 10]: One half of the fines were already recovered with the initial 2-slot setup, with results being similar for air and vacuum tests; using the wider slot gap for coarser inputs, the contamination with particles smaller than 75 microns was only around 1.5 percent [20, p. 10]. Publication of the results for the final design (7 slots) is still pending but seem promising since the 2-slot setups already indicate a success. By way of contrast, Berggren's other separator, the rotating cone seemed less successful; the early model did not deliver as promised and "experimentation showed that different approaches were needed to perform the desired particle size separations" [20, p. 7]. A scaled up and overall iterated design still failed to reproduce the mass distribution around the cone's circumference in vacuum under otherwise similar conditions [20, p. 9].

3.1.2 Electrostatic Beneficiation

In the main source's summary, Rasera et al. conclude that "*electrostatic* methods have been studied the most" and accordingly outnumber the publications of gravitational and magnetic beneficiation [11, p. 13]. Three main techniques were identified that dominate the pertinent literature [11, p. 7]:

- Conductive induction with slide separators
- Tribocharging with plate separators
- Electrostatic travelling wave

Starting with the former, William N. **Agosto**, who published several relevant papers during the 1980s and 90s, can be considered as one of the most active scientists in conductive induction for lunar SRU. In **1983** [57], he compared roller-type separators (as mentioned in 2.1.2.2.1 & shown in figure 6) to slide-type ones using a binary mixture of ilmenite and olivine (10:90 mass ratio in four size fractions) [11, p. 7]. When assessing their performance (by ilmenite grade) and usability, he found that the latter was superior after one pass. Agosto accordingly employed *slide-type separators* in his future experiments, despite the narrowed recovery (which is to be expected, as mineral enrichment exhibits "a grade-recovery relationship in which a relatively small fraction of the desired mineral can often be recovered at very high grade" [20, p. 5]). In the same essay, he noted that *temperature* would also play a major role in electrostatic enrichment, as heating the feed and air around it was able to significantly boost the performance. These two findings have been quantified and visualized in tables:

Table 9: Comparison of separator types (L) and effect of heating on electrostatic separation (R) [11, p. 7]

Size Fraction [μm]	Drum		Slide			Sample	Size Fraction [μm]	28 °C		180–190 °C	
	Grade [$wt.\%$]	Recovery [$wt.\%$]	Grade [$wt.\%$]	Recovery [$wt.\%$]				Grade [wt-%]	Recovery [wt-%]	Grade [wt-%]	Recovery [wt-%]
45–90	29	29	98	29		Anorthite/ Pyroxene [50/50]	90–150	60	<1	73	54
90–150	53	64	90	38							
150–250	78	91	95	68		Olivine/ Anorthite [10/90]	150–250	66	1	94	34
250–500	80	87	79	82							

The improvement of grade and recovery that came along with elevated temperatures can be explained by the increased conductivity of semi-conductors and the prevention of water adsorption for $T \geq 100°C$. The latter effect can alternatively be achieved by pretreating the processed material

i.e., through cleaning it with a solvent like isopropyl alcohol. Doing so while also using a hand magnet to attract agglutinates and soil metal would remove the undesired <45 µm fraction as a side effect, states Agosto, who consequently applied this procedure prior to all future experiments [11, p. 7]. It should be noted that the filtered constituents account for approx. 40% of the regolith [44, p. 1], so that the validity of Agosto's findings may be limited.

The feed rate Agosto used during his experiments was set to $6g/s$ and $7g/s$. The aluminum induction charging electrodes were tested at a maximum field strength of $+7kV/cm$ and $+4.7kV/cm$, which had a great impact on recovery (improvements over 100% were achieved), so that +5kV was selected as the nominal field strength for subsequent testing [11, p. 7]. During the tests it was also found that semi-conductors would not only be charged by the induction charging electrode, but also through contact with the metal slide – a side-effect that leads to deteriorated predictability. The tribocharging caused semi-conductive pyroxene to obtain a negative charge; depending on the polarity of the electrode, this either added up or cancelled out with the induced charge (a negative polarity induces a positive charge and vice versa). To augment the negative tribocharge gained, Agosto recommends working with a *positive polarity* only in the context of slide-type separators.

In later studies (**1984** [44] and **1985** [52]), Agosto started working with more realistic material mixtures like the simulant KSC-1 or even real lunar samples and exposed his setup to more representative environmental conditions (nitrogen atmosphere or vacuum) [11, p. 8]. The separator's design was iterated accordingly (see figure 19). When assessing the ilmenite concentration, it can be said that the new setup outperformed the former one; whilst this is partially attributable to the improved design, the enhanced performance under nitrogen (7.9 wt.% to 90±7 wt.%) and in vacuum (9.8 wt.% to 78±8 wt.%) is certainly also caused by physical influence factors (like gas ionization or fluid drag) [11, p. 8].
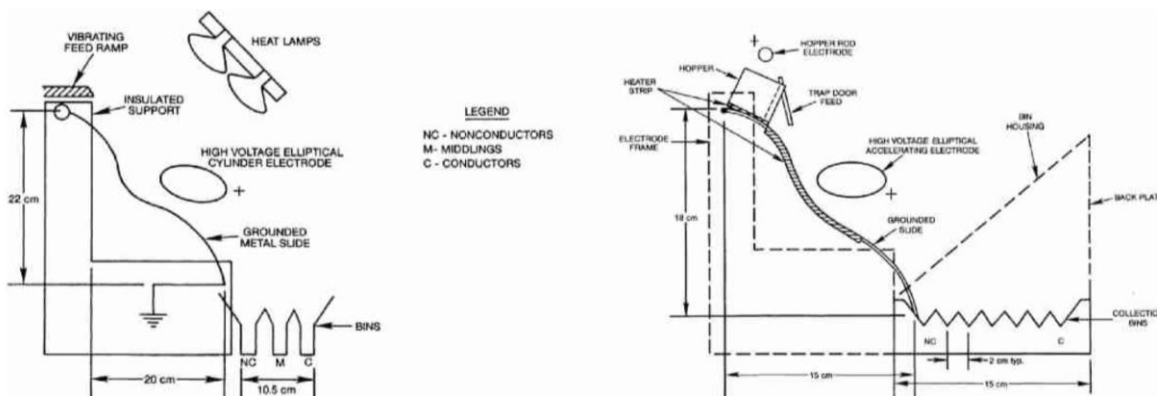
Figure 19: Slide separator setups used for testing in air (L) and with nitrogen or vacuum (R) [11, p. 8]

Continuing with the second technique addressed in the main source – *tribocharging and plate separation* – it should first be noted that there are two ways of separating the tribocharged particles: Either by means of *uniform* electrostatic fields, achieved using parallelly oriented plate electrodes, or through *non-uniform* fields, where the dielectrophoresis force comes into play (consult 2.1.2.2.1 for more information), which occur when the plates are angled with respect to one another [11, p. 9]. The configuration can further be clustered into *vertically* oriented (where gravity drives the particle motion) or *horizontally* aligned (need for an artificial conveyance).

There are two parties who mainly investigated these kinds of separators in the context of lunar applications: Li et al. – a group from the University of Kentucky – and their colleagues from Kennedy Space Center (NASA): Trigwell, Quinn, and Captain et al. In **1999**, the group led by T.X. **Li** [58] built a separator that "employed a pneumatically-driven vertical parallel plate separator with a copper tribocharger" as shown in figure 20 to perform tests on "individual [lunar] minerals (ilmenite, fosterite, albite, augite or quartz), on binary and ternary mixtures, and on a custom regolith simulant" [11, p. 9]. In particular, the experimental setup included a vibratory feeder to pour the respective mixture into copper tubes of 6.35 mm diameter, which bore loops that acted as triboelectric chargers [58, p. 135]. A carrying gas flow (nitrogen at an average gas velocity of 15m/s) then pneumatically pushed the particles down the loops, forcing particle-particle and particle-wall interactions to occur, effectively charging the material. After exiting the loops, the charged particles passed through an electric field provided by rectangle copper electrode plates of 38.1 x 14 cm, which were distanced by 10 cm [58, p. 135]. The electric field strength was quantified as 200 kV/m, powered by a high DC voltage. All the above-mentioned components were fitted into a rectangle plexiglas chamber of 61 cm (height) x 15.2 cm x 17.8 cm. Several experiments were conducted using this setup in a laboratory environment (room temperature of 298K and relative humidity of 50-60% [58, p. 135]); in the first run, the researchers funneled each mineral type individually (results to be found in figure 20). Thereafter, they experimented with binary mixtures of ilmenite and one of the other minerals, respectively. When mixed with fosterite, ilmenite charged negatively, whereas it charged positively in combination with the other three minerals (accordingly deflected to the negative electrode) [58, p. 139]. This led to the conjecture that particle-particle interactions would dominate the bulk charging behavior (at least in a pneumatic system) [11, p. 9]. Next, the team used ternary mixtures and found that ilmenite would land in the central collection hoppers when fosterite was also present in the feed, reasoning that it would prevent the target mineral from attaining charge [11, p. 9]. This finding was backed by the last experiments when complex simulants (of more than four constituents) were used.
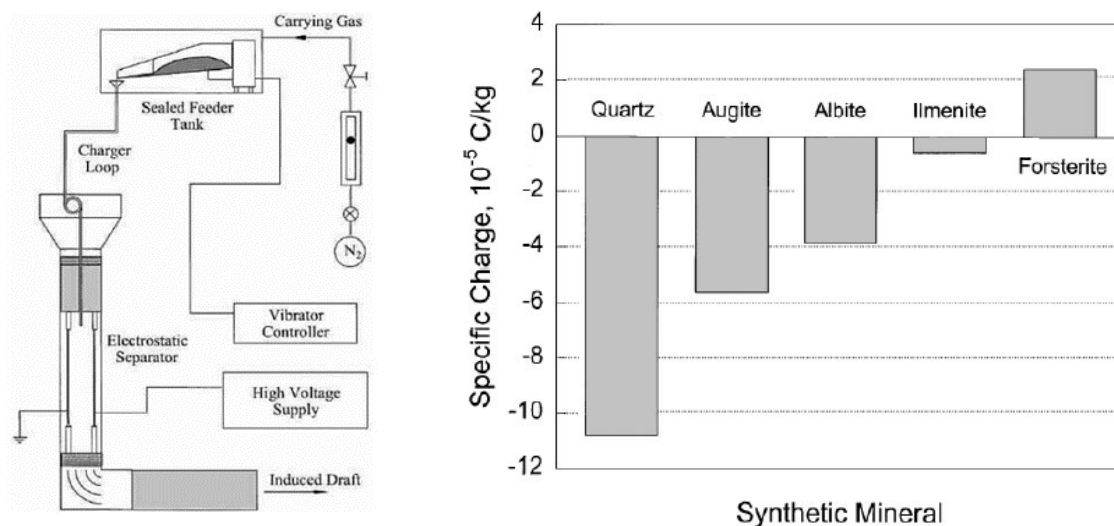

Figure 20: Schematic (L) and measured specific charge (R) for Li et al.'s system [58, 135-138]

Trigwell et al. took a similar approach in **2006** [59], as they also used a pneumatically driven, vertical plate separator, powered by a high DC voltage (±15kV). The electrodes in their setup were tilted by 4°

each (non-uniform field); the tribochargers were horizontally-oriented and made of aluminium and PTFE this time [11, p. 9]. Also, instead of using a simple mixture of synthetic minerals, a more realistic regolith simulant – namely MLS-1 – was fed to the separator this time. Dividing this simulant into size fractions (ranging from<25 µm to >100 µm) before experimenting with it, they found that the larger fraction charged more successfully than the smaller one (note that this observation may be caused by smaller particles readily adhering to the charger) [11, p. 9]. The design was iterated in **2007**: **Captain** [60] replaced the pneumatic conveyor with a free-fall setup, where gravity would draw the particles "through an aluminium block with a zig-zag path machined into it" [11, p. 9]. With respect to the processed material, Captain opted for the lunar simulant JSC-1 and decided to work with a narrow size fraction (ranging from 50-75 µm), only. Re-running the experiment under the new conditions revealed that iron-rich minerals like ilmenite tended to charge positively (except for ferrite, which charged negatively), so that they were attracted by the negative electrode.

NASA's tribocharging research efforts were extended by experiments of **Trigwell** in **2009** [61]. This study focused on comparing different materials for the static mixers (see figure 21). Copper, aluminium, and PTFE were shortlisted. To test the materials' tribocharging performance, Trigwell worked with the 50-75 µm size fraction JSC-1 just like Captain but added JSC-1A and KSC-1 to the list for completeness. Other factors, like the electrode charge, the charging block geometry, and the measuring technique (XPS and Raman spectroscopy) stayed the same for the sake of comparability. The experiments that followed can be recognized as successful, since ilmenite was significantly enriched from the KSC-1. When using copper, iron-bearing minerals were stringently consolidated at the negative electrode. In the case of the JSC-1 and -1A simulants, the data provided by Trigwell in his paper is too scares to make any judgement (lacking in the spectroscopy measurements or a modal mineralogy assessment).
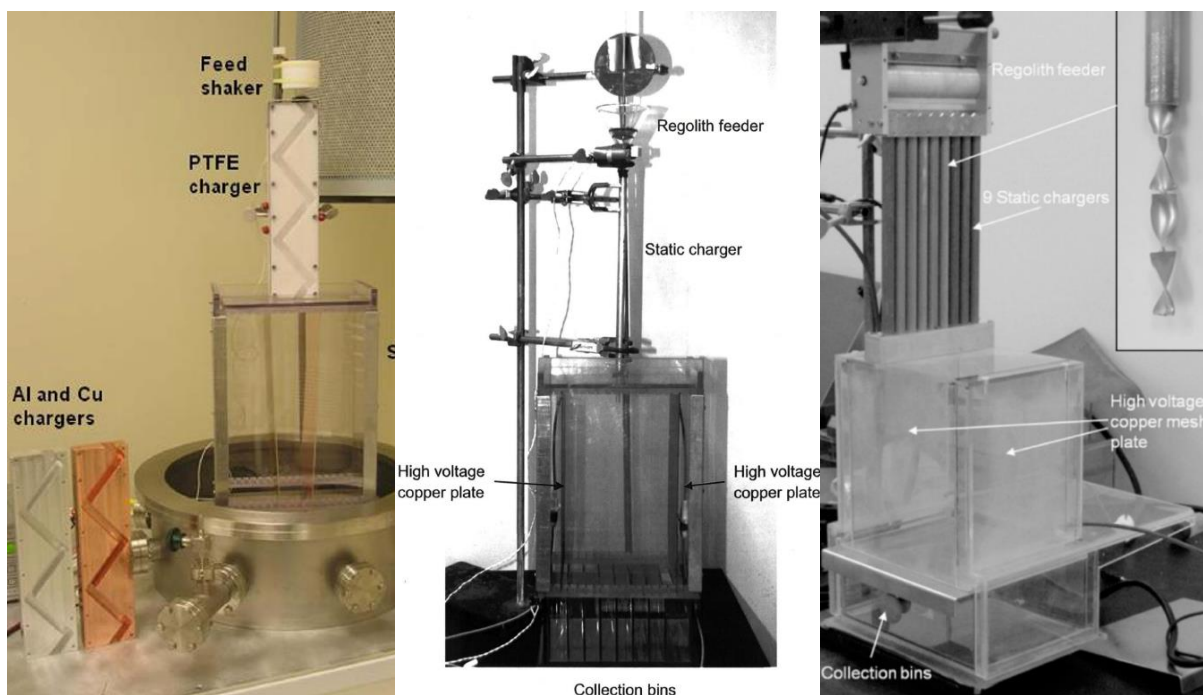

Figure 21: Iterating NASA's separator: From Trigwell (2009, 2012) to Quinn (2012) [61], [62], [63]

The last modification to the experimental setup made by **Trigwell** was shared with the public in **2012** [62] (see figure 21). With the aim of improving flexibility, the machined charging blocks were now replaced with interchangeable tubes – also made from copper, aluminium, and PTFE – with internal baffles.   The electrode voltage was now made adjustable and the maximum voltage was doubled (up to ±30kV). More collection hoppers could be accommodated now (up to 7), so that the resolution of the measurements could be increased. JSC-1A was still used, but the other derivatives were replaced by NU-LHT-2M (with an additive of +5% ilmenite). Despite the modified setup, the measurements were surprisingly close to the ones from three years earlier: Titanium was enriched by +67%, while the iron concentration increased by +33%. Real regolith (Apollo 14 samples) was now also tested. In this context, it was found that ±15kV and aluminum tubes achieved optimal separation with the samples, leading to a Ti- and Fe-enrichment of up to +164% and +12%, respectively. The main source concludes that "these results suggest that tribocharging and parallel plate separation is a viable approach for lunar mineral beneficiation" [11, p. 9].

With the aim of testing the separator under low gravity conditions, **Quinn** took the separator on parabolic flights in **2012** [63]. To prepare the apparatus for the plane journey, the team upgraded the design once more (see figure 21) by increasing the number of static chargers (nine tubes) – which were now only made from one material (aluminum) – and by optimizing the collector bin design to maximize efficiency. Due to technical constraints, the experiments onboard the aircraft had to be made under atmospheric pressure, instead of vacuum. Several electrostatic field strengths were tested on a total of two flights (by applying voltages of ±8, 10, 12kV on the first and 13, 15, 20kV on the second) using the <1 mm fraction of NU-LHT-2m (10 wt.% ilmenite was added for the second round for the sake of detectability). Analyzing the data obtained during those flights, the researchers found that ilmenite would always obtain little – if any – positive charge, so that it would land in the central or positive hopper with a statistical significance, no matter the voltage applied. For the first set of electrode voltages, enrichment was quantified as 60.3% with a recovery of 69.4% after a single pass. Applying the second series of voltages, while using the ilmenite-enriched simulant yielded even better results (enrichment of 106% [note that recovery plummeted to 23.9%]). This tendency showed throughout all tests, so that Quinn et al. concluded: Higher voltages lead to higher-grade ilmenite outputs, while recovery is better with lower-voltage tests. One should bear in mind that the validity of this statement is questionable, as the testing parameters were inconsistent.

As can be seen in figure 22, the team of **Berggren**, too, incorporated plate separation to electrostatically discriminate between conducting and non-conducting particles in their LSPS (**2011** [20]). However, unlike all the other researchers, Berggren and his team relinquished the common 'static tribochargers and vertical plates'-scheme; instead, "a basic two-plate induced-charge system" was designed, where the charge is implanted "as material flows over [a] grounded [stainless steel] plate" [20, p. 15] and the separation is achieved through a high-tension electrostatic field coming from a parallel copper plate with positive polarity, which would attract charged, conducting particles (leaving non-conductors at the bottom, where they are split from the rest). The E-field is powered by a high-voltage (*short*: HV) module capable of delivering 12,000 volts of potential. Test were run using synthetic mixtures and the lunar regolith simulants of choice, JSC-1A and NU-LHT-2M.

The experiments indicated that Berggren's electrostatic separator is yet to be revised, as only moderate enrichment was achieved, and programmatic drawbacks were revealed. Generally, multistage processing (refeeding the concentrate of one run to further boost concentration) was needed to achieve notable changes in grade (up to six runs). Human attention was also demanded for maintenance, as a periodic removal of waste products was mandatory to avoid constipation. Lastly, it was noted that "gentle placement of the feed particles onto the grounded plate was important" [20, p. 16] as allowing particles to bounce on the grounded plate measurably impaired their charging.
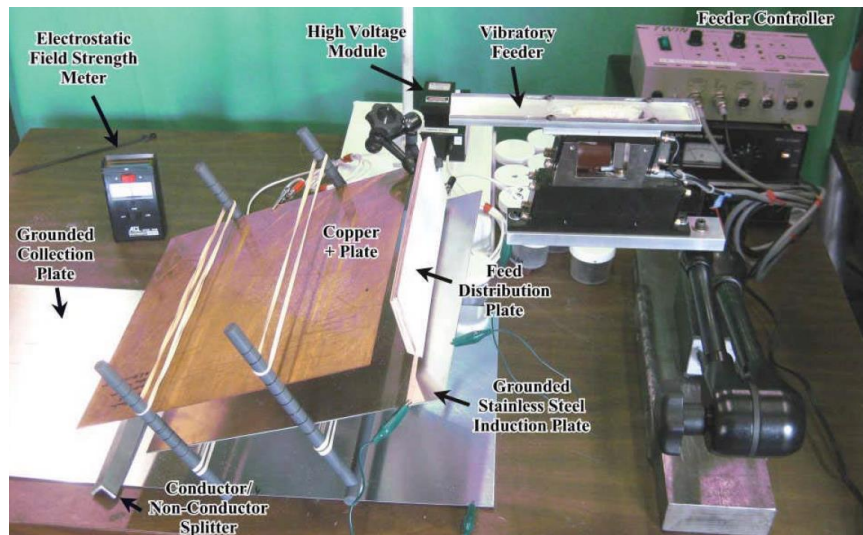
Figure 22: Electrostatic plate separator of Berggren et al. [20, p. 16]

The last concept portrayed in the main source – the *electrostatic travelling wave* (*short*: ETW) – is simultaneously the most recent advancement in the domain of electrostatic separation for lunar applications, although its use is not limited to beneficiation (also demonstrated for cleaning solar panels and space suit). It was intensively pushed by scientists from the Waseda University in Japan – first and foremost by Kawamoto and Adachi – since the beginning of the 21st century. The setup that underlies the Japanese ETW-experiments is visualized in figure 23 and concisely summarized hereupon: A power supply generates four alternating rectangular voltages, which are phase shifted by 90° through a microcontroller. The voltages are linked to parallel copper electrodes, which are printed on a non-conductive particle conveyor [64, p. 70]. When the current flows, a non-uniform electrostatic field is generated between the electrodes [11, p. 11]; with the voltages being phase-shifted, a travelling wave seems to appear. Charged particles located on the conveyor would now be affected by the resulting Coloumb and dielectrophoresis forces and consequently 'hop' in the direction of the ETW [64, p. 70]. The altitude of this parabolic hop is size-dependent, which can be exploited by attaching collection boxes at different heights to the end of the conveyor. In **2004**, **Kawamoto and Seki** [65] showed that even uncharged carrier particles can be affected by the ETW, as the contact with (an acetate rayon surface of) the conveyor would already tribocharge them with a charge of -0.01 and -0.03 µC/g, enough for them to respond to the modulated travelling wave: "When the travelling wave was initialized, this charge was enough for the Coulomb force to become dominant and drive their motion. As they moved, they gained additional charge through tribocharging as they collided with other particles and the insulation, augmenting the Coulomb force" [11, p. 11].

Figure 23: Schematic and photo of the ETW-experiment setup by Adachi et al. [64, pp. 70-72]

In **2017**, **Adachi** et al. [64] demonstrated the utility of this technique in the context of lunar beneficiation. In doing so, the researchers used the experimental setup outlined above to process the <106 µm fraction of the Japanese regolith simulant FJS-1 under vacuum and in air. In particular, 5 gram of the simulant were fed from the right side with the aid of a vibration supplier, which consisted "of a mechanical sieve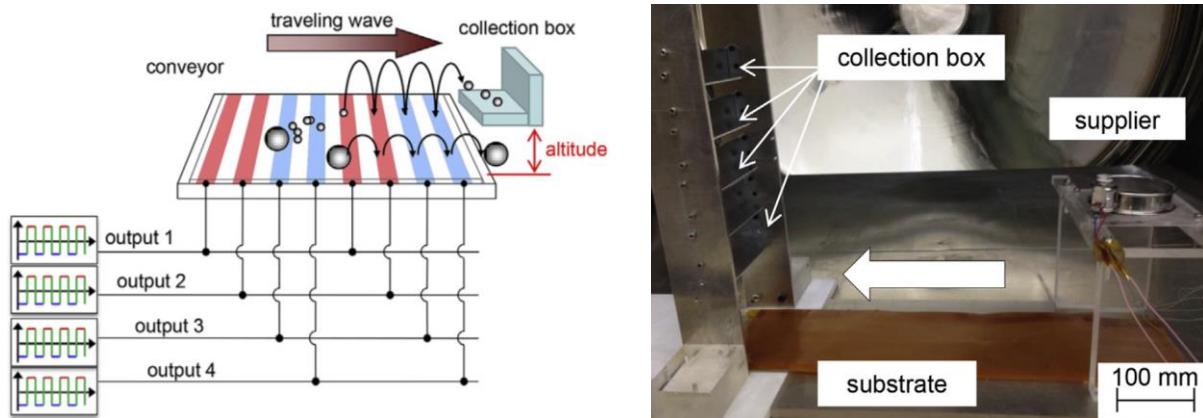 (mesh size: 0.5 mm) and a DC vibration motor (FA-130RA, Mabuchi Motor) " [64, p. 72]. The conveyor was made from an acrylic plate that was covered by a polyimide substrate of 0.1 mm thickness, 128 mm length and 490 mm length. The collection boxes were made from 25 x 25 cm L-profiles, mounted 100, 150, 200, and 250 mm above the ground (see figure 23). The test results indicated that the presence of air would impair the device's performance, "as fluid drag strongly influenced particle motion" [11, p. 11]. Under vacuum, however, the separation was significant and met the theoretic predictions well. Adachi and his colleagues conclude their work by noting that they adapted their numerical calculations to the lunar gravity and predict a successful particle separation, expecting the separator "to extract particles smaller than approximately 10 mm" [64, p. 76].

3.1.3 Magnetic Beneficiation

As can be inferred from table 8, sundry studies were undertaken to also demonstrate the feasibility of *magnetic* beneficiation in the lunar context. Magnetically processing lunar regolith "for both early-stage sizing and gangue removal as well as for the enrichment of specific minerals" [11, p. 12] was, among others, done by R.R. **Oder and** L.A. **Taylor**. In **1990** [66] and **1991** [45], they used a so-called *Frantz isodynamic separator* (see figure 24) – a patented device that induces strong magnetic fields in order to sort dry mineral grains according to their susceptibility, splitting the incoming feed into two channels – to successfully separate paramagnetic oxides like ilmenite from paramagnetic pyroxene. They reported: "Ilmenite concentrates in the magnetic susceptibility interval extending approximately from 80 to 400 x 10^{-6} *cc/gm* and the [...] pyroxene concentrates in the interval from 20 to 80 x 10^{-6} cc/gm" [45, p. 5368]. When repeating this experiment with real lunar soil, they achieved moderate success, as they recovered 22 wt.% of the ilmenite from an immature highland sample (native FeO content of 0.6 vol.%) and 57% from an immature mare sample (5.6 vol.% FeO) [11, p. 12]. These results correlate with the data gathered by **Taylor** in **1992** [41], which showed that the 90-150 µm fraction of Apollo samples 10058 could be upgraded from 16% to 52%, while the 45-90 µm fraction of samples

10058 and 71055 were boosted to an ilmenite concentration of 62% and 72%, respectively [11, p. 13]. In **2005**, **Taylor** [40] proposed that relatively weak, hand-held permanent magnets can be used to remove the problematic dust fraction (which is ferromagnetic, as 90% of the <10 μm fraction carry the np-Fe^0 patina mentioned in 2.2.1.2) and to filter undesired np-Fe^0-bearing agglutinates (which make up 80% of the <10 μm fraction) from the regolith. Thus, handheld magnets may represent an efficient and inexpensive method for sizing and gangue removal prior to further enrichment steps [11, p. 13].

Figure 24: Frantz Isodynamic Separator with external magnet and two-channel track [67]

This idea was seized and advanced by H. **Kawamoto and** H. **Inoue**. While working on methods suitable for removing regolith particles from spacesuit fabrics in **2012** [68], the researchers were able to capture the <53 μm size fraction of FJS-1 simulant using permanent magnets. In terms of numbers, they "successfully removed between 50 and 70% of the simulant from the fabric" [11, p. 13], though expecting higher rates for experiments with real regolith (as FJS-1 has a lower relative magnetic permeability [1.073 for FJS-1 vs. 1.311 for regolith] and a higher share in non-magnetic components).

Berggren and colleagues, who were already mentioned in the preceding chapters, also employed magnetic beneficiation in their Lunar Soil Particle Separator, as posed in their paper from **2011** [20]. They opted for a drum separator that featured "fixed magnets inside a rotating drum" [20, p. 11], which was chosen for its "compact size, wide range of operating parameters [...], [few] moving parts, and its low power requirement" [20, p. 11]. In their experimental assembly, the authors implemented "grade N-50 neodymium-iron-boron permanent magnets for enriching magnetic and paramagnetic materials from binary mixtures and lunar simulants" [11, p. 13].

The schematic and photo to be found in figure 25 show the setup in greater detail: First, the processed material is fed into the system from right above the drum's top. The feed lands on the polycarbonate tubing of the outer cylinder. As this cylinder turns, while the arc-shaped, nickel-plated magnets remain stationary, non-magnetic particles would be "propelled by dynamic forces and [...] projected away from or fall from the rotating cylinder", whereas "magnetic particles are attracted to the magnets attached to a fixed inner cylinder" and only fall "when they pass out of the influence of the magnetic field" [20, p. 12]. Following the perceptions from first-order experiments, Berggren noted that fine-tuning is needed when it comes to the operational speed, which dominates the grade-recovery relationship (low speed for high grade but low mass; high speed for higher flow rate with poor quality), and the gap between rotor and stator (to avoid strongly magnetic particles sticking to the outer cylinder). Berggren also observed that narrow size ranges are needed for an efficient operation of the drum separator [20, p. 12].
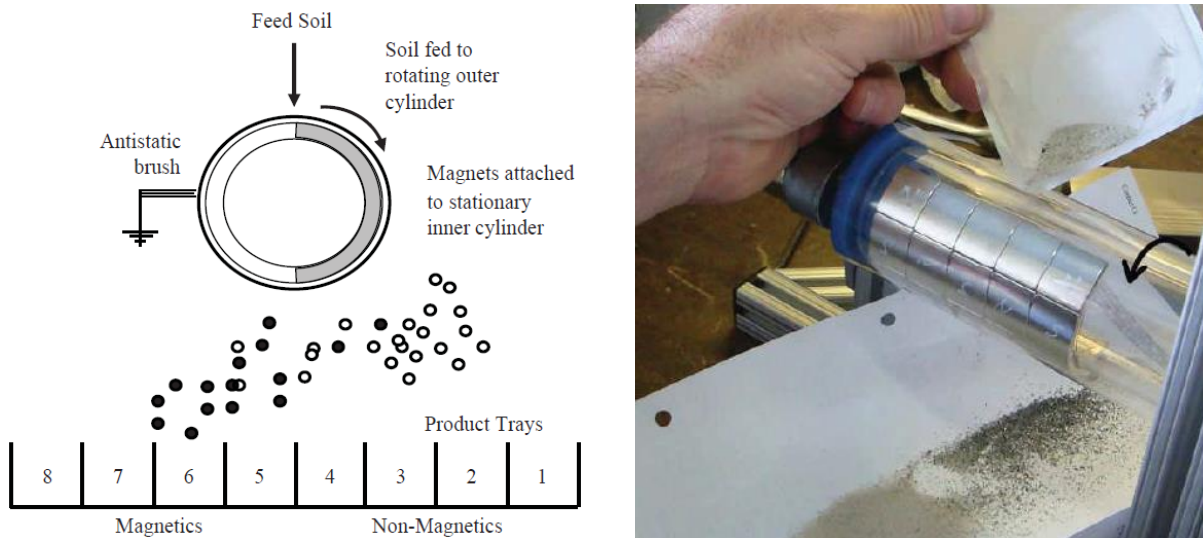
Figure 25: Schematic and photo of Berggren's permanent magnet drum separator [20, p. 12]

The permanent magnets served their purpose well during experiments: When trying to concentrate iron oxide from quartz sand, the grade was successfully increased from 10 to 87 wt.%; the experiment was rerun with ilmenite as the target mineral, now yielding a grade of 75 wt.% after three passes. However, when feeding lunar simulant to the apparatus, the results were rather sobering: No significant upgrade was achieved when testing with simulant JSC-1A; the resulting values were more encouraging when using NU-LHT-2M, where Berggren et al. managed to boost iron oxide-rich minerals from 4 wt.% to 10.5 wt.% [11, p. 13]. Nevertheless, the separator was still able to effectively control the size distribution.

The beneficiation-related efforts of J.G. **Williams** and his fellow researchers were already displayed in chapter 3.1.1 – but the team's scheme, deliberated in **1979** [16], did not only consider gravitational separation, but also included a third section (see figure 26), where pre-sized "particles are separated into ilmenite and tailings by magnetic separators" [16, p. 276]. Unfortunately, the authors fail to outline the specific technique for their sequence, so that no further information can be given.
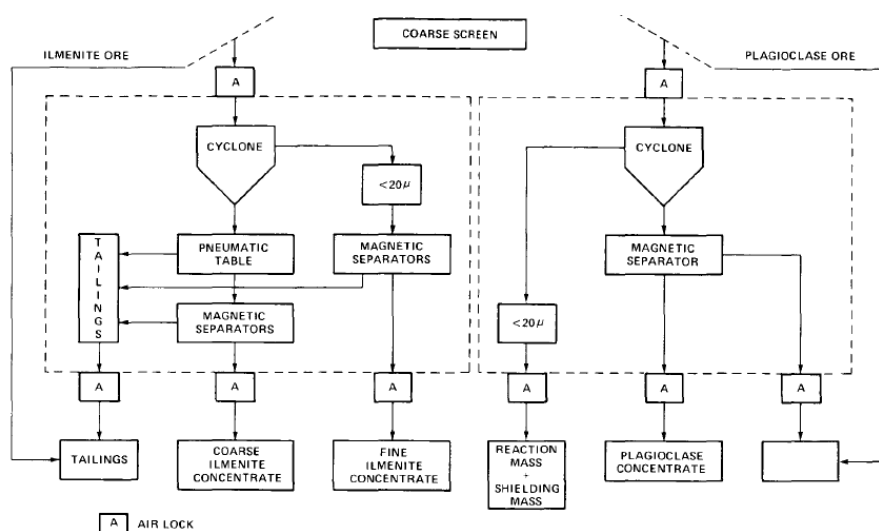
Figure 26: The beneficiation scheme drafted by Williams et al. in 1979 [16, p. 277]

Lastly, one more author – who was already cited in chapter 3.1.2 – should be named before closing chapter 3.1, as he also dealt with magnetic beneficiation: William N. **Agosto**. The scientist not only investigated electrostatic beneficiation, but also looked at mineral separation incorporating drum magnets at scale for oxygen and metal production. In a paper released in **1981** [69], he proposed a corresponding process (see figure 27) and mathematically demonstrated that it could be capable of producing an output of up to 500 tons of lunar iron-nickel alloy per year [11, p. 13]. In **1984** [44], he used magnetic separation in practice, as a pretreatment step in his electrostatic separation study: "Prior to electrostatic separation of the 10084 lunar sample, agglutinates and soil metal amounting to 37 wt% were removed with a hand magnet. Virtually all the soil ilmenite was retained in the nonmagnetic fraction" [44, p. 1]. This procedure was also applied during his experiments in **1985** [52]; the fact that "the ferromagnetic agglutinates had been removed with a permanent magnet" [44, p. 1] in advance may have paved the way for the solid performance of his electrostatic separator.
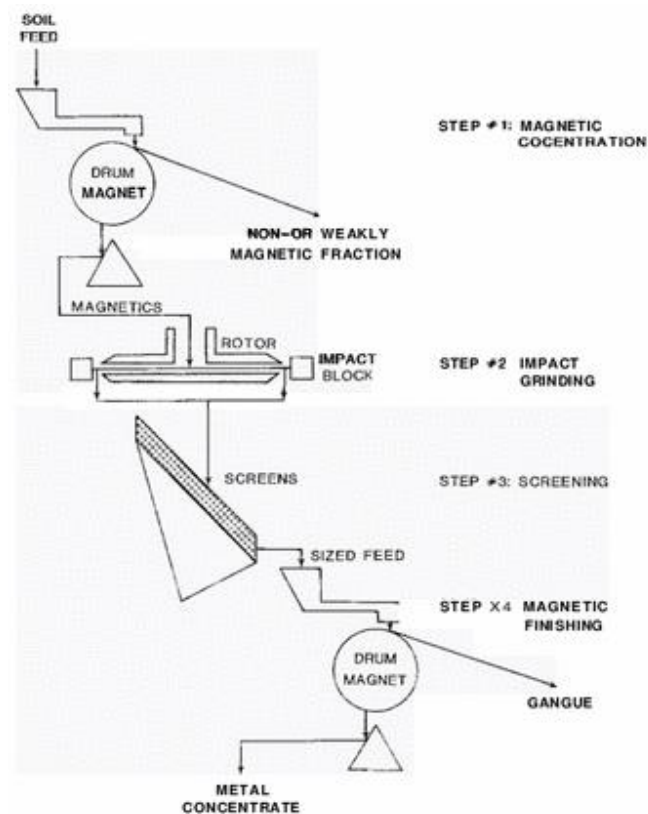
Figure 27: Flow sheet of magnetic beneficiation by Agosto [69]

3.2 Requirements & Specifications

With the first WP being accomplished, a profound stock of knowledge regarding previous lunar beneficiation experiments is now at disposal. Having recourse to this stock helps in shaping SMU's beneficiation apparatus. In a first step, this will be done through technical *requirements* (*short*: RQ), i.e., characteristics to be met by the product as well as *specifications* that particularize its future properties. In this context, RQs act as a design guideline for the whole development process, as they

embody the initial needs (the input). Specifications, on the other hand, indicate the system's prospective performance by quantifying how well it will work (the output). This chapter's purpose is to derive a catalogue of such statements and metrics for the laboratory testbed, in order to facilitate the ensuing WPs (for instance the concept generation, component selection, and design phases).

Normally, a good starting point for the derivation of such a catalogue would be the expectations expressed by the main stakeholders (e.g., a customer). In view of the ISRU value chain for oxygen production (see chapter 2.1), this role is epitomized by the extraction step, as its efficiency greatly depends on the quality of the feedstock provided by the beneficiation testbed (as explained in 2.1.3). Since no O_2 extraction reactor will be built over the course of SMU's research activities, there is no internal party that could issue a set of useful demands. To circumvent this conjuncture, well-founded assumptions must be made. Acquiring these was done by summarizing the values found in the papers reviewed in chapter 3.1 in the form of a table: As can be seen below, all relevant sources referred to by Rasera et al. were listed one above the other, while the most important quantities mentioned by the respective authors make up the columns. This includes the key performance metrics for beneficiation (grade, recovery, and enrichment ratio, as explained in chapter 2.1.2), as well as the particle size (further split into minimum and maximum particle size) in micrometers and feed rate (in kilograms per hour). An arithmetic average was calculated for each column to prevent anomalies from distorting the outcome. Contextual information (like subprocesses, simulant types, and materials used in the experiments) was also collected (to be found in annex 4) to help in classifying the given values.

Table 10: Summary of specifications given in secondary sources

Author	Year	Initial Grade	Final Grade	Recovery	Enrichment	Size Range [μm]	Size min. [μm]	Size max. [μm]	Feed rate [kg/h]
Gravitational									
Wilkinson	2011	-	-	-	-	75-150	75	150	13
Magnetic									
Williams	1979	5	17		2,2…3,7	20-200	20	200	-
Oder	1989	-	-	-	-	45-150	45	150	-
Taylor	1992	-	40	-	-	45-90 and 90-150	45	150	-
Beggren	2011	4	10,5	-	2,625	150-425	150	425	6
Electrostatic									
Adachi	2017a	-	-	-	-	<106	-	-	-
Agosto	1984	10	54	45	5,4	90-150	90	150	-
Williams	1979	5	-	-	-	20/200	20	200	-
Agosto	1983	10	90	38	9	45-90, …, 250-500	45	500	21,60
Agosto	1985	7,30	51	-	6,99	90-150, 150/200	90	200	25,2
Captain	2007	10	-	-	-	50-75	50	75	-
Li	1999	14,28	37		2,59	75-106	75	106	-
Quinn	2012	10	20,6	69,4	2,06	<1000	-	-	0,3
Trigwell	2006	-	-	-	-	<25, >100	-	-	"6l/min"
Trigwell	2009	10	-	-	-	50-75	50	75	-
Trigwell	2012	2,8	11,5	-	4,11	50-75,75-100	50	100	-
Additional Sources									
Beggren	2021	-	70	50	-	150-425	150	425	20
Agosto	1985	9,5	38	-	4	-	-	-	-
Ø		8,16	39,96	50,60	4,60		68,21	207,57	14,35

Additionally, existing extraction studies containing preliminary feedstock requirements were consulted to validate the calculated mean values. By way of example, Gibson and Knudsen published a patent for a device capable of extracting oxygen from concentrated lunar ilmenite in 1996 [70], in which the authors state that the envisioned reactor would accept particle sizes of 20 to 200 micrometers. This seems to correlate with the calculated values in a sufficient manner.

The specifications gathered in table 6 were then used as a steppingstone to deliberate the technical requirements. In a first step, each RQ was formulated as "an unambiguous statement that identifies a product characteristic or constraint" [71, p. 75] that could either be tested or measured. When being integrated into the RQ catalogue thereafter, each of these *statements* was assigned a unique *identification number* (for the sake of traceability) and supplemented with additional attributes like the *RQ level* (a standard 3-tier space engineering hierarchy consisting of system, subsystem, and component-level was applied). Ultimately, they were grouped according to their respective *RQ type*.

Many different types of technical requirements exist that may be used to characterize a product in different regards. A highly esteemed standard like the European Cooperation for Space Standardization (*short*: ECSS) distinguishes 12 different classes in its document ECSS-E-ST-10-06C [72]. However, to stay on top of things, this catalogue is confined to the most relevant of the 12 RQ types:

- **Functional** Requirements
- **Performance** Requirements
- **Environmental** Requirements
- **Operational** Requirements
- **Interface** Requirements
- **Design** Requirements

On that note, *functional RQs* are statements that "define what the product shall perform, in order to conform to the needs / mission statement or requirements of the user" [72, p. 18]. They form the catalogue's basis, as they pave the way for the more specific RQ types. From there on, the *performance RQs*, which "quantify to what level the functional requirement will be fulfilled" [71, p. 79], can be derived. The environmental RQs, on the other hand, define the external conditions (of physical, thermal, or electrical nature, for example) under which the testbed will be operated. They interrelate with the challenges described in chapter 2.3 (only the laboratory environment is relevant for the testbed) and are complemented by the *operational RQs*, which themselves specify the mode of control and the degree of autonomy that the product offers under given circumstances. Lastly, the *design RQs* regard the constraints imposed on the design (e.g., by the facility) and the construction standards applied [72]. This affects the selection of components and materials, but also dimensions and margins.

It should be noted that the RQ (& specification) catalogue that was conceived in the above explained manner is an ever-expanding document and will, thus, mature with every new WP, so that no final version exists at this point in time. However, an excerpt of the current version is provided in table 11 for demonstration purposes, while a more in-depth and recent list will be provided in annex 4. Each requirement shown in this list adheres to the general rules stated in the above mentioned ECSS document, as they were expressed in an unambiguous, unique, complete, and verifiable way. Moreover, they flow down adequately from top (system-level) to bottom (component-level). In order to maintain transparency in the making of the given tables, a few requirements shall be explicated exemplarily and elaborated upon before closing this subchapter:

- **SMU_BEN_002 & _003:** Main functions needed to accomplish the mission objective defined (turning the raw material into an ilmenite-rich and size-sorted feedstock that is chemically and physically suitable for extraction through hydrogen reduction, as explained in 2.1.2 & .3)

- **SMU_BEN_007:** Feed rate as inferred from mean value in table 11; rounded to the next highest integer; moderately high margins added to permit adaptability during experiments
- **SMU_BEN_008:** Max. & min. particle size approximated by mean values in table 11; upper limit rounded; lower limit corrected with value from Gibson and Knudsen's reactor; thresholds aligned with the properties of the simulant / size of nominal ilmenite grains (as mineralogy and particle size are intertwined [as elucidated in 2.2.2])
- **SMU_BEN_009, _010 & _011:** Min. performance parameters derived from mean values in table 11; rounded to a reasonably close number; aligned with the initial ilmenite content of the utilized simulant (LMS-1 as declared in 2.2.1.3 and annex 2)
- **SMU_BEN_012, _013, _014 & _015:** Guaranteeing the operability of the system under laboratory conditions; keeping humidity reasonably small to avoid caking of the simulant
- **SMU_BEN_020 & _021:** Assuring that the testbed can be brought to and operated in a vacuum chamber outside the DLR entities
- **SMU_BEN_049:** Rejection of ferromagnetic constituents necessary to filter undesired np-Fe^0-bearing dust and ferrous agglutinates, to improve feedstock quality [16, p.2]

Table 11: An excerpt of the requirments & specifications catalogue featuring the system level RQs

RQ ID	RQ Type	RQ Statement
SMU_BEN_001	Functional RQ	The beneficiation testbed shall be able to receive, convey and process lunar regolith simulant (LHS-1, LMS-1 or LHS-1D) as a raw material.
SMU_BEN_002	Functional RQ	The beneficiation testbed shall be able to filter specific particle sizes of the raw material.
SMU_BEN_003	Functional RQ	The beneficiation testbed shall separate the ore mineral ilmenite from other constituents within the raw material.
SMU_BEN_004	Functional RQ	The beneficiation testbed shall be able to dispense a feedstock of size-sorted material rich in the ore mineral.
SMU_BEN_005	Functional RQ	The beneficiation testbed shall be able to dispense waste streams of undesired tailings and gangue minerals.
SMU_BEN_006	Performance RQ	The amount of lunar regolith simulant that can be received by the testbed shall at least be 1 kg or 1 liter, respectively.
SMU_BEN_007	Performance RQ	The rate at which the lunar regolith simulant can be conveyed and processed by the testbed shall be 15±5 kg/h.
SMU_BEN_008	Performance RQ	The particles size to be filtered by the testbed shall range from 0 to 20 μm and from 200 μm onwards.
SMU_BEN_009	Performance RQ	The final grade of the ore mineral within the feedstock dispensed by the testbed shall be at least 40 wt.%
SMU_BEN_010	Performance RQ	The recovery of the ore mineral within the feedstock dispensed by the testbed shall be at least 50 wt.%
SMU_BEN_011	Performance RQ	The enrichment ratio of the ore mineral within the feedstock dispensed by the testbed shall at least be 4.5.
SMU_BEN_012	Environmental RQ	The beneficiation testbed shall be able to operate under Earth's gravitational acceleration of 9.81 m/s^2.
SMU_BEN_013	Environmental RQ	The beneficiation testbed shall be able to operate under atmospheric pressure (10^5 Pa) and vacuum (up to 10^-10 Pa).
SMU_BEN_014	Environmental RQ	The beneficiation testbed shall be able to operate at a standard temperature of 293.15K (±5K).
SMU_BEN_015	Environmental RQ	The beneficiation testbed shall be able to operate at an air humidity lower than 60 %.
SMU_BEN_016	Operational RQ	The beneficiation testbed shall be operable by a single, (HV-)qualified experimenter.
SMU_BEN_017	Operational RQ	The beneficiation testbed shall accept an input of multiple control parameters from the operator prior to the experiment's start.
SMU_BEN_018	Interface RQ	The beneficiation testbed shall offer a permanent connection to the ground and a firm stand during experiments.
SMU_BEN_019	Interface RQ	The beneficiation testbed shall connect to one or more Schuko electrical socket(s), i.e., AC 230V 50Hz.
SMU_BEN_020	Design RQ	The beneficiation testbed shall be designed in a moveable manner, allowing it to be transported to different locations when not in use.
SMU_BEN_021	Design RQ	The beneficiation testbed shall fit through standard door frames without disassembly.

3.3   Concept Generation

The following lines are devoted to the generation of a powerful concept for SMU's laboratory testbed. Based on the findings and outcomes of the literature review as well as the requirement catalogue expounded on the preceding pages, chapter 3.3 will deal with the selection of adequate beneficiation processes, the arrangement of those processes in a feasible setup (while also itemizing the system into distinct units), and the visualization of the devised ideas in terms of sketches. With the extensiveness of this set of tasks turning the conceptualization into an excessively large WP, a separate section will be dedicated to each of those aspects, proceeding in the following order:

- Filtering, assessing, and selecting suitable **processes** (3.3.1)
- Conflating the processes in a detailed **setup**, including a schematic and a product tree (3.3.2)
- Drafting design **sketches** to visualize the verbally expressed ideas (3.3.3)

3.3.1 Processes

Many different studies that regarded the beneficiation of lunar regolith have been explored during the literature review in chapter 3.1, revealing a great number of practically proven processes that could be employed within the testbed. This knowledge is complemented and backed by theoretically implementable beneficiation methods, as introduced in the foundations chapter (2.1.2). However, the infobesity that comes along with such a manifold of sources makes it hard to immediately see the bigger picture behind dry lunar beneficiation at this stage. To produce relief, a hierarchical overview was created that *filters* the mentioned processes out of the texts and clusters them into three separation categories (dark orange boxes in figure 28), boosting lucidity, comparability, and ratability:
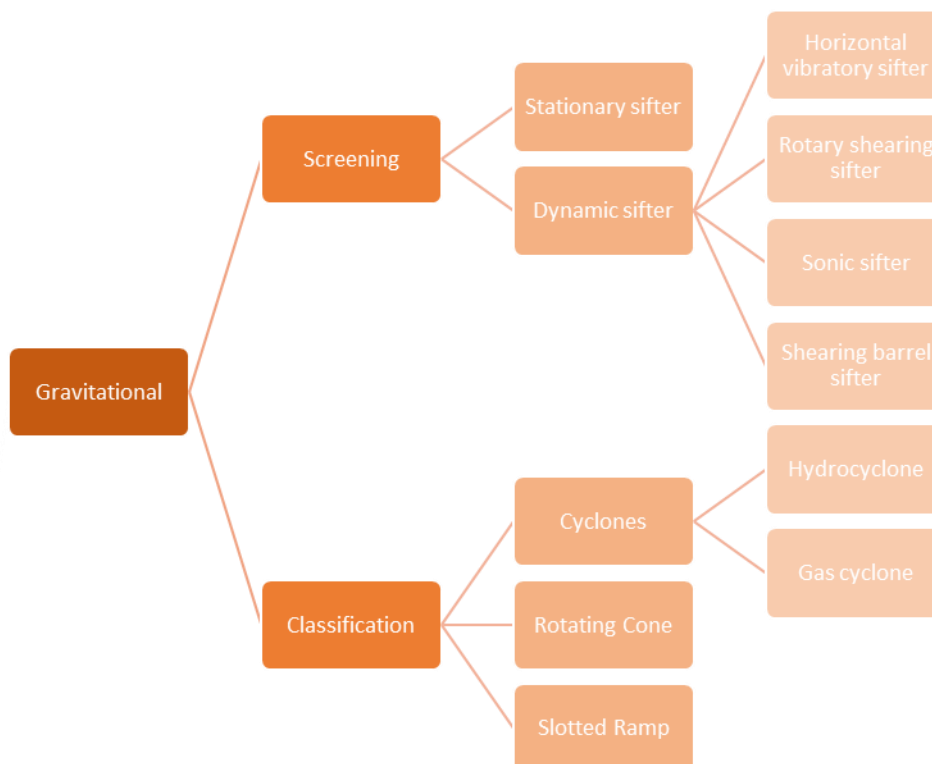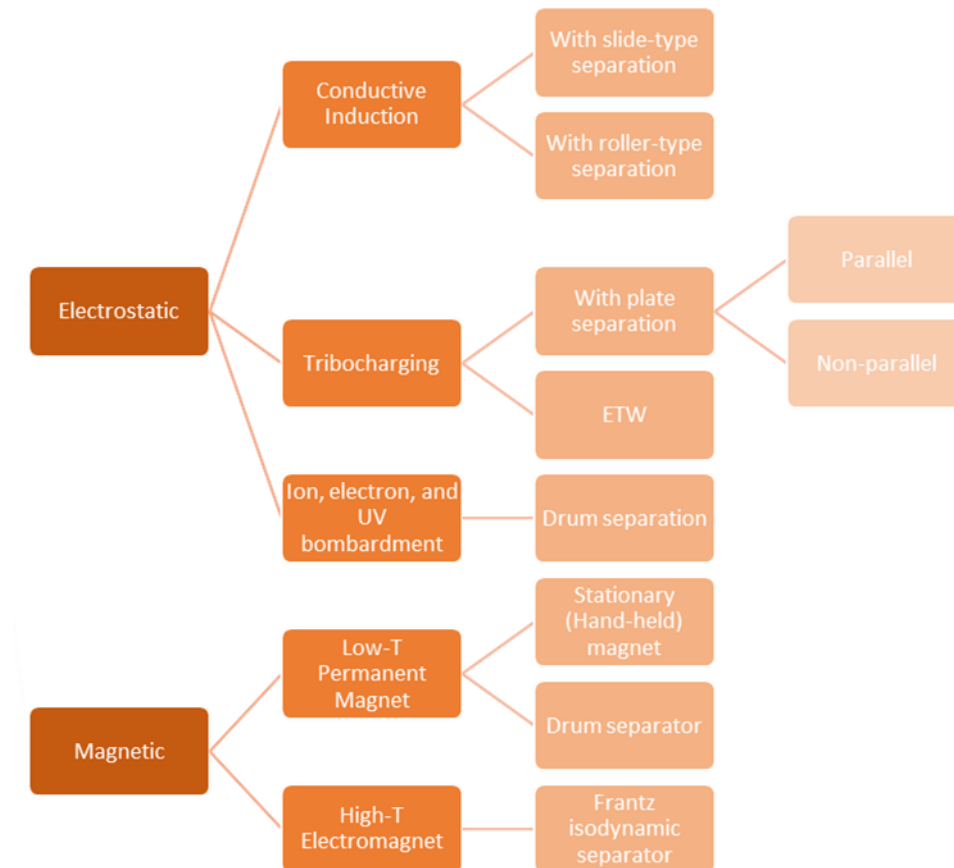
Figure 28: Overview of the known processes for lunar dry beneficiation grouped in three categories

When it comes to the process *assessment & selection*, letting all the above indexed subprocesses (bright orange boxes) compete against each other in one big evaluation scheme, in order to elect the one winner, would normally be considered a good approach. Nonetheless, when revising the RQ catalogue conceived in chapter 3.2, it becomes apparent that a single process alone will fail to fulfill all the demanded system-level functions at once. In fact, each separation category has its own raison d'être – a quality that only it can offer or an aspect in which it rigorously outcompetes the others. Accordingly, the strengths of all three categories (which will be outlined in 3.3.1.1, .2 & .3) should be combined, rather than neglected, so that the strategy of choice is to only compare cognate processes (of equal origin) and nominate one winning process per category. The application of this assessment approach for gravitational, electrostatic, and magnetic beneficiation will be constituted hereupon.

3.3.1.1 Gravitational Processes

Beginning with gravitational separation methods: They are best at exploiting specific mechanical attributes within the raw material – such as particle size or density – to distinguish the ore mineral from other tailings in the simulant, thereby helping to increase the ilmenite grade (*chemical dressing*) and attain the correct feedstock size distribution (*physical preparation*). In view of table 3, lunar soil samples indicate that pure ilmenite grains never exceed diameters of 500 µm, but mostly remain smaller than 250 µm, making them easily filterable for gravitational separators. The importance of gravitational beneficiation is additionally underscored by the fact that the degree of liberation

(the ratio of a mineral occurring as free particles to the total amount of that mineral [free and locked]) increases with decreasing grain size, resulting in a purer outcome, which translates into a higher final grade (consult chapter 2.2.2 for further information).

To identify the most advantageous subprocess in the domain of gravitational separation, a classic decision matrix was utilized. A decision matrix is a simple, yet powerful evaluation tool that supports its user in selecting the best option by analyzing and rating the performance of several alternatives. It does so in a systematical and methodically correct manner, while being less complex, thus, less labor-intensive than tools like the weighted multi-criteria decision analysis, but also less subjective than methods like the Pugh Matrix (where the arbitrary selection of a reference biases the outcome). In it, assessment *criteria* are listed in the first column (each forming a new row) and *weighted* according to subjective importance in the second column, while all *alternatives* are itemized next to them, each creating a column themselves [73]. In the course of this assessment (depicted in table 12), the criteria were conceived during a brainstorming session and inspired by attributes mentioned in literature (e.g., by Allen Wilkinson [chapter 3.1.1]) or RQs; alternatives were taken from figure 28. The matrix elements forming in the middle are used to score the fulfillment of the respective criterion by the currently rated alternative. The scale chosen in this particular case ranges from **0** (= criterion not fulfilled at all) to **5** (= criterion completely fulfilled). Lastly, the penultimate row is used to *sum* up the weighted scores ($weighting\ factor * score$) of each alternative, whereas the last row awards a *rank* to them according to their cumulative performance.

Table 12: Decision matrix for evaluating the subprocesses of gravitational beneficiation

		Alternatives				
	Weight	Stationary Screening	Dynamic Screening	Cyclones	Rotating Cone Separator	Slotted Ramp Separator
Environmental Independence	0.15	2	4	1	2	3
Simplicity & Reliability	0.05	4	3	2	3	4
Energy Efficiency	0.1	5	4	1	3	4
Volume & Mass	0.1	5	4	3	4	3
Technology Readiness	0.15	4	5	4	3	3
Process Integrability	0.15	0	4	2	4	5
Adjustability & Scalability	0.05	4	5	3	5	4
Performance	0.2	1	5	4	2	4
Cost & Dev. Effort	0.05	5	3	3	3	4
Sum	1.0	2.7	4.3	2.65	3	3.75
Rank	-	4	1	5	3	2

(The leftmost column spanning the criteria rows is labelled "Criteria".)

A succinct reasoning for the awarding of scores in an exemplary case will be provided in the following: Stationary screening devices depend on a firm gravitational pull for particle conveyance. Thus, under the low-g environment found on the Moon and with the absence of an externally induced de-blinding motion, the system is prone to clogging, which will put its main function at risk on a regular basis. Other environmental challenges, however, such as a varying air pressure (vacuum on the Moon or atmospheric pressure in the lab) or different radiation levels do not affect the devices performance, so that a score of **2** was arrived at regarding the *environmental independence*. Relinquishing complex and failure-prone mechanisms makes the system appear robust, so that a **4** was given for its *simplicity & reliability* (one point was deducted as wear and tear remains an issue). This also attributes to the great performance in the following categories: Being independent of an external energy source (no power consumed), occupying only little space (format of a thin sheet with low design height), and being light weight like no other alternative (only the metal sieve insert attributes to the total mass) makes it stand out from the competitors, so that **5** points were rewarded in view of *energy efficiency, volume & mass*. As a matter of fact, it is also the oldest technique for size sorting in terrestrial applications, so that its *technology readiness* was rated with **4** (minus one point, as it was not investigated into for lunar applications). The earlier mentioned drawback (the proneness to clogging) paired with the absence of a reject-outlet makes a continuous operation impossible and has accordingly led to a **zero**-rating in view of the process integrability, as periodic maintenance by an operator becomes inevitable (which is tolerable although costly in the lab but becomes a showstopper when transferred to space). This also severely impairs the overall *performance*, as stationary screening only delivers acceptable results when processing coarse material, so that only **1** point was awarded. Its *adjustability & scalability*, on the other hand, can be described as good, since key parameters (aperture size, shape, screen material & flexure) can be adapted to the specific needs and scale. The *cost & development effort* are very moderate, which was acknowledged by a score of **5** points. Multiplying all the above-listed numbers with their respective weighting factor and summing up the weighted scores eventually led to a sum of **2.7**. When comparing this sum to the ones from the other alternatives, it shows that stationary screening comes fourth, indicating that it should not be favored.

This procedure was repeated for dynamic screening, cyclones, the rotating cone separator, and the slotted ramp separator, too. For the sake of this paper's conciseness, an in-depth reasoning for the scoring of all other alternatives was outsourced to annex 5, which the interested reader is encouraged to consult. The main part of this thesis will hence focus on the results and winners of each category. In the case of gravitational separation, the decision matrix implied that dynamic screening devices are the most promising solution. They first and foremost convince by their outstanding *performance*, but also offer an excellent *technology readiness* as well as optimal *adjustability & scalability* capabilities. With a **3** being the lowest score, it seems to succeed all along the line. This may be explained by the fact that it inherits the potential of the stationary screens, whilst remedying its penalties. It is therefore selected as the gravitational beneficiation process to be pursued in later concept generation steps. All in all, the scoring made in table 12 correlates with and was established on observations made earlier or reported within literature: Classification-based devices like cyclones turned out not to be competitively viable, as they demand a liquid carrier medium (see 2.1.2.1), while screening techniques like dynamic sifters prevail as the most trusted size beneficiation method.

3.3.1.2 Electrostatic Processes

The unique strength of electrostatic beneficiation lies in the *mineral enrichment* efficacy it provides. Being without equal in this regard, achieving the ilmenite grade, recovery, and enrichment ratio stipulated in the RQ catalogue (SMU_BEN_009…_011) will make the implementation of it inevitable. All its subprocesses follow the same principle, as they work by imparting charge on the bulk material in a first step and by discriminating its constituents based on their differences in electric conductivity as a second stage. At this, the poorly chargeable ilmenite will retain only little or no charge (due to its relatively high conductivity; consult 2.2.2 for further explanation) whereas the undesired tailings like pyroxene will become highly polarized, which can be exploited by a suitable separation apparatus, effectively partitioning the bulk into different fractions. A decision matrix, which followed the procedure outlined on the previous pages, was also used to ordain the best option for this category. The outcome of the completed assessment is exhibited in table 13 below.

Table 13: Decision matrix for evaluating the subprocesses of electrostatic beneficiation

		Weight	Alternatives				
			Conductive Induction + slide separator	Conductive Induction + roller separator	Tribocharging + Plate Separator	Tribocharging + Electrostatic Travelling Wave	Ion, electron & UV bombardment + Drum separation
Criteria	Environmental Independence	0.15	2	3	4	2	3
	Simplicity & Reliability	0.05	4	3	4	2	3
	Energy Efficiency	0.1	2	1	3	4	3
	Volume & Mass	0.1	3	3	4	4	3
	Technology Readiness	0.15	3	2	5	3	1
	Process Integrability	0.15	4	5	5	3	5
	Adjustability & Scalability	0.05	3	5	3	4	5
	Performance	0.2	4	3	5	3	3
	Cost & Dev. Effort	0.05	3	3	3	2	3
Sum		1.0	3.15	3.05	4.3	3	3.1
Rank		-	2	4	1	5	3

A justification for the respective scoring of all alternatives can again be found in annex 5. With a big lead of 1.15 points, tribocharging in conjunction with plate separation seems to dominate the field and will accordingly be nominated as the process to represent electrostatic beneficiation in the testbed. The technique convinces with an excellent *performance*, which into the bargain "has been tested in more environmental conditions than any other method" [11, p. 11] (engendering a high *technology readiness*). Being the process of choice for so many researchers in the domain of lunar SRU

while prevalently yielding splendid results entailed a **5** in both criteria. Its sound *environmental independence*, superb *simplicity & reliability* and small *volume & mass* were rewarded with a **4**. This appraisal again coincides with statements from literature, where tribocharging is described as "the simplest method considered for imparting charge on particles" [11, p. 6] and emphasized that "it employs simple, light-weight and low-mass components" [11, p. 11]. It is further highlighted that the nature of the lunar environment "is ideal for triboelectrification and electrostatic separation, [as] the lack of moisture prevents the regolith grains from sticking together, and the lower gravitational pull increases separation of the charged particles, all of which enhance mineral segregation" [59]. Only the mediocre *energy efficiency* (due to the usage of high voltage power supplies), *adjustability & scalability*, and increased *cost & development effort* (suitable static chargers are not commercially available and must, thus, be designed and manufactured individually) can be seen as downsides that slightly lower the median.

3.3.1.3 Magnetic Processes

The exceptional feature offered by magnetic beneficiation is its ability to remove the problematic dust proportion within the lunar regolith (*sizing*) as well as superfluous agglutinates (*gangue removal*). On the one hand, dedusting is beneficial because the minute dust particles contain virtually no single-domain ilmenite grains (as explained in 2.2.2). On the other hand, their abrasiveness and tendency to adhere to surfaces would severely disturb subsequent enrichment or extraction steps, while contributing to the system's attrition. Furthermore, agglutinates would add to the impurity of the feedstock, so that an ideal feedstock should have few agglutinates, only [41, p. 1416]. Magnetic beneficiation is possible because of the ferromagnetic patina that covers more than 90 percent of the <10 µm section [11, p. 12] and because of the magnetically susceptible np-Fe0 droplets engulfed by agglutinitic glass (see chapter 2.2.1.2). As these unwanted entities are gradually filtered out, the grade of the ore mineral within the simulant can also be passively increased. Strong magnetic fields (>2 T) can even be used to further boost the ilmenite grade, by distinguishing even dia- or paramagnetic particles from one another (*mineral enrichment*).

The third and final decision matrix can be found on the next page. The scoring in table 14 was again substantiated in bullet points, to be found in annex 5. This time, the winner is the permanent magnet drum separator. Crucial for its victory was, among other factors, its *environmental independence*, as variations in air pressure (Berggren already tested it under atmosphere and in vacuum) or gravity (the rotational speed can be adjusted to compensate low gravity) do not affect the system. Its *process integrability* is also splendid, considering that it is an automatable process, which can be operated in a free-fall setup. Such a device would also inherit a tremendous *adjustability & scalability*, insomuch that the number of magnets can be increased to enhance the separator's capacity without changing the overall design, whilst many parameters can be fine-tuned to a given scenario (divider angle, separation point etc.). Ergo, **5** points were given for these criteria. Beyond that, it earned **4** points for its good *energy efficiency* (a low-power, small-scale DC motor suffices). Moreover, it is a comparably compact and lightweight device, so that **4** points were awarded for the criterion *volume & mass*. Again, literature seems to agree with these valuations, as was already mentioned in chapter 3.1.3.

The *simplicity & reliability* did not exceed **3** points, as the technique involves an incremented number of parts – some of them moving at high speeds – which might eventually lead to deterioration or failure during continuous operation. Its *technology readiness* was also estimated to be medium (**3**), as it is highly used in terrestrial applications, but novel for extraterrestrial usage. Its *performance* is double-edged, as "nearly complete recovery of the magnetic materials at very high grade" [20, p. 13] was achieved with a binary mixture, whereas "success with the simulants […] was more modest" [11, p. 13]; to acknowledge this duality, a **3** was awarded. And lastly, the *cost & development* effort was also rated with a **3**, majorly due to the long time needed for the design work.

Table 14: Decision matrix for evaluating the subprocesses of magnetic beneficiation

		Weight	Alternatives		
			Stationary Permanent magnet	Permanent Magnet Drum Separator	Frantz Isodynamic Separator
Criteria	Environmental Independence	0.15	3	5	1
	Simplicity & Reliability	0.05	5	3	3
	Energy Efficiency	0.1	5	4	1
	Volume & Mass	0.1	5	4	1
	Technology Readiness	0.15	5	3	5
	Process Integrability	0.15	1	5	3
	Adjustability & Scalability	0.05	4	5	2
	Performance	0.2	1	3	4
	Cost & Dev. Effort	0.05	5	3	1
	Sum	1.0	3.25	3.9	2.65
	Rank	-	2	1	3

Having elected the winning process for magnetic beneficiation concludes the process assessment & selection. The *permanent magnet drum separator* – along with *dynamic screening* and *tribocharging & plate separator* – will be implemented in the testbed's *setup*, which will be regarded in the following.

3.3.2 Setup

As implicated on page 53, combining the winning processes in order to best exploit their individual strengths is the basis of the deceived testbed's setup. This *multi-stage* approach is not only necessary to fulfill all the system-level functional requirements, but it also follows the example of the *Swiss cheese model*, an often-used engineering method that helps in mitigating risk. The model prevents

single points of failure from endangering the mission objective by adding layers of security – slices of 'cheese' in figure 29 – that may compensate the malfunction ('hole') of another member of the system ('cheese loaf'). In our case, this would mean that if the electrostatic separation alone would not yield the demanded feedstock quality (e.g., because the simulant fails to represent the electric conductivity of lunar regolith), the magnetic separation would make up for this shortcoming by attributing to the mineral enrichment. Thus, the diversification will assure both efficiency (ilmenite increments add up) and reliability (if one process fails, the outcome will still be acceptable) of the system. A multi-stage approach is also encouraged by other researchers. Berggren, for instance, denotes "that a combination of magnetic and electrostatic separation […] could produce even higher ilmenite concentrations" [20, p. 4] and later concludes that the "results suggested that a combined magnetic-electrostatic processing approach would [be] best for concentrating lunar soil ilmenite" [20, p. 5].
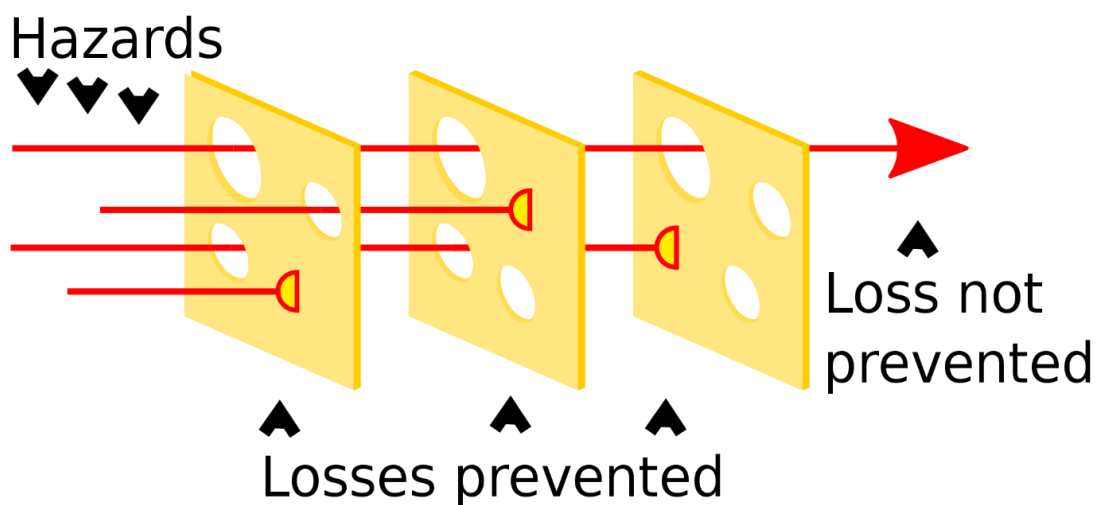

Figure 29: A visualization of the Swiss cheese model [74]

Having decided for a multi-stage approach, the next step in drafting an adequate setup is to put the winning processes in a reasonable *order*. At this, dynamic screening would be a good candidate for the first beneficiation process in the arrangement, as size separation is often considered to be a pre-step to mineral enrichment, increasing its efficiency ("In general, the separations are better when narrowly sized particles are fed" [20, p. 12]) while already advancing the feedstock. Next would be the permanent magnet drum separator, which would remove the dust fraction as well as impurities such as ferromagnetic agglutinates. Dumping the tiniest particles within the simulant prior to electrostatic beneficiation is also suggested by the scientific community, since dust "particles were found to charge up significantly and stick to the chargers and walls, inhibiting regolith flow and preventing other particles from impacting the chargers" [62]. This makes tribocharging in conjunction with a plate separator the last process. Putting electrostatic beneficiation at the end of the chain seems to align well with the procedure authors like Williams [16] suggested, as shown in chapter 3.1.

Having opted for a sequence enables us to come up with a rough *schematic*, which will be a template for the subsequent sketches and later design work. Adding necessities like an inlet, which gathers and stores the raw material until the experiment is started, or an outlet that collects the different waste streams to the above-described order of processes leads to the scheme depicted on the next page.
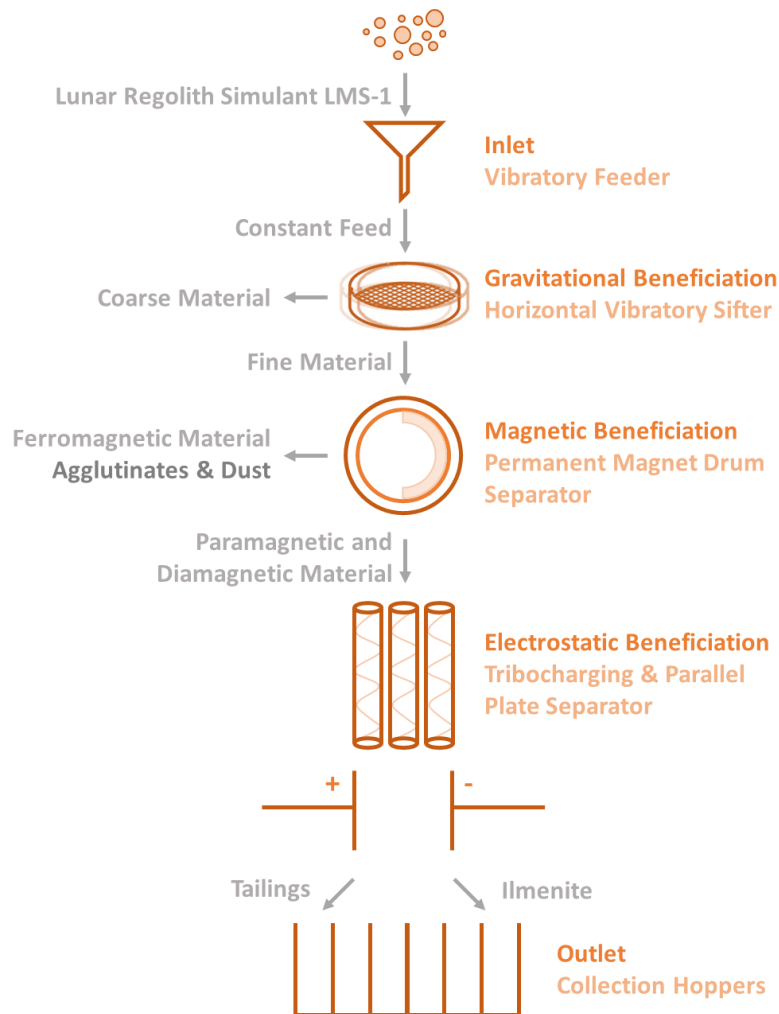
Figure 30: Schematic of the testbed's setup

In view of figure 30, some further aspects of the testbed's *setup* have already been *detailed*. In particular, the three main subsystems (referring to the physical units responsible for the realization of the selected processes) were arranged vertically. Thus, gravity becomes the mode of conveyance, turning the testbed into a free-fall system. This averts the necessity of complex artificial conveyors, making components like pneumatic pumps or conveyor belts untenable, whereby the system becomes simpler, thus, more robust. This configuration is also favorable in consideration of future applications on the Moon, as the low gravity that leads to a decelerated particle flow will result in an overall elevated yield [59]. The type of inlet was defined as a vibratory feeder, as it is the most common (used by Li [58, p. 135], Berggren [20, p. 18] and others) and most abundantly available solution on the market (used in many research domains, from agriculture and the food industry to pharmacy). Furthermore, such devices are precisely tunable, easing the fulfilment of RQ SMU_BEN_007. The process of dynamic screening will be executed by a horizontal vibratory sifter, as these kinds of devices possess the longest heritage, offer a high commercial availability, and experience low wear. Moreover, the electrodes used within the plate separator will be oriented parallelly, so that the electrostatic field between it will be of uniform nature, making it easier to predict a particle's motion within it (by avoiding the dielectrophoresis force; see 3.1.2). Lastly, plain collection hoppers will serve as the outlet, which could be made from easily manufacturable materials like polymers.

The last step within subchapter 3.3.2 is advocated by the methodical breakdown of the system. A *product tree* is the most popular method in this regard, as it helps in identifying all the necessary subsystems and components. The final product tree is provided in annex 6 and briefly described hereupon. In the product tree, the system (the beneficiation testbed) has been split into **6** *subsystems*:

- **Subsystem 1:** Inlet
- **Subsystem 2:** Gravitational Separator
- **Subsystem 3:** Magnetic Separator
- **Subsystem 4:** Electrostatic Separator
- **Subsystem 5:** Outlet
- **Subsystem 6:** Structure

This division made it possible to extend the RQ catalogue by several entries and refine it according to the selected processes, as can be tracked in annex 4. Vice-versa, the necessary *components* were derived from the RQ catalogue (e.g., rollers to fulfill SMU_BEN_020). While most parts are directly listed underneath their respective subsystem, others were additionally grouped into assemblies for the sake of clarity (stator, rotor, and support; charger and separator). All in all, **36** entries were listed on the component level. It should be noted that this only comprises the number of different parts, not their total number (as some parts will be needed in large quantities, such as profiles, nuts, and bolts).

3.3.3 Sketches

The antecedent subchapters already contributed to the generation of an auspicious concept by identifying the processes and describing the setup needed to meet the system's desired range of functions. However, they describe the testbed in a verbal manner, only; thus, it remains hard to vividly imagine its appearance. Chapter 3.3.3 is about to change that by offering a graphic visualization of the fully assembled device and its individual subsystems in the following figures and in annex 7.
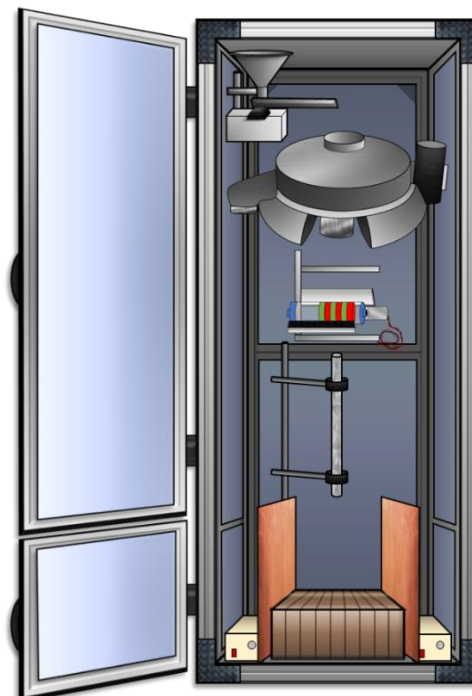

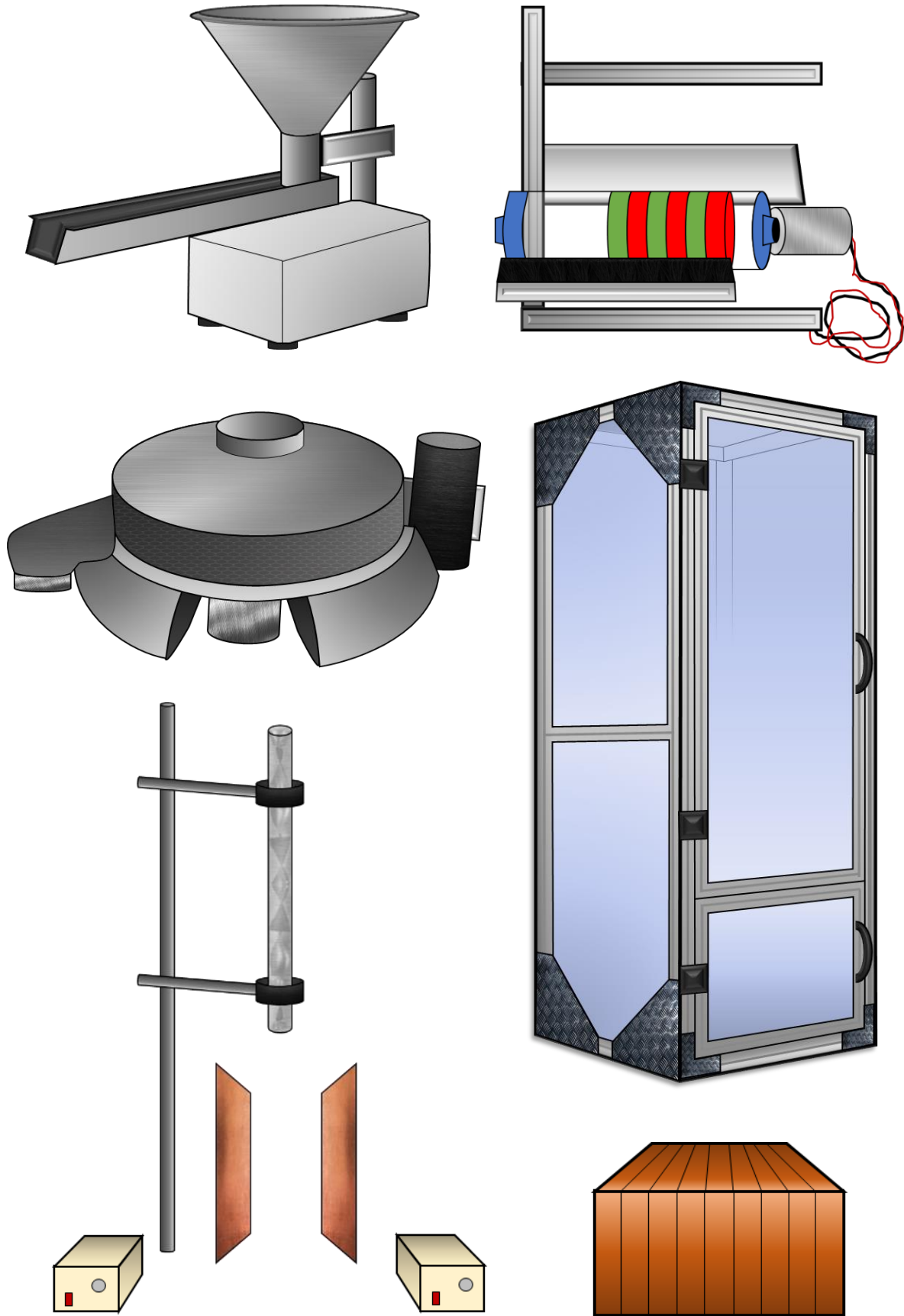**Figure 31: Sketch of the beneficiation testbed at system-level**

Figure 32: Detailed sketches of all subsystems (inlet, mag. sep., grav. sep., structure, elec. sep.& outlet)

3.4 Calculation & Dimensioning

Up to this point, three essential WPs have been tackled, which brought the laboratory test stand into being, while the development process progressed steadily. What is still missing, though, is a quantitative characterization of the system, which would assure that the desired functions and specifications can eventually be reached, while predetermining its most essential dimensions. To remedy this situation, a multitude of relevant design calculations will be performed within chapter 3.4, including the computation of both the magnetic (3.4.1) and electric (3.4.2) subsystems.

3.4.1 Computing the Magnetic Separator

The first calculation to be presented as part of chapter 3.4.1 regards the *capacity* of the permanent magnet drum separator as a function of the *rotational velocity*. This step is prerequisite to fulfill requirement SMU_BEN_007 in conjunction with SMU_BEN_049 (see chapter 3.2), whereat it defines the basic dimensions of the drum rotor and prepares the component selection efforts (see 3.5) by narrowing down the potentially to-be-used DC-motor and magnets. By computing the revolutions per minute (*short*: RPM) that the rotor will have to spin at, it furthermore supports experimenters that will work with the testbed in finding the right process parameters (as inferred in 3.1.3). The calculation is based on the formulas provided in the essay '*Development and Applications of a Drum Medium-Intensity Permanent Magnetic Separator*' by Cao Zhi Liang and others published in 1996 [75].

The formula for the capacity given by Liang et al. comprises the length of the drum L, the linear drum velocity v, the diameter of a particle r_p, the looseness of the feed f (often called porosity), and its mean density ρ [75, p. 138]:

$$Q = L * v * r_p * f * \rho \tag{10}$$

As our final aim is to compute the RPM needed to achieve a given capacity, rearranging the equation to solve for v is the next step. Thereinafter, the linear velocity can be substituted by its counterpart, the angular velocity ω (angular change in position), times the radius of the circular path of motion r (the outer radius of the drum). Lastly, ω (radians per second) in return can be converted into the rotational frequency n (RPM):

$$v = \frac{Q}{L * r_p * f * \rho}$$

$$\omega * r = \frac{Q}{L * r_p * f * \rho}$$

$$\frac{n}{60 \frac{s}{min}} * 2\pi * \frac{rad}{(1/min)} = \frac{Q}{L * r_p * f * \rho * r}$$

$$n = \frac{Q}{L * r_p * f * \rho * r * 2\pi} * 60 \frac{s}{min} * \frac{(1/min)}{rad}$$

With the formula at hand, the values can be inserted. At this, the mean particle size and uncompressed bulk density from the data sheet of the used mare simulant LMS-1 (annex 2) were taken as r_p and ρ. The looseness of the feed is exemplified by the porosity of in-situ lunar regolith at depths up to 60 cm, which was listed in table 2. L and r, the dimensions of the rotor, were predefined in accordance with the design and arc segment magnets used by Berggren (K&J Magnetics AX2C45-N and –S [20, p. 12]). Since only a fraction of the rotor length will be equipped with magnets, the effective length L_{eff} will be put into the equation instead. It was derived as the width of five arc segment magnets stacked together. Lastly, the needed capacity to conform with the RQ catalogue is the nominal flow rate converted into kilograms per second. In numbers, this looks as follows:

$$r_p = 50 \; \mu m = 50 * 10^{-6} m$$

$$\rho = 1.56 \frac{g}{cm^3} = 1{,}560 \frac{kg}{m^3}$$

$$f = 46\% = 0.46$$

$$L = 200 \; mm = 200 * 10^{-3} m$$

$$r = 32.575 mm = 32.575 * 10^{-3} m$$

$$L_{eff} = b_{mag} * n_{mag} = 19{,}05 * 10^{-3} m * 5 = 95{,}25 * 10^{-3} m$$

$$Q = 15 \frac{kg}{h} = 0{,}00416667 \frac{kg}{s}$$

Putting these numbers into the equation now yields the *minimum rotational frequency n_{min}*:

$$n_{min} = \frac{0{,}00416667 \frac{kg}{s}}{95{,}25 * 10^{-3} m * 50 * 10^{-6} m * 0{,}46 * 1{,}560 \frac{kg}{m^3} * 32.575 * 10^{-3} m * 2\pi} * 60 \frac{s}{min}$$

$$* \frac{(1/min)}{rad} = 357.4034 \; \frac{1}{min}$$

Multiplying it with a reasonable safety factor of 2 yields the *wanted rotational frequency n_{wanted}*:

$$n_{wanted} = n_{min} * S = 357.4034 * 2 = 714.8067 \; \frac{1}{min}$$

Accordingly, a DC motor that can provide around 715 RPM should be suited to do the job. This seems to correlate with Berggren's motor choice surprisingly well, as he opted for a "variable speed gear motor (700 rpm at 13 volts dc; Buehler gearhead motor, MPJA part 16392)" [20, p. 12]. As foreboded earlier, this only holds true when arc segment magnets are used that have dimensions similar to the above-mentioned models, which should be a premise during the component selection phase.

The other set of equations presented in Liang's paper shall be the subject of the second and last calculation within this subchapter. It regards the separation of particles from the rotor due to the forces acting on them. In this context, three forces reign the principle of separation on a permanent magnet drum separator, which are mapped in the following illustration.
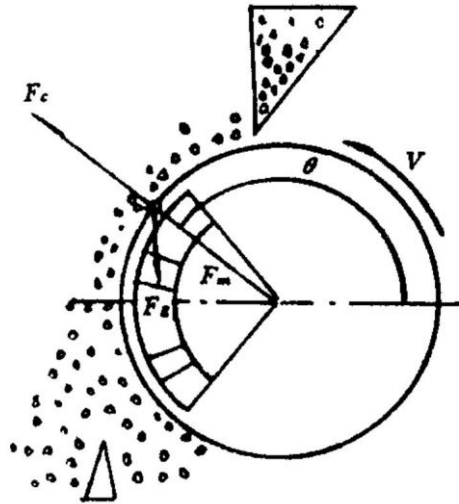
Figure 33: Forces acting on a particle processed by a permanent magnet drum separator [75, p. 137]

The abbreviations in figure 33 stand for the forces already mentioned and described in 2.1.2 (a slightly different, but more precise formula for the magnetic force was given on page 13 and could be used alternatively). Their equations are given below [75, p. 137]:

- **Magnetic Force:** $F_m = \chi H \frac{dH}{dx}$
- **Centrifugal Force:** $F_c = \frac{mv^2}{R}$
- **Force of Gravity:** $F_g = mg$

According to Liang et al., merging the components of the forces yields the collection force applied to the magnetic material at the separation point [75, p. 137]:

$$\mu \chi H \frac{dH}{dx} \geq \mu m \frac{mv^2}{R} + mg * \sin(\Theta) - \mu mg * \cos(\Theta) \tag{11}$$

In our magnetic separator, ferromagnetic particles are supposed to remain stuck on the rotating drum when it turns with the previously determined RPM (left term of formula 11 dominates), whereas para- and diamagnetic minerals like ilmenite should be thrown off at some point by the drum's motion, following its own trajectory (magnetic attraction becomes inferior so the right side of equation 11 prevails). Checking the feasibility of the magnetic separator by assuring that this really is the case, is the very aim of this calculation.

Even though formulae exist to quantify the attractive force of a permanent magnet, it soon becomes apparent that an analytic contemplation does not get us very far, as the magnetic field intensity $\vec{H}$ and the magnetic field gradient $\frac{d\vec{H}}{dx}$ both sharply vary with the position of the respective particle within the magnetic field, which cannot be regarded by hand. To circumvent this fact, numeric simulations were preferred for the determination of the magnetic force. The open-source application FEMM (acronym for Finite Element Method Magnetics) was used to model a 2D-section of the separator such that its magnetic field could be simulated. This was done by firstly adding nodes, which could then be connected to circular arcs. The dimensions of these geometries were adapted to the size of the K&J

Magnetics arc segments (1 1/8" outer radius; 1" inner radius; 3/4" thickness; 45°). Secondly, the areas enclosed by these geometries were assigned the corresponding materials, so that the program can simulate their magnetic properties; Neodymium with a grade of N50 was selected to match Berggren's magnets, air was chosen for the surrounding fluid. Before starting the simulation, the alternation of polarities was set. The simulation's result is depicted hereunder:
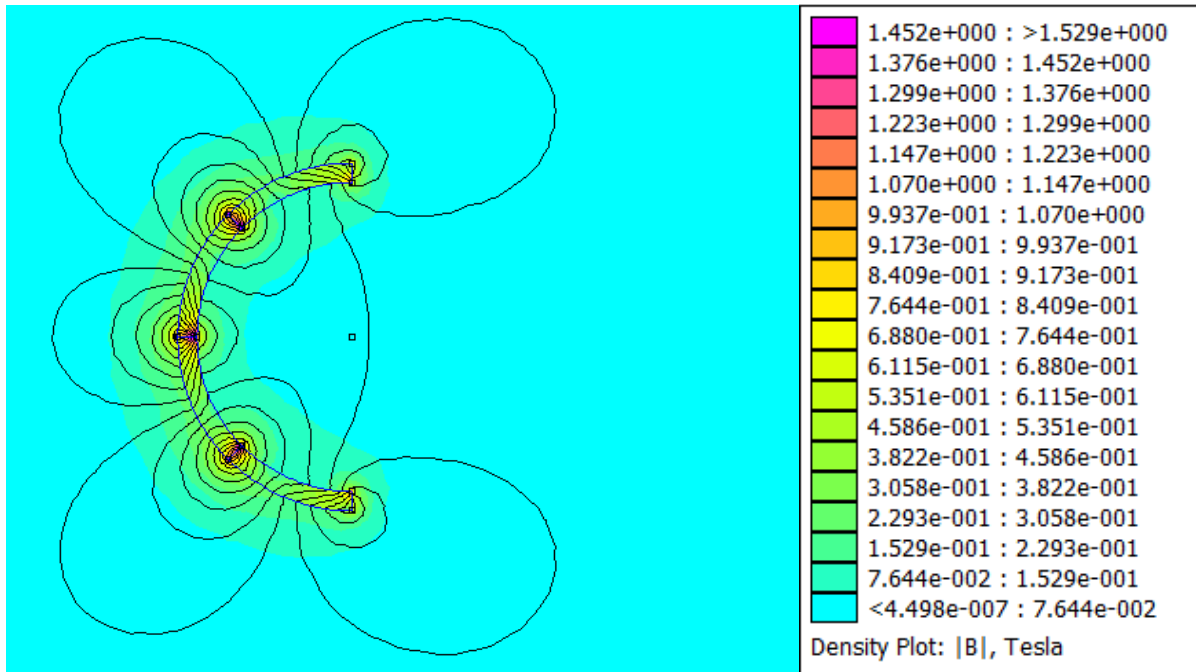

Figure 34: FEMM simulation of the magnetic field

Seeing that the simulation outputs reasonable results (field lines follow correct path and values are in the right order of magnitude) motivates to utilize this model for the determination of the magnetic forces that act upon both ilmenite and ferrous particles in the field at two different locations (at 90°, where the particles are fed, and at 135°, a likely separation point). Therefore, circular areas of a diameter that matches the average grain size were plotted and assigned with suitable properties (susceptibility values given in 2.2.2 were used to create custom materials). The gap between particles and the magnet was chosen to mimic the outer tube. Screenshots of the investigation's results are shown in annex 8.

Using the values output by the numeric simulation, we can finally calculate all forces to be inserted into formula 11. Starting with the easiest: The force of gravity is the product of mass and gravitational acceleration (9.81 $\frac{m}{s^2}$ on Earth, as explained in 2.3). The unknown mass can be substituted by the product of the density and volume ($V = \frac{4}{3}\pi r_{average}^3 = \frac{4}{3}\pi * (0,006\ cm)^3 = 9,0478 * 10^{-7}\ cm^3$ for an idealized, spherical shape) of an average ilmenite grain (properties defined in 2.2.2):

$$F_g = mg = \rho V g = 4.75 \frac{g}{cm^3} * (9,0478 * 10^{-7}\ cm^3) * 9.81 \frac{m}{s^2}$$
$$= 4.2977 * 10^{-9} kg * 9,81 \frac{m}{s^2} = 4.2160 * 10^{-8} N$$

Next, the centrifugal force is the previously calculated mass of an ilmenite particle multiplied by the linear velocity of the drum squared, divided by its diameter (the r from calculation 1 doubled). Beforehand, the earlier elucidated relation between linear and angular velocity was now applied the other way around to get from the RPM of the first calculation to the corresponding linear velocity:

$$\omega = \frac{n}{60\frac{s}{min}} * 2\pi * \frac{rad}{(1/min)} = \frac{357.4034\frac{1}{min}}{60\frac{s}{min}} * 2\pi * rad = 37.4272\frac{rad}{s}$$

$$v = \omega * r = 37.4272\frac{rad}{s} * (32.575 * 10^{-3}m) * \frac{1}{rad} = 1.2192\frac{m}{s}$$

$$F_c = \frac{mv^2}{R} = \frac{4.2977 * 10^{-9}kg * \left(1.2192\frac{m}{s}\right)^2}{65.15 * 10^{-3}m} = 9.8054 * 10^{-8}N$$

Lastly, the directional components of the magnetic force vector determined during the FEMM analysis will have to be merged to obtain the magnitude of the magnetic force on the ilmenite grains:

$$\left|\vec{F}_{m,90°}\right| = \sqrt{F_{m,x}^2 + F_{m,y}^2} = \sqrt{(8.0772 * 10^{-10}N)^2 + (2.19893 * 10^{-8}N)^2} = 2.2004 * 10^{-8}N$$

$$\left|\vec{F}_{m,135°}\right| = \sqrt{F_{m,x}^2 + F_{m,y}^2} = \sqrt{(8.46491 * 10^{-10}N)^2 + (1.35906 * 10^{-8}N)^2} = 1.3617 * 10^{-8}N$$

At last, we can insert the calculated forces into a tidied formula 11, while also applying the values for the coefficient of friction μ (the tabular value for polycarbonate was chosen for it is Berggren's drum material [20, p. 12] and shall, thus, be premised henceforth) and the respectively observed angle θ.

$$\mu * F_m \geq \mu m * F_c + F_G * \sin(\Theta) - \mu * F_G * \cos(\Theta)$$

$$0.31 * 2.2004 * 10^{-8}N$$
$$< 0.31 * 9.8054 * 10^{-8}N * 1.68409 * 10^{-7}N + 4.2160 * 10^{-8}N$$
$$* \sin(90°) - 0.31 * 4{,}2160 * 10^{-8}N * \cos(90°)$$

$$6.8213 * 10^{-9}N < 4.2160 * 10^{-8}N$$

$$0.31 * 1.3617 * 10^{-8}N$$
$$< 0.31 * 9.8054 * 10^{-8}N * 1.68409 * 10^{-7}N + 4.2160 * 10^{-8}N$$
$$* \sin(135°) - 0.31 * 4{,}2160 * 10^{-8}N * \cos(135°)$$

$$4.2213 * 10^{-9}N < 3.9053 * 10^{-8}N$$

It can be seen, that – at both positions – the ilmenite particle will not readily adhere to the drum but will instead be propelled and projected away by the dominant dynamics, meeting the earlier stated expectations. Realizing that the magnetic forces on ferrous particles (see annex 8) are orders of magnitude higher than the right term's results makes the repetition of this procedure needless, as it already indicates that they will stick to the surface with great confidence. Thus, the feasibility of the magnetic separator's concept is quantitatively safeguarded.

3.4.2 Computing the Electrostatic Separator

The other half of chapter 3.4 is allotted to the quantitative delineation of the testbed's electrostatic subsystem. Subchapter 3.4.2 will therefore depict how the homogeneous electric field and the parallel plate separator that creates it were quantitatively characterized. In a second step, the trajectory of a given mineral grain in such a field is computed and will be presented as part of a parametric model.

The parallelly orientated electrodes of the electrostatic separator can be described through the physics theory of the parallel-plate capacitor. The field lines of the homogeneous electrostatic field it creates accordingly flow from plus to minus, as can be seen in figure number 35.
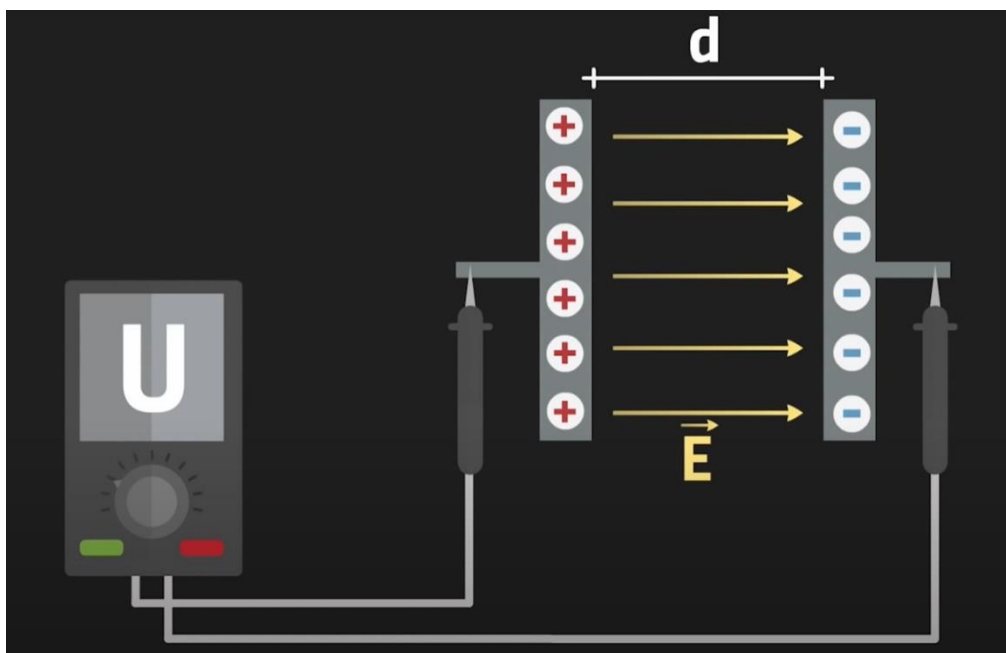

Figure 35: Schematic of a parallel-plate capacitor and the homogeneous electric field it creates [76]

As implied in the illustration, a mathematic connection between U (the voltage applied to the electrodes), the distance d between the plates, and the electric field strength $\vec{E}$ exists [76]:

$$U = \vec{E} * d \tag{12}$$

With respect to the values of these parameters, U can be dimensioned freely, while this decision defines the maximum voltage that the to-be-selected HV DC power supply (from the product tree) must be able to provide. In this context, example values from 3.1.2 were used as a point of reference:

- **Li, 1999:** $U = 0 \dots 20kV$ [58, p. 135]
- **Trigwell, 2006:** $U = 5 \dots 30kV$ [59, p. 4]
- **Trigwell, 2009:** $U = \pm 15kV$ [61, p. 1062]
- **Trigwell, 2012:** $U = \pm 30kV$ [62, p. 4]

Based on this, a value of ±25 kV was selected, which is a new premise for the component selection WP. The distance d is a dimension that can be chosen more or less arbitrarily; however, a smaller gap is preferable to acquire a high field strength. On the other hand, the gap should not be too small, to

prevent particles from colliding with the electrodes (a contact-free deviation of the particle's trajectory is preferred to avoid adherence to the plates). The consultation of chapter 3.1.2 implied that 10 cm would be a reasonable value, which was among others suggested by Li [58, p. 135]. Formula 12 can now be rearranged to solve for the missing quantity $\vec{E}$:

$$\vec{E} = \frac{U}{d} = \frac{|\pm 25kV|}{0.1m} = \frac{50kV}{0.1m} = 500\,\frac{kV}{m}$$

Quantifying the energy of the electric field would be the next goal. In order to do so, formula 13 [76] must be used beforehand to calculate the capacity of the plate capacitor:

$$C = \varepsilon_0 * \varepsilon_r * \frac{A}{d} \tag{13}$$

It is calculated as the relative permittivity of the vacuum ε_0 (a natural constant of $8.85 * 10^{-12}\frac{F}{m}$) multiplied by the relative permittivity of dielectric ε_r (the material between the plates), again multiplied by the quotient of a plate's area A and the distance d. For air as the medium, ε_r acquires a value of 1,00059. Nevertheless, we will primarily regard the vacuum-case, making it a neutralized factor of 1. A is again a parameter that can be chosen to scale the respective component. Trigwell, for instance, used rectangular copper-clad plates of 6" $*$ 12" [59, p. 5] (roughly 465 cm²), which is similar in surface area to what Li suggested (38.1 cm $*$ 14 cm [58, p. 135], resulting in approx. 533 cm²). A commercially available plate capacitor in a comparable shape and format was already sought in order to have reliable values for the calculation (the process of finding it will be elaborated during 3.5); its dimensions are 28.3 cm $*$ 28.3 cm. As a consequence, the capacity of the separator in vacuum is:

$$C_{vac} = 8.85 * 10^{-12}\frac{F}{m} * 1 * \frac{0{,}283m * 0{,}283m}{0{,}1m} = 7{,}0879pF$$

With that said, formula 14 [76] finally yields the energy of the electric field:

$$E_{el} = \frac{1}{2} * C * U^2 \tag{14}$$

$$E_{el,vac} = \frac{1}{2} * 7{,}0879pF * (50kV)^2 = 8.8598 * 10^{-3}W$$

This concludes the first task of 3.4.2, as the parallel-plate separator and its electric field are now sufficiently characterized. During the process, all major variables regarding the power supply (U) and plates (d, A) have been dimensioned. The now following, second calculation will be based on these parameters with the aim of computing the particle trajectory in the above-characterized electric field.

Two forces govern the trajectory of a mineral grain in a parallel-plate separator as part of a free-fall system in vacuum (i.e., neglecting air drag). The Coulomb force, which represents the characteristic electrostatic force present in a homogeneous electric field (as explained in 2.1.2.2.1), acts in the y-axis (horizontally). The force of gravity, which was already referred to multiple times now, acts in the x-direction (vertically). As such, they follow the superposition principle, as is depicted in figure 36 on the next page.
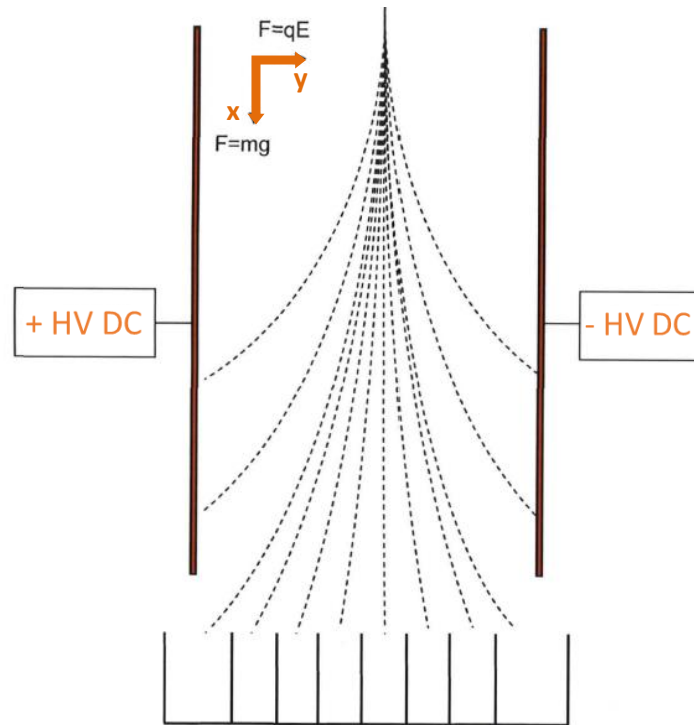
Figure 36: Trajectories of different particles in a homogeneous electric field [62, p. 18]

According to formula 2 given in chapter 2.1.2.2.1, the Coulomb force equals the product of the electric field strength (known) and the particle's electric charge (unknown). The missing quantity – the maximum charge that a particle may obtain from tribocharging – can be computed using yet another formula from the foundations chapter: The Harper equation (eq. 5). This shall be done exemplarily for an ilmenite grain ($\phi_{p,ilmenite} = 4.29$ eV from annex 3) and an olivine grain ($\phi_{p,alu} = 7.9$ eV) of 50 μm gran size (average for particles within the LMS-1 simulant), which triboelectrically charge with aluminum walls (the material that performed optimally [3.1.2], with $\phi_{s,alu} = 4.28$ eV [61, p. 1064]):

$$\frac{q_{p,max,ilmenite}}{m} = 2.66 * 10^{-13} \left(\frac{\phi_s - \phi_p}{\rho_p * r_p^2}\right) \left(8.85 + 1.151 \log_{10} r_p\right)$$

$$= 2.66 * 10^{-13} \left(\frac{4.28 \ eV - 4.29 eV}{4750 \frac{kg}{m^3} * (5 * 10^{-5}m)^2}\right) (8.85 + 1.151 * \log_{10}(5 * 10^{-5}m))$$

$$= -8{,}7349 * 10^{-10} \frac{C}{kg}$$

$$\frac{q_{p,max,olivine}}{m} = 2.66 * 10^{-13} \left(\frac{\phi_s - \phi_p}{\rho_p * r_p^2}\right) \left(8.85 + 1.151 \log_{10} r_p\right)$$

$$= 2.66 * 10^{-13} \left(\frac{4.28 \ eV - 7.9 eV}{3250 \frac{kg}{m^3} * (5 * 10^{-5}m)^2}\right) (8.85 + 1.151 * \log_{10}(5 * 10^{-5}m))$$

$$= -4.62144 * 10^{-7} \frac{C}{kg}$$

Multiplying the obtained values with the respective grain mass is done in an effort to pave the way for the calculation of the Coulomb forces acting on the two particles. The grain masses are derived in the way outlined in 3.4.1 (densities are taken from annex 3). All three steps are conducted hereupon:

$$V_{idealized\ sphere} = \frac{4}{3}\pi r_{average}^3 = \frac{4}{3}\pi * (0.005cm)^3 = 5.2360 * 10^{-7}\ cm^3$$

$$m_{ilmenite} = \rho V = 4.75\frac{g}{cm^3} * (5.2360 * 10^{-7}\ cm^3) = 2.4871 * 10^{-6}g = 2.4871 * 10^{-9}kg$$

$$m_{olivine} = \rho V = 3.25\frac{g}{cm^3} * (5.2360 * 10^{-7}\ cm^3) = 1.7017 * 10^{-6}\ g = 1.7017 * 10^{-9}kg$$

$$q_{p,max,ilmenite} = \frac{q_{p,max,ilmenite}}{m} * m_{ilmenite} = -8{,}7349 * 10^{-10}\frac{C}{kg} * 2.4871 * 10^{-9}kg$$
$$= -2.1725 * 10^{-18}C$$

$$q_{p,max,olivine} = \frac{q_{p,max,olivine}}{m} * m_{olivine} = -4.62144 * 10^{-7}\frac{C}{kg} * 1.7017 * 10^{-9}kg$$
$$= -7.8643 * 10^{-16}C$$

$$\vec{F}_{C,ilmenite} = q_{p,max,ilmenite} * \vec{E} = -2.1725 * 10^{-18}C * 5000{,}000\frac{V}{m} = -1.0863 * 10^{-12}N$$

$$\vec{F}_{C,olivine} = q_{p,max,olivine} * \vec{E} = -7.8643 * 10^{-16}C * 500{,}000\frac{V}{m} = -3.9322 * 10^{-10}N$$

The negatively charged particles will accordingly be dragged towards the positively charged electrode. It can already be seen that the resulting Coulomb forces differ by orders of magnitude – implying that the two minerals can be separated noticeably. The pull of gravity will, on the other hand, let the particles cascade downwards. It can be quantified following the procedure elucidated in 3.4.1:

$$F_{g,ilmenite} = m_{ilmenite} * g = 2.4871 * 10^{-9}kg * 9.81\frac{m}{s^2} = 2.4398 * 10^{-8}N$$

$$F_{g,olivine} = m_{olivine} * g = 1.7017 * 10^{-9}kg * 10^{-9}kg * 9.81\frac{m}{s^2} = 1.6694 * 10^{-8}N$$

As both forces permanently act on the particles, their positions and velocities in x- and y-direction are subject to a constant change, or mathematically speaking: They are functions of time. This is taken into account by the following equations of motion [76]:

$$x(t) = -\frac{1}{2} * g * t^2 + x_0 \tag{15}$$

$$v_x(t) = -g * t \tag{16}$$

$$y(t) = \frac{1}{2} * \frac{U}{d} * \frac{q}{m} * t^2 \tag{17}$$

$$v_y(t) = \frac{U}{d} * \frac{q}{m} * t \tag{18}$$

Using these formulae to calculate the variables at multiple instants in time by hand would quickly turn out to be too laborious or would entail a poor resolution (if a small sampling rate was chosen instead). This problem is exacerbated by the fact that other particle parameters (different mineral types [i.e., particle work function ϕ_p] and sizes r_p) and boundary conditions (different static charger material [i.e., surface work function ϕ_s], gravitational acceleration g, U, A or d) should be simulatable. To make allowance of these functions, a parametric model (see annex 9) that accepts user inputs via various preference panels and outputs the resulting values in a table was deliberated, which is based on equations 15 to 18. The table of values was further used to plot the trajectories in a 2D diagram:

Figure 37: Resulting trajectory plotted on a 2D-diagram as the output of the parametric model

It shows that – using static chargers made from aluminum under terrestrial gravity – ilmenite grains would always land in the central collection hopper (because $\vec{F}_{C,ilmenite} \ll F_{g,ilmenite}$), whereas minerals with a better chargeability like olivine would experience an appreciable deviation, which would draw them towards the positive electrode. This observation proves the feasibility of the electrostatic separation subsystem within our beneficiation testbed, which successfully concludes chapter 3.4 at last. The interested reader may find additional plots with other preferences in annex 9.

3.5 Component Selection

If all the parts listed in the product tree were meant to be newly developed and custom-built, we could already proceed to the design activities, as a quantitively validated concept is now at hand. However, designing and manufacturing everything in-house is too expensive, for one thing, and way too labor-intensive to be realized by one engineer as part of a six-month thesis, for the other. Thus, the nomination of ready-made, commercial off-the-shelf (*short*: COTS) parts will be an intermediate step, to be parenthesized between the calculation and design chapters. In the course of this, an internet research was done in an effort to scan the market for potential products. Generally, laboratory-certified or industry-ready solutions were focused on, as they are best-suited for the testbed. Promising candidates for the more complex, yet most essential units were shortlisted in the form of tables, which are portrayed in annex 10. This pertains the vibratory feeder (inlet), sifter (gravitational separator), arc segment magnets (magnetic separator), and HV DC power supply (electrostatic separator). Thereupon, a winner was selected, to be implemented in the test stand's prospective CAD model. These leading products shall be introduced succinctly, so that the reader may get an idea as to their range of function and unique selling points. It was assured that all selected products would accord to the applicable RQs, which will be highlighted throughout this subchapter.

Starting with the inlet: It is supposed to continuously convey a uniform stream of the bulk regolith simulant and feed it into the vibratory sifter (SMU_BEN_033). Furthermore, it was stipulated that it should consists of two units – the *vibratory feeder* itself and an external control panel, which enables the operator to adjust the feed rate during the experiment (SMU_BEN_034). Consulting the RQ catalogue, it should further be compatible to Schuko sockets (SMU_BEN_038) and the European power grid (230 V @ 50 Hz AC). A device that meets these and the other inlet-related criteria is the *Laborette 24* (see figure 38) by *Fritsch*, a German manufacturer for laboratory equipment.

Figure 38: The vibratory feeder of choice - the Laborette 24 - and its external control unit [77]

Its V-shaped, stainless-steel channel in conjunction with the microprocessor-controlled vibration motor allow for a very precise and fine-tunable flow rate, while also offering a surprisingly broad range of $1 \dots 1500 \frac{g}{min}$ [77] (fulfilling SMU_BEN_035 with ease). Its 1.4 Liter funnel – also made from stainless-steel – conforms to SMU_BEN_006 with a comfortable margin. Besides, the height of this funnel (with respect to the channel) can be adapted to the bulk material's properties. Moreover, the device convinces with a low noise level (approx. $L_{pAd} = 34dB$) and compact size ($44 * 14 * 34\ cm$) [77], so that it supposedly aligns with SMU_BEN_037. Bearing all these factors in mind, it was chosen as the COTS inlet for SMU's beneficiation test bench.

With regards to the gravitational separator, **16** suitable *sifter* models by **11** different manufacturers were identified during the market analysis – most of them of European origin, whereas many others are sold by Asian companies. The *Russel Compact Sieve* (see figure 39) by the British enterprise *Russel Finex* is the winner of this shortlist.

Figure 39: Russel Compact Sieve on an optional stand [78]

This circular vibratory sifter can effectively remove oversize from the bulk material (SMU_BEN_040). The oversize is ejected to the side (SMU_BEN_042), whereas the good part cascades downwards and exits the sifter axially, where it may be received by the magnetic separator (SMU_BEN_041). This secures continuous operation, as no manual removal of the accumulating oversize is needed (which would have been necessary with e.g., the JEL Fix II by the J. Engelsmann AG [annex 10]). Moreover, it is trusted by many different industries and used for several different tasks, "including sieving pharmaceutical powders, various food powders and powder paint" [78]. While it is indeed well-suited for screening powders at industrial scales, it was also used in research and explicitly mentioned in lunar beneficiation studies by Wilkinson [56]. Its compact form factor is also a persuading attribute, as the sifter will probably be the biggest part of the testbed, therefore defining its width and length. As the Russel Finex' product line also offers auxiliary ultrasonic deblending gear, SMU_BEN_043 is satisfied, too (its necessity shall be tested during experiments). Beyond that, a "tool-

free, quick-release mechanism allows for easy disassembly and cleaning" [78], minimizing the assembly time. In addition, the housing that encloses the mesh screen, prevents dust and fumes from escaping, mitigating the hazard of dust explosions. Lastly, a "rubber suspension system dampens mechanical noise, ensuring quiet operation" [78] and an optimal force transmission (SMU_BEN_048).

Concerning magnetic beneficiation, the best fitting *arc segment magnets* were looked for. During this search, neodymium-iron-boron (NdFeB) was set as the material, for it offers a remarkably high magnetic flux density (strongest permanent magnets commercially available). These state-of-the-art magnets are graded according to their maximum energy product, which directly relates to their pull force. Beyond this factor, the COTS magnets were evaluated based on their dimensions (which should be similar to the ones from chapter 3.4.2), price, and direction of magnetization (radial, diametral, or axial). The winner was the often-cited *AX2C45-N* and *-S* by *K&J Magnetics*.
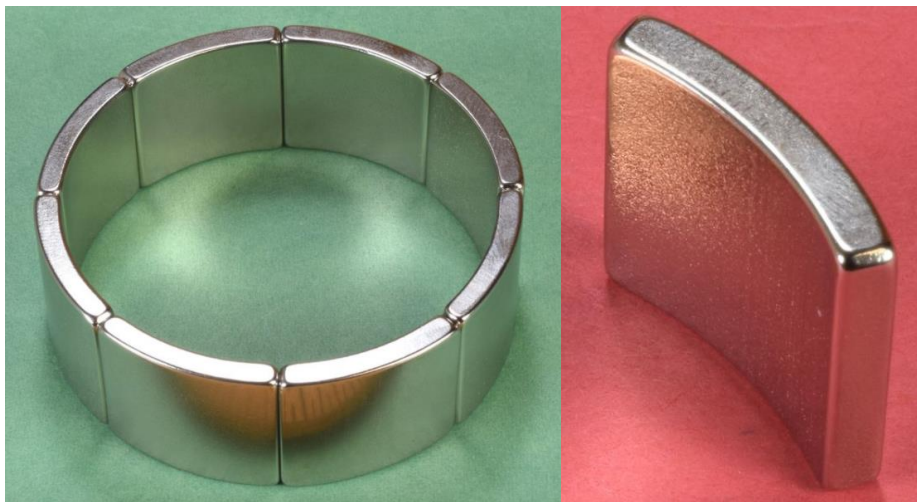

Figure 40: Arc segment magnets by K&J Magnetics (in a ring of alternating polarity and single copy) [79]

First and foremost, this decision is based on its pertinent heritage, as its utility for lunar mineral enrichment was already demonstrated in experiments by Berggren. Secondly, another arc segment magnet with such a high grade (N50) and corresponding pull force (12.6 lbs [79]) was not found. Even if compromises in terms of grade were to be made, a product of a grade higher than 42 in conjunction with these dimensions (1.1/8" o.r. x 1" i.r. x 3/4"x 45° [79]) was not found. Another attribute seldom found amongst competitors was the radial magnetization (diametral or axial magnetization is not favored for the use in a drum separator). Lastly, its nickel coating will prevent corrosion in the long run, making it a durable and maintenance-free solution. Since this exact model was opted for, the calculations of 3.4.1 are still valid and do not need to be adapted, making the development process a lot more efficient.

In this context, a suitable DC motor was also identified (without the methodical approach, as it is less of a mission-critical part). The RS PRO brushed geared DC motor was selected. It can spin at 897 RPM ($n_{wanted} = 714.8067 \frac{1}{min}$) and deliver a torque of 10 Ncm through a 6 mm wide and 12 mm long chamfered shaft [80]. It will be powered by the Basetech BT-153 DC power supply, which was selected for its superior cost-benefit ratio ($U_{DC} = 0 \dots 15\ V$; $I = 0 \dots 3\ A$; $P_{max} = 45\ W$) [81].

Speaking of power, the *HV DC power supply* for the electrostatic separator was again found during a market examination (in annex 10). The seven shortlisted products were compared in terms of output and input voltage, power, application area, and price (which will not be disclosed, as most prices were available on request, only). In doing so, the *PHYWE 13671-93* (see figure 41 left) was selected as the winner. It exactly matches the previously computed output voltage ($U_{wanted} = \pm 25$ kV from 3.4.2), provides an excellent value at a very low cost (competitors would often cost 2-3 times as much), and comes in a portable, impact-proof, and stackable casing [82]. Furthermore, it is compatible with the 230 V grid (SMU_BEN_038) and offers high safety (short-circuiting-proof and safety jack sockets used).

Figure 41: The PHYWE HV DC power supply (L) and plate capacitor (R) [82]

PHYWE is a German business that develops, manufactures, and sells scientific equipment for research and educational purposes. Hence, it does not only offer electronics, but also other accessories needed for popular experiments. One of them demonstrates Coulomb's Law and involves a ready-for-use plate capacitor (see figure 41 R) and HV-suited cables. Buying all components for the separator assembly from one supplier guarantees compatibility and safety of operations (both top-priority features), as not only the components on an individual level, but also the setup as a whole was already tested and validated. Thus, the $28.3\ cm * 28.3\ cm * 0.4\ cm$ aluminum plate capacitor with insulating stems (*06233-00*) and the $30kV$, 1000 mm long cords (*07367-00*) are nominated alongside the power supply.

With respect to the other assembly of the electrostatic separator – the charger – there is only one COTS part to be selected: The heat tape (used to heat the feed and air around it to increase the conductivity of the minerals, effectively boosting the separation performance as suggested by Agosto in 3.1.2). The German brand ISOHEAT offers an abundant catalogue of different options. The MiL-HT-PSG (PTFE-isolated; 230 V AC; $T_{max} = 260°C$; IP 64 splashproof) was chosen in this regard [83].

Lastly, to conform with SMU_BEN_028, the structural components will be selected from the product catalogue of *ITEM*, a German manufacturer for modular aluminum profiles and accessory. This process, however, will be explained in more detail (while citing the applicable RQs) over the course of the subsequent chapter, as it is part of the design process, which will be elaborated hereupon.

3.6 Design

Heretofore, the beneficiation test bench has been characterized verbally, visually, in numbers, by use of diagrams, and through tables; hence, the basis for a methodically sound apparatus has already been set. With all the necessary data at disposal, the aggregated information can now be incorporated into a 3D model using CAD applications. This job will be carried out using Dassault Systèmes' CATIA V5 (the construction program used at the DLR subsidiary in Bremen). As such, chapter 3.6 will minutely portray the work done during the design process; it is further divided into subchapters to emphasize the transition from a conceptual, preliminary (3.6.1) to a more technical, detailed design (3.6.2).

3.6.1 Preliminary Design

Commencing with the preliminary design (*short*: PD): It is an effort to translate the 2D sketches into 3D models, to materialize the product tree or, taken all together, to bridge a gap between the concept (3.3) and detailed design activities [55]. Over the course of the PD, new *CATPARTs* (native CAD format; lower tier) will be designed from scratch in line with the dimensions from 3.4 using CATIA's *Part Design* and *Generative Shape Design* (*short:* GSD) workbenches, while digital representations of the chosen COTS components (3.5) will be recreated from technical drawings or *STEP* (neutral CAD format) files. Furthermore, the components will be assembled in *CATPRODUCTs* (upper tier) and integrated into one big file. Packaging these units within this file using CATIA's *Assembly Design* tools will be done thereupon to refine the system configuration and avoid collisions. Lastly, parametric-associative models of the designated structural elements will be created, whose dimensions are coupled to this configuration, allowing them to smoothly wrap around the other subsystems in an agile manner. Now, before elucidating the PD work in greater detail, the result of this first half of the design process are shown with the aim of enhancing the reader's imagination throughout subchapter 3.6.1:
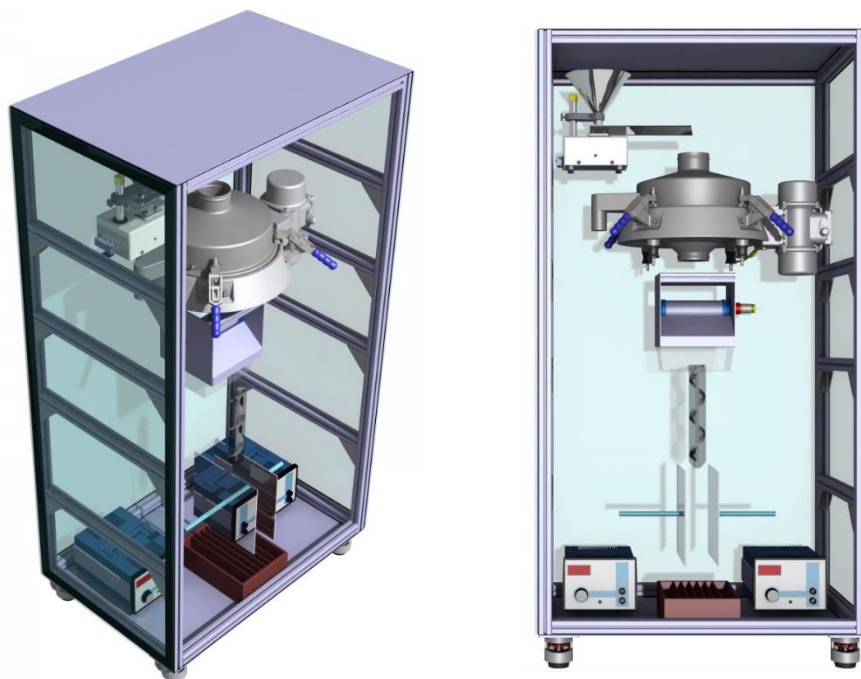

Figure 42: Rendered images showing different perspectives of the PD's outcome

Starting from the top: The 3D models of the *Laborette 24* and the *Russel Compact Sieve* shown in figure 42 were derived from STEP models, which were provided by their respective manufacturer after a formal purchase request, sent as part of the upcoming production planning (3.7). In the meanwhile (and for the most part of the design phase), rough dummies were used instead to block the installation space to be occupied by these not-yet-available models. In the process of creating the dummies, publicly available sources (websites, datasheets, etc.) were consulted to obtain their rough geometry and external dimensions; an appropriate offset was added supplementarily. For illustrative purposes, a screenshot showing these dummies in comparison to their later STEP models is provided here below:
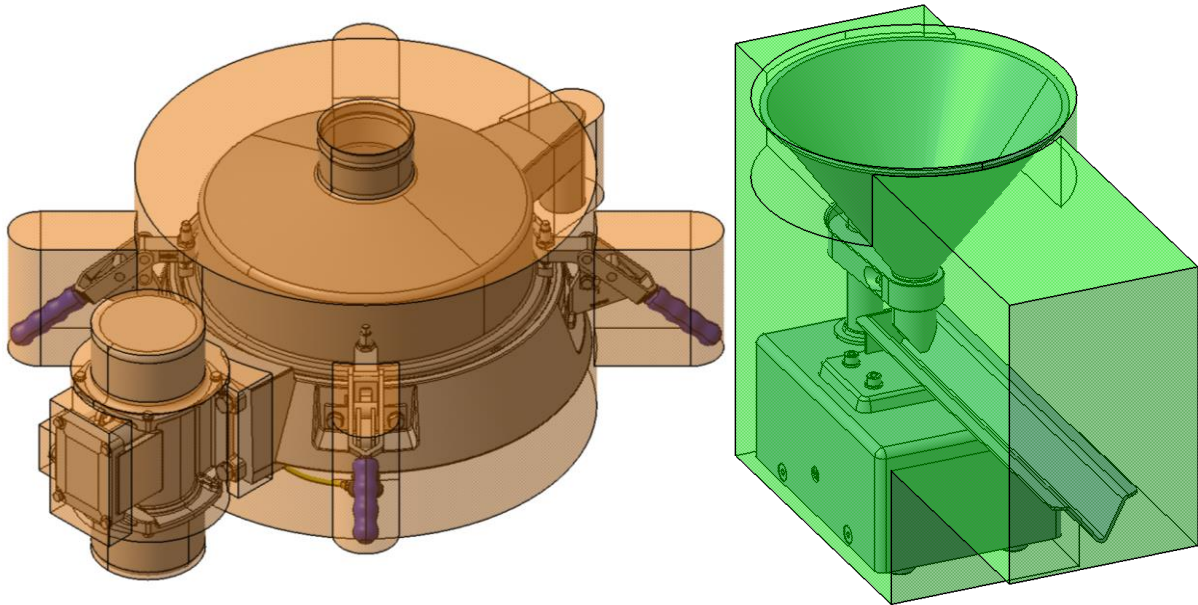

Figure 43: Dummies representing the installation space to be occupied by the sifter (L) and feeder (R)

Continuing downwards, the next subsystem in the chain is the magnetic separator. It was newly developed and built around the selected magnets. Its design started with the *inner tube* of the stator, which was created extruding a circular profile with a diameter of 25.4 mm, i.e., 1" (3.5) by 200 mm (3.4.1). Offsetting the resulting cylinder by 0.32 mm, i.e., 0.125" (chosen as the wall thickness to match the magnet's imperial dimensions) and enclosing the surfaces finished this part. The *arc segment magnets*, which would sit on the side of this tube, were modeled using the dimensions from 3.5 and duplicated to form a row of five magnets (3.4.1) with four magnets per column ($4 * 45° = 180°$). The *outer tube* (rotor) was designed thereinafter; its inner diameter was set as the magnet's outer diameter plus an air gap of 1 mm. Again, an offset was created and filled to convert the shape into a solid. At the tubes' end, *caps* were designed using CATIA's pad, chamfer, and fillet functions. They encapsule the tubes (preventing dust from entering) and hold the assemblies in place. *Ball bearings* were inserted between them, to allow for a low-friction rotation of the outer tube, while the inner one remains stationary (a placeholder was inserted during 3.6.1 and will be specified as part of 3.6.2). This compound was then integrated into a *frame* consisting of four line 6 ITEM profiles ($30 * 30 \, mm$ [84]) of 230 mm length and two end plates ($230 * 230 * 0.25 \, cm$), which support the stator and rotor. Flat plastic panels would act as a *covering* and conceal the frame's top and sides. The selected *DC motor* was recreated based on a technical drawing and attached to the right plate of the frame.

A bent sheet-metal part was then constructed to form a *ramp* that collects the dia- and paramagnetic constituents within the simulant, which would fall off the drum due to the superior dynamic forces (3.4.1), effectively separating the flow into two portions. The ferromagnetic tailings, which would stick to the drum, would be brushed off by an antistatic *brush*, whose design is inspired by domestic appliance. It was positioned at the separator's back (0° in reference to 3.4.1) and fixed to the profiles. The tumbling-down tailings would be caught and stored in a 2-liter, frustum-shaped *vessel*, attached to the separator's bottom (7° draft angle). When all these parts are put together, the preliminary magnetic separator bears a striking resemblance to its idol (the 2D sketch provided in figure 32):
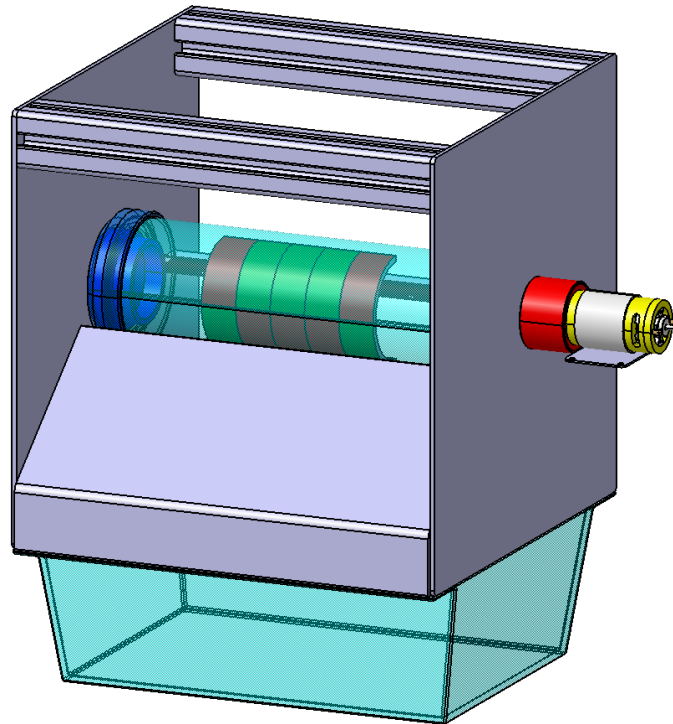

Figure 44: Close-up of the magnetic separator's PD model

Having passed the magnetic separator, the ilmenite-containing portion would fall into the electrostatic separator's charger, whose design is to be regarded next. Encapsuled by a thin-walled *outer tube* ($d_i = 50\ mm; t = 2\ mm$), the *static mixer* (responsible for tribocharging the grains) is the assembly's centerpiece. Its corkscrew-shaped surface was derived from a rectangular profile and a helix spline ($h = 575mm$; 5 revolutions), which were fused using the sweep command within the GSD workbench. A central rod ($d_o = 10\ mm$) clings to the swept surface, thus, stabilizes the static mixer and prevents particles from taking a shortcut. At the bottom – were the static mixer ends – the outer tube is tapered to a small outlet diameter of 20 mm, so that the material can be interspersed slowly and precisely into the middle of the electrostatic field. The separator assembly's *parallel plates* resemble the PHYWE 06233-00 and accordingly measure $28.3 * 28.3 * 0.4\ cm$. Their insulating stems (used as the interface to the *isolating retainer*) are 190 mm long and 16 mm in diameter. As most residual parts (stand, isolating retainer, and heat tape) do not affect the installation space, their design was shifted to 3.6.2. Thus, remodeling the HV DC power supply selected in 3.5 concludes the PD of the electrostatic separator. Again, this step was done using the dimensions provided in data sheets and drawings.

At the test stand's bottom, the highly chargeable tailings and the ilmenite-rich feedstock would fall into different compartments of the outlet's *collection hopper*. It was designed within the Part Design: A $310 * 230 * 100\ mm$ pad was created first. Based on a sketch of rectangular profiles, the drafted filleted pocket command ($d = 5\ mm; \alpha = 5°; R = 2.5\ mm$) was then used to create the different compartments. At this, the inner compartments are very narrow (providing a high separation resolution), while the outermost are wider (to collect the more chargeable gangue minerals with the smallest grain sizes) following the probable trajectories computed in 3.4.2. In general, the hopper is molded so that particles cannot get trapped (e.g., by avoiding flat, horizontal surfaces, or undercuts).

As outlined in this subchapter's intro, all the designed CATPARTs (component-level) mentioned above were organized and managed in CATPRODUCTs (subsystem-level). Integrating these subsystem groups into one big file (system-level) was the next step. It allowed to resemble the setup (see figure 45) and package the installation space. At this, the Assembly Design workbench was used to identify an arrangement that would occupy a low volume, while also obeying a general clearance of 10 mm (taking precautions for potential tolerances and dynamic behaviour that might otherwise lead to collisions or interference). The subsystems were first brought to their designated position using the *move* toolbar (manipulation and snap tools). Subsequently, they were statically determined using the *constraints* toolbar (through coincidence, contact, offset, or angular constraints until all six degrees of freedom were defined), consequently anchoring the desired location. The result of this procedure is a mature system-level configuration that can be used to design the last subsystem: The structure.
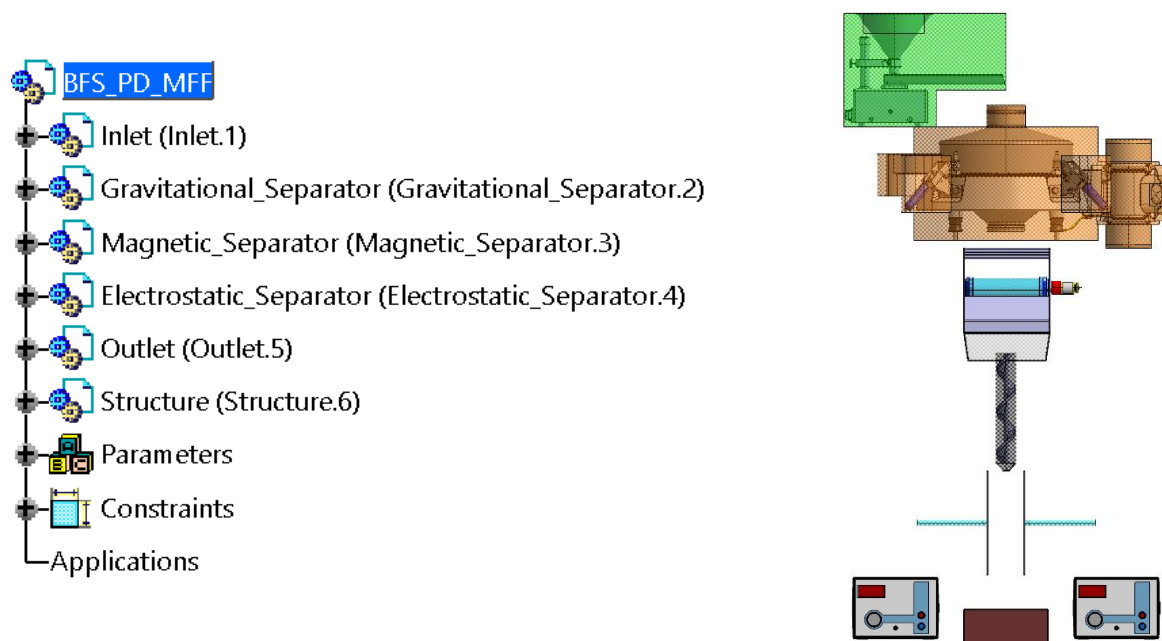
Figure 45: Resembling the product tree & schematic in CATIA's specification tree (L) and workspace (R)

As mentioned earlier, the structure was developed as a parametric-associative model. This means that its dimensions are not defined in the form of explicit, static numbers but rather as dynamic formulae, which themselves relate to a small set of parameters – variables that can be entered by the user. Broadly speaking, a change of these parameters would trigger an update cycle, which would automatically generate a new geometry that is adapted to the new input.

For a start, this affects the *profiles*. They were designed by projecting the $40 * 40\ mm$ cross section of a generic ITEM line 8 profile [84] onto a sketch plane and extruding it by its parametric lengths:

- **Height strut:** $L_h = 1787\ mm$
- **Width strut:** $L_w = 979\ mm$
- **Depth strut:** $L_d = 650\ mm$

Four profiles per dimensional direction would form the scaffolding (already fulfilling SMU_BEN_025). Eight more were added in the y-direction, to be used as a mechanical interface between the structure and the other subsystems (SMU_BEN_023). They are mounted to the scaffolding by 80 * 80 mm *support angles*; sixteen copies were positioned in the structure's CATPRODUCT. Thereafter, solid *panels* were created and attached to the scaffold's sides (SMU_BEN_022); two-millimeter-thick metal plates were chosen for bottom and top, whereas transparent polymer plates of 8 mm thickness were selected for the sides (to offer the visibility that is demanded by SMU_BEN_027). During 3.6.2, these materials shall be further specified, bearing in mind the corrosion-resistance-RQ SMU_BEN_032. A thin layer of *elastomers* was inserted between all panels and profiles, thereby sealing the system against dust (SMU_BEN_031) and dampening vibrations coming from the other subsystems (SMU_BEN_026). Lastly, four lockable *rollers* were added to the PD structure. Even though these rollers would increase the testbed's total height by approx. 100 mm, the system remains small enough to conform to SMU_BEN_029, while still providing the system's transportability (SMU_BEN_020) and the steady footing during experiments (SMU_BEN_018) demanded in the RQ catalogue.

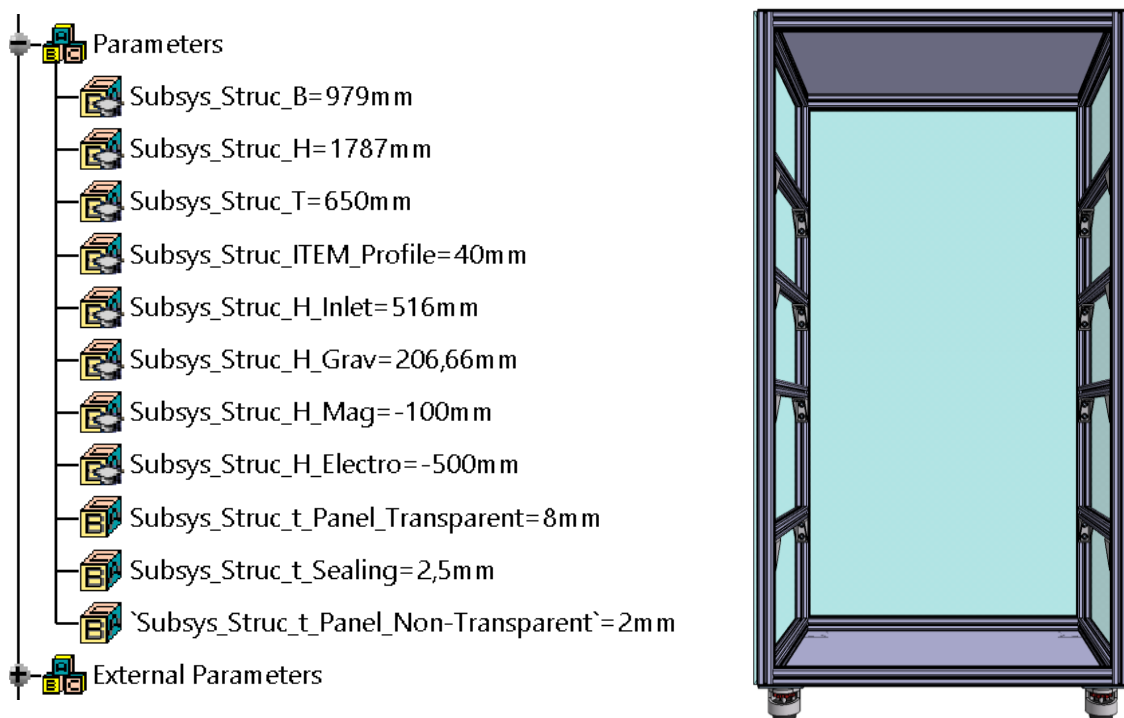**Figure 46: Parametric-associative model of the structure (R) based on user-selected parameters (R)**

Having obtained a viable structure concludes the first half of the design phase and, with it, subchapter 3.6.1, too. All files were archived (high-res images can be found in annex 11) and a duplicate of the system design was created, which will serve as a basis for the now upcoming, detailed design phase.

3.6.2 Detailed Design

Having dealt with things like the configuration and layout of the beneficiation testbed, the previously shown PD primarily focused on the parts' geometry and the system-level volume, rather than more technical aspects (like *joining technologies* and *manufacturing techniques* to be used, *materials* to be assigned, or *standards* to be applied). Characterizing this missing facet while also improving the general design maturity is the aspiration of the detailed design (*short*: DD) phase. Thus, the second half of the design process is largely dedicated to the execution of the following tasks:

- **Iterating** the design and increasing the level of detail for self-made components (e.g., ramp)
- **Specifying** machine elements and catalogue parts (e.g., ball bearings, bolts, and nuts)
- **Adding** the CAD models for components that are still missing (e.g., heat tape)
- **Replacing** placeholders and parametric models with their COTS counterpart (e.g., profiles)
- **Deliberating** the fixture of the other subsystems to the structure (e.g., stand, retainer)

Altogether, these activities will engender the final CAD models (see annex 12 for rendered images) and enhance the testbed's technical specificity to such an extent that will entitle us to proceed to the last WP of the development process i.e., the production planning.

Starting with the magnetic separator: It was almost completely rethought, because it was realized that several drawbacks and pitfalls had been incorporated into its PD model. First and foremost, this affects the ramp – an until now static part; it was substituted with an *adjustable divider*, so that the separation point becomes fine-tunable (finding the sweet spot will be the task of future experimenters). This divider consists of a 229 mm wide and 55 mm high, filleted aluminum (chosen for its low magnetic susceptibility) plate. It has two threads at the end of each side, which would fit into slots in the frame's end plates. *M3 nuts* on the outside could then be loosened to adjust the divider (between +30° and -30°) and fastened to perform the experiment. A consequence of this design change was that the DC motor could no longer remain at its current position, as it would block the divider's path. Therefore, the motor was tilted by 90° and attached to the end plate via a *galvanized angle connector*. Furthermore, it was found that the magnetic separator was unnecessarily bulky, so that the ITEM profiles were moved closer together, sharply reducing the dimensions of the frame's end plate (now $200 * 200 * 2.5\ mm$), which should further be made from aluminum (avoiding bimetallic corrosion). However, the resulting compactness of the subsystem necessitated a better guidance of the material flow to prevent particles from getting stuck. Therefore, the lateral covering (made from transparent polycarbonate for its high impact strength compared to other transparent polymers) was tilted so it would cover the slots of the profiles. The top and bottom covering were reshaped into *funnels* that would guide the material onto the drum (for the first) and into the charger or vessel (for the latter). What results is a tooth-shape that can be best seen in a 2D-section (left side of figure 47 on the next page). In an effort to specify the magnetic separator's machine elements, the *DIN 625-61809* ($d = 45mm$; $D = 58$; $w = 7mm$ [85]) were chosen to substitute the ball bearing placeholders of the PD model, as they best approximate the size of the surrounding caps. The caps' design was adapted to accommodate and hold them via an interlocking snap-fit. Another joining technology implemented into the magnetic separator is the friction fit; at this, ITEM's *T-Slot Nuts 6 St M5, bright zinc-plated* in

conjunction with *M5x10 dome-head screws* were used to attach the coverings to the frame's profiles in regular patterns. Dome-head screws were also used to assemble the frame and to fasten the angle connector to it (M5x20 and M2.5x10). A single *M8x20 hexagon socket head cap screw* secures the stator at the end plate opposing the DC motor. Moreover, an adhesive bond was chosen for the connection between the magnets and the inner tube; the security level S 4 of DIN 2304 was assigned in this case. At last, adding a CAD file for the DC power supply selected during 3.5 (Basetech BT-153) and replacing it with the former placeholder finalized the magnetic separator's DD model:
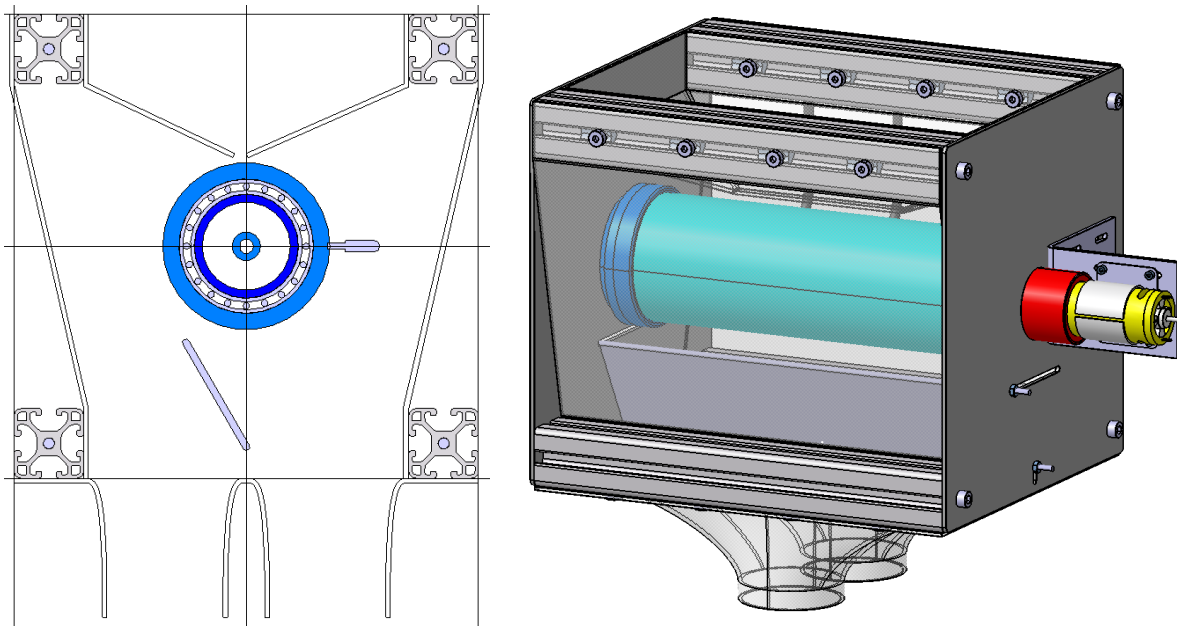

Figure 47: 2D-section (L) and close-up (R) of the magnetic separator's DD model

Having completed the DD work for the magnetic separator, the attention turned towards the ensuing subsystem. The transformation of the electrostatic separator was chiefly concerned with assembly number one. At this, an adapter piece was appended to the outer tube, gradually widening its diameter at the top ($R_{i,top} = 27.5\ mm$) to make for a firm friction fit with the two adjacent funnels. Further, aluminum was chosen as the basic material for both the outer tube and static mixers (in accordance with the findings from 3.4.2), as using different materials for the adjacent units might have deteriorated the process of tribocharging and led to adherence-based losses in recovery. Speaking of the static mixer: Its geometry was simplified and its pieces merged, so it could be milled from a single block of metal. At this, it appeared that separately swept surfaces (joined and filleted) would offer a better force flow and grip than the earlier design concept. Moreover, it was possible to increase the whole assembly's length. As such, adding several revolutions to the helix guide curve will increase the number of possible particle-particle and particle-wall interactions during experiments, effectively boosting the tribocharging efficacy. The heat tape, which would wrap around the outer tube following the charger's helix, was designed thereafter following the data given in ISOHEAT's product catalogue (25 * 7 mm). Lastly, inserting a new CATPART for the stand (holding the charger) and isolating retainer (holding the parallel plates) concluded the work invested into the DD electrostatic separator. Both parts consist of three units each: A pedestal (base plate and barrel-shape), a stainless-steel rod (M10; $l_{stand} = 1000\ mm$ and $l_{iso.retainer} = 370\ mm$), and clamps (round clamps and boss head clamps).

The outlet subsystem was also extended with newly modeled CATPARTs; more specifically, an oversize container was added to the sifter's sidewise outlet, and a vessel for ferromagnetic tailings was created and attached to the second funnel of the magnetic separator. Both containers shall be mounted to their respective counterpart using hose clamps; the clamps were specified as DIN 3017. The already existing collection hopper, on the other hand, would be held in position by two L-shaped guide rails made from aluminum. These shall be glued to the structure's bottom plate using a metal-metal adhesive (again following DIN 2304). Since only modest claims must be asserted as to the containers' accuracy and mechanical load capacity, it was decided that they shall be produced via rapid prototyping. More specially, additive manufacturing using a polylactic acid filament is suggested, for it is easily printable, biodegradable, inexpensive and offer high stiffness and strength [86].
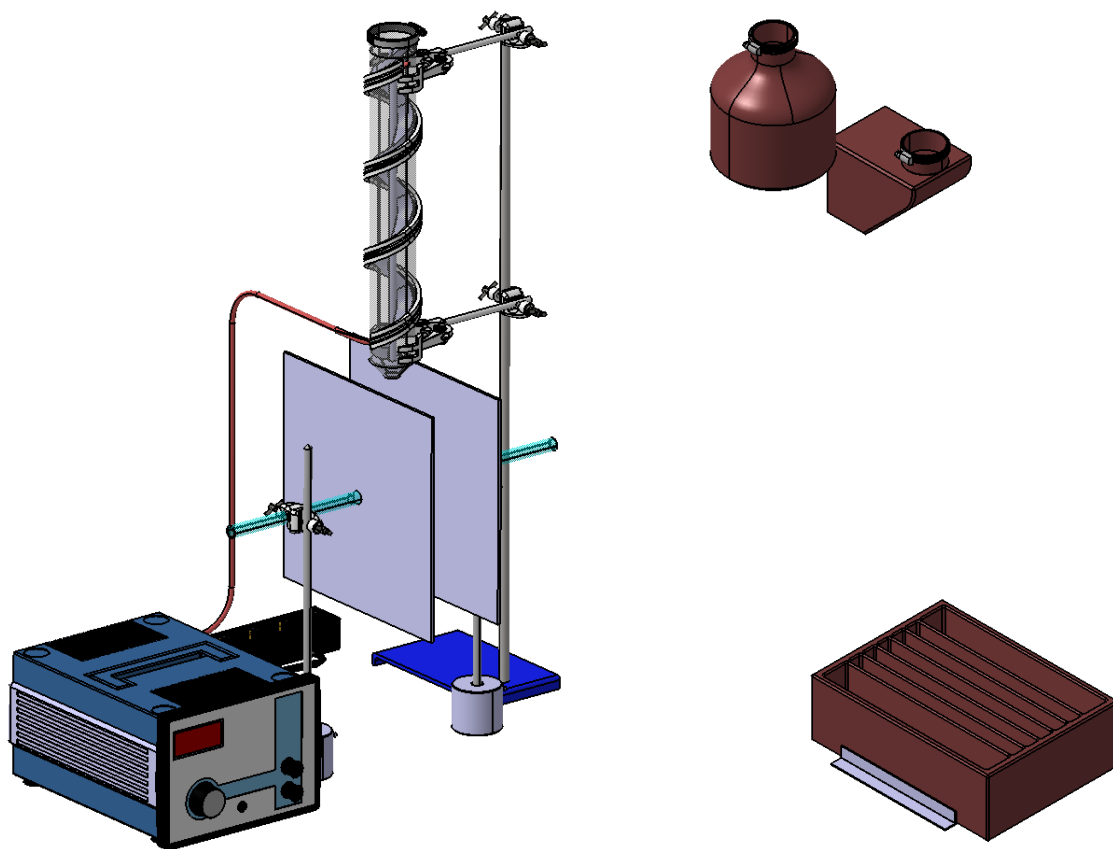
Figure 48: DD models of the electrostatic separator (L) and outlet (R) subsystems

In what follows, the DD of the structure (see figure 49) shall be dealt with. In a first step, the parametric profiles from the PD were replaced with the COTS *Profile 8 40x40 E, natural*, in the form of pre-cut delivery units. Yet, the number of profiles mentioned in the PD did not suffice to satisfy SMU_BEN_024; thus, another eight profiles of this type had to be added at the front side in an effort to construct two separately open- and closeable swing doors. Thereat, different types of fastening elements were used to connect all profiles together (see annex 12 for images of their CAD files):

- The *Automatic-Fastening Set 8, stainless* is used to assemble the scaffolding
- The *Automatic Angle Bracket Set 8 80x80 Al* is used to attach the crossbars to the scaffolding
- The *Automatic Flat Bracket Set 8 80x40 Al* is used to assemble the smaller bottom door
- The *Automatic Flat Bracket Set 8 120x120 Al* is used to assemble the bigger top door

Figure 49: DD model of the structure

The doors were attached to the scaffolding by hinges of the type *8 Al FP0-270° light*, for they are inherently sturdy, offer the widest opening angle, and produce the smallest door gap (0.1 mm) of all ITEM solutions. Keeping this gap as small as possible is needed to prevent dust from escaping. Hence, sealing the rest of the gap (4 mm) is important, too, so that the *Door Stop Seal 8 40* was inserted on the other sides, where it additionally "stops the door leaf flush with the profile's outer face" [84]. In addition, *Cover Profile 8 32x4* – an elastic and non-slip cover for a profile's groove – was inserted below both doors to narrow their gap, dampen vibrations coming from the other subsystems, and maintain cleanliness. Also inserted into the doors' profile grooves was the *Lip Seal 8 2-4 mm*. This was not only done to satisfy SMU_BEN_031 yet again, but also to fasten the panel elements, which shall be regarded next.

The choice of materials for the panels announced in 3.6.1 was done reviewing the range of products found in ITEM's catalogue. At this, the options for transparent panels are acrylic glass, polycarbonate, and glycol-modified polyethylene terephthalate, also known as PTE-G [84]. Since – unlike the magnetic separator that involves parts rotating at high speeds – the structure does not have to be impact-proof, the use of polycarbonate or PTE-G can be considered as overengineering. Thus, the economical, but highly transparent *Acrylic Glass 4 mm XT, clear* was preferred for the side panels and doors. Its "resistance to numerous aggressive chemical agents" and "good resistance to water, alkalis and aqueous solutions containing inorganic salts" [84] makes it an ideal fit in light of SMU_BEN_032. This also holds true for the *Sheet Material Al 2mm, natural anodized*, which was selected as the panelling of the laboratory testbed's bottom and top, for it is a stable and durable metal that comes at moderate costs, only. As mentioned above, the door panel would be inserted into the grooves and held by the lip seal. This is different for the scaffolding, where fixing the panels in the groove is not an option, as it would interfere with the crossbars. It was found that the easiest way to mount the panels onto the outside of the profiles are *T-Slot Nuts 8 St M8, stainless* in conjunction with *Flat Mushroom Head Screws M8x16* (which reduce contact pressure through an integrated collar); all alternative ITEM

panel fasteners seemed unsuitable, as they would either position the panel flush with the profiles or aligned with the groove. This combination was added at regular intervals and bore holes were drilled into the panels at the given positions. This was also done for the elastomers underneath them, which are further specified as cuttings of an ethylene propylene diene monomer tape (self-adhesive), which shall be 40 mm wide to cover the whole contact face (a thickness of 2.5 mm was assumed). The last component to be replaced from the PD structure's model are the rollers. At this, the *Jacking Castors D62 120x120* were chosen, for they combine a castor with a height-adjustable, non-slip knuckle foot [84]. This feature might also be taken advantage of to level the test stand in an uneven environment. Each castor has a load capacity of 3400 N and is attached to the scaffold's bottom profiles using *Button-Head Screws M8*. The final model of the structure subsystem was arrived at adding the following additional components to the CATPRODUCT:

- The *Handle PA 80* and *Handle PA 120* are used to open and close the doors for maintenance
- The *Door Lock 6-8 Zn* is used to temporarily lock the doors during experiments
- The *Angle Bracket 8 160x160-40 Al M8* is used to stiffen the bottom of the structure
- The *Automatic Angle Bracket Set 8 40x40 Al* is used to stiffen the top of the structure

Integrating everything into the finished structure was the last step within the design WP and will, thus, bring chapter 3.6 to a close. As implied during 3.6.1, the dummies for the vibratory feeder and sifter were replaced by their original 3D models. The feeder is connected to the structure via a moveable rack (to ease the filling of simulant), whereas the sifter is fastened to the crossbars via stationary beams. The DD magnetic separator model was inserted beneath them, and its position adapted to the revised geometry; more specifically, the funnel-shape at its top made possible to move it along the positive z-axis and, thus, minimize the distance to the sifter's outlet, enabling a more direct and secure transmission of bulk material. Universal brackets tie its frame to two beams, which in return attach the aggregate to the structure. At last, the reworked versions of the electrostatic separator and outlet were deployed on the structure's bottom and aligned with the axis of the magnetic separator's outlet.

Figure 50: Rendering of the DD system model as the outcome of the design effort

3.7 Production Planning

Owing to chapter 3.6, a mature and well-deliberated model of the beneficiation testbed exists. However, the outcome of this thesis is not meant to remain a digital file forever. Instead, it is planned to actually build and utilize the test stand in the future. For that reason, one last WP is yet to be regarded within the framework of the development process: The production planning. This WP comprises all actions needed to ensure that the impending manufacturing and assembly of the apparatus is prepared in an optimal manner. As it is the very centerpiece of the production planning, chapter 3.7 will emphasize the procurement-related activities. Such being the case, it will demonstrate how documents like a *bill of materials* (*short*: BOM) or *technical drawings* have been derived from the CAD data, which in return were needed to issue *enquiries*, request *quotations*, or place *orders*.

The first step in facilitating the testbed's transition from a computer file to a physical object was to create *subsystem-level BOMs*. CATIA has a tool built into its Assembly Design workbench for this particular task. To make use of it, a number was assigned to each component in the specification tree (integer mode) and the relevant properties to appear in the BoM (number, quantity, type, etc.) were selected. The raw list was exported and saved as a CSV file (tabular data stored in plain text). Rearranging, rectifying, and formatting the raw list was done afterwards using Microsoft Excel. Lastly, adding columns with auxiliary information that might come in handy during the sourcing (e.g., suggestions regarding potential manufacturing techniques, comparable products, or contemplable suppliers) yielded one workable table per subsystem. By way of example, the electrostatic separator's BOM is given here below:

Table 15: Bill of materials for the electrostatic separator

Amount	Part Number	Type	Description	Specifications	Material
1	Static Mixer	Custom	Lathing	⌀ 50 mm	Aluminium
1	Outer Tube	Custom	Bending & Welding	⌀ 52 mm	Aluminium
1	Heat Tape	COTS	ISOHEAT MiL-HT-PSG	25 x 7 mm	PTFE
1	Stand: Base Plate Pedestal	COTS	PHYWE 39124-21	21 x 13 cm	Coated Steel
1	Stand: Rod	COTS	PHYWE 02031-00	M10 x 1000 mm	Stainless-Steel
2	Stand: Round Clamps	COTS	PHYWE 37716-00	80 mm	Cast Iron, Cork
1	HV DC Power Supply	COTS	PHYWE 13671-93	370 x 236 x 168 mm	Polymers
2	Parallel Plates	COTS	PHYWE 06233-00	283 x 283 x 4 mm	Aluminium
2	Cables	COTS	PHYWE 07367-00	1000 mm	n.a.
1	Retainer: Barrel Pedestal	COTS	PHYWE 02004-55	⌀ 60 mm x 55 mm	Coated Steel
1	Retainer: Rod	COTS	PHYWE 02031-00	M10 x 370 mm	Stainless-Steel
4	Retainer: Boss Head Clamps	COTS	PHYWE 37697-00	16 mm	Zinc
1	AC Power Strip	COTS	AS Schwabe 38609	1.5 m; IP44	Polymers

Even though this set of tables makes it easy to get a condensed overview (which is favorable, e.g., during building), in terms of procurement it is often of greater benefit to group components according to suppliers, rather than subsystems. This especially holds true for the order at ITEM. This company offers an online tool, whose algorithm can read tables that exclusively feature ITEM commodities to deduce a shopping cart from it in an automated manner, equally reducing effort and time spent during an enquiry. Therefore, a set of *order lists* was issued, too, which enumerates all the COTS components to be bought from a respective vendor, including applicable features (like article number, length, and width). When inquiring custom parts, on the other hand, the more suitable document is a *technical drawing* (see figure 51). They precisely outline the geometry and symbolically communicate technical properties of the component through standardized perspectives and notation. One drawing was issued per custom component using CATIA's Drafting workbench. At this, the ISO standard and an A3 sheet style were applied. Each page layout features at least three views (front, top, and left plus detailed, section or isometric views if applicable), the essential dimensions, a frame, and a title block. Clear instructions for the manufacturer were added when needed (e.g., demanding deburring or defining accepted tolerances). An example for both document types – the reseller-specific order list and a technical drawing – can be found in annex 13.
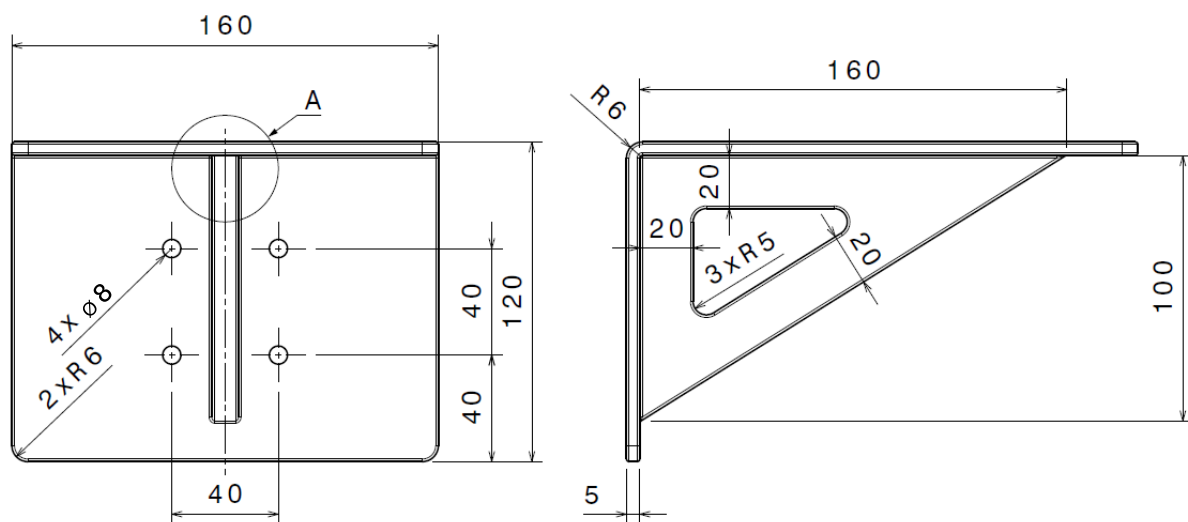

Figure 51: Extract from a technical drawing showing the retaining plate for the inlet's rack

Having gathered all the necessary documentation (BOM, order lists, and technical drawings), the active procurement could commence: Inquiries and tenders were sent via mail to the respective reseller, correspondence was held with their representatives, and meetings were hosted with their salesmen. As part of this, 3D models were exchanged where necessary (as mentioned during 3.6.1). When it came to the final purchase transaction, DLR's internal procurement system was preferably used; products not appearing in the system were order via external shops. The invoices and shipping confirmations were stored and shared with the accounting department (see annex 13 for an example). Lastly, manuals to be consulted during the erection of the test stand and prior to its initial operation were downloaded and archived to ease the work of research assistants and experimenters alike. The completion of WP7 not only concludes the main part of this document, but also managed to bridge a gap between the development process and the assembly, integration, and test (*short*: AIT) phase.

Chapter 4   Summary

The initial objective of this thesis was to develop a test bench that is capable of concentrating the mineral ilmenite from a lunar regolith simulant under laboratory conditions, for the purpose of demonstrating the technology readiness of beneficiation in the greater context of in-situ oxygen production on the Moon. To that end, a systematic development process consisting of seven work packages was suggested to acquire a methodically sound end product. Following the order of this process, the most distinctive perceptions shall be synthesized hereinafter.

As part of the first WP, the most relevant studies and scientific publications were reviewed. It was found that a great number of processes exists in the research field of lunar minerals beneficiation, which have been investigated by researchers who all used different setups and, thus, reported varying results. These processes can be formally divided into gravitational, magnetic, and electrostatic beneficiation, whereat the latter has been studied the most. In the case of gravitational beneficiation, the processes can be categorized into screening and classification techniques; screening was often referred to as the more reliable choice, whereas it was pointed out that classification methods – like the use of cyclones – are often less-suited for the use in outer space or would impose more technical challenges. Concerning electrostatic beneficiation, it was realized that conductive induction with slide separators, tribocharging with plate separators, and the electrostatic travelling wave dominate the pertinent literature; the first two seemed to achieve a significant mineral enrichment, whereas the latter is preferably used for size sorting. Lastly, magnetic beneficiation was either done using permanent magnets of low field strengths or electromagnets of high field strengths; these could either be used stand-alone or incorporated into e.g., a drum separator.

During the second WP, requirements and specifications were gathered to facilitate the testbed's ongoing development. It was decided that – in the absence of an internal stakeholder – reference values from literature are needed to continue the work in this regard. It was ascertained that a minimum final grade of 40 wt. %, a recovery of at least 50 wt. %, and an enrichment ratio of 4.6 would make for reasonable starting points. Additionally, studies that dealt with oxygen reaction indicated that a particle size range between 20 µm and 200 µm should be targeted. Based on these findings, a system-level catalogue of 21 entries was derived. As the development process proceeded, this catalogue was expanded with lower-level entries.

The third WP was dedicated to the generation of a potent and feasible concept. In a first step, the beknown processes were filtered, assessed, and selected (one process per beneficiation category). In doing so, it was found that dynamic screening would outcompete the other gravitational processes, for it offers a remarkably high technology readiness, is easily adjust- and scalable, and exhibits a supreme performance. Further, tribocharging in conjunction with plate separation was found to be the best choice respecting electrostatic processes for similar qualities; it is further extremely well integrable. In view of magnetic beneficiation, which seems to be best at dedusting, gangue removal, and mineral enrichment, the permanent magnet drum separator won the assessment. It is convincing due to its environmental independence, compact size, low power demand and superb controllability.

With the aim of taking advantage of these processes' individual strengths and maintaining reliability, a multi-stage approach was opted for – following the example of the Swiss cheese model. At this, a sequence and setup were chosen that would exploit the synergy effect; a vertical free-fall system turned out to be the best option for both terrestrial and lunar applications. It was illustrated in the form of a schematic, a product tree, and sketches, which facilitated the remaining development steps.

With the aid of WP number four, the validity of the conceived concept was quantitatively audited. It was computed that the magnetic drum separator would have to spin at a rotational frequency of approx. 357 RPM to reach a previously defined capacity. Therefore, it was estimated that the DC motor that spins the drum must be capable of delivering a rotational frequency of up to 715 RPM. Using a numeric simulation tool to model the magnetic field of the drum separator, it was further evinced that the paramagnetic ilmenite grains could be successfully separated from ferromagnetic constituents at the predetermined nominal drum velocity. Calculations regarding the electrostatic separator showed that the potential between the electrodes of the plate separator should be in the order of magnitude of ±25 kV to discriminate different particles under terrestrial gravity and in vacuum. Beyond that, it was calculated that a plate surface area of around 800 cm^2 and a plate distance of 10 cm would make for good dimensions. Moreover, the trajectories of different mineral grains under both lunar and terrestrial gravitation were modeled, whereat different tribocharger materials (different work functions) were tested; is shows that aluminum can be considered a good material under laboratory conditions, as it achieves a distinct separation of mineral grains in vacuum.

Amidst WP five, suitable commercial off-the-shelf components were nominated. In an effort to identify the available options for the most essential parts of each subsystem, the market was firstly screened for laboratory-certified or industry-ready products. Concerning the inlet's vibratory feeder, five viable commodities were found and listed along with their qualities (application area, feed rate, hopper volume, and size). Regarding the gravitational beneficiation's sifter, 16 products could be shortlisted. Furthermore, five different arc segment magnets were detected and compared according to their grade, size, angle, magnetization direction, and price. And lastly, six different HV DC power supplies, to be used with the electrostatic plate separator, were assessed after gleaning data like input and output voltage, as well as the maximum power. The winner of each category was briefly introduced and reconciled with the requirements catalogue.

Designing the laboratory test bench was the subject of the sixth WP. Its purpose was to convert the previously gathered ideas and information into mature and manufacturable 3D models using the CAD software CATIA V5. A bipartite structure was applied: The first part – the preliminary design – was concerned with the conceptual aspects of mechanical engineering like the geometry of parts and the volumetric configuration of the assemblies within the over-all system. At this, it was realized that a dynamic, parametric-associative model is best at deriving optimal dimensions for the structural elements. On the contrary, the second phase a.k.a. the detailed design focused on more technical aspects – especially originating from the subdiscipline of manufacturing engineering – to increase the system's technical specificity. Defining materials, mounting, and standards was done in parallel with the iteration of the part-designs and the apposition of new models. Over the course of the DD, flaws

on the component-level have been eradicated (e.g., replacing a static ramp of the magnetic separator with a dynamically controllable divider), the performance of assemblies has been improved (e.g., by prolonging the length of the electrostatic separator's charger), and the subsystems have been conflated (e.g., by deliberating a mechanical interface).

Lastly, the seventh and, thus, final WP was concerned with facilitating the production of the test stand. Since bringing the digital models into the physical world will be the follow-up action to this thesis, the procurement of parts had to be taken care of over the course of this development process. Documents that are required in this regard like bills of materials (one per subsystem) and technical drawings (for mechanically manufactured parts) were derived from the CAD models and utilized when issuing inquiries and sending purchase requests.

The completion of all seven WPs concluded the development work and with it, the practical part of this thesis. After a final review, all data have been reviewed, approved, and submitted.

Figure 52: Artistic impressions of SMU's beneficiation test stand inside the laboratory of DLR Bremen

Chapter 5   Conclusion & Outlook

In retrospect, it can be said that the goal of this thesis has been accomplished entirely, as a well-conceived and feasible beneficiation testbed has been delivered. Following a systematic sequence of activities that embraced methods from numerous engineering and science branches ensured a high quality at all levels. Therethrough, the way for well-founded experiments in the laboratory and representative study results has been paved. These experiments and findings, in return, will help in closing the research gaps mentioned in the introduction; hence, the scientific community's call to action – the request to demonstrate the feasibility of mineral beneficiation in the context of in-situ oxygen production on the Moon – has been answered by the SMU research group.

Despite the resounding success that this thesis has brought, dealing with potential error sources is part of any good conclusion, as reflecting the own work in a critical manner is the very essence of science. At this, one blind spot might be the geometry of the electrostatic separator's charger: Even though a smooth flow of the lunar regolith simulant was made allowance for during the detailed design phase, it cannot be validated by digital means, but needs to be tested under appropriate ambient conditions in real life. Thus, it is suggested that – before commissioning the custom static mixer – a pretrial shall be conducted, which will proof that the flow does not get interrupted, in order to confirm the adequacy of the design. In this regard, the effect of surface roughness and especially the angle of inclination on the adherence of the bulk material to the surface should be examined. If needed, the design should be adapted according to the pretrial's findings.

Furthermore, the hazard of dust formation during the experiments should be borne in mind. To elaborate, the smallest fraction of regolith simulant might be whirled up by rapid movement – for example due to the vibration of the sifter – and consequently form a combustible cloud of solid particles suspended in the oxygen-rich air. This will likely turn out to be a baseless concern in the end. Nevertheless, if the accumulation of dust should actually be observed during an experiment, the system must be switched off immediately, to mitigate the risk of a spark (coming from any of the electronics) igniting it. An easy countermeasure to prevent such a calamity might be the use of flexible connectors that would envelop the crossover from one subsystem to the other (e.g., from the feeder to the sifter), thereby withholding the awhirl powder. This could either be self-made – potentially from polythene sheets – or bought as an optional accessory (e.g., by the sifter's vendor).

Moreover, it should be noted that in case the electrostatic plate separator fails to reproduce the mineral enrichment targets stated in the RQ catalogue ab initio – for instance because the flight paths of particles under atmospheric conditions vigorously differ from the predicted trajectories under vacuum – there are several set screws to correct the shortcoming. For example, the distance between the plates (nominally set to 10 cm) could be reduced to increase the electric field strength. Alternatively, the voltage applied to the electrodes might be doubled by connecting a second HV DC power supply in parallel (this should only be done after consulting the manufacturer and executed under the guidance of HV-qualified personnel). Vice versa, if particles were to collide with and accumulate at the plates, the field strength should be reduced accordingly.

Lastly, one of the biggest uncertainties does not directly affect the testbed, but rather the material it processes: The simulants LHS-1, LMS-1, and LHS-1D were carefully chosen by the SMU research group. However, a simulant remains a simulant and can only mimic the properties of real lunar regolith to a certain extent. Thus, it may fall short of expectations regarding the size distribution (especially the correlation between grain size and mineralogy), magnetic attributes or electrostatic properties. Since the success of the apparatus heavily relies on the correct replication of these characteristics, it is yet to be found out if the beneficiation testbed can live up to its full potential.

Having reviewed the outcome with integrity, we can now dare a glance towards the future work. In the near term, the AIT is going to be of top priority. Provided that all required components are shipped in time, the assembly will start directly after the submission of this document (February 2022). At this point in time, the vibratory feeder has already arrived, just like many COTS components of the electrostatic separator. The arc segment magnets and structural elements should follow shortly, which augurs excellent conditions for an expeditious construction procedure. Erecting the structure will most probably be the first step, which will include metalworking-related activities like bolting, deburring, drilling, grinding, and cutting. Later, once the other subsystems come into play, electrical work like soldering and wiring will join in. Once all the other subsystems will have been put together, too, they will be integrated into the structure in the manner outlined during the design chapter, whereat the system is complemented. When the test stand is completely mounted and all subsystems are integrated, the testbed will be moved into the laboratory, where it will be inspected and tested. At first, all its basic functions shall be checked on an individual basis (one subsystem at a time). If this trial yields a positive result, the system can be tested as a whole. If the device in its entirety also demonstrates nominal behaviour, it is verified and approved for usage.

This will enable researchers of the SMU group to finally conduct beneficiation-related experiments. In a first series of experiments, the overall performance of the apparatus shall be measured. This will require an a priori verification of the input simulant's composition (in comparison to its datasheet) as well as an a posteriori analysis of the output feedstock (measuring the final grade), so that recovery and enrichment ratio can be computed. At this, it is recommended that the ilmenite content within the material shall be determined via spectroscopic methods. If a spectrometer is not available, this task could be outsourced to an external laboratory. Once the first experiments are finished, a second series of studies could investigate how much each beneficiation step attributes to the overall improvements (one of the many advantages of having pursued a multi-stage setup). In addition, prospective experiments may be directed at the improvement of the system, for instance by trying different mesh sizes for the sifter or by adjusting the rotational velocity and divider angle of the magnetic separator (varying the separation point will influence the grade-recovery-relationship). Further, the electrostatic separator's voltage may be altered to find an optimal mineral separation.

No matter what the experiments will be targeting: They will eventually lead to new insights for the scientific community and, thus, be a valuable contribution to mankind's stock of knowledge in the field of lunar mineral beneficiation. With beneficiation being a vital part of in-situ oxygen production, this will be of paramount importance to make the vision of a lunar outpost for human spaceflight a reality.

Bibliography

[1]   E. M. Jones, *Apollo 11: Transcript and Commentary*. One Small Step. Accessed: Jun. 11 2021. [Online]. Available: https://www.hq.nasa.gov/alsj/a11/a11.step.html

[2]   Wikipedia, *Moon.* [Online]. Available: https://en.wikipedia.org/w/index.php?title=Moon&oldid=1027938331 (accessed: Jun. 11 2021).

[3]   NASA, *The Moon is a School for Exploration: Science Mission Directorate.* [Online]. Available: https://science.nasa.gov/science-news/science-at-nasa/2007/14feb_school (accessed: Jun. 11 2021).

[4]   J. Pinson, "Moon May Hold Billions of Tons of Subterranean Ice at Its Poles," *Eos Transactions American Geophysical Union*, 2020, doi: 10.1029/2020EO151889.

[5]   Wikipedia, *Lunar soil.* [Online]. Available: https://en.wikipedia.org/w/index.php?title=Lunar_soil&oldid=1034953503 (accessed: Aug. 19 2021).

[6]   A. Abbud-Madrid, "Why Space Resources: The Moon, Asteroids, Mars, and Back to Earth," in *Space Resources Week*, Virtual, 2021.

[7]   K. Sacksteder and G. Sanders, "In-Situ Resource Utilization for Lunar and Mars Exploration," in *45th AIAA Aerospace Sciences Meeting and Exhibit*, Reno, Nevada, Aug. 2007.

[8]   K. Hadler, D. J. P. Martin, J. Carpenter and J.J. Cilliers, "A universal flowsheet and terminology for in situ resource utilization (ISRU): 50th Lunar and Planetary Science Conference 2019," 2019.

[9]   ESA, *The Moon as a spaceport to the Universe.* [Online]. Available: http://www.esa.int/ESA_Multimedia/Images/2019/10/The_Moon_as_a_spaceport_to_the_Universe (accessed: Jun. 14 2021).

[10] ESA, *ESA Space Resources Strategy.* [Online]. Available: https://sci.esa.int/documents/34161/35992/1567260390250-ESA_Space_Resources_Strategy.pdf (accessed: Jun. 15 2021).

[11] J. N. Rasera, J. J. Cilliers, J. A. Lamamy, and K. Hadler, "The beneficiation of lunar regolith for space resource utilisation: A review," *Planetary and Space Science*, vol. 186, p. 104879, 2020, doi: 10.1016/j.pss.2020.104879.

[12] International Space Exploration Coordination Group, *In-Situ Resource Utilization Gap Assessment Report.* [Online]. Available: https://www.globalspaceexploration.org/wordpress/wp-content/uploads/2021/04/ISECG-ISRU-Technology-Gap-Assessment-Report-Apr-2021.pdf (accessed: Jun. 20 2021).

[13] P. Zabel, "Synergetic Material Utilization: Combining ISRU and ECLSS," in *Planetary and Terrestrial Mining Sciences Symposium: Global Perspectives*, Virtual, 2021.

[14] K. Hadler *et al.,* "A universal framework for Space Resource Utilisation (SRU)," *Planetary and Space Science*, vol. 182, p. 104811, 2020, doi: 10.1016/j.pss.2019.104811.

[15] G. H. Just, K. Smith, K. H. Joy, and M. J. Roy, "Parametric review of existing regolith excavation techniques for lunar In Situ Resource Utilisation (ISRU) and recommendations for future excavation experiments," *Planetary and Space Science*, vol. 180, p. 104746, 2020, doi: 10.1016/j.pss.2019.104746.

[16] R. J. Williams, D. S. McKay, D. Giles, and T. E. Bunch, "Mining and Beneficiation of Lunar Ores: Technical papers derived from the 1977 Summer Study," *Space Resources and Space Settlements*, p. 275, 1979.

[17] K. Hadler, J. Rasera, R. Cruise, Y. Yu, S. Witchalls, and J. Cilliers, "Beneficiation of Lunar Regolith: Progress and Challenges," in *Planetary and Terrestrial Mining Sciences Symposium: Extraction and Processing*, Virtual, 2021.

[18] G. Heiken, D. Vaniman, and B. M. French, *Lunar sourcebook: A user's guide to the moon*. Houston: Cambridge University Press / Lunar and Planetary Institute, 2005.

[19] Wikipedia, *Mineral processing.* [Online]. Available: https://en.wikipedia.org/w/index.php?title=Mineral_processing&oldid=1032803314 (accessed: Aug. 20 2021).

[20] M. Berggren, R. Zubrin, P. Jonscher, and J. Kilgore, "Lunar Soil Particle Separator," *49th AIAA Aerospace Sciences Meeting*, p. 436, 2011.

[21] C. Panda, *Working and Principle of Vibratory Sifter.* [Online]. Available: https://pharmaceuticalupdates.com/2020/04/28/working-and-principle-of-vibratory-sifter/ (accessed: Aug. 23 2021).

[22] JXSC Mine Machinery, *Mineral Processing Equipment and Solutions by JXSC Mine Machinery: Hydrocylone - Mineral Processing.* [Online]. Available: https://mineraldressing.com/equipment/hydrocylone/ (accessed: Aug. 23 2021).

[23] H. R. Manouchehri, K. Hanumantha Rao, and K. S. E. Forssberg, "Review of electrical separation methods," *Mining, metallurgy & exploration*, vol. 17, no. 3, pp. 139–166, 2000, doi: 10.1007/BF03402842.

[24] Wikipedia, *Beneficiation.* [Online]. Available: https://en.wikipedia.org/w/index.php?title=Beneficiation&oldid=1039413932 (accessed: Aug. 23 2021).

[25] S. Rosenblum and K. Brownfield, "MAGNETIC SUSCEPTIBILITIES OF MINERALS," *U.S. GEOLOGICAL SURVEY*, 2000. [Online]. Available: https://pubs.usgs.gov/of/1999/0529/report.pdf

[26] C. Schwandt, J. A. Hamilton, D. J. Fray, and I. A. Crawford, "The production of oxygen and metal from lunar regolith," *Planetary and Space Science*, vol. 74, no. 1, pp. 49–56, 2012, doi: 10.1016/j.pss.2012.06.011.

[27] Wikipedia, *Redox.* [Online]. Available: https://en.wikipedia.org/w/index.php?title=Redox&oldid=1034565056 (accessed: Aug. 18 2021).

[28] Wikipedia, *Acid.* [Online]. Available: https://en.wikipedia.org/w/index.php?title=Acid&oldid=1035245449 (accessed: Aug. 18 2021).

[29] Wikipedia, *Dissociation (chemistry).* [Online]. Available: https://en.wikipedia.org/w/index.php?title=Dissociation_(chemistry)&oldid=1033241584 (accessed: Aug. 18 2021).

[30] Wikipedia, *Electrolysis.* [Online]. Available: https://en.wikipedia.org/w/index.php?title=Electrolysis&oldid=1036060147 (accessed: Aug. 18 2021).

[31] Wikipedia, *Pyrolysis.* [Online]. Available: https://en.wikipedia.org/w/index.php?title=Pyrolysis& oldid=1039053643 (accessed: Aug. 18 2021).

[32] M. A. Gibson and C. W. Knudsen, "LUNAR OXYGEN PRODUCTION FROM ILMENITE," *Lunar Bases and Space Activities of the 21st Century*, pp. 543–549, 1985. [Online]. Available: https:// ui.adsabs.harvard.edu/abs/1985lbsa.conf.543G/abstract

[33] H. M. Sargeant *et al.,* "Hydrogen reduction of lunar samples in a static system for a water production demonstration on the Moon," *Planetary and Space Science*, vol. 205, p. 105287, 2021, doi: 10.1016/j.pss.2021.105287.

[34] M. Okrusch and S. Matthes, *Mineralogie: Eine Einführung in die spezielle Mineralogie, Petrologie und Lagerstättenkunde,* 9th ed. Berlin, Heidelberg: Springer Berlin Heidelberg, 2014.

[35] R. R. Oder, L. A. Taylor, and R. Keller, "Magnetic characterization of lunar soils," *Abstracts of the Lunar and Planetary Science Conference*, vol. 20, p. 804, 1989. [Online]. Available: http:// adsabs.harvard.edu/abs/1989LPI…20.804O

[36] Wikipedia, *Mineral.* [Online]. Available: https://en.wikipedia.org/w/index.php?title=Mineral& oldid=1033138418 (accessed: Jul. 15 2021).

[37] Wikipedia, *Breccia.* [Online]. Available: https://en.wikipedia.org/w/index.php?title=Breccia& oldid=1030163010 (accessed: Jul. 15 2021).

[38] C. Meyer, "Lunar Regolith," *NASA Lunar Petrographic Educational Thin Section Set*, pp. 46–48, 2003. [Online]. Available: https://curator.jsc.nasa.gov/lunar/letss/regolith.pdf

[39] R. V. Morris, G. Klingelhöfer, R. L. Korotev, and T. D. Shelfer, "Mössbauer mineralogy on the Moon: The lunar regolith," *Hyperfine Interactions*, vol. 117, no. 1, pp. 405–432, 1998, doi: 10.1023/A:1012699511670.

[40] L. A. Taylor, H. H. Schmitt, W. D. Carrier, and M. Nakagawa, "The Lunar Dust Problem: From Liability to Asset," in *1st Space Exploration Conference: Continuing the Voyage of Discovery*, Orlando, Florida, 2005.

[41] L. A. Taylor *et al.,* "Magnetic Beneficiation of High-Ti Mare Basalts: Petrographic Analyses," *Abstracts of the Lunar and Planetary Science Conference*, vol. 23, p. 1415, 1992. [Online]. Available: https://ui.adsabs.harvard.edu/abs/1992LPI…23.1415T/abstract

[42] S. K. Runcorn *et al.,* "Magnetic properties of Apollo 11 lunar samples," *Proceedings of the Apollo 11 Lunar Science Conference*, vol. 3, pp. 2369–2387, 1970. [Online]. Available: https:// ui.adsabs.harvard.edu/abs/1970GeCAS…1.2369R/abstract

[43] P. Metzger, "Deep Reduction of Energy: Requirement for Lunar Ice Extraction," in *Space Resources Week*, Virtual, 2021.

[44] W. N. Agosto, "Electrostatic Separation and Sizing of Ilmenite in Lunar Soil Simulants and Samples," *LUNAR AND PLANETARY SCIENCE XV*, vol. 15, p. 1, 1984. [Online]. Available: http:// adsabs.harvard.edu/abs/1984LPI…15…1A

[45] R. R. Oder, "Magnetic separation of lunar soils," *IEEE Trans. Magn.*, vol. 27, no. 6, pp. 5367– 5370, 1991, doi: 10.1109/20.278841.

[46] G. Arrhenius, S. K. Asunmaa, and R. W. Fitzgerald, "ELECTROSTATIC PROPERTIES OF LUNAR REGOLITH," *Lunar and Planetary Institute*, pp. 30–32.

[47] C. Sipe *et al.,* "Creation, Methodology, and Applications of High Fidelity Simulated Lunar Agglutinates," in *Planetary and Terrestrial Mining Sciences Symposium: Simulants*, Virtual, 2021.

[48] L. A. Taylor, C. M. Pieters, and D. Britt, "Evaluations of lunar regolith simulants," *Planetary and Space Science*, vol. 126, pp. 1–7, 2016, doi: 10.1016/j.pss.2016.04.005.

[49] Exolith Lab, *LMS-1 Lunar Mare Simulant.* [Online]. Available: https://exolithsimulants.com/collections/regolith-simulants/products/lms-1-lunar-mare-simulant (accessed: Aug. 3 2021).

[50] Wikipedia, *Ilmenite.* [Online]. Available: https://en.wikipedia.org/w/index.php?title=Ilmenite&oldid=997720214 (accessed: Jul. 29 2021).

[51] R. R. Oder, "Magnetism of Lunar Soils," *Space Studies Institute*, 1992. [Online]. Available: http://ssi.org/Magnetism_of_Lunar_Soils.pdf

[52] W. N. Agosto, "Electrostatic Concentration of Lunar Soil Minerals," *Lunar Bases and Space Activities of the 21st Century*, p. 453, 1985. [Online]. Available: https://ui.adsabs.harvard.edu/abs/1985lbsa.conf.453A/abstract

[53] A. Radl, K. M. Neumann, and H. Wotruba, "From lunar regolith to oxygen and structural materials: RWTH Aachen's integrated conceptual design," in *Space Resources Week*, Virtual, 2021.

[54] W. J. Scott, "GEOPHYSICS FOR MINERAL EXPLORATION: A Manual for Prospectors," 2014. [Online]. Available: https://www.gov.nl.ca/iet/files/mines-prospector-matty-mitchell-virtual-geophysics-mineral-exploration-march2014.pdf

[55] Wikipedia, *Engineering design process.* [Online]. Available: https://en.wikipedia.org/w/index.php?title=Engineering_design_process&oldid=1038610711 (accessed: Aug. 31 2021).

[56] A. Wilkinson, "Size Beneficiation of Regolith for Simplicity and Efficiency," *Planetary & Terrestrial Mining and Sciences Symposium*, 2011. [Online]. Available: https://isruinfo.com/public/index.php?page=srr_12_ptmss

[57] W. N. Agosto, "Electrostatic separation of binary comminuted mineral mixtures," *Space Manufacturing*, p. 315, 1983.

[58] T. Li, H. Ban, J. Hower, J. Stencel, and K. Saito, "Dry triboelectrostatic separation of mineral particles: a potential application in space exploration," *Journal of Electrostatics*, vol. 47, no. 3, pp. 133–142, 1999, doi: 10.1016/S0304-3886(99)00033-9.

[59] S. Trigwell, J. Captain, J. Captain, E. E. Arens, J. W. Quinn, and C. I. Calle, "Electrostatic Beneficiation of Lunar Simulant," Berkeley, CA, 2006. [Online]. Available: https://ntrs.nasa.gov/citations/20130011155

[60] J. Captain, S. Trigwell, E. Arens, A. Biris, J. Quinn, and C. Calle, "Tribocharging lunar simulant in vacuum for electrostatic beneficiation," in *AIP Conference Proceedings*, pp. 951–956.

[61] S. Trigwell, J. G. Captain, E. E. Arens, J. W. Quinn, and C. I. Calle, "The Use of Tribocharging in the Electrostatic Beneficiation of Lunar Simulant," *IEEE Trans. on Ind. Applicat.*, vol. 45, no. 3, pp. 1060–1067, 2009, doi: 10.1109/TIA.2009.2018976.

[62] S. Trigwell, J. Captain, K. Weis, and J. W. Quinn, "Electrostatic beneficiation of lunar regolith: Applications in In-situ Resource Utilization," *J. Aero. Eng.*, vol. 26, no. 1, p. 30, 2012, doi: 10.1061/(ASCE)AS.1943-5525.0000226.

[63] J. Quinn, J. G. Captain, K. Weis, E. Santiago-Maldonado, and S. Trigwell, "Evaluation of Tribocharged Electrostatic Beneficiation of Lunar Simulant in Lunar Gravity," *J. Aero. Eng.*, vol. 26, no. 1, p. 37, 2012. [Online]. Available: https://ntrs.nasa.gov/citations/20110016172

[64] M. Adachi, H. Moroka, H. Kawamoto, S. Wakabayashi, and T. Hoshino, "Particle-size sorting system of lunar regolith using electrostatic traveling wave," *Journal of Electrostatics*, vol. 89, pp. 69–76, 2017, doi: 10.1016/j.elstat.2017.08.002.

[65] H. Kawamoto, K. Seki, and N. Kuromiya, "Mechanism on traveling-wave transport of particles," in *NIP & Digital Fabrication Conference*, Society for Imaging Science and Technology, Ed., pp. 1019–1026.

[66] R. R. Oder and L. A. Taylor, "Magnetic beneficiation of highland and hi-ti mare soils: magnet requirements," in *Engineering, Construction, and Operations in Space II*, 1990, pp. 133–142.

[67] S.G. Frantz Co., *L-1 Isodynamic Laboratory Separator.* [Online]. Available: https://www.sgfrantz.com/laboratory-separators/l-1-isodynamic-laboratory-separator/ (accessed: Sep. 27 2021).

[68] H. Kawamoto and H. Inoue, "Magnetic Cleaning Device for Lunar Dust Adhering to Spacesuits," *J. Aerosp. Eng.*, vol. 25, no. 1, pp. 139–142, 2012, doi: 10.1061/(ASCE)AS.1943-5525.0000101.

[69] W. N. Agosto, "Beneficiation and powder metallurgical processing of lunar soil metal," Princeton, NJ, USA, May. 18 1981 - May. 21 1981.

[70] M. A. Gibson and C. W. Knudsen, "Apparatus for manufacture of oxygen from lunar ilmenite," US005536378A, USA 309,990, Jul 16, 1996.

[71] O. Romberg and A. Martelo, "Space Systems Engineering / Concurrent Engineering: Lecture," DLR, Universität Bremen, Bremen, 2020.

[72] ECSS Executive Secretariat, "ECSS-E-ST-10-06C: Technical requirements specification," *European Cooperation for Space Standardization*, Mar. 2009.

[73] Wikipedia, *Decision matrix.* [Online]. Available: https://en.wikipedia.org/w/index.php?title=Decision_matrix&oldid=993728786 (accessed: Dec. 15 2022).

[74] Wikipedia, *Swiss cheese model.* [Online]. Available: https://en.wikipedia.org/w/index.php?title=Swiss_cheese_model&oldid=1067134469 (accessed: Jan. 6 2022).

[75] C. Z. Liang, "Development and Applications of a Drum Medium–Intensity Permanent Magnetic Separator," *Magnetic and Electrical Separation*, vol. 7, no. 3, pp. 133–144, 1996, doi: 10.1155/1996/12318.

[76] Physik - simpleclub, *E-Felder: Zusammenfassung*, 2016. Accessed: Jan. 8 2022. [Online]. Available: https://www.youtube.com/watch?v=YOfIgmeCwbo&ab_channel=Physik-simpleclub

[77] FRITSCH GmbH, *LABORETTE 24: Vibratory Feeder with V-shaped channel.* [Online]. Available: https://www.fritsch-international.com/sample-preparation/dividingfeeding/vibratory-feeders/details/product/laborette-24-with-v-shaped-channel/ (accessed: Jan. 10 2022).

[78] Russell Finex Ltd., *Circular Vibrating Screeners & Vibratory Sieves: Round Screeners.* [Online]. Available: https://www.russellfinex.com/en/separation-equipment/screening-machines/vibratory-sieves/ (accessed: Jan. 10 2022).

[79] K&J Magnetics, Inc., *Arc Segments: AX2C45-N.* [Online]. Available: https://www.kjmagnetics.com/proddetail.asp?prod=AX2C45-N (accessed: Jan. 11 2022).
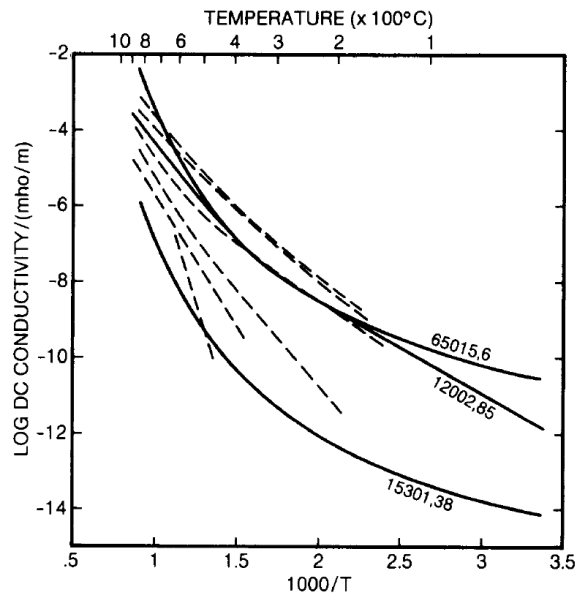
[80] RS Components Ltd., *RS PRO Brushed Geared DC Geared Motor: 7.92 W, 12 V, 10 Ncm, 897 rpm, 6mm Shaft.* [Online]. Available: https://export.rsdelivers.com/product/rs-pro/950d111/rs-pro-brushed-geared-dc-geared-motor-792-w-12-v/4540827 (accessed: Jan. 16 2022).

[81] Conrad Electronic SE, *Labornetzgerät: Basetech BT-153.* [Online]. Available: https://www.conrad.de/de/p/basetech-bt-153-labornetzgeraet-einstellbar-0-15-v-dc-0-3-a-45-w-anzahl-ausgaenge-1-x-393647.html#productDownloads (accessed: Jan. 16 2022).

[82] PHYWE Systeme GmbH und Co. KG, *Bestellkatalog: 2017/2018.* [Online]. Available: https://cdn02.plentymarkets.com/jd5w7us67fek/frontend/Onlineshop/Kataloge/2020/00202-01_Bestellkatalog_2017_2018_gesamt_web.pdf (accessed: Jan. 11 2022).

[83] ISOHEAT GmbH, *PTFE-insulated heating tape: series MiL-HT-PSG.* [Online]. Available: http://www.isoheat.de/fileadmin/downloads/public/produkte/heizleitungen_heizbaender/eng/MiL-HT-PSG_e.pdf (accessed: Jan. 16 2022).

[84] item Industrietechnik GmbH, *Product Catalogue: MB Building Kit System.* [Online]. Available: https://product.item24.de/en/products/product-catalogue/products/mb-building-kit-system-1001009411/ (accessed: Jan. 13 2022).

[85] SKF GmbH, *Rillenkugellager: 61809-2RS1.* [Online]. Available: https://www.skf.com/de/products/rolling-bearings/ball-bearings/deep-groove-ball-bearings/productid-61809-2RS1 (accessed: Jan. 16 2022).

[86] Simplify3D, *Ultimate Materials Guide: Tips for 3D Printing with PLA.* [Online]. Available: https://www.simplify3d.com/support/materials-guide/pla/ (accessed: Jan. 15 2022).

Annex

A1 – Further Information on Lunar Regolith

Fig. 9.48. Electrical conductivity of lunar samples. DC conductivity (vertical axis) is plotted as a function of inverse temperature in kelvins (bottom horizontal axis) and temperature (top horizontal axis), using the equations given in the text. In general, conductivity increases with increasing temperature for both lunar soil and rock samples. Dashed curves (from *Schwerer et al.,* 1974) are for samples 10048, 15058, 15418, 15555, 68415, and 68815. Solid curves (*Olhoeft et al.,* 1973a) give data for two soil samples (12002,85 and 15301,38) and one rock (65015,6).

TABLE 9.16. Summary of dielectric sounding results.

System	Wavelength (m)	Relative Dielectric Permittivity	Loss Tangent	References
Surveyor				
Surveyor 1	0.023	2.40±0.50	—	*Muhleman et al.* (1969)
Surveyor 3	0.023	2.07±0.11	—	*Muhleman et al.* (1969)
Surveyor 5	0.023	2.00±0.16	—	*Muhleman et al.* (1969)
Surveyor 7	0.023	3.28±0.40	—	*Muhleman et al.* (1969)
Surveyor 3	0.023	3.7±0.5–1.0	(0.0257±0.005) ρ (where ρ is density)	*Brown et al.* (1967)
Apollo 17 SEP				
First 7±1m depth		3.8±0.2	0.08±0.04	*Strangway et al.* (1975)
Next 100±10m		7.5±0.5	0.035±0.025	*Strangway et al.* (1975)
Remainder		9	—	*Strangway et al.* (1975)
Luna 9	0.17	2.7±0.9	—	*Kroupenio* (1971)
Luna 11		2.85±0.15	—	*Kroupenio* (1971)
Luna 13		4.4±2.1	—	*Kroupenio* (1971)
Luna 14	0.17	2.9±0.1	—	*Kroupenio* (1971)
Luna 16	0.031	2.15±0.35	—	*Kroupenio* (1973)
Luna 17	0.031	2.3±0.4	—	*Kroupenio* (1973)
Luna 19		2.35±0.65	—	*Kroupenio et al.* (1975)
Luna 19		3.2±0.2	—	*Kroupenio et al.* (1975)
Luna 20		1.7±0.2	—	*Kroupenio et al.* (1975)
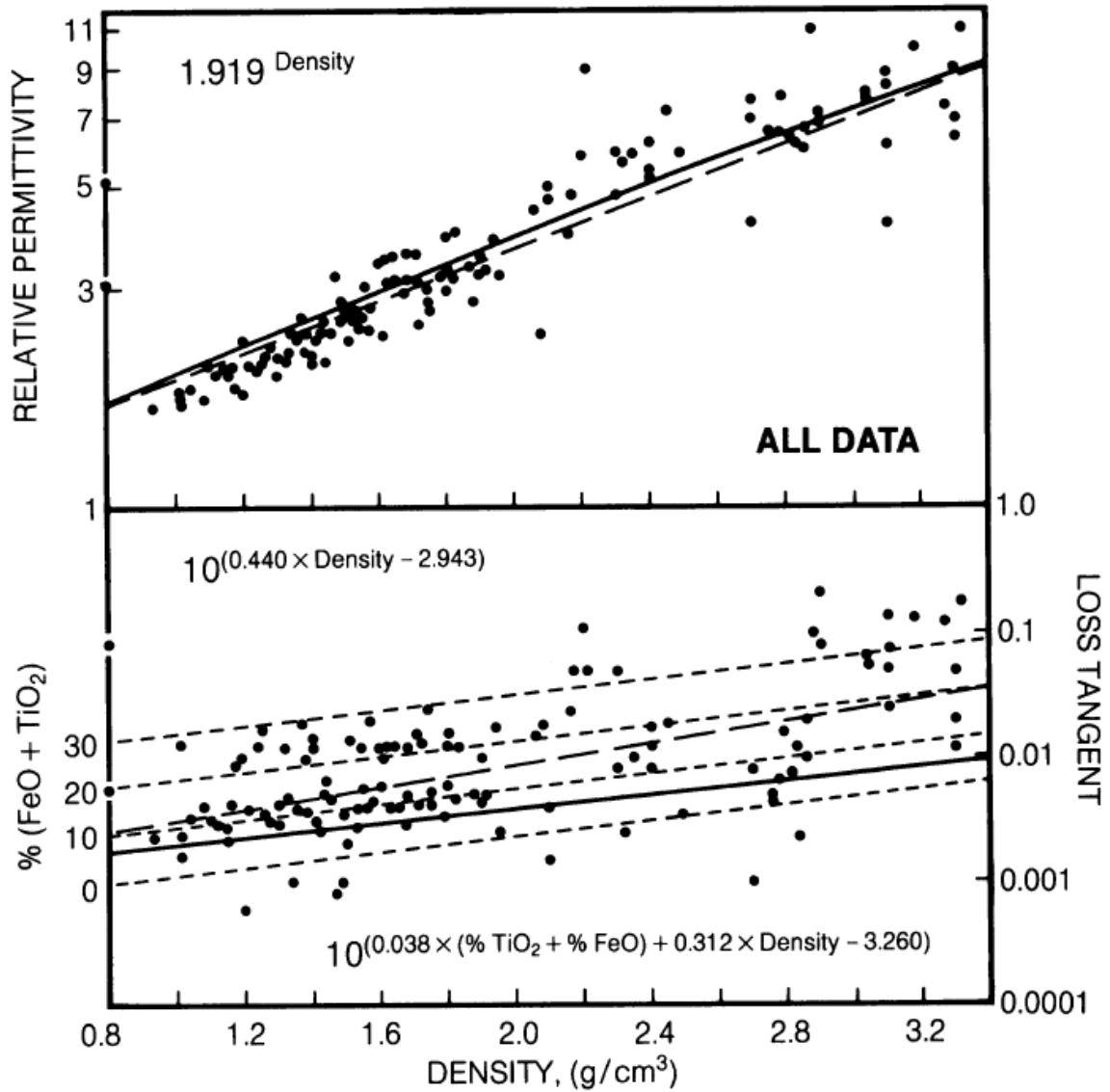
Fig. 9.52. Relative dielectric permittivity (upper vertical axis) and loss tangent (lower right vertical axis) for lunar materials as functions of bulk density (horizontal axis) and %(TiO₂ + FeO). Data points represent all samples from Table A9.16. Both permittivity and loss tangent increase with increasing density. The permittivity plot (upper) shows two theoretical fits to the data points: the Bruggeman-Hanai-Sen (BHS) mixing formula (*Sen et al.*, 1981) (solid line; see text for details) and a least-squares power-law fit (*Olhoeft and Strangway*, 1975) (dashed line). The loss tangent plot (lower) shows three theoretical fits to the data: the equivalent BHS formula (solid line), the two-dimensional regression to the power-law formula (given in upper left) (dashed line), and three-dimensional regression (light dashed lines) of variance as a function of density and selected values of %(TiO₂ + FeO) (light dashed curves for 0%, 10%, 20%, and 30%).

Source: Lunar sourcebook. A user's guide to the moon by Heiken, Grant; Vaniman, David; French, Bevan M. (2005)

A2 – Further Information on Simulants

LHS-1 Lunar Highlands Simulant | **Fact Sheet**
January, 2021

Simulant Name: LHS-1 Lunar Highlands Simulant
Simulant Type: General purpose
Reference Material: Average lunar highlands
Uncompressed Bulk Density: 1.30 g/cm^3
Mean Particle Size: 60 μm
Median Particle Size: 50 μm
Particle Size Range: <0.04 μm – 400 μm

Mineralogy

As mixed.

Component	Wt.%
Anorthosite	74.4
Glass-rich basalt	24.7
Ilmenite	0.4
Olivine	0.3
Pyroxene	0.2

Safety

See SDS for details. Primary hazard is dust inhalation; wear a respirator in dusty conditions.

Bulk Chemistry

Measured by XRF.

Oxide	Wt.%
SiO_2	48.1
Al_2O_3	25.8
CaO	18.4
Fe_2O_3	3.7
K_2O	0.7
MgO	0.3
MnO	0.1
P_2O_5	1.0
TiO_2	1.1
SO_3	0.3
Cl	0.4
SrO	0.1
Total	99.9

Particle Size Distribution

FTIR Spectrum

Photo credit Matthew Villegas. FTIR spectrum courtesy of Katerina Slavicinska, Bennett Lab, UCF. Apollo particle size data adapted from the Lunar Soils Grain Size Catalog, Graf, 1993.

LMS-1 Lunar Mare Simulant | **Fact Sheet**
January, 2021

Simulant Name: LMS-1 Mare Simulant
Simulant Type: General purpose
Reference Material: Average lunar maria
Uncompressed Bulk Density: 1.56 g/cm³
Mean Particle Size: 50 µm
Median Particle Size: 45 µm
Particle Size Range: <0.04 µm – 300 µm

Mineralogy

As mixed.

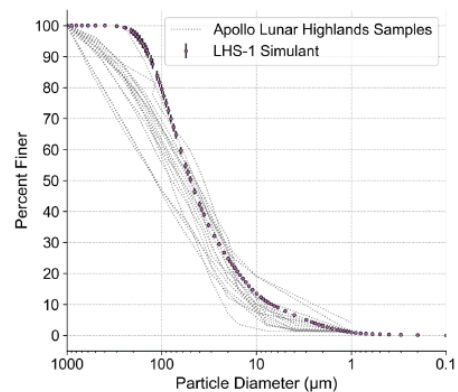| Component	Wt.%
Pyroxene	32.8
Glass-rich basalt	32.0
Anorthosite	19.8
Olivine	11.1
Ilmenite	4.3

Safety

See SDS for details. Primary hazard is dust inhalation; wear a respirator in dusty conditions.

Bulk Chemistry

Measured by XRF.

Oxide	Wt.%
SiO_2	40.2
Al_2O_3	14.0
CaO	9.8
Fe_2O_3	13.9
K_2O	0.6
MgO	12.0
MnO	0.3
P_2O_5	1.0
TiO_2	7.3
Cl	0.4
Cr_2O_3	0.3
NiO	0.2
SrO	0.1
Total	**100.0**

Particle Size Distribution
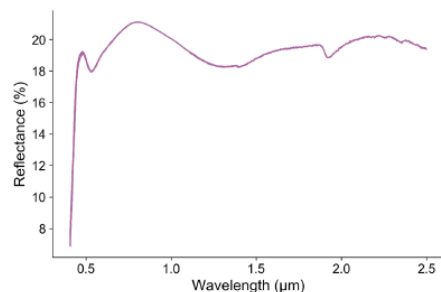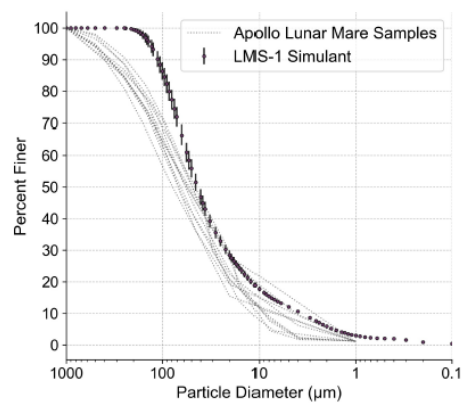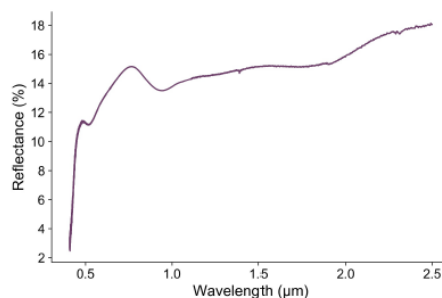

FTIR Spectrum

Photo credit Matthew Villegas. FTIR spectrum courtesy of Katerina Slavicinska, Bennett Lab, UCF. Apollo particle size data adapted from the Lunar Soils Grain Size Catalog, Graf, 1993.

EXOLITH LAB

LHS-1D Dust Simulant | Fact Sheet

January, 2021

Simulant Name: LHS-1D Dust Simulant
Simulant Type: Extra-fine lunar highlands simulant for dust studies
Reference Material: Average lunar highlands
Uncompressed Bulk Density:
Mean Particle Size: 7 μm
Median Particle Size: 5 μm
Particle Size Range: <0.04 – 35 μm

Mineralogy

As mixed.

| Component	Wt.%
Anorthosite	74.4
Glass-rich basalt	24.7
Ilmenite	0.4
Olivine	0.3
Pyroxene	0.2

Safety

See SDS for details. Primary hazard is dust inhalation; wear a respirator in dusty conditions.

Bulk Chemistry

Measured by XRF.

Oxide	Wt.%
SiO_2	48.1
Al_2O_3	25.8
CaO	18.4
Fe_2O_3	3.7
K_2O	0.7
MgO	0.3
MnO	0.1
P_2O_5	1.0
TiO_2	1.1
SO_3	0.3
Cl	0.4
SrO	0.1
Total	99.9

Particle Size Distribution

FTIR Spectrum

In progress.

Photo credit Matthew Villegas.

Source: *https://exolithsimulants.com/collections/regolith-simulants*

A3 – Further Information on Ilmenite & Tailings

TABLE 1. Significant Lunar Minerals..

	Mineral	Dana #	Mohs Hardness	Spec Gravity	Chemical Composition	%*
Plagioclase	Anorthite	76.1.3.6	6	2.75	$CaAl_2Si_2O_8$	A
	Bytownite	76.1.3.5	6.0-6.5	2.73	$(Ca,Na)(Si,Al)_4O_8$	M
	Labradorite	76.1.3.4	7	2.71	$(Ca,Na)(Si,Al)_4O_8$	M
Olivine	Fayalite	51.3.1.1	6.5-7.0	4.39	Fe_2SiO_4	m
	Forsterite	51.3.1.2	6.5-7.0	3.24	Mg_2SiO_4	M
Pyroxene	Clinoenstatite	65.1.1.1	5.0-6.0	3.4	$Mg_2[Si_2O_6]$	M
	Pigeonite	65.1.1.4	6	3.3	$(Mg,Fe^{+2},Ca)_2[Si_2O_6]$	M
	Hedenbergite	65.1.3a.2	6	3.5	$CaFe^{+2}[Si_2O_6]$	m
	Augite	65.1.3a.3	5.5-6.0	3.3	$(Ca,Na)(Mg,Fe,Al,Ti)[(Si,Al)_2O_6]$	M
	Enstatite	65.1.2.1	5.0-6.0	3.4	$Mg_2[Si_2O_6]$	A
O	Ilmenite	4.3.5.1	5.5	4.72	$Fe^{+2}TiO_3$	m
Spinel	Spinel	7.2.1.1	7.5-8.0	3.56	$MgAl_2O_4$	m
	Hercynite	7.2.1.3	7.5-8	3.93	$Fe^{+2}Al_2O_4$	m
	Ulvospinel	7.2.5.2	5.5-6.0	4.7	$TiFe^{+2}_2O_4$	m
	Chromite	7.2.3.3	5.5	4.7	$Fe^{+2}Cr_2O_4$	m
S	Troilite	2.8.9.1	4	4.75	FeS	t
PO4	Whitlockite	38.3.4.1	5	3.12	$Ca_9(Mg,Fe^{+2})(PO_4)_6(PO_3OH)$	t
	Apatite	41.8.1.0	5	3.19	$Ca_5(PO_4)_3(OH,F,Cl)$	t
	Native Iron	2.9.1.1	4.5	7.87	Fe	t

* - Typical relative abundance, A-abundant, M-major, m-minor, t-trace.

Source: https://www.nasa.gov/sites/default/files/atoms/files/significant_lunar_minerals.pdf

Table 1. *WFs and Q of several minerals*

Mineral	WF (eV)	Charge (Q)
olivine	7.90 ± 0.35	1696 ± 243
plagioclase	5.58 ± 0.38	3309 ± 264
pyroxene	5.14 ± 0.36	3615 ± 250
ilmenite	4.29 ± 0.11	4207 ± 76

Source: "INDICATION OF MINERAL WORK FUNCTION IN LUNAR DUST ELECTROSTATIC MIGRATION"
by Xiongyao Li, Hong Gan, Bing Mo, Shijie Wang, Hong Tang, Guangfei Wei, Yu-Yan Sara Zhao (1993)
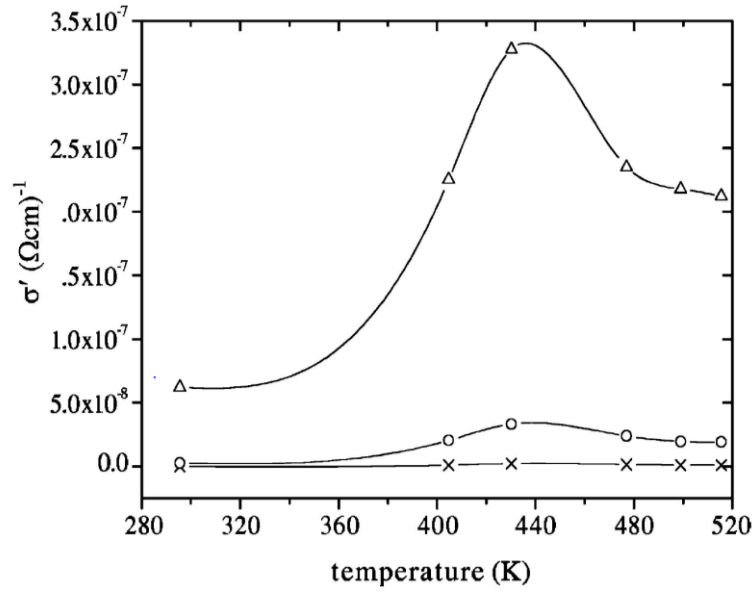
Figure 3 A plot of the real conductivity against temperature for the Microwave treated Ilmenite samples at three chosen frequencies (10^{-2} ($\times$), 10^3 ($\circ$) and 10^5 Hz ( )). The solid line is a spline fit to the data showing a peak temperature (T_p) around 440 K.
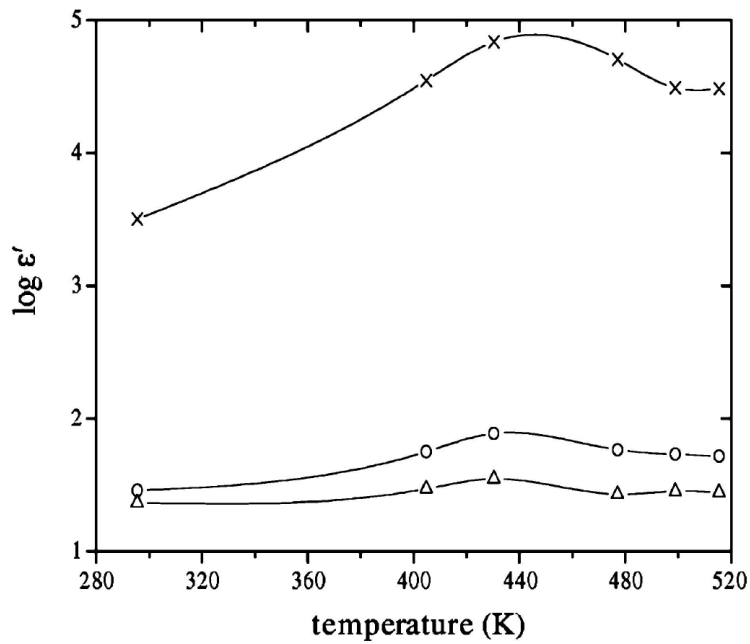
Figure 6 A plot of the dielectric constant against temperature for the Microwave treated Ilmenite samples at three chosen frequencies (10^{-2} ($\times$), 10^3 ($\circ$) and 10^5 Hz ( )). The solid line is a spline fit to the data from which T_p can be estimated around 440 K.

Source: *"An investigation on electrical properties of microwave treated natural ilmenite (FeTiO3)"*
by Chiteme, C.; Mulaba-Bafubiandi, A. F. (2006)

A4 – Requirements & Specifications cont'd

Contextual Information for Specifications found in Literature

Author	Year	Sub-Processes	Process Parameter	Mixture
Gravitational				
Wilkinson	2011	Screening	Rotary shearing vs. horizontal vibratory sifter	LHT-2M, JSC-1A, OB-1
Magnetic				
Williams	1979	n/a	220 tons per hour (only in theory)	high-titanium, mature mare soil 70215
Oder	1989	Frantz Isodyn. Sep.	-	1g of highland soil 64421
Taylor	1992	Frantz Isodyn. Sep.	-	immature soil 71061 (a typical Apollo ...)
Beggren	2011	Magnetic Drum Sep.	3545 Gauss	JSC-1A and Nu-LHT-2M
Electrostatic				
Adachi	2017a	ETW	parallel copper electrodes & polyimide substrate; 18µm th	FJS-1
Agosto	1984	Conductive induction & slide separator	T=190; 5kV/cm;	KSC-1 & Apollo 10084
Williams	1979	Charging Electrodes & Free Fall Separation		n/a
Agosto	1983	Conductive induction & slide separator	T=28 & 180...190C, "+-7kV and +-4.7kV, later 5kV"	Binary Mixture
Agosto	1985	Conductive induction & slide separator	T=100...200C	Apollo 11 soil.
Captain	2007	tribocharging & plate separation	materials: copper, alu, PTFE, stainless steel; 50deg incline	JSC-1 & KSC-1
Li	1999	tribocharging & plate separation	200 kV/m	Custom
Quinn	2012	tribocharging & plate separation	Text(+-12kV and +-20kV; 18g simulat); 2nd feed rate 0.18	NU-LHT-2M.
Trigwell	2006	tribocharging & plate separation	4deg charged to +-15 kV	JSC-1 & MLS-1
Trigwell	2009	tribocharging & plate separation	Parallel electrodes charged to +-15 kV	JSC-1 & JSC-1A & KSC-1
Trigwell	2012	tribocharging & plate separation	up to +-30kV (12 and 24 were used), 7 bins	JSC-1A & NU-LHT-2M & Apollo 14163 /
Additional Sources				
Beggren	2021	Multi-Stage	1kg/day oxygen; >10kV plate voltage, low current	JSC-1A and Nu-LHT-2M
Agosto	1985	Conductive induction & slide separator	-	Apollo 11 soil.

Requirements Catalogue for System- and Subsystem-Level (CW 45)

RQ ID	RQ LVL	RQ Type	RQ Title	RQ Statement	Specs
SMU_BEN_001	System	Functional RQ	Input	The beneficiation testbed shall be able to receive, convey and process lunar regolith simulant (LHS-1, LMS-1 or LHS-1D) as a raw material.	
SMU_BEN_002	System	Functional RQ	Particle sizing	The beneficiation testbed shall be able to filter specific particle sizes of the raw material.	
SMU_BEN_003	System	Functional RQ	Mineral enrichment	The beneficiation testbed shall separate the ore mineral ilmenite from other constituents within the raw material.	
SMU_BEN_004	System	Functional RQ	Output I	The beneficiation testbed shall be able to dispense a feedstock of size-sorted material rich in the ore mineral.	
SMU_BEN_005	System	Functional RQ	Output II	The beneficiation testbed shall be able to dispense waste streams of undesired tailings and gangue minerals.	
SMU_BEN_006	System	Performance RQ	Input mass / volume	The amount of lunar regolith simulant that can be received by the testbed shall at least be 1 kg or 1 liter, respectively.	1 kg / 1l
SMU_BEN_007	System	Performance RQ	Input rate	The rate at which the lunar regolith simulant can be conveyed and processed by the testbed shall be 15±5 kg/h.	15 kg/h
SMU_BEN_008	System	Performance RQ	Size range	The particles size to be filtered by the testbed shall range from 0 to 20 μm and from 200 μm onwards.	20...200 μm
SMU_BEN_009	System	Performance RQ	Grade	The final grade of the ore mineral within the feedstock dispensed by the testbed shall be at least 40 wt.%	40%
SMU_BEN_010	System	Performance RQ	Recovery	The recovery of the ore mineral within the feedstock dispensed by the testbed shall be at least 50 wt.%	50%
SMU_BEN_011	System	Performance RQ	Enrichment factor	The enrichment ratio of the ore mineral within the feedstock dispensed by the testbed shall at least be 4.5.	4.5
SMU_BEN_012	System	Environmental RQ	Gravity	The beneficiation testbed shall be able to operate under Earth's gravitational acceleration of 9.81 m/s^2.	9.81 m/s^2
SMU_BEN_013	System	Environmental RQ	Pressure	The beneficiation testbed shall be able to operate under atmospheric pressure (10^5 Pa) and vacuum (up to 10^-10 Pa).	10^5 Pa... 10^-10 Pa
SMU_BEN_014	System	Environmental RQ	Temperature	The beneficiation testbed shall be able to operate at a standard temperature of 293.15K (±5K).	293.15K (±5K).
SMU_BEN_015	System	Environmental RQ	Humdity	The beneficiation testbed shall be able to operate at an air humidity lower than 60 %.	60 %.
SMU_BEN_016	System	Operational RQ	Operator	The beneficiation testbed shall be operable by a single, (HV-)qualified experimenter.	
SMU_BEN_017	System	Operational RQ	Control	The beneficiation testbed shall accept an input of multiple control parameters from the operator prior to the experiment's start.	

SMU_BEN_018	System	Interface RQ	Mech. Connection	The beneficiation testbed shall offer a permanent connection to the ground and a firm stand during experiments.	
SMU_BEN_019	System	Interface RQ	Elec. Connection	The beneficiation testbed shall connect to one or more Schuko electrical socket(s), i.e., AC 230V 50Hz.	
SMU_BEN_020	System	Design RQ	Transportability	The beneficiation testbed shall be designed in a moveable manner, allowing it to be transported to different locations.	
SMU_BEN_021	System	Design RQ	Dimensions	The beneficiation testbed shall fit through standard door frames without disassembly.	
SMU_BEN_022	Subsystem	Functional RQ	Structure: Casing	The structure shall encase the other subsystems, physically separating them from the surrounding.	
SMU_BEN_023	Subsystem	Functional RQ	Structure: Hold	The structure shall be able to hold the other subsystems in place by offering mechanical attachment points.	
SMU_BEN_024	Subsystem	Functional RQ	Structure: Accessibility	The structure shall be open- and closeable to allow temporal access to the other subsystems for maintenance and equipping.	
SMU_BEN_025	Subsystem	Functional RQ	Structure: Mech. Loads	The structure shall absorb the system's mechanical loads and transfer them to the ground.	
SMU_BEN_026	Subsystem	Functional RQ	Structure: Vibrations	The structure shall dampen the vibrations induced by the other subsystems to avoid resonance.	
SMU_BEN_027	Subsystem	Functional RQ	Structure: Visibility	The structure shall allow for continuous observation of the beneficiation process by the operator.	
SMU_BEN_028	Subsystem	Design RQ	Structure: Modularity	The structure shall primarily be built from ITEM's modular assortment, as decided by the head of the SMU research group.	
SMU_BEN_029	Subsystem	Design RQ	Structure: Max. Dimens.	The structure shall not exceed 195 cm x 92 cm, as given by the door frame of the EDEN laboratory at the DLR institute in Bremen.	195*92 cm
SMU_BEN_030	Subsystem	Design RQ	Structure: Min. Dimens.	The outer structural elements shall have a minimum distance of 10 mm to other subsystems.	10 mm
SMU_BEN_031	Subsystem	Design RQ	Structure: Dust	The structure shall be sealed against dust (IP 50), containing whirled up lunar regolith simulant inside the system.	IP 50
SMU_BEN_032	Subsystem	Environmental RQ	Structure: Detergent	The outer structural elements shall be resistant towards detergents and corrosion.	
SMU_BEN_033	Subsystem	Functional RQ	Inlet: Feeding	The inlet shall dispense the raw material at a constant rate into the gravitational separator.	
SMU_BEN_034	Subsystem	Functional RQ	Inlet: Control	The inlet shall be controllable before and during the experiment by qualified staff.	
SMU_BEN_035	Subsystem	Performance RQ	Inlet: Feed Rate	The feed rate at which the raw material shall be dispensed by the inlet is 15 kg/h.	15 kg/h
SMU_BEN_036	Subsystem	Design RQ	Inlet: External Panel	The inlet's vibratory feeder and control panel shall be separable from one another.	

ID	Type	RQ Type	Category	Requirement	Value
SMU_BEN_037	Subsystem	Design RQ	Inlet: Size	The inlet shall not occupy more than 25% of the system's total volume.	25%
SMU_BEN_038	Subsystem	Interface RQ	Inlet: Power	The inlet shall be connected to a regular socket (as specified in SMU_BEN_019) via an in-built cable.	
SMU_BEN_039	Subsystem	Interface RQ	Inlet: Mounting	The inlet shall provide its own pedestal to stand in an upright position on a planar element within the structure.	
SMU_BEN_040	Subsystem	Functional RQ	Grav. Ben.: Separation	The gravitational separator shall receive the raw material fed by the inlet and discriminate its particles according to their size.	
SMU_BEN_041	Subsystem	Functional RQ	Grav. Ben.: Wanted	The gravitational separator shall forward the wanted fraction to the magnetic separator.	
SMU_BEN_042	Subsystem	Functional RQ	Grav. Ben.: Unwanted	The gravitational separator shall forward the unwanted size fraction to a waste container.	
SMU_BEN_043	Subsystem	Functional RQ	Grav. Ben.: De-blinding	The gravitational separator shall prevent (actively or passively) the blinding of its mesh.	
SMU_BEN_044	Subsystem	Performance RQ	Grav. Ben.: Size Good	The gravitational separator shall concentrate particles less than or equal to 200 μm and forward them to the magnetic separator.	
SMU_BEN_045	Subsystem	Performance RQ	Grav. Ben.: Size Bad	The gravitational separator shall reject particles bigger than 200 μm and release them to the outlet's waste container.	
SMU_BEN_046	Subsystem	Design RQ	Grav. Ben.: Mesh	The gravitational separator shall have a mesh-size of 200 μm.	
SMU_BEN_047	Subsystem	Interface RQ	Grav. Ben.: Power	The gravitational separator shall be connected to a Schuko socket (as specified in SMU_BEN_019) via an in-built cable.	
SMU_BEN_048	Subsystem	Interface RQ	Grav. Ben.: Mounting	The gravitational separator shall be mountable to an external structure.	
SMU_BEN_049	Subsystem	Functional RQ	Mag. Ben.: Separation	The magnetic separator shall remove ferromagnetic tailings (e.g., agglutinates) from para- and diamagnetic particles.	
SMU_BEN_050	Subsystem	Functional RQ	Mag. Ben.: Sizing	The magnetic separator shall remove the dust fraction of the sieved material.	
SMU_BEN_051	Subsystem	Performance RQ	Mag. Ben.: Size Range	The magnetic separator shall remove particles with a grain size of 0 to 20 μm by exploiting their greater susceptibility.	
SMU_BEN_052	Subsystem	Design RQ	Mag. Ben.: Controlability	The magnetic separator shall have an adjustable divider that allows for controllability	
SMU_BEN_053	Subsystem	Interface RQ	Mag. Ben.: Sizing	The magnetic separator shall be powered by a laboratory power supply, which rectifies and transforms the power from the socket.	
SMU_BEN_054	Subsystem	Functional RQ	Elec. Ben.: Separation	The electrostatic separator shall partition minerals based on differences in conductivity.	200°C

A5 – Further Reasoning for Process Assessment

Dynamic Screening

- **Environmental Independence:** Movement (vibration or rotation) provided by dynamic mechanism helps particles to move down despite low-g environment; vacuum and radiation are of no concern
- **Simplicity & Reliability:** Complexity of apparatus slightly increased (electrical motor is a single point of failure), but on the other hand reliability increased as blinding less of an issue
- **Energy Efficiency:** Low electric energy consumption due to minute movement only (low kinetic and potential energy required)
- **Volume & Mass:** Bigger than stationary sifter, but smaller than cyclones / slotted ramp separator
- **Technology Readiness:** Very well established on Earth; COTS available; almost all studies use a dynamic sifter
- **Process Integrability:** Continuous operation possible; easy to integrate; no maintenance needed when suitable de-blinding insert utilized
- **Adjustability & Scalability:** Available in all sizes and shapes; design parameters easily adaptable to needs (same as for stationary screening
- **Performance:** sizing good, mineral enrichment rather limited, same like stationary
- **Cost & Dev. Effort:** Low dev. Effort (COTS available; select size ranges and you have your main design parameter [mesh size]), but costs are higher due to motor

Cyclones

- **Environmental Independence:** Classification with process-fluid unfavorable for extraterrestrial applications; losses are to be expected due to pressure potential
- **Simplicity & Reliability:** Involves a gas that may escape the system, leading to failure of mission; pump prone to failure, but no moving parts and low-wear
- **Energy Efficiency:** Creating & maintaining flow costs energy (permanently)
- **Volume & Mass:** Volume intense, as reliant on high inner surface area & height; mass low due to thinness of sheet metal
- **Technology Readiness:** Well-established on Earth, but no experimental proof of concept for extraterrestrial application
- **Process Integrability:** Air locks needed for vacuum, which makes vertical orientation (needed for free-fall system) impossible.
- **Adjustability & Scalability:** Easily pre-dimension-able, as dimensions and air pressure can be adjusted to granulate. But not much control during operation
- **Performance:** No scientifically sound data for lunar application, but assumed as moderate
- **Cost & Dev. Effort:** Medium costs; COTS abundantly available, but only few of them for solid-solid separation

Rotating Cone Separator

- **Environmental Independence:** Air drag under atmospheric pressure distorts experiment; different cone shape and rotational speed needed for different gravitational acceleration on Moon and Earth (in the laboratory)
- **Simplicity & Reliability:** Motor for rotating cone is single point of failure; many moving parts (rotation at high RPM rates will eventually cause wear & tear)

- **Energy Efficiency:** Electric energy will be needed constantly – its quantity is determined by design and weight of cone (so that moderate score given)
- **Volume & Mass:** Diameter of cone must be big for good resolution of particle distribution
- **Technology Readiness:** No real heritage in terrestrial mining industry; however, Berggren's design seems promising and will be iterated in the future
- **Process Integrability:** Can be mounted with ease, but the big field of distribution means that regolith is not dispensed at one single spot, making it hard to funnel the outgoing material
- **Adjustability & Scalability:** RPM (main parameter) can be adjusted during operation, meaning performance can be controlled without design change; very well scalable
- **Performance:** Improvement of the grade reported by Berggren was not satisfying, but rather moderate
- **Cost & Dev. Effort:** Single parts are rather cheap, but dev. effort is medium

Slotted Ramp Separator

- **Environmental Independence:** A drag not such an issue (as velocity of particles remains small); two separate designs will be needed for different gravity on Moon and Earth
- **Simplicity & Reliability:** No noticeable wear & tear, only a couple of parts will face abrasion over time; Only release of particles is handled non-mechanically
- **Energy Efficiency:** No external electric energy needed, but high potential energy needed (the greater the difference in height, the better for this type of separator)
- **Volume & Mass:** Fairly large volume occupied, but mass should be somewaht small
- **Technology Readiness:** Concept has only been proven by Berggren in lunar context so far, no comparable techniques found in terrestrial industries
- **Process Integrability:** Can be integrated between regolith feeder and ensuing mineral enrichment steps easily
- **Adjustability & Scalability:** Design is adjustable, but only in advance (no controllability during operation); very well scalable
- **Performance:** Seems promising, with some uncertainty
- **Cost & Dev. Effort:** Single parts are very cheap, but dev. effort is medium

Conductive Induction (both for slide separator and roller separator)

- **Environmental Independence:** Will work under different atmospheric conditions (Earth atmosphere / nitrogen / vacuum), but presence of a surrounding fluid makes a big difference (as reported by Agosto in 1985 [see 3.1]: Ionized gas may contribute to particle charging and fluid drag may lead to to partial density segregation of ilmenite / increase the transit time)
- **Simplicity & Reliability:** Structure of slide separator is very simple and has no moving parts; Roller type separator has only few moving parts; both rely on electrode that may fail
- **Energy Efficiency:** Extensive heating is needed for this method, which is very energy intensive; the slide separator needs a lot of potential energy (same explanation as for slotted ramp holds true), but no additional electric energy; the roller separator additionally needs an engine that turns the drum
- **Volume & Mass:** Slide separator is rather big and bulky; roller is cylindrical and has high front area utilization; mass should be lower for sheet-metal slide
- **Technology Readiness:** Only one researcher (Agosto) was active in the field of conductive induction for lunar SRU; the papers he published are almost 40 years old; As slides were preferential, it was more deeply investigated (research in conductive induction + roller separator has halted as a consequence); mineral fines were neglected by Agosto

- **Process Integrability:** Both offer rather good integrability; axis of incoming and outgoing material flow fully vertical for roller/drum types (not the case for slide, where it is 45 deg, not allowing fully vertical material flow for free-fall separator)
- **Adjustability & Scalability:** Both variants are scalable, but only roller type is fully adaptable (slide only adjustable during design phase; no controllability after manufacturing; roller can be adjusted without design changes (through RPM)
- **Performance:** Literature reports that it may be hard to efficiently separate minerals with high resistivity using induction charging (as mentioned in chapter 2); semi-conductors would also be charged through tribocharging (friction with the metal slide) – which leads to deteriorated predictability (chapter 3)
- **Cost & Dev. Effort:** Costs are medium; designing the slide would be easier (geometric simplicity) than designing the roller separator (more parts involved)

Tribocharging & Plate Separator

- **Environmental Independence:** Static chargers are reliant on gravity, so different design will be needed for Moon and Earth – however, pneumatic conveyance may be employed to compensate for low-g; atmospheric pressure does not seem to play a major role
- **Simplicity & Reliability:** Tribocharging is repeatedly referred to as the simplest process for imparting charge on particles; static chargers work independently (do not rely on external power supply), so no blackout would impair its performance, (only plates would be affected)
- **Energy Efficiency:** High potential energy needed; high voltage power supply needed
- **Volume & Mass:** Low-mass components can be employed; big height due to static chargers
- **Technology Readiness:** Has been tested under more conditions than any other method for lunar SRU
- **Process Integrability:** Integration easily viable; axis of incoming and outgoing material flow fully aligned (perfect for free-fall setup)
- **Adjustability & Scalability:** Dimensions of static chargers can be adapted to flow rate (but only in advance, not during operation); Voltage of plates can be adjusted during operation
- **Performance:** Rasera concluded that tribocharging together with parallel plate separators are capable of enriching minerals in the context of lunar ISRU.
- **Cost & Dev. Effort:** Easy to develop; COTS parts abundantly available

Tribocharging & ETW

- **Environmental Independence:** Different gravitational potential translates into completely different dimensions; air drag may play a major role in particle trajectory and demands counter measures (as hinted by the authors themselves)
- **Simplicity & Reliability:** The whole system contains no more than three main units only: power supply, microcomputer, particle conveyor, and hopper; but despite low number of parts, those parts are rather complex compared to other techniques; stability relies on sophisticated electronics
- **Energy Efficiency:** Four low-voltage lines needed (energy consumption rather medium)
- **Volume & Mass:** Fairly compact experimental setup (30 cm in height for lab testing)
- **Technology Readiness:** Only 1 group of Japanese researchers investigated this technology for lunar SRU; low TRL so far; material flow tested so far only very small (5 g)
- **Process Integrability:** integrating this system is possible, but comes at an elevated effort (as hoppers are not in one plane but stacked on top of each other); horizontal process chain preferred, vertical alignment rather difficult

- **Adujustability & Scalability:** adjustability generally good (via microcomputer); the author (Adachi) remarks that the scaling of such a system is generally possible (by widening the width of the conveyor and installing the collection boxes parallelly (meaning that major design changes would be needed)
- **Performance:** Sizing performance is generally very good, but the mineral enrichment not persuasive
- **Cost & Dev. Effort:** Many complex electronics involved; no COTS solutions available; all in all rather expensive; relies on coding (extra effort)

Ion, electron & UV Bombardment & Drum separation

- **Environmental Independence**: Ion bombardment demands a gaseous medium like air to be ionized, which is hard to be stored and impractical on the moon (as explained by Manouchecheri: The negative corona is only possible to be generated in gases that provide electron attachment).
- **Simplicity & Reliability:** Three main components only ([corona-generating] electrode, earthed metallic surface and gas to ionize); very similar to induction & roller separator
- **Energy Efficiency:** depends on beam type: ion bombardment (corona discharge) = high voltage electrode, lightning bolts are sign of energy losses; electron more energy efficient; UV most likely best
- **Volume & Mass:** Same as for other drum/roller separators mentioned above
- **Technology Readiness:** Not demonstrated for lunar purposes, but good terrestrial heritage (as mentioned by Manouchecheri)
- **Process Integrability:** Same as for conductive induction & roller separator; axis of incoming and outgoing material flow fully vertical for roller/drum types
- **Adjustability & Scalability:** Just like other roller separators (RPM adjustable); voltage adjustability gives new degree of feedome
- **Performance:** Solid performance on Earth, not yet tested for lunar application, so average value assumed
- **Cost & Dev. Effort:** Same as for roller separator with conductive induction nominated as the most favorable process

Stationary Permanent Magnet

- **Environmental Independence:** Air pressure, temperature and other env. factors do not have a big influence; however, with low g comes clogging and adherence may become a big issue due to charge
- **Simplicity & Reliability:** The simplest technique possible; no moving parts; not affected by power outage
- **Energy Efficiency:** No electric energy consumed; no other form of energy must be applied
- **Volume & Mass:** Small dimensions are viable; magnets alone have comparably small mass (as no extra parts are required, as it is the case for other technologies)
- **Technology Readiness:** Permanent magnets have been used a lot on Earth and in Space
- **Process Integrability:** When integrated into a bigger system, a permanent magnet becomes prone to clogging and needs frequent maintenance / cleaning, as it cannot be deactivated
- **Adjustability & scalability:** Magnetic attraction / repulsion force and size can be chosen freely
- **Performance:** Oly dedusting is possible with low-T hand magnets – even most agglutinates will not be attracted; mineral enrichment is not feasible this way
- **Cost & Dev. Effort:** Comparably cheap; no development effort (magnets are COTS parts)

Permanent Magnet Drum Separator

- **Environmental Independence:** Operability in vacuum and atmosphere already proven; The controllability of the drum motor makes it adaptable to lunar and terrestrial gravity
- **Simplicity & Reliability:** Only few moving parts used; almost no wear and tear; very sturdy
- **Energy Efficiency:** Only a small and efficient DC motor that turns the cylinder is powered; permanent magnets do not consume any energy
- **Mass & Volume:** Cylindrical shape of the drum offers high surface area to volume ratio (optimally exploiting the volume); The device built by Berggren was very compact
- **Technology Readiness:** Feasibility only demonstrated in one study, but it is recent / topical (not as ancient as e.g., Agosto's findings); very common in the terrestrial industry
- **Process entertainability:** no maintenance necessary, brush cleans of remainder, free-fall feed on drum is perfect; different flows separatable with adjustable metal surface
- **Adjustability & Scalability:** Easily adjustable through various parameters (controlling speed etc.); only increase nr. of magnets or dimensions to scale up
- **Performance:** Sound dedusting performance, as small particles highly attracted to low T magnets; ferrous agglutinates easily removed; enrichment ratio rather limited with simulants as portrayed by Berggren
- **Cost & Dev. Effort:** Cheap components; modest development effort

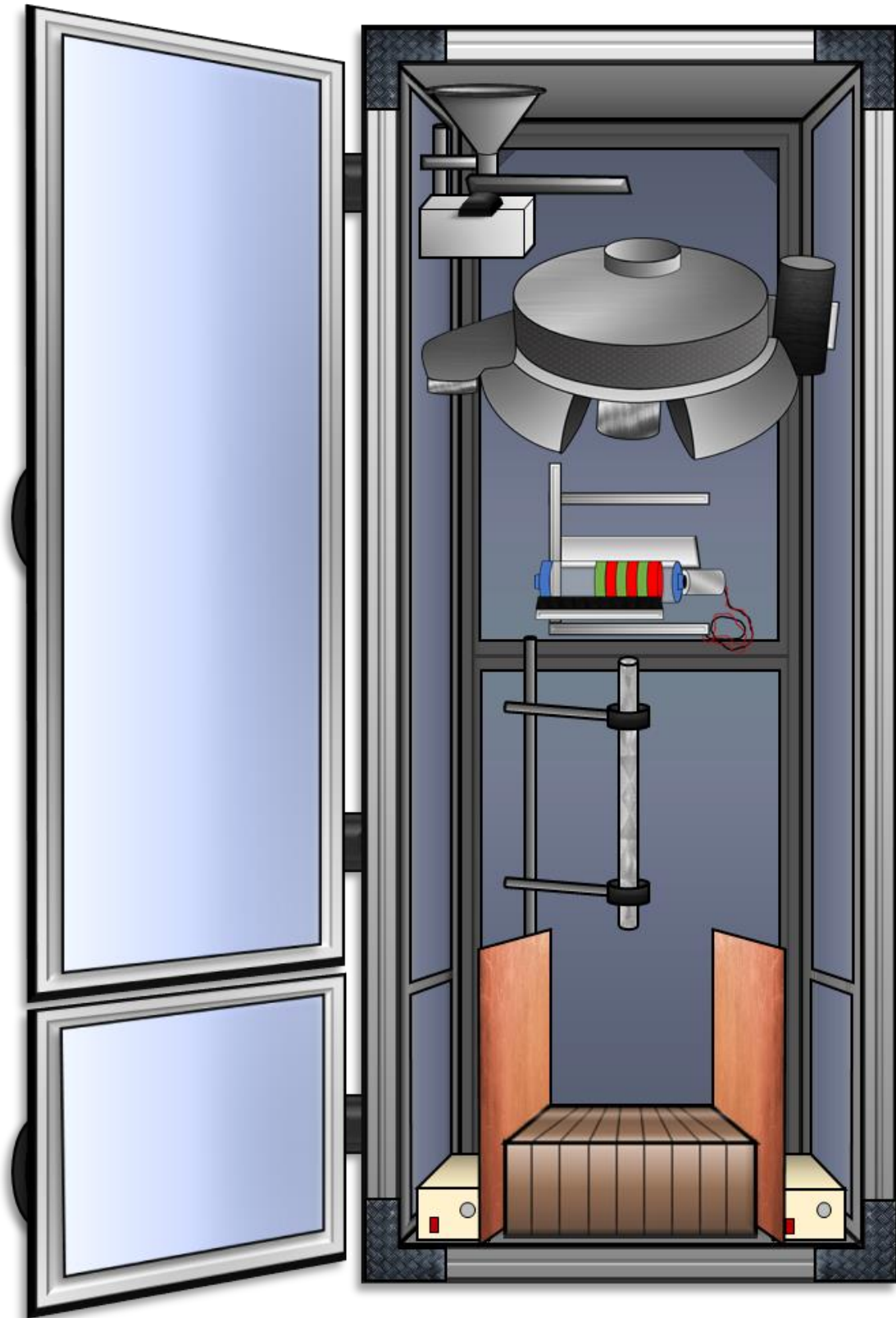**Frantz Isodynamic Separator**

- **Environmental Independence:** Designed for laboratory environment only (the product's datasheet declares a narrow temperature window); not designed for use in outer space, but should be okay with vacuum
- **Simplicity & Reliability:** Complex electromagnetic product, which involves many parts; magnetic coils with high electrical load are prone to failure; reliability still seems very high
- **Energy Efficiency:** A regular power supply, that generates high currents is involved (adjustable to over 2.5 amperes), thus, poor energy efficiency
- **Mass & Volume:** Data sheet reveals huge dimensions (81x81x41 cm) and high mass (150kg)
- **Technology Readiness:** The device is commercially available, is in use since decades and comes with a warranty
- **Process Integrability:** The product can be switched to vertical mode (called the vertical feed mode of operation); in this mode, only low feed rate possible (9kg/h)
- **Adjustability & Scalability:** Poor scalability, as only one model / size available (L-1 model), but orientation & susceptibility adjustable (as described on website)
- **Performance:** Best mineral enrichment results of all magnetic beneficiation techniques (studies)
- **Cost & Dev. Effort:** 5000 USD excluding shipping costs and tax; no development effort

A6 – Product Tree

System: Beneficiation Testbed

Subsystem 1: Inlet
- Vibratory Feeder
- Feeder Controller

Subsystem 2: Gravitational Separator
- Sifter
- De-blinding Unit

Subsystem 3: Magnetic Separator
- **Assembly 1:** Stator
  - Inner Tube
  - Arc Segment Magnets
  - Caps
  - Ball Bearings
- **Assembly 2:** Rotor
  - Outer Tube
  - DC-Motor
  - DC Power Supply
  - Wiring
  - Caps
  - Brush
- **Assembly 3:** Support
  - Frame
  - Covering
  - Ramp / Divider
  - Funnels

Subsystem 4: Electrostatic Separator
- **Assembly 1:** Charger
  - Static Mixer
  - Outer Tube
  - Heat Tape
  - Stand
- **Assembly 2:** Separator
  - HV DC Power Supply
  - Parallel Plates
  - Cables
  - Isolating Retainer

Subsystem 5: Outlet
- Oversize Container (Grav. Beneficiation)
- Ferromagnetics Vessel (Mag. Beneficiation)
- Collection Hopper (Elec. Beneficiation)

Subsystem 6: Structure
- Profiles
- (T-slot) Nuts & Bolts
- Panels
- Support Angles
- Rollers
- Handles
- Elastomers (Sealing & Dampening)
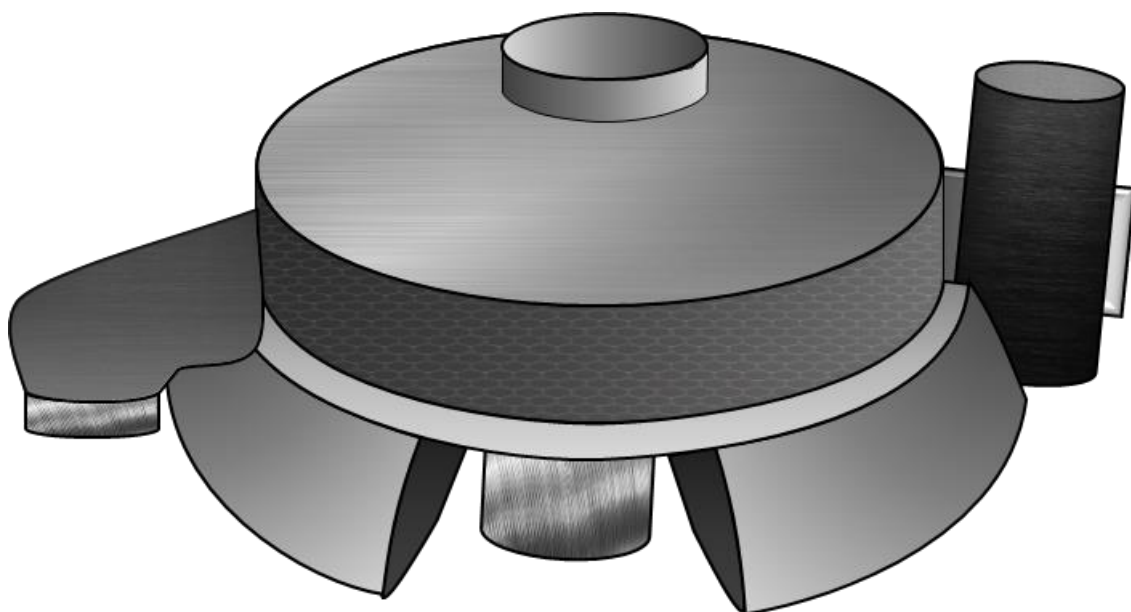
A7 – Sketches in High Resolution

System: Beneficiation Testbed

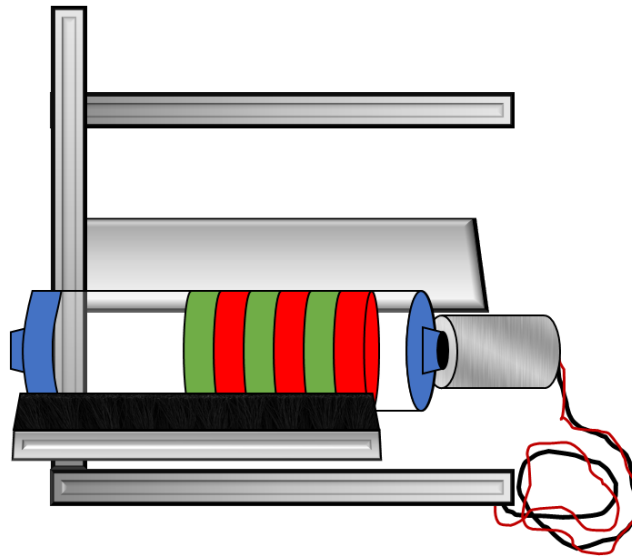**Subsystem 1: Inlet (Vibratory Feeder)**
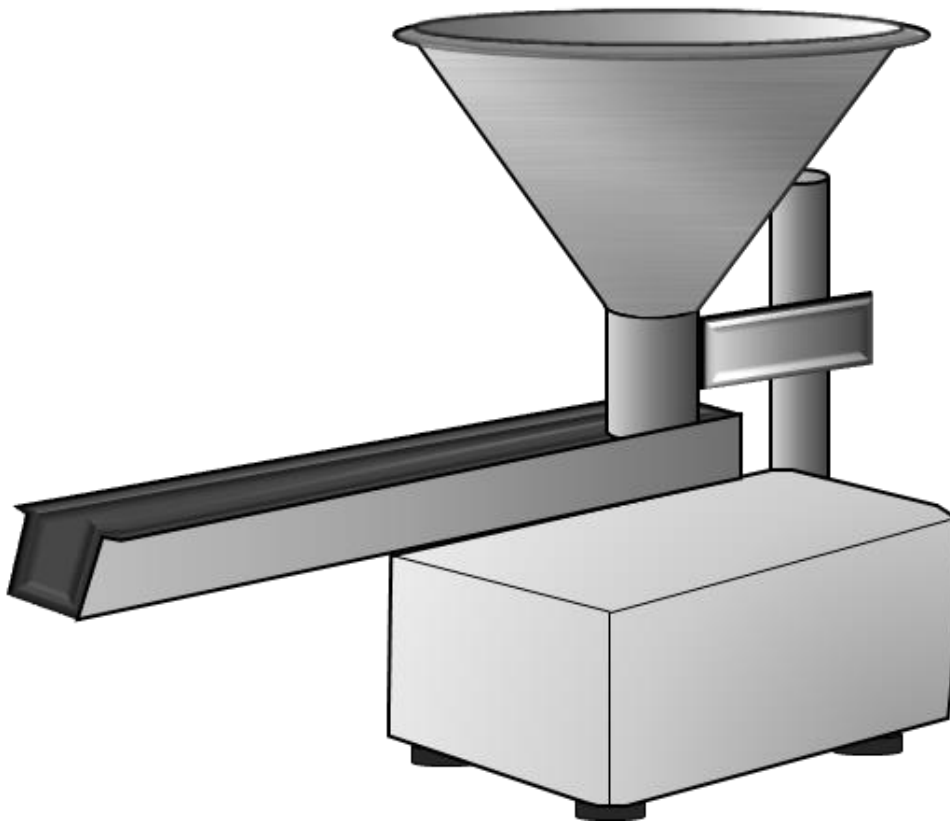
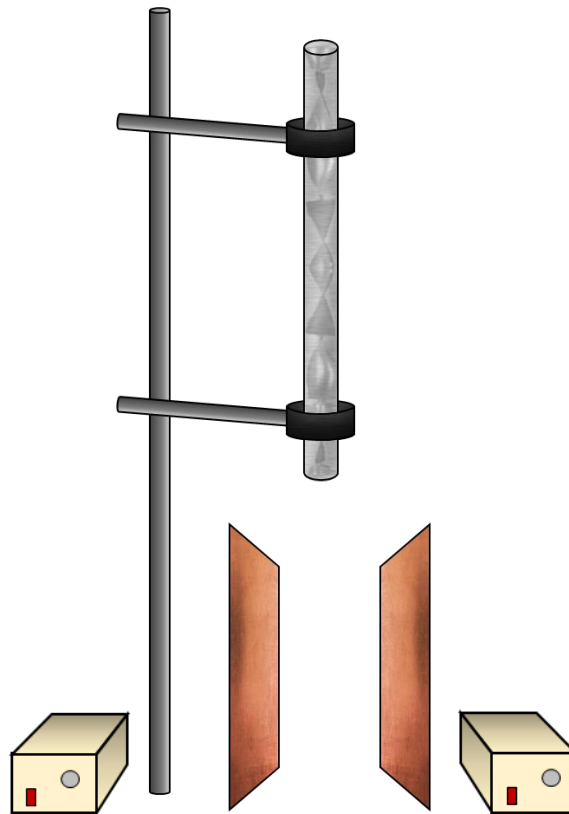**Subsystem 2: Gravitational Separator (Horizontal Vibratory Sifter)**
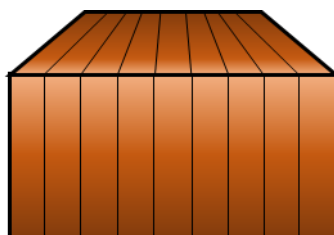
Subsystem 3: Magnetic Separator (Permanent Magnet Drum Separator with Stator and Rotor)
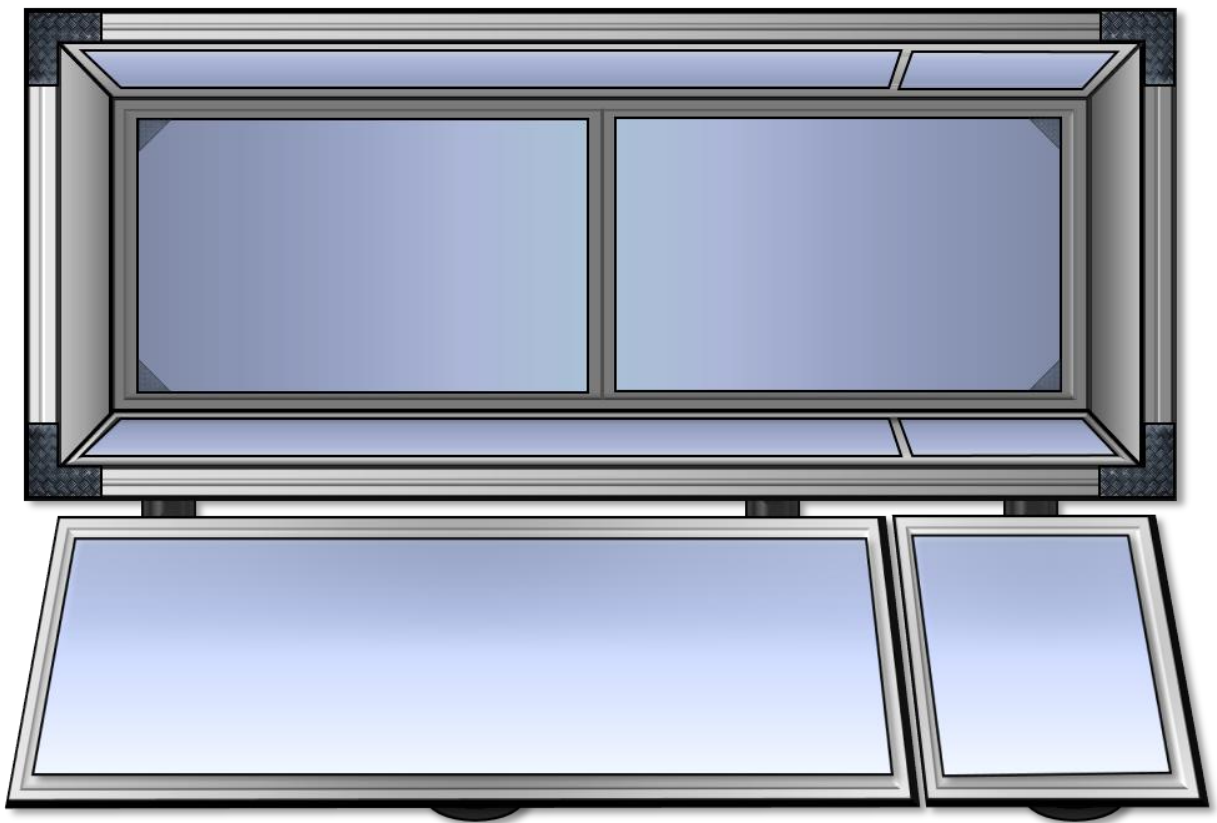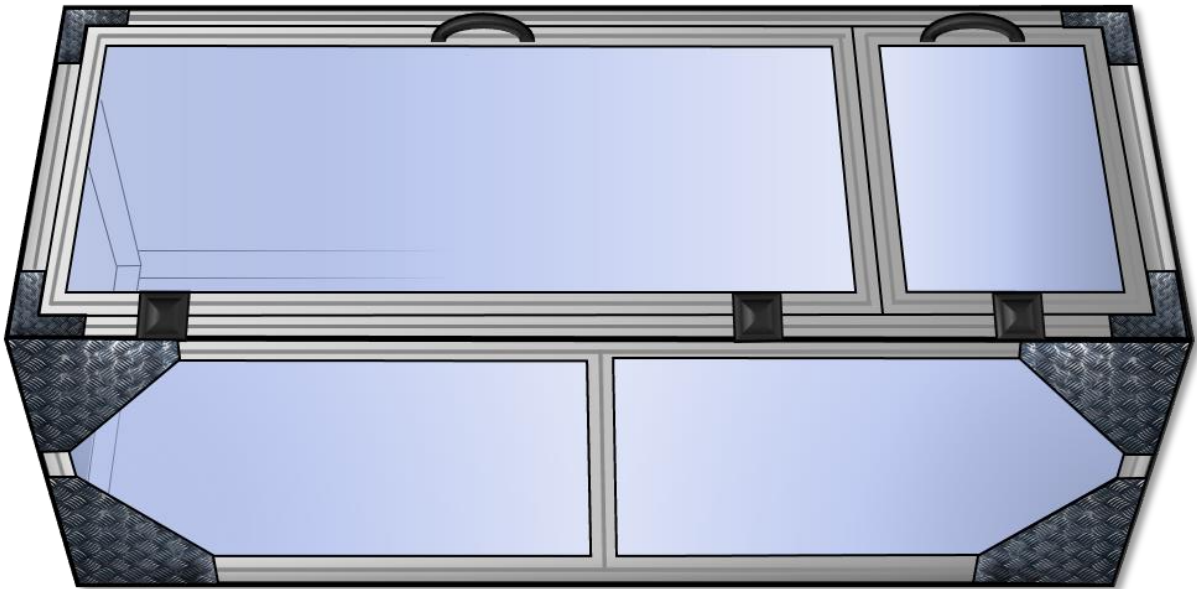

Subsystem 4: Electrostatic Separator (Static Tribocharger and Electrostatic Separator)

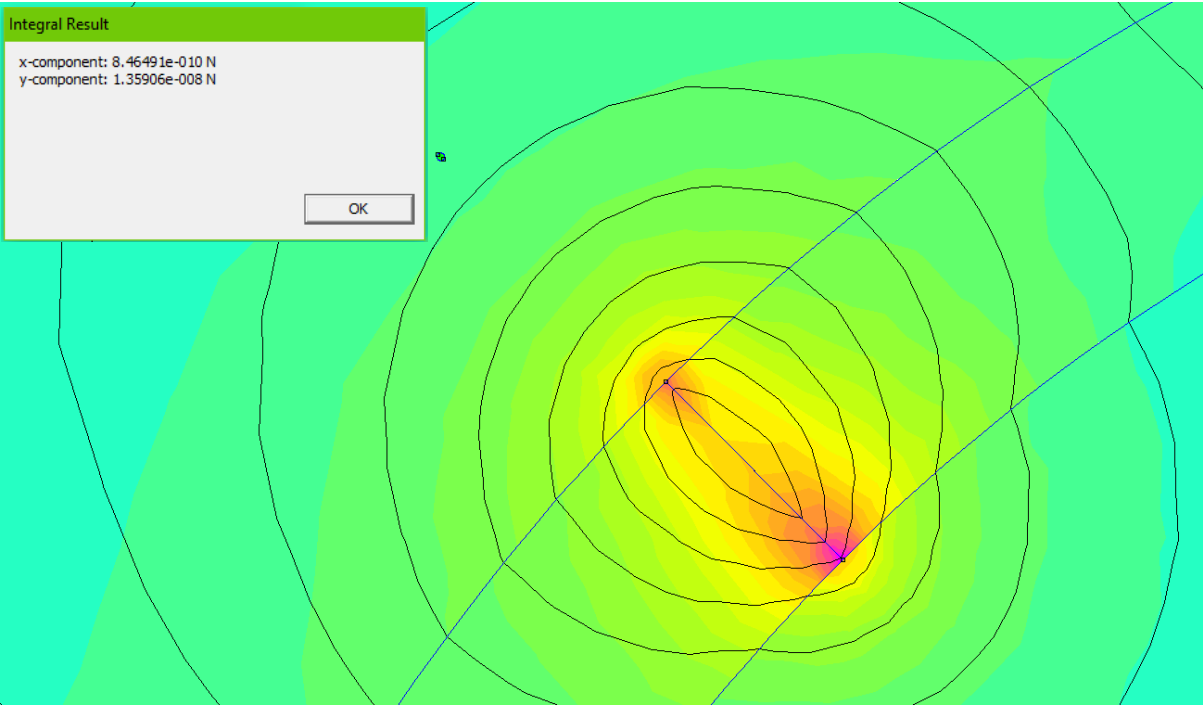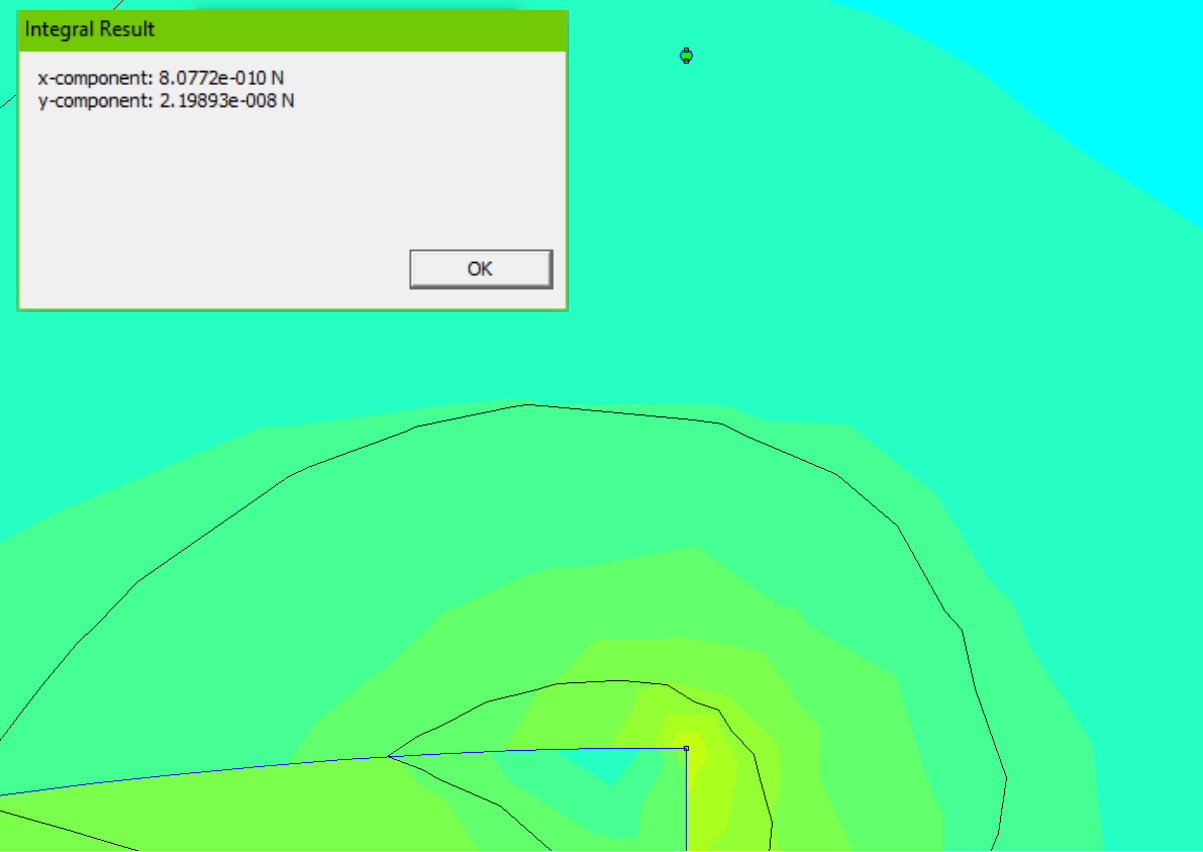
Subsystem 5: Outlet (Collection Hopper)

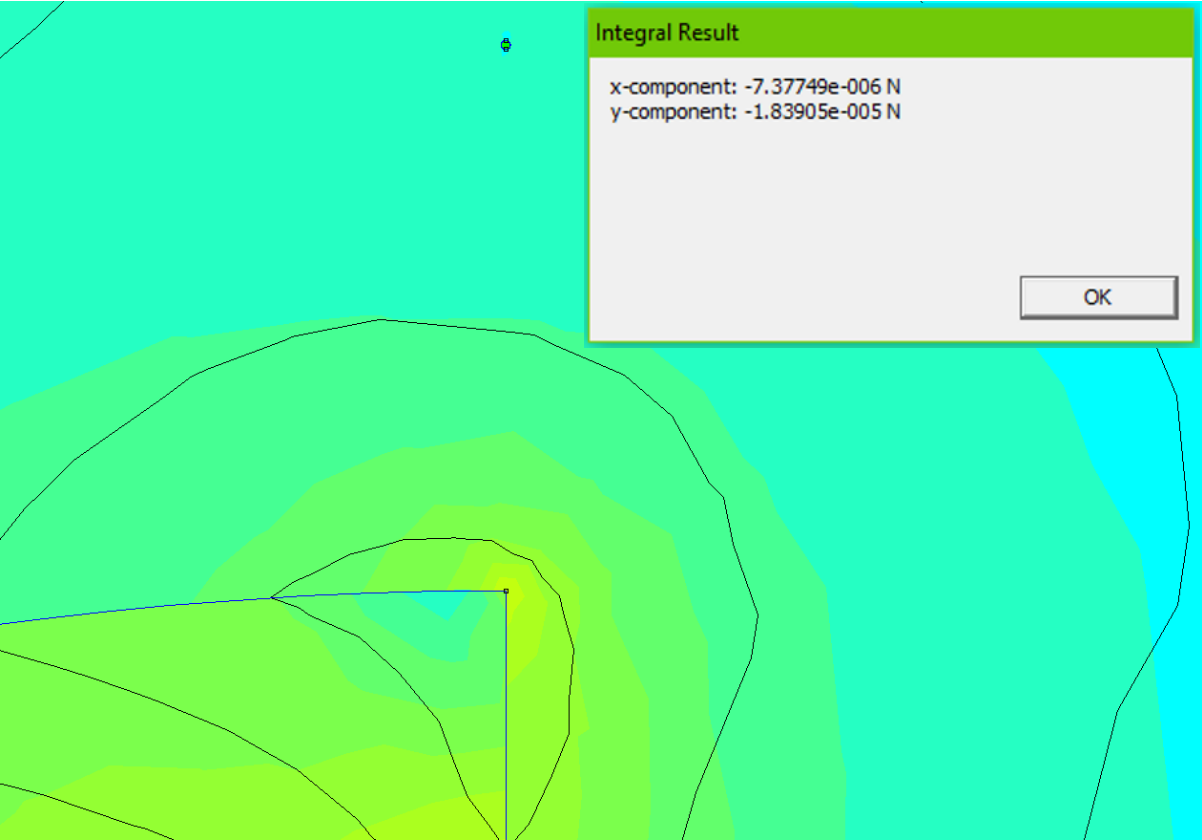**Subsystem 6: Structure**

A8 – Numeric Determination of Magnetic Forces

Ilmenite Grains (at 90° and 135°)

Iron Particles (at 90° and 135°)

Integral Result

x-component: -7.37749e-006 N
y-component: -1.83905e-005 N

OK

Integral Result

x-component: 0.000112969 N
y-component: -0.000139651 N

OK
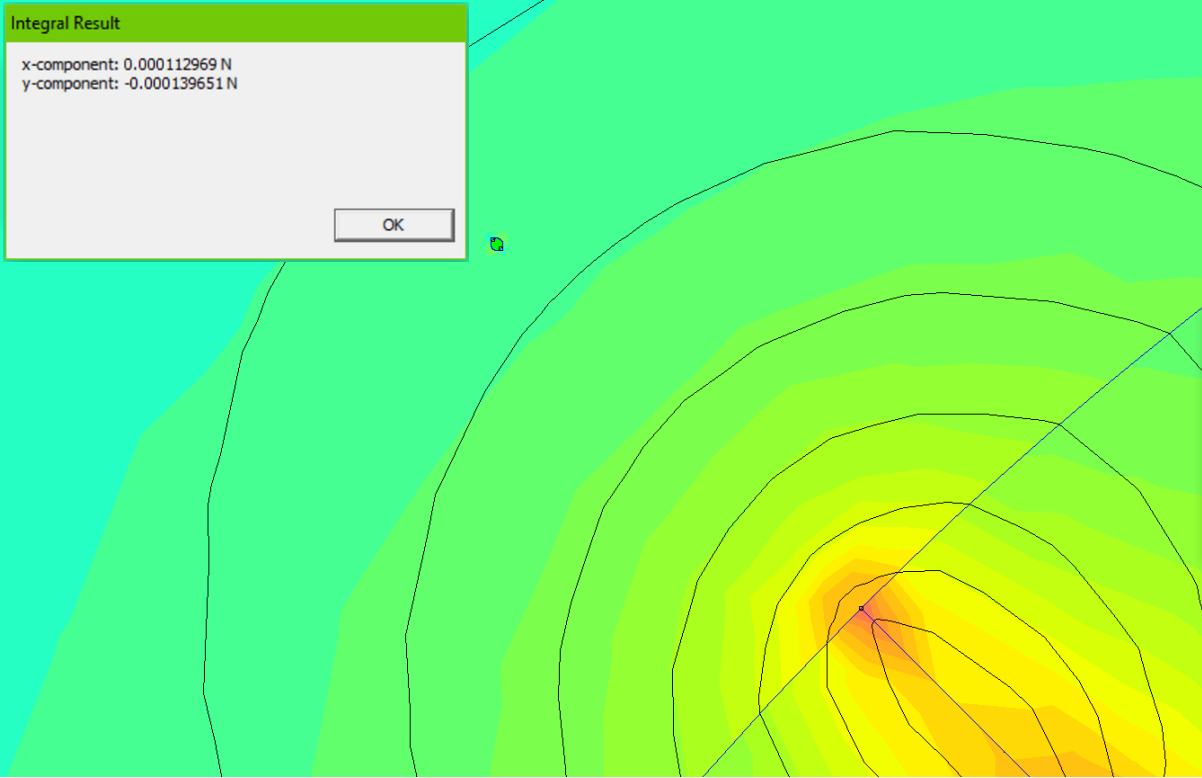
A9 – Parametric Model for Electrostatic Separation

Preference Panels

Variable	Unit	Value
U	V	50000
d	m	0,1
L	m	0,283
g	m/s^2	9,81
t_f	s	0,240200392
φ_s	eV	4,28
r_p	m	0,000025
q/m ilmenite	C/kg	-3,18351E-09
q/m olivine	C/kg	-1,68432E-06
q/m plagioclase	C/kg	-7,21402E-07
q/m pyroxene	C/kg	-3,9408E-07

Charger Material
Al

Planet
Earth

Selection Options & Underlying Data

Material	Work Function
Al	4,28
Cu	4,65
SS	5,04
PTFE	5,75

Planet	Gravitational Acceleration
Earth	9,81
Moon	1,625

Table of Resulting Values

i	t	x (mm)	v_x(m/s)	y_ilmenite	y_olivine	y_plagiocl	y_pyroxene	v_y ilmenite (m	v_y olivine (m	v_y plagio	v_y pyroxe
1	4,8040E-03	-1,1320E-01	-4,7127E-02	-1,8368E-05	-9,7179E-03	-4,1622E-03	-2,2737E-03	-7,6468E-06	-4,0458E-03	-1,7328E-03	-9,4658E-04
2	9,6080E-03	-4,5280E-01	-9,4255E-02	-7,3471E-05	-3,8872E-02	-1,6649E-02	-9,0948E-03	-1,5294E-05	-8,0915E-03	-3,4656E-03	-1,8932E-03
3	1,4412E-02	-1,0188E+00	-1,4138E-01	-1,6531E-04	-8,7461E-02	-3,7460E-02	-2,0463E-02	-2,2940E-05	-1,2137E-02	-5,1984E-03	-2,8397E-03
4	1,9216E-02	-1,8112E+00	-1,8851E-01	-2,9388E-04	-1,5549E-01	-6,6595E-02	-3,6379E-02	-3,0587E-05	-1,6183E-02	-6,9312E-03	-3,7863E-03
5	2,4020E-02	-2,8300E+00	-2,3564E-01	-4,5919E-04	-2,4295E-01	-1,0406E-01	-5,6842E-02	-3,8234E-05	-2,0229E-02	-8,6640E-03	-4,7329E-03
6	2,8824E-02	-4,0752E+00	-2,8276E-01	-6,6124E-04	-3,4984E-01	-1,4984E-01	-8,1853E-02	-4,5881E-05	-2,4275E-02	-1,0397E-02	-5,6795E-03
7	3,3628E-02	-5,5468E+00	-3,2989E-01	-9,0002E-04	-4,7618E-01	-2,0395E-01	-1,1141E-01	-5,3528E-05	-2,8320E-02	-1,2130E-02	-6,6261E-03
8	3,8432E-02	-7,2448E+00	-3,7702E-01	-1,1755E-03	-6,2195E-01	-2,6638E-01	-1,4552E-01	-6,1175E-05	-3,2366E-02	-1,3862E-02	-7,5727E-03
9	4,3236E-02	-9,1692E+00	-4,2415E-01	-1,4878E-03	-7,8715E-01	-3,3714E-01	-1,8417E-01	-6,8821E-05	-3,6412E-02	-1,5595E-02	-8,5192E-03
10	4,8040E-02	-1,1320E+01	-4,7127E-01	-1,8368E-03	-9,7179E-01	-4,1622E-01	-2,2737E-01	-7,6468E-05	-4,0458E-02	-1,7328E-02	-9,4658E-03
11	5,2844E-02	-1,3697E+01	-5,1840E-01	-2,2225E-03	-1,1759E+00	-5,0363E-01	-2,7512E-01	-8,4115E-05	-4,4503E-02	-1,9061E-02	-1,0412E-02
12	5,7648E-02	-1,6301E+01	-5,6553E-01	-2,6449E-03	-1,3994E+00	-5,9936E-01	-3,2741E-01	-9,1762E-05	-4,8549E-02	-2,0794E-02	-1,1359E-02
13	6,2452E-02	-1,9131E+01	-6,1266E-01	-3,1041E-03	-1,6423E+00	-7,0341E-01	-3,8425E-01	-9,9409E-05	-5,2595E-02	-2,2527E-02	-1,2306E-02
14	6,7256E-02	-2,2187E+01	-6,5978E-01	-3,6001E-03	-1,9047E+00	-8,1579E-01	-4,4564E-01	-1,0706E-04	-5,6641E-02	-2,4259E-02	-1,3252E-02
15	7,2060E-02	-2,5470E+01	-7,0691E-01	-4,1327E-03	-2,1865E+00	-9,3650E-01	-5,1158E-01	-1,1470E-04	-6,0686E-02	-2,5992E-02	-1,4199E-02
16	7,6864E-02	-2,8979E+01	-7,5404E-01	-4,7021E-03	-2,4878E+00	-1,0655E+00	-5,8207E-01	-1,2235E-04	-6,4732E-02	-2,7725E-02	-1,5145E-02
17	8,1668E-02	-3,2715E+01	-8,0116E-01	-5,3083E-03	-2,8085E+00	-1,2029E+00	-6,5710E-01	-1,3000E-04	-6,8778E-02	-2,9458E-02	-1,6092E-02
18	8,6472E-02	-3,6677E+01	-8,4829E-01	-5,9511E-03	-3,1486E+00	-1,3486E+00	-7,3668E-01	-1,3764E-04	-7,2824E-02	-3,1191E-02	-1,7038E-02
19	9,1276E-02	-4,0865E+01	-8,9542E-01	-6,6307E-03	-3,5082E+00	-1,5026E+00	-8,2080E-01	-1,4529E-04	-7,6869E-02	-3,2923E-02	-1,7985E-02
20	9,6080E-02	-4,5280E+01	-9,4255E-01	-7,3471E-03	-3,8872E+00	-1,6649E+00	-9,0948E-01	-1,5294E-04	-8,0915E-02	-3,4656E-02	-1,8932E-02
21	1,0088E-01	-4,9921E+01	-9,8967E-01	-8,1001E-03	-4,2856E+00	-1,8355E+00	-1,0027E+00	-1,6058E-04	-8,4961E-02	-3,6389E-02	-1,9878E-02
22	1,0569E-01	-5,4789E+01	-1,0368E+00	-8,8900E-03	-4,7035E+00	-2,0145E+00	-1,1005E+00	-1,6823E-04	-8,9007E-02	-3,8122E-02	-2,0825E-02
23	1,1049E-01	-5,9883E+01	-1,0839E+00	-9,7165E-03	-5,1408E+00	-2,2018E+00	-1,2028E+00	-1,7588E-04	-9,3052E-02	-3,9855E-02	-2,1771E-02
24	1,1530E-01	-6,5203E+01	-1,1311E+00	-1,0580E-02	-5,5975E+00	-2,3974E+00	-1,3096E+00	-1,8352E-04	-9,7098E-02	-4,1587E-02	-2,2718E-02
25	1,2010E-01	-7,0750E+01	-1,1782E+00	-1,1480E-02	-6,0737E+00	-2,6014E+00	-1,4211E+00	-1,9117E-04	-1,0114E-01	-4,3320E-02	-2,3665E-02

i	t	x (mm)	v_x(m/s)	y_ilmenite	y_olivine	y_plagiocl	y_pyroxene	v_y ilmenite (r	v_y olivine (m	v_y plagic	v_y pyroxe
26	1,2490E-01	-7,6523E+01	-1,2253E+00	-1,2417E-02	-6,5693E+00	-2,8137E+00	-1,5370E+00	-1,9882E-04	-1,0519E-01	-4,5053E-02	-2,4611E-02
27	1,2971E-01	-8,2523E+01	-1,2724E+00	-1,3390E-02	-7,0844E+00	-3,0343E+00	-1,6575E+00	-2,0646E-04	-1,0924E-01	-4,6786E-02	-2,5558E-02
28	1,3451E-01	-8,8749E+01	-1,3196E+00	-1,4400E-02	-7,6188E+00	-3,2632E+00	-1,7826E+00	-2,1411E-04	-1,1328E-01	-4,8519E-02	-2,6504E-02
29	1,3932E-01	-9,5201E+01	-1,3667E+00	-1,5447E-02	-8,1728E+00	-3,5004E+00	-1,9122E+00	-2,2176E-04	-1,1733E-01	-5,0251E-02	-2,7451E-02
30	1,4412E-01	-1,0188E+02	-1,4138E+00	-1,6531E-02	-8,7461E+00	-3,7460E+00	-2,0463E+00	-2,2940E-04	-1,2137E-01	-5,1984E-02	-2,8397E-02
31	1,4892E-01	-1,0879E+02	-1,4609E+00	-1,7651E-02	-9,3389E+00	-3,9999E+00	-2,1850E+00	-2,3705E-04	-1,2542E-01	-5,3717E-02	-2,9344E-02
32	1,5373E-01	-1,1592E+02	-1,5081E+00	-1,8808E-02	-9,9511E+00	-4,2621E+00	-2,3283E+00	-2,4470E-04	-1,2946E-01	-5,5450E-02	-3,0291E-02
33	1,5853E-01	-1,2327E+02	-1,5552E+00	-2,0002E-02	-1,0583E+01	-4,5327E+00	-2,4761E+00	-2,5234E-04	-1,3351E-01	-5,7183E-02	-3,1237E-02
34	1,6334E-01	-1,3086E+02	-1,6023E+00	-2,1233E-02	-1,1234E+01	-4,8115E+00	-2,6284E+00	-2,5999E-04	-1,3756E-01	-5,8916E-02	-3,2184E-02
35	1,6814E-01	-1,3867E+02	-1,6495E+00	-2,2500E-02	-1,1904E+01	-5,0987E+00	-2,7853E+00	-2,6764E-04	-1,4160E-01	-6,0648E-02	-3,3130E-02
36	1,7294E-01	-1,4671E+02	-1,6966E+00	-2,3805E-02	-1,2594E+01	-5,3942E+00	-2,9467E+00	-2,7529E-04	-1,4565E-01	-6,2381E-02	-3,4077E-02
37	1,7775E-01	-1,5497E+02	-1,7437E+00	-2,5145E-02	-1,3304E+01	-5,6981E+00	-3,1127E+00	-2,8293E-04	-1,4969E-01	-6,4114E-02	-3,5024E-02
38	1,8255E-01	-1,6346E+02	-1,7908E+00	-2,6523E-02	-1,4033E+01	-6,0102E+00	-3,2832E+00	-2,9058E-04	-1,5374E-01	-6,5847E-02	-3,5970E-02
39	1,8736E-01	-1,7218E+02	-1,8380E+00	-2,7937E-02	-1,4781E+01	-6,3307E+00	-3,4583E+00	-2,9823E-04	-1,5778E-01	-6,7580E-02	-3,6917E-02
40	1,9216E-01	-1,8112E+02	-1,8851E+00	-2,9388E-02	-1,5549E+01	-6,6595E+00	-3,6379E+00	-3,0587E-04	-1,6183E-01	-6,9312E-02	-3,7863E-02
41	1,9696E-01	-1,9029E+02	-1,9322E+00	-3,0876E-02	-1,6336E+01	-6,9967E+00	-3,8221E+00	-3,1352E-04	-1,6588E-01	-7,1045E-02	-3,8810E-02
42	2,0177E-01	-1,9968E+02	-1,9793E+00	-3,2401E-02	-1,7142E+01	-7,3421E+00	-4,0108E+00	-3,2117E-04	-1,6992E-01	-7,2778E-02	-3,9756E-02
43	2,0657E-01	-2,0931E+02	-2,0265E+00	-3,3962E-02	-1,7968E+01	-7,6959E+00	-4,2041E+00	-3,2881E-04	-1,7397E-01	-7,4511E-02	-4,0703E-02
44	2,1138E-01	-2,1916E+02	-2,0736E+00	-3,5560E-02	-1,8814E+01	-8,0581E+00	-4,4019E+00	-3,3646E-04	-1,7801E-01	-7,6244E-02	-4,1650E-02
45	2,1618E-01	-2,2923E+02	-2,1207E+00	-3,7195E-02	-1,9679E+01	-8,4285E+00	-4,6042E+00	-3,4411E-04	-1,8206E-01	-7,7976E-02	-4,2596E-02
46	2,2098E-01	-2,3953E+02	-2,1679E+00	-3,8866E-02	-2,0563E+01	-8,8072E+00	-4,8111E+00	-3,5175E-04	-1,8610E-01	-7,9709E-02	-4,3543E-02
47	2,2579E-01	-2,5006E+02	-2,2150E+00	-4,0574E-02	-2,1467E+01	-9,1943E+00	-5,0226E+00	-3,5940E-04	-1,9015E-01	-8,1442E-02	-4,4489E-02
48	2,3059E-01	-2,6081E+02	-2,2621E+00	-4,2319E-02	-2,2390E+01	-9,5897E+00	-5,2386E+00	-3,6705E-04	-1,9420E-01	-8,3175E-02	-4,5436E-02
49	2,3540E-01	-2,7179E+02	-2,3092E+00	-4,4101E-02	-2,3333E+01	-9,9935E+00	-5,4591E+00	-3,7469E-04	-1,9824E-01	-8,4908E-02	-4,6383E-02
50	2,4020E-01	-2,8300E+02	-2,3564E+00	-4,5919E-02	-2,4295E+01	-1,0406E+01	-5,6842E+00	-3,8234E-04	-2,0229E-01	-8,6640E-02	-4,7329E-02

Plot of the Results (using copper chargers on the Earth at U$_{max}$)

Plot of the Results (using PTFE chargers on the Moon at U$_{max}$)
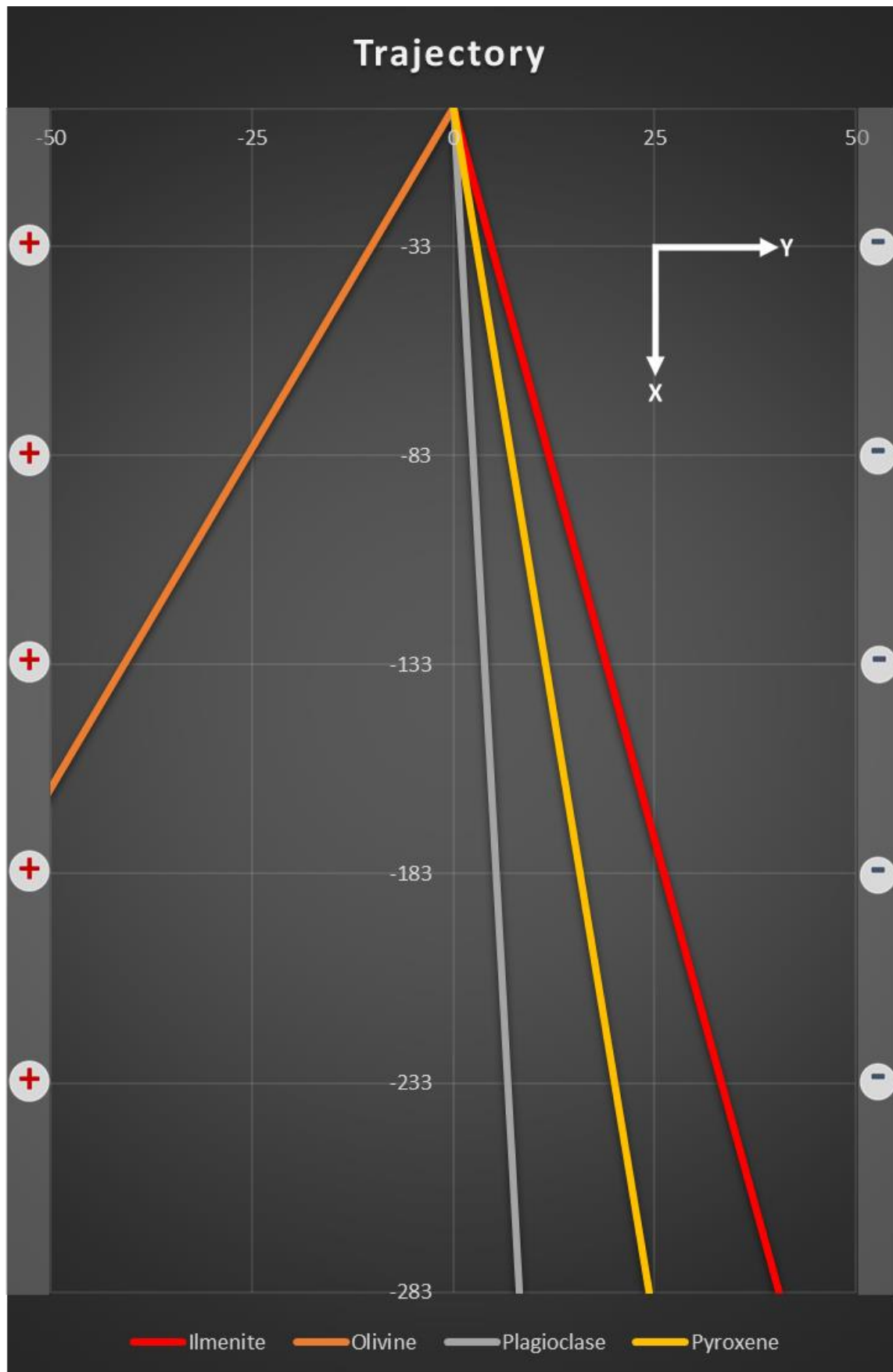
Plot of the Results (using stainless steel chargers on the Moon at 0.5*U_max)

A10 – Market Screening Matrices

Inlet: Vibratory Feeders

Model	Manufacturer	Reseller	Description	Application	Feed Rate	Hopper Volume	Size
DR100	Retsch	Retsch	Vibratory Feeder with U-shape channel	Laboratory (food, agriculture, chemicals, polymers, sand, minerals, ...)	0.5...5 dm³/min	2.65...3.5 L	42 x 26 x 28 cm
Laborette 24	Fritsch	Fritsch	Vibratory Feeder with V-shape channel	Laboratory (food, plastics, chemicals, pharma, metal powder...)	1...1500 g/min	1.4 L	44 x 14 x 34 cm
Lambda Doser	Lambda	Lambda	Powder Dosing Unit with storage vessel	Laboratory (liquids, metal powders, chalk, coal, biomass)	0...999 n/a	1 L	30 x 18 x 14 cm
DS28	Brabender	Direct Industry	Single Screw Feeder	Laboratory (food, plastics, chemicals, pharma)	5-150 dm³/h	n/a	67 x 35 x 55 cm
n/a	n/a	eBay	Electromagnetic Vibrating Feeder Small	Industry (chemicals, grain processing)	1 t/h	n/a	n/a

Gravitational Separator: Horizontal Vibratory Sifters

| Model	Manufacturer	Reseller	Description	Application
Compact Sieve	Russelfinex	Russelfinex	Industrial Check Screening Machinery	Research (Wilkinson 2011) & Industry (Chemicals, Coatings, Ceramics, Metal Powders, …)
Mini Sieve	Russelfinex	Russelfinex	Industrial Check Screening Machinery	Industry (Chemicals, Coatings, Ceramics, Metal Powders, …)
Eco Separator	Russelfinex	Russelfinex	Grading Sieve, Round Separator	Industry (Food & Beverage, Pharmaceuticals, Chemicals, Coatings, …)
Sieb-maschine	Vibrotech	Vibrotech GmbH	Vibrationstaumelsiebmaschine / Separator	Feststoff- / Flüssigkeitsseparierung
AS 200	Retsch	Retsch	Vibratory Sieve Shaker	Laboratory & Research
CXX-276h	YUCHENGTECH	Amazon	Automatic Sifter Shaker Machine	Domestic (Flour)
XZS-800	CAPSULCN	iPharmachine	Fine Powder Screening Machine	Industry (Pharmaceuticals)
XZS-400	CAPSULCN	iPharmachine	Powder Sifter Machine	Industry (Pharmaceuticals)
VPB/VPM C-Line	Virto Cuccolini	Virto Cuccolini	Industrial Check Screening Machinery	Industry (Food & Powders)
Analysette 3	Fritsch	LabShop	Vibratory Sieve Shaker	Laboratory & Research
JEL Fix II	J. Engelsmann AG	J. Engelsmann AG	Vibration Screening Machine for protective screening	Industry (Chemical, Plastic, Pharmaceutical, Food)
JEL Konti II	J. Engelsmann AG	J. Engelsmann AG	Vibration Screening Machine for grading	Industry (Chemical, Plastic, Pharmaceutical, Food)
n/a	Erimaki	Erimaki	Direct discharge screen with one side motor	Quality Assurance (Powder, Liquids)
VRS	Allgaier	Allgaier	Vibration-Round-Screener for control screening	Dedusting, Dewatering
Vibrall	Allgaier	Allgaier	Vibration-Round-Screener for control screening	Industry (Dry Bulk Goods)
n/a	n/a	Kaufland	Electric, Automatic Vibratory Sifter for Granular Powder	Domestic (Flour)

Magnetic Separator: NdFeB Arc Segment Magnets

Model	Manufacturer	Reseller	Grade	Size	Angle	Magnetization	Price
AX2C45-N and -S	K&J Magnetics Inc.	K&J Magnetics Inc.	N50	1 1/8" o.r. x 1" i.r. x 3/4" x 45º	45	radial	$7.94
n/a	Magnosphere	Amazon	N42	4mm x 25mm, InnenR 33,5mm	45	diametral	7,48 €
n/a	Magengine	Direct Industry	n/a	n/a	n/a	n/a	n/a
TR-028.5-25-20-NN	Neomagnete	Neomagnete	45SH	R28,5-r25x20mm	60	n/a	5,91 €
N-SEG-425-N and -S	Magnosphere	Magnosphere	N42	4 x 25mm, InnenR 33,5mm	45	radial	5,86 €

Electrostatic Separator: HV DC Power Supplies

Model	Manufacturer	Reseller	Description	Application	Output Voltage	Input Voltage	Power
F121CT®	EMCO	arrow.com	Compact High-Voltage Module for DC/DC Voltage Conversion	Research (Berggren 2011)	0...±6 kV	0...15 V DC	10 W
MJ Series	Glassman	Helios Power Solutions	Regulated High-Voltage DC Module with AC/DC Voltage Conversion	Research (Trigwell 2009)	0...+/-30 kV	105...125 V / 210...250 V AC	15 W
M-Power Line	Fug	Fug	Compact High-Voltage Power Supply with AC/DC Voltage Conversion	Laboratory (test stands, ion sources, particle accelerators, photomultipliers)	0...+/-10/30/50 kV	230 V AC	200/500/1000W
13671-93	PHYWE	PHYWE	High-Voltage Power Supply with AC/DC Voltage Conversion and Display	Laboratory & Education	0...±25 kV	230 V AC	60 W
LNC Serie	Heinzinger	Heinzinger	High-Voltage Table-Mounted Power Supply	Industry, Laboratory, Automation & Medical	0...+/-30 kV	230 V AC	60 W
HVGEN_POS_30KV	Highvoltageshop	Highvoltageshop	Positive High-Voltage DC Generator	Domestic / DIY	+30 kV	12V DC	4.8 W
HVGEN30_v1	Highvoltageshop	Highvoltageshop	Adjustable High-Voltage Power Supply with Current Limitation	Domestic / DIY	0...+30 kV	12 V DC	n/a

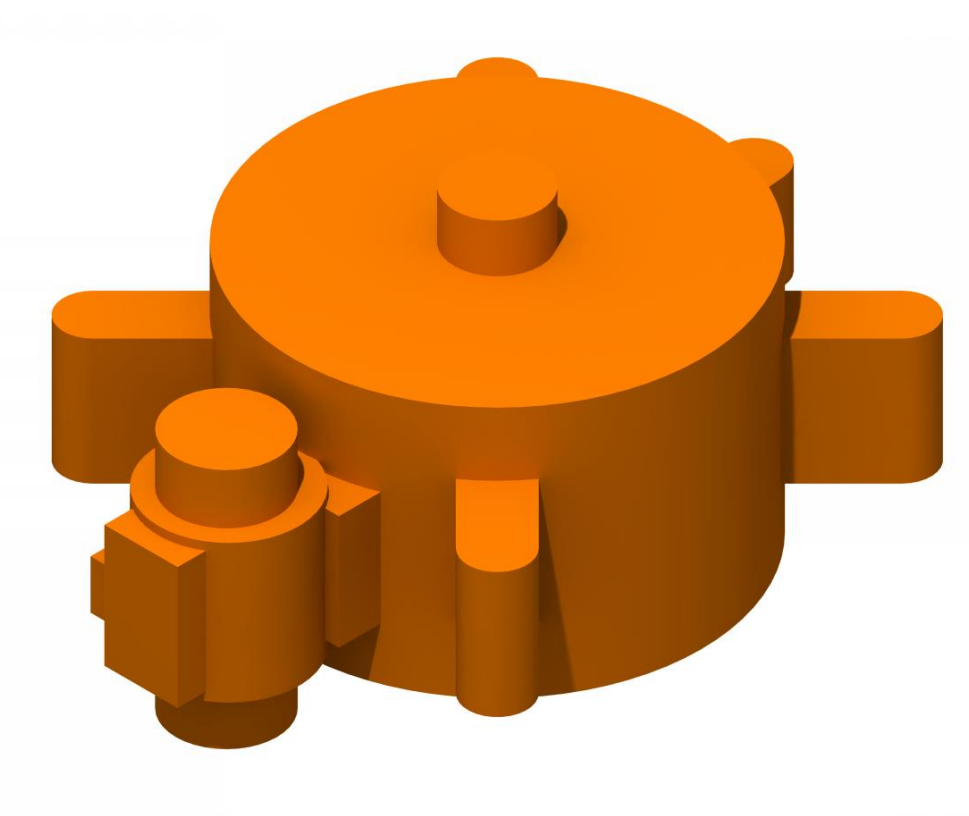# A11 – PD Models in High Resolution
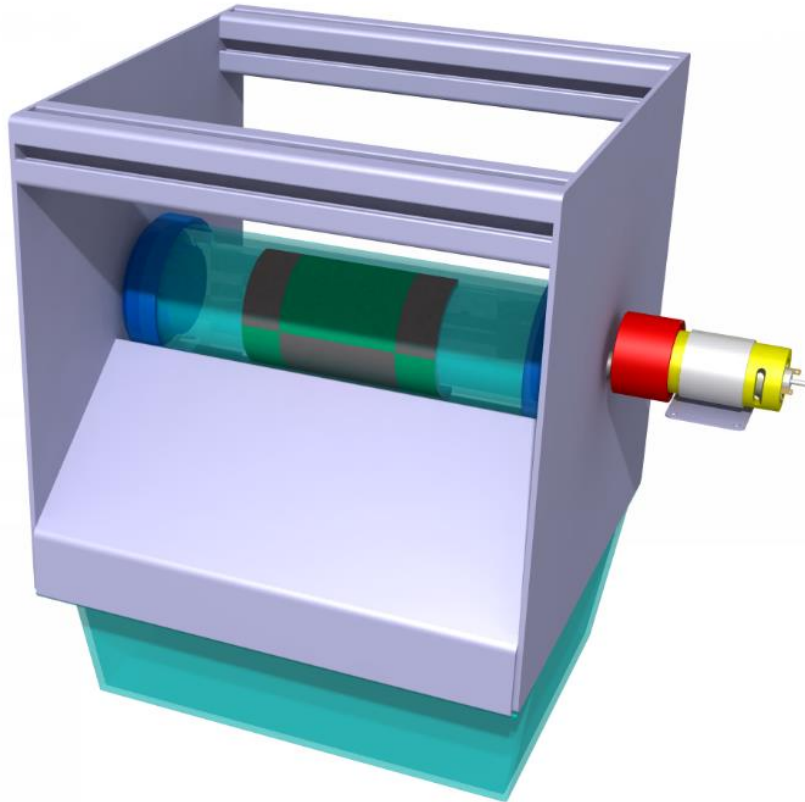
System: Beneficiation Testbed
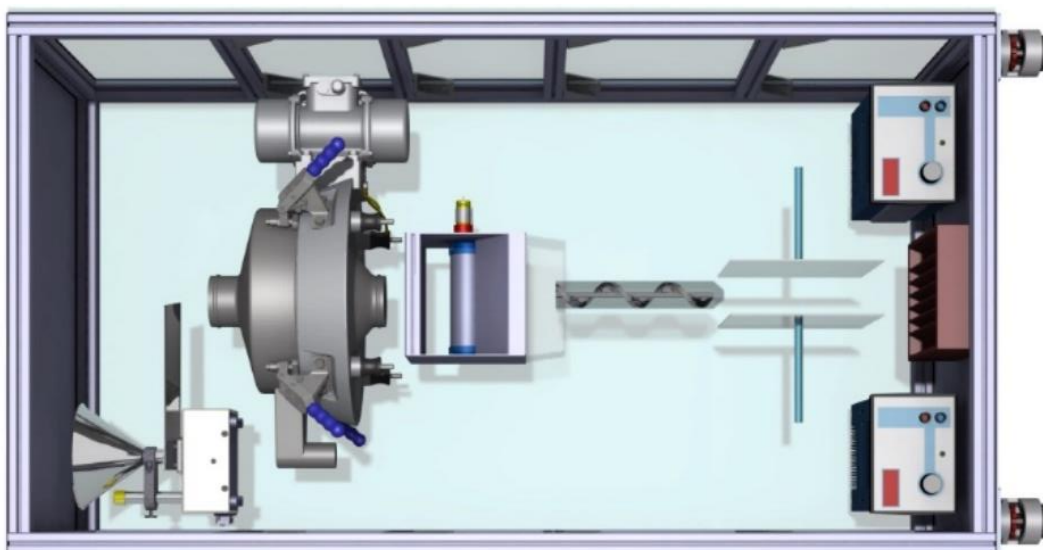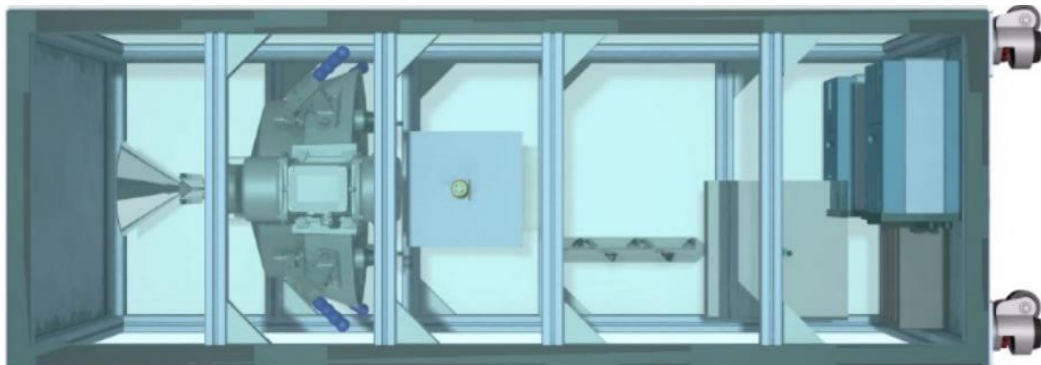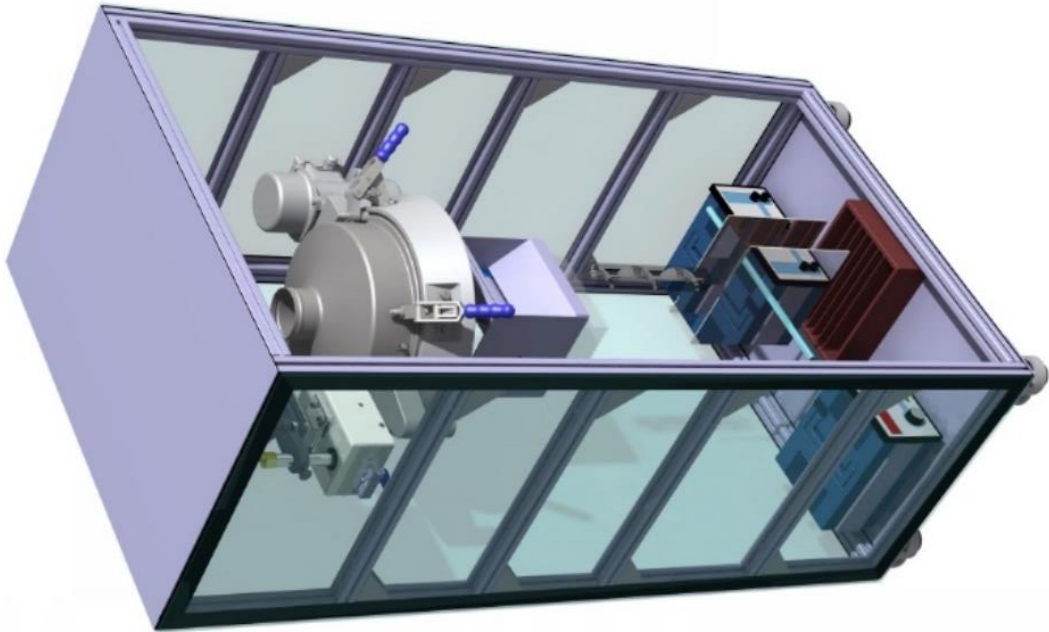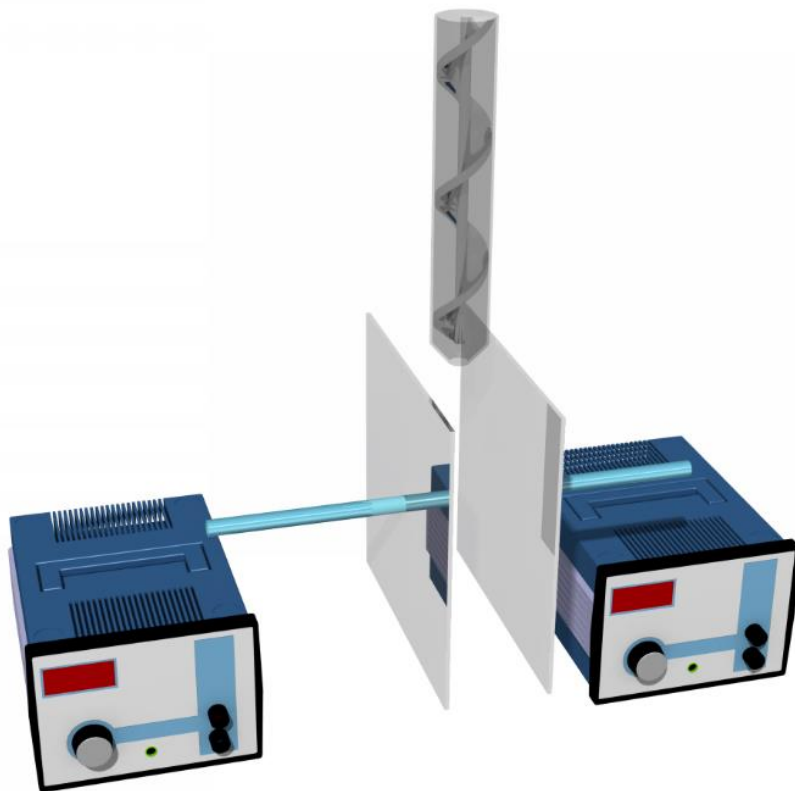
Subsystem 1: Inlet (Dummy)
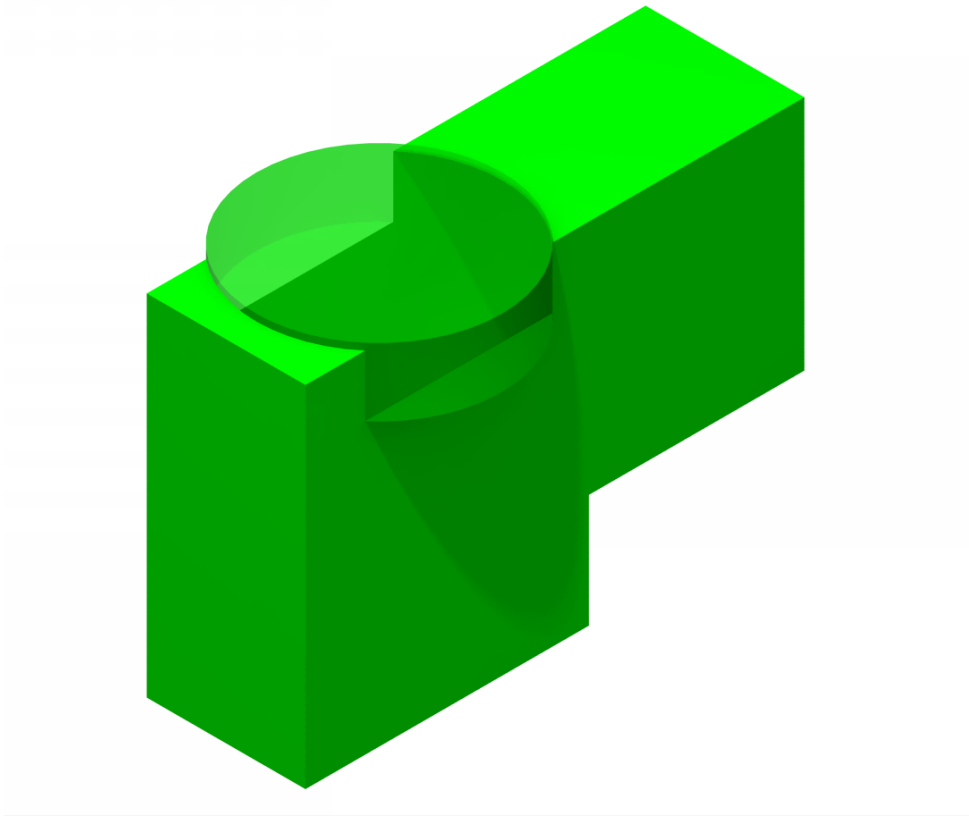
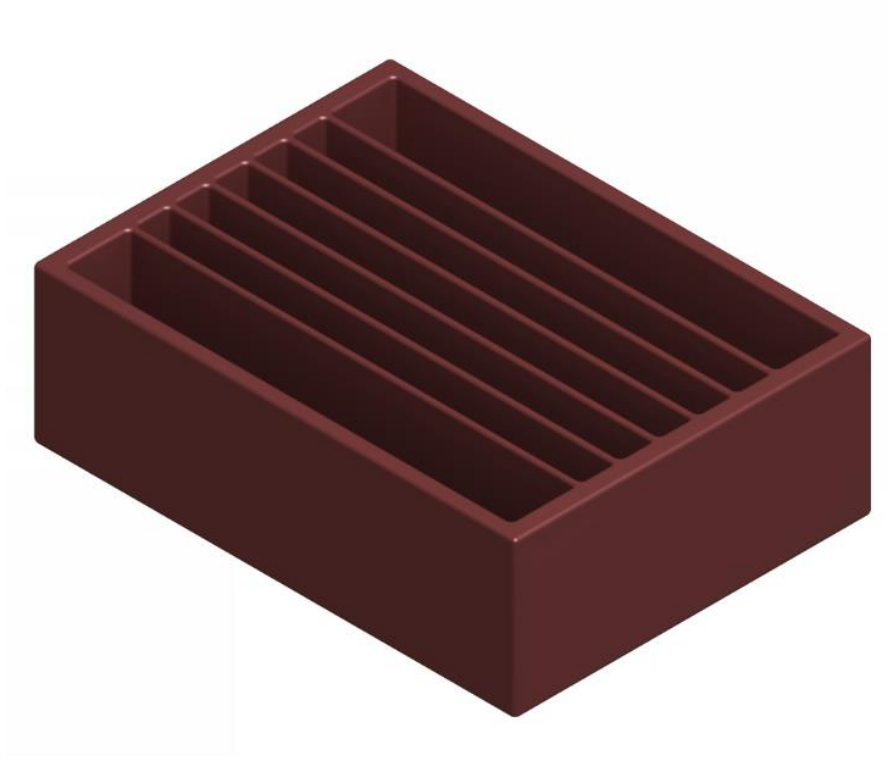**Subsystem 2: Gravitational Separator (Dummy)**

Subsystem 3: Magnetic Separator

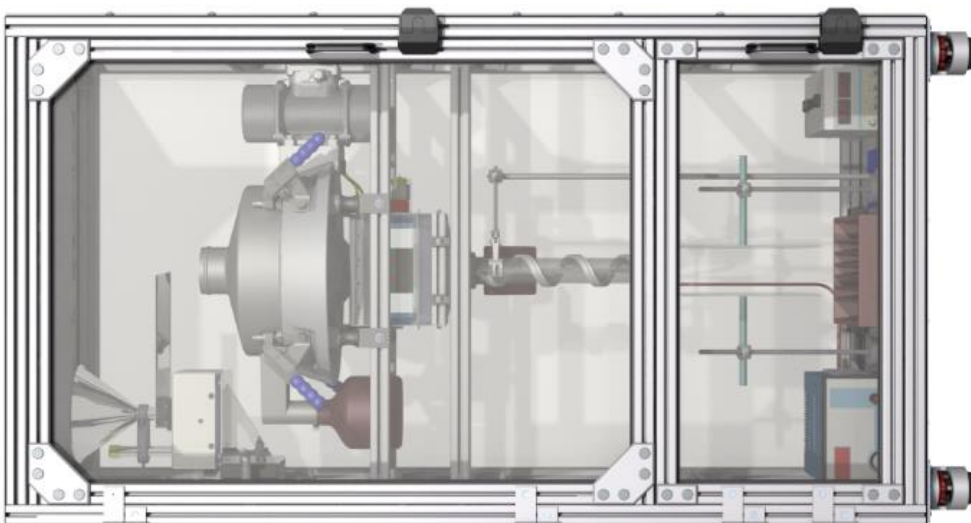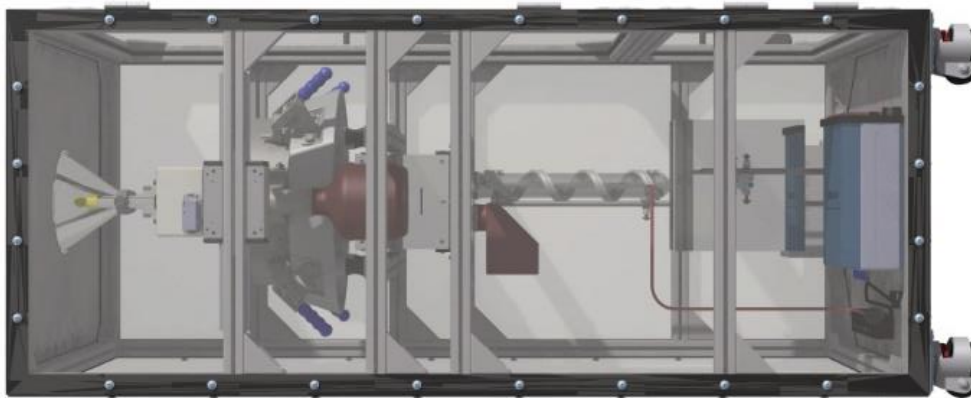**Subsystem 4: Electrostatic Separator**
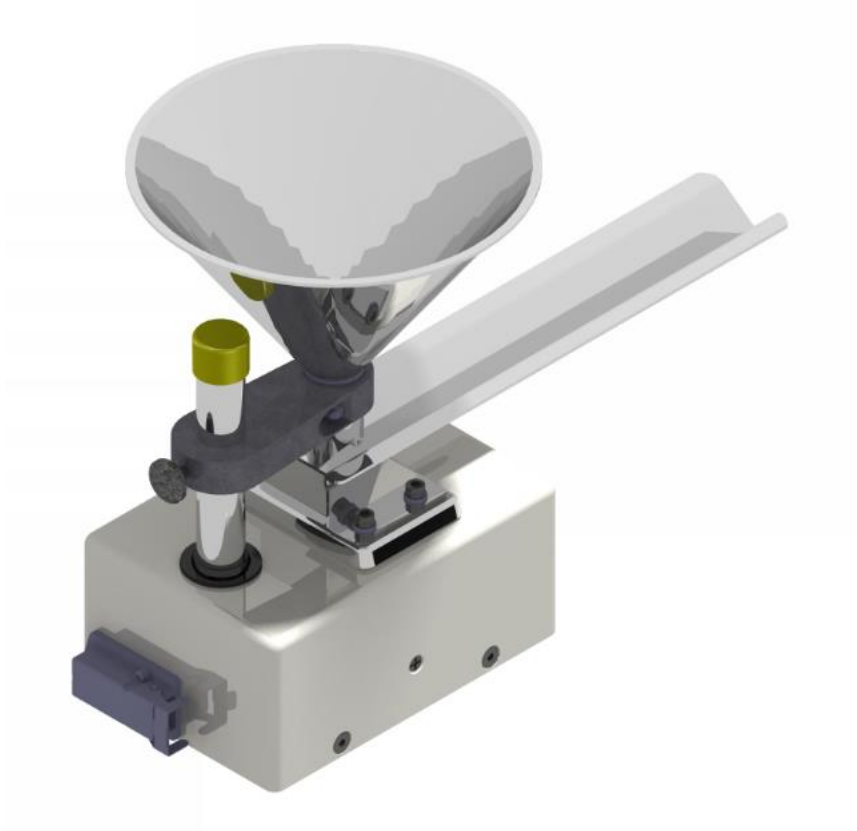
Subsystem 5: Outlet

Subsystem 6: Structure
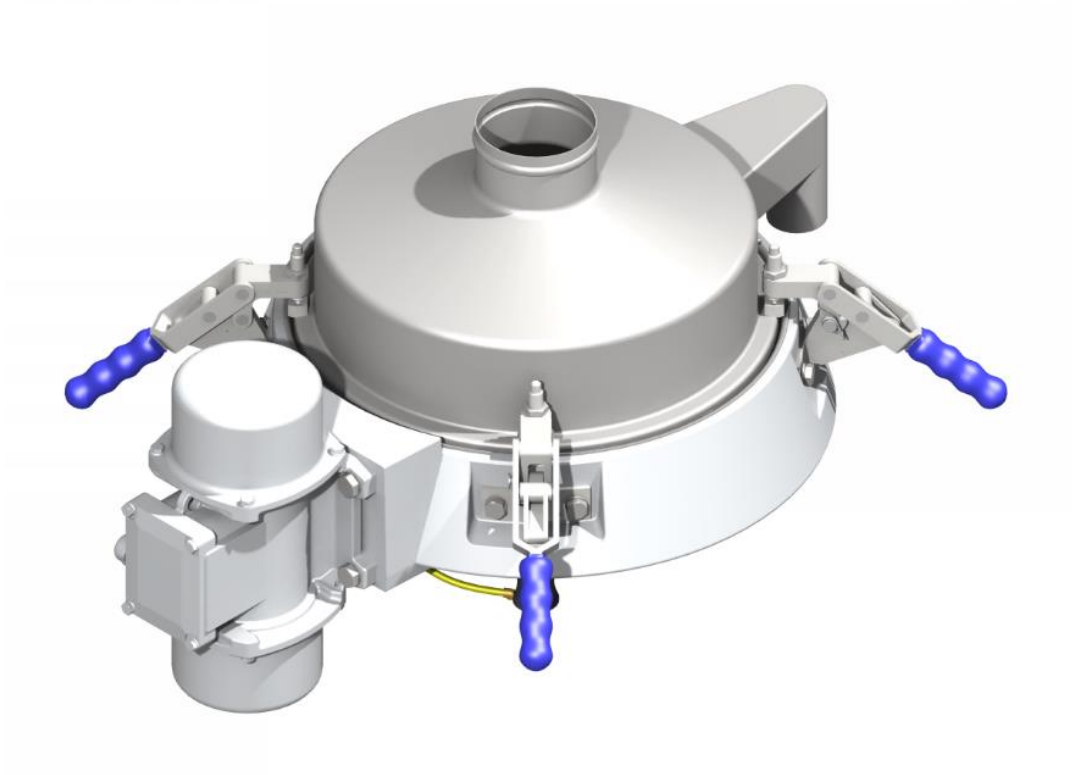
A12 – DD Models in High Resolution

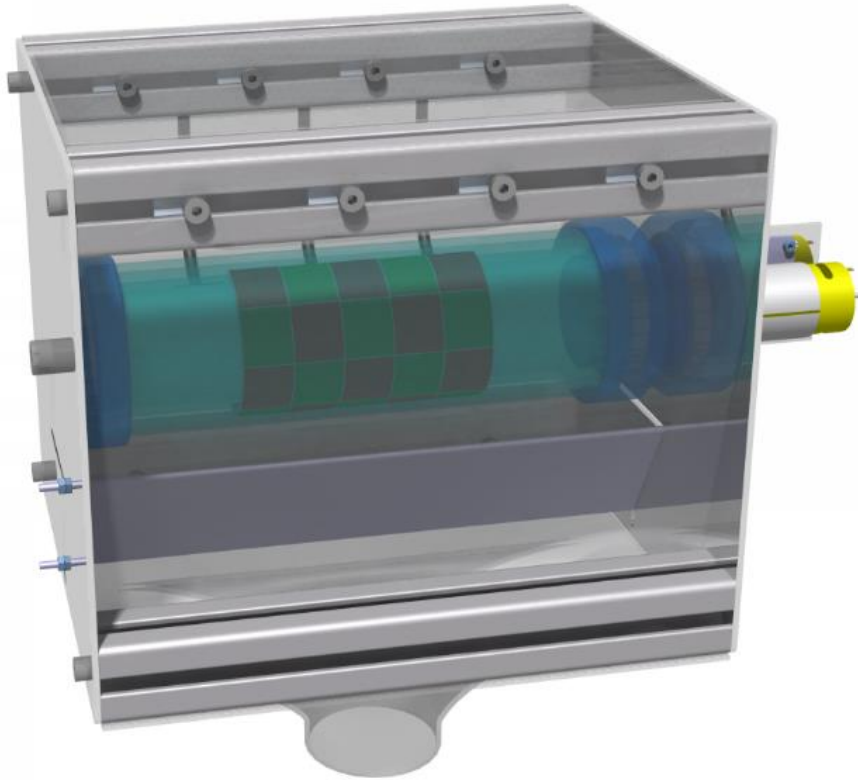**System: Beneficiation Testbed**
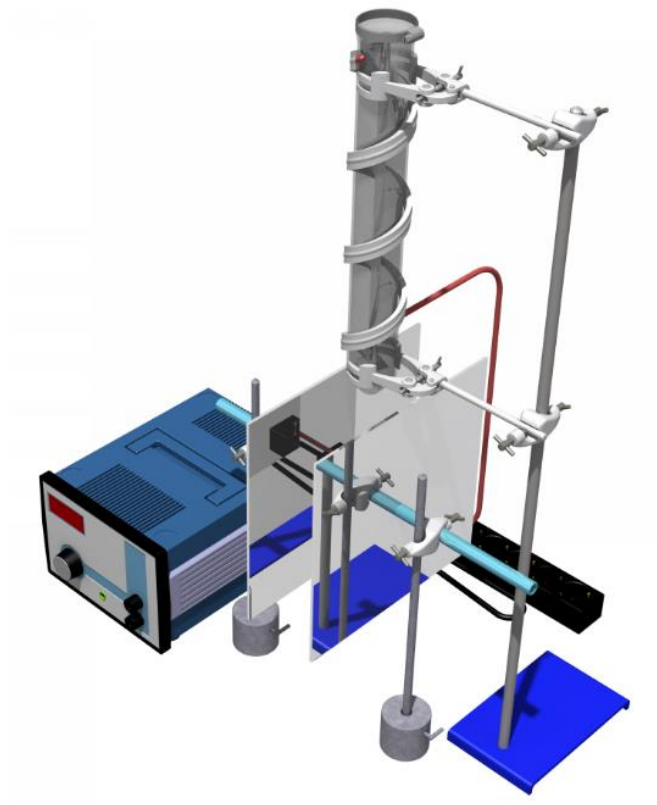
Subsystem 1: Inlet
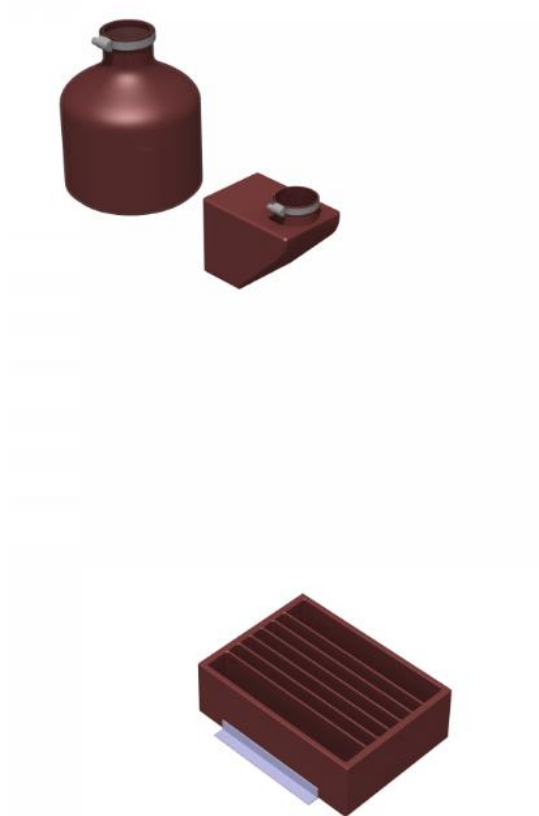

Subsystem 2: Gravitational Separator

Subsystem 3: Magnetic Separator

Subsystem 4: Electrostatic Separator
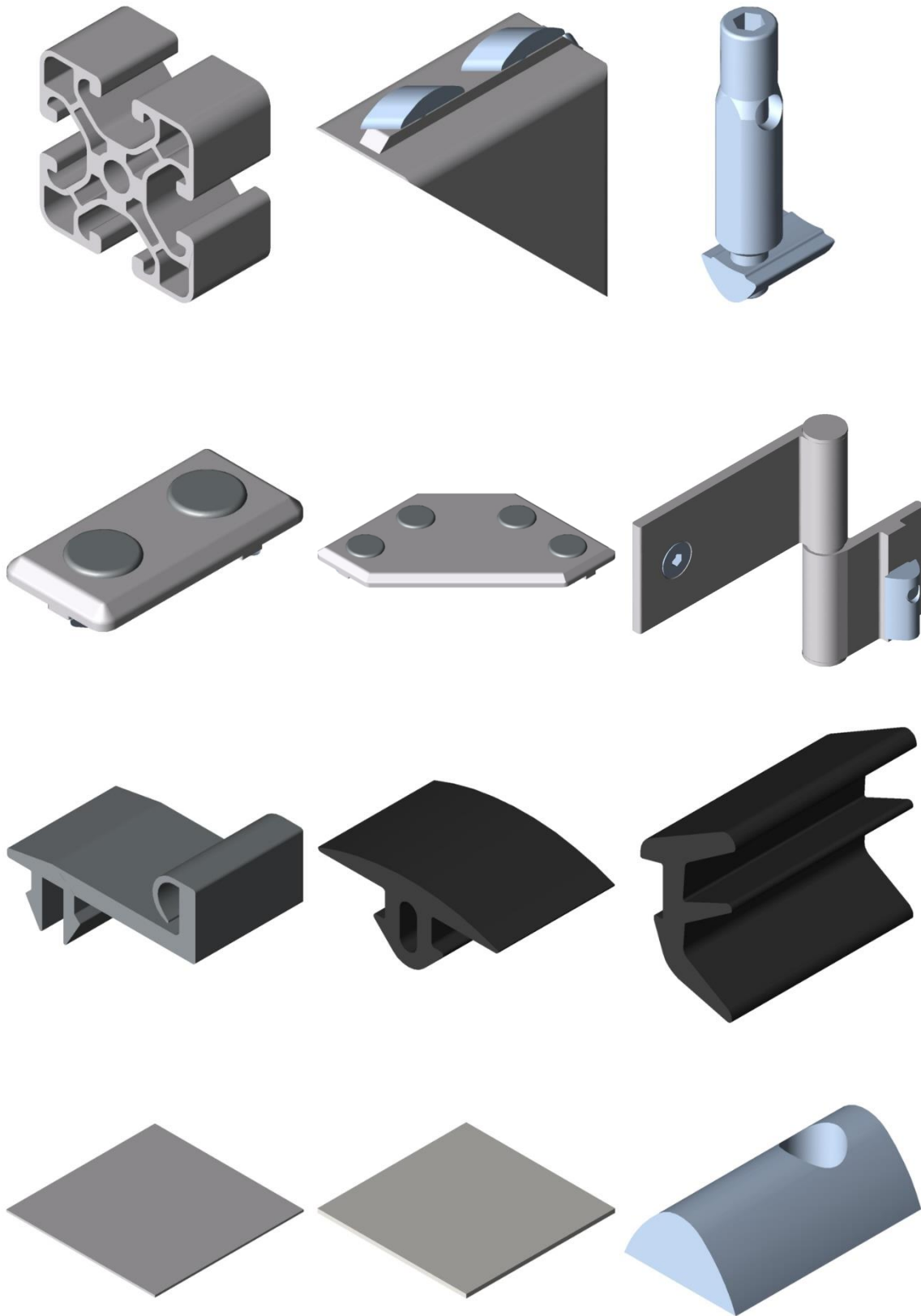
Subsystem 5: Outlet
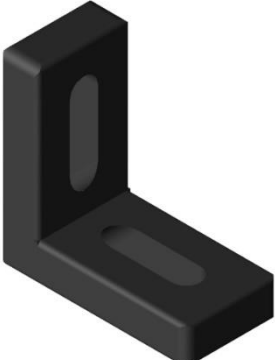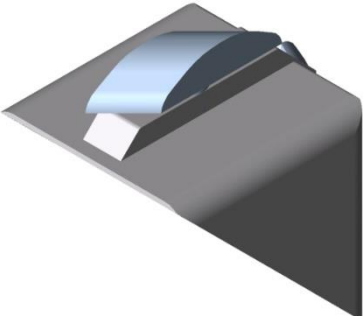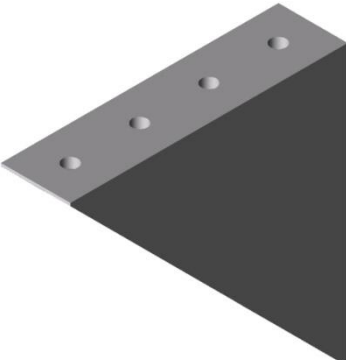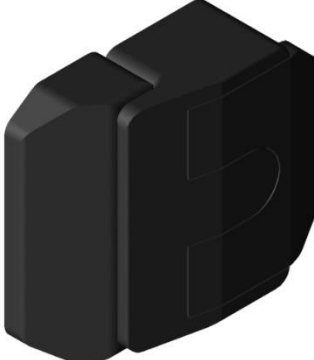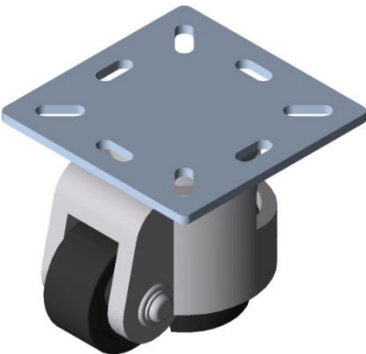

Subsystem 6: Structure

Components: Types of Structural Components (in the order of appearance in chapter 3.6.2)
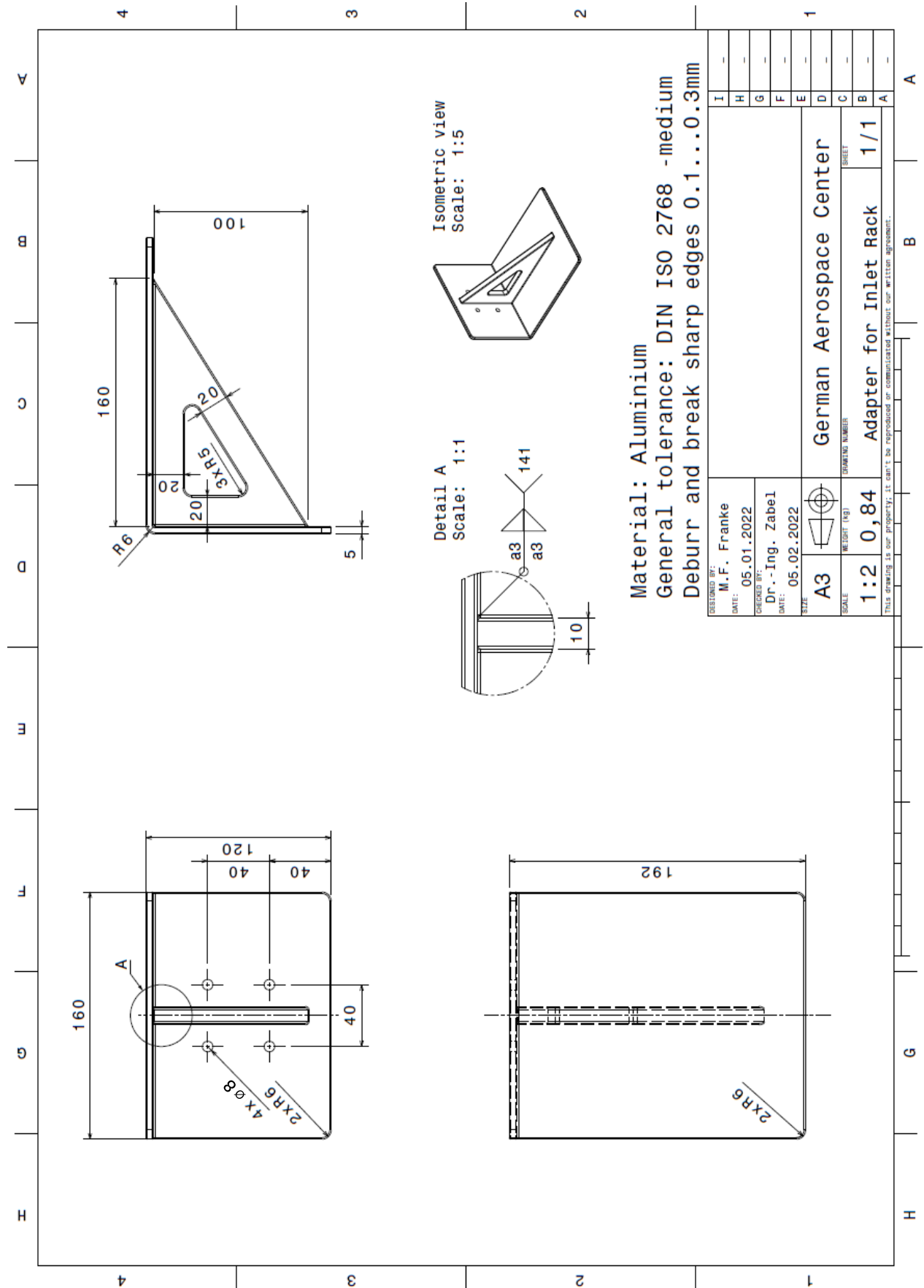
A13 – Procurement Documentation

Example of a reseller-specific order list: ITEM Enquiry "DLR_SMU_BEN_MFF" (24.01.2022)

Pos.	Amount	Article-No.	Article	Length[mm]	Width[mm]
1.0	1	0.0.658.32	Slide LRF 8 D10 120x160		
2.0	1	0.0.463.65	Slide Clamp 8 heavy-duty		
3.0	8	7.0.000.09	Profile 8 40x40 E, natural	907	
3.1	8	0.0.026.30	Saw Cut for Small Cross-Sections		
4.0	112	8.0.000.78	Flat Mushroom Head Screw M8x16, bright zinc-plated		
5.0	136	0.0.388.49	T-Slot Nut 8 St M8, stainless		
6.0	32	0.0.440.58	Automatic-Fastening Set 8, stainless		
7.0	4	0.0.419.06	Profile 6 30x30 light, natural	230	
7.1	4	0.0.026.30	Saw Cut for Small Cross-Sections		
8.0	32	0.0.419.43	T-Slot Nut 6 St M5, bright zinc-plated		
9.0	4	0.0.474.60	Bracket 40x40x20 Zn, black		
10.0	4	0.0.388.51	T-Slot Nut 8 St M6, stainless		
11.0	4	8.0.003.24	Flat Mushroom Head Screw M5x20, zinc-plated		
12.0	4	8.0.003.50	Flat Mushroom Head Screw M6x20, zinc-plated		
13.0	4	7.0.000.09	Profile 8 40x40 E, natural	1.788,00	
13.1	4	0.0.026.30	Saw Cut for Small Cross-Sections		
14.0	12	7.0.000.09	Profile 8 40x40 E, natural	665	
14.1	12	0.0.026.30	Saw Cut for Small Cross-Sections		
15.0	1	0.0.473.08	Sheet Material Al 2mm, natural anodized	987	745
15.1	1	0.0.475.48	Saw Cut for Panel Elements Cat. 1		
16.0	1	0.0.473.08	Sheet Material Al 2mm, natural anodized	987	745
16.1	1	0.0.475.48	Saw Cut for Panel Elements Cat. 1		
17.0	2	0.0.492.09	Acrylic Glass 4mm XT, clear	1.788,00	745
17.1	2	0.0.475.48	Saw Cut for Panel Elements Cat. 1		
18.0	1	0.0.492.09	Acrylic Glass 4mm XT, clear	1.788,00	987
18.1	1	0.0.475.48	Saw Cut for Panel Elements Cat. 1		
19.0	4	0.0.667.44	Jacking Castor D62 120x120		
20.0	16	0.0.642.56	Automatic Angle Bracket Set 8 80x80 Al		
21.0	4	0.0.615.45	Hinge 8 Al FP0-270° light		
22.0	2	0.0.617.32	Door Stop Seal 8 40, grey similar to RAL 7042	907	
22.1	2	0.0.026.30	Saw Cut for Small Cross-Sections		
23.0	4	0.0.619.56	Angle Bracket 8 160x160-40 Al M8, aluminium		
24.0	4	0.0.642.54	Automatic Angle Bracket Set 8 40x40 Al		
25.0	1	0.0.617.32	Door Stop Seal 8 40, grey similar to RAL 7042	1.708,00	
25.1	1	0.0.026.30	Saw Cut for Small Cross-Sections		
26.0	2	0.0.488.45	Door Lock 6-8 Zn		
27.0	4	7.0.000.09	Profile 8 40x40 E, natural	902	
27.1	4	0.0.026.30	Saw Cut for Small Cross-Sections		
28.0	2	7.0.000.09	Profile 8 40x40 E, natural	400	
28.1	2	0.0.026.30	Saw Cut for Small Cross-Sections		

29.0	1	0.0.429.02	Cover Profile 8 32x4, black	902	
30.0	2	0.0.391.35	Handle PA 120, black		
31.0	4	0.0.436.83	Lip Seal 8 2-4mm, black	822	
32.0	1	0.0.492.09	Acrylic Glass 4mm XT, clear	845	422
32.1	1	0.0.475.48	Saw Cut for Panel Elements Cat. 1		
33.0	2	0.0.436.83	Lip Seal 8 2-4mm, black	400	
34.0	4	0.0.642.53	Automatic Flat Bracket Set 8 80x40 Al		
35.0	2	7.0.000.09	Profile 8 40x40 E, natural	1.136,00	
35.1	2	0.0.026.30	Saw Cut for Small Cross-Sections		
36.0	1	0.0.492.09	Acrylic Glass 4mm XT, clear	1.158,00	845
36.1	1	0.0.475.48	Saw Cut for Panel Elements Cat. 1		
37.0	2	0.0.436.83	Lip Seal 8 2-4mm, black	1.136,00	
38.0	4	0.0.642.55	Automatic Flat Bracket Set 8 120x120 Al		
39.0	20	8.0.003.83	Flat Mushroom Head Screw M8x22, zinc-plated		
40.0	8	8.0.003.80	Flat Mushroom Head Screw M8x20, zinc-plated		
41.0	2	0.0.442.03	Shaft-Clamp Profile 8 D10, natural	500	
41.1	2	0.0.026.30	Saw Cut for Small Cross-Sections		
42.0	2	0.0.401.09	Shaft D10, bright	500	
42.1	2	0.0.294.06	Saw Cut for Shafts		

Example of a Technical Drawing: Adapter for Inlet Rack (Interface between Structure and Inlet)

Isometric view
Scale: 1:5

Detail A
Scale: 1:1

Material: Aluminium
General tolerance: DIN ISO 2768 -medium
Deburr and break sharp edges 0.1...0.3mm

DESIGNED BY:	M.F. Franke	
DATE:	05.01.2022	
CHECKED BY:	Dr.-Ing. Zabel	
DATE:	05.02.2022	

German Aerospace Center

SHEET 1/1

DRAWING NUMBER

Adapter for Inlet Rack

SIZE A3

WEIGHT (kg) 0,84

SCALE 1:2

This drawing is our property; it can't be reproduced or communicated without our written agreement.

Example of an Invoice: K&J Magnetics, Inc. (14.12.2021)

K&J Magnetics, Inc.
18 Appletree Lane
Pipersville, PA 18947
www.kjmagnetics.com

1249872   1249872

INVOICE	REP 1: REP 2:		12/14/2021	U1074404	CC	1249872

Dlr E.v. Michel Franke Robert-hooke-str. 7 K24 Bremen, Bremen 28359 Germany Email: michel.franke@dlr.de	Dlr E.v. Michel Franke Robert-hooke-str. 7 K24 Bremen, Bremen 28359 Germany Ship via DHL Express Worldwide

AX2C45-N	ARC, 1-1/8" or x 1" ir x 3/4" x 45º, N50, NI, North	10	$7.94	$79.40
AX2C45-S	ARC, 1-1/8" or x 1" ir x 3/4" x 45º, N50, NI, South	10	$7.94	$79.40

Subtotal	$158.80
Shipping	$37.77
	$196.57

All Products: HTS: 8505.11.0070, ECCN: EAR99
All Products manufactured in China   *D.Gober 12/14/2021*

Thanks for your business. Have a great day!